

University of St Andrews



Full metadata for this thesis is available in
St Andrews Research Repository
at:

<http://research-repository.st-andrews.ac.uk/>

This thesis is protected by original copyright

NOVEL BARIUM CONTAINING COMPLEXES

**A THESIS SUBMITTED FOR THE DEGREE OF
DOCTOR OF PHILOSOPHY**

BY

JASON A.P. NASH



TL
B 770.

This Ph.D. dissertation is dedicated to my family,
friends and most of all, my father ;
Lt.Cmdr.G.E.Nash R.N.,R.I.N., for which I hope
this Ph.D. dissertation is a fitting tribute to him.

DECLARATION

I, Jason Adam Peregrine Nash hereby certify that this thesis has been composed by myself, that it is a record of own work and that it has not been accepted in partial or complete fulfilment of any other degree or professional qualification.

Signed:

Date 22/12/94

I was admitted to the Faculty of Science of the University of St. Andrews under Ordinance General No.12 on 14th October, 1991 and as a candidate for the degree of Ph.D. on 1st October, 1992.

Signed:

Date 22/12/94

I hereby certify that the candidate has fulfilled the conditions of the resolution and the Regulations appropriate to the degree of Ph.D.

Signature of Supervisor

Date 22/12/94

In submitting this thesis to the University of St. Andrews I understand that I am giving permission for use in accordance with the regulations of the University Library for the time being in force, subject to any copyright vested in the work not being affected thereby. I also understand that the title and abstract will be published and that a copy of the work may be made and supplied to any bona fide library or research worker.

ACKNOWLEDGEMENTS

First, I would like to thank my supervisor, Professor Cole-Hamilton for his support, discussions, and his never-ending patience. Drs. Steve Cook and Barbara Richards for their constructive discussions on Chemistry and Cricket. Associated Octel Ltd., for their financial assistance and the operating of an STA service (Mr Barry Cheeseman). Professor Michael Hitchman and Dr.Sarkis Shamilian for their constructive advice.

I would also like to thank Dr. Douglas "sarcastic * * * * * " Foster and Mr. Peter "sweeping statement" Pogorzelec, for their direction in ways of good practical chemistry, their continuing encouragement, and their invaluable help which was gratefully appreciated. Colin Grubb for his guidance in the art of subtlety (or lack of it !!!), Russell "Odd Job" Clarke for his humour in thinking that Airdrie Football team are the best team in Europe ???!!!, and all the other members of labs 334-337 for their constant supply of glassware, solvents and their friendship. Dr. John Barnes and Mr. John Paton from the University of Dundee for their guidance and showing me an insight into the world of X-ray crystallography, as well as helping me to solve the crystal structures of [Cu(POUND)₂] and [Ba(TDFND)₂ .tetraglyme]. Dr. Phil Lightfoot from the University of St.Andrews for his X-ray crystallographic solutions of [Cu(TMMHD)₂] and [Ba([18](Me)₄N₄(Py₂)(Cl₂).3H₂O].

I would also like thank Sylvia Smith for the microanalysis undertaken, Melanja Smith for giving me time on the N.M.R. machines as well as some help in obtaining some ¹³⁵Ba N.M.R. spectra. Bobby Cathcart in the workshop, Colin Millar for running the Mass spectroscopic service and Jim Bews for his help with my computer problems. Finally, I would like to especially thank Karen, for putting up with me through the years of my Ph.D and the support that she gave me, and to my family for their constant help and support.

ABSTRACT

A series of barium(II) and copper(II) complexes of “scorpion tail” β -diketonates were produced and analysed. From the X-ray crystal structure of [Cu(POUD)₂], all of the scorpion tail barium and copper complexes are assumed to be polymeric in the solid state and are shown to be involatile under STA or vacuum conditions. Although, in solution, they are probably monomeric.

The barium containing bibracchial pendant arm macrocycles (1), (2) and (3) have been produced and their volatility analysed. Although, the barium pendant arm macrocycles, [7,16-bis(3-carboxypropanoyl)-1,4,10,13-tetraoxa-7,16-diazacyclooctadecane barium (II)] (1) and [7,16-bis(Z-3-carboxypropenoyl)-1,4,10,13-tetraoxa-7,16-diazacyclooctadecane barium (II)] (2) were formed in the neutral state (the carboxylate function deprotonated), barium pendant arm macrocycle - [(N,N-Carboxymethyl)-4,13-diaza-18-crown-6-barium(II) bromide dihydrate] (3) was isolated as the barium bromide salt.

In all three cases, cis and trans isomers were isolated, and in all three cases, the macrocyclic complexes were shown to be involatile either by STA or vacuum conditions. The lack of volatility is due to the inter / intramolecular hydrogen bonding which will take place between the water molecules and the barium complex.

The most successful volatile precursor which was prepared, involved the synthesis of the complexes of 2,2,6,6-tetramethylmercaptohept-4-en-3-one. The copper (II) complex was shown to be extremely volatile.

The X-ray crystal structure of [Cu(TMMHD)₂] shows that the complex is essentially monomeric and hence, the lack of intermolecular interactions contributes towards its enhanced volatility.

[Ba(TDFND)₂.tetraglyme] is a nine coordinate, monomeric solid with no evidence of hydrogen bonding or van der Waals bonding, which may explain why the barium complex volatilises without decomposition.

CONTENTS

CHAPTER 1 - SUPERCONDUCTING MATERIALS AND THEIR USES

1.1.	What is superconductivity?	1
1.2.	Different types of superconductor	1
1.3.	The structure of a superconductor	5
1.4.	The mechanism of superconductivity	8
1.5.	The properties of superconductor	10
1.5.1.	Meissner effect	11
1.5.2.	Josephson effect	11
1.6.	Applications of superconductors	12
1.7.	Why CVD ?	14
1.8.	Requirement of a CVD precursor	17
1.9.	Non-fluorinated barium containing precursors v's fluorinated barium containing precursors	17
1.1.0.	References	19

CHAPTER 2 - A REVIEW OF ALL POTENTIAL VOLATILE BARIUM COMPOUNDS

2.1.	Introduction	22
2.2.	Barium β -diketonates	23
2.2.1.	Non-fluorinated barium β -diketonate complexes	23
2.2.2.	Non-fluorinated polyether barium β -diketonate complexes	26
2.2.3.	Fluorinated barium β -diketonates	31
2.2.4.	Polyether adducts of perfluorinated barium β -diketonates	35

2.3.	Barium β -ketoiminate complexes	38
2.4.	Barium Alkoxides and Siloxides	42
2.4.1.	Barium monodentate, monofunctional alcoholates	42
2.4.2.	Barium oligoether alcoholates	46
2.4.3.	Barium polyfunctional alcoholates	47
2.4.4.	Crown ether adducts of barium alkoxides	50
2.5.	Barium siloxides	50
2.6.	Organometallic barium compounds	52
2.6.1.	Simple barium metallocenes	53
2.6.2.	Other arenes and larger metallocenes	58
2.6.3.	Polyether " scorpion tail " metallocenes	60
2.7.	Barium silyl amides	61
2.7.1.	Other barium trimethylsilyl compounds	63
2.7.2.	Barium cyclophosphazene complexes	64
2.8.	Barium carboxylates	66
2.9.	References	68

CHAPTER 3 - SCORPION-TAIL BARIUM β -DIKETONATES

3.1.	Introduction	76
3.2.	Ligand preparation	79
3.3.	Keto-Enol Tautomerism	81
3.4.	IR Data of the ligands	82
3.5.	^1H N.M.R. Data of the ligands	82
3.6.	^{13}C N.M.R. Data of the ligands	87
3.7.	Microanalysis of the ligands	87
3.8.	Reactions of the scorpion tail β -diketones with BaH_2 in toluene	87
3.9.	IR Data of the barium complexes	88

3.1.0.	¹ H N.M.R. Data of the barium complexes	89
3.1.1.	¹³ C N.M.R. Data of the barium complexes	89
3.1.2.	Microanalysis of the barium complexes	92
3.1.3.	STA Analysis	93
3.1.3.1.	[Ba(ODD) ₂]	93
3.1.3.2.	[Ba(DOTD) ₂]	94
3.1.3.3.	[Ba(POUD) ₂]	94
3.1.3.4.	[Ba(TPOUD) ₂]	95
3.1.4.	Why are the barium complexes decomposing?	96
3.1.5.	The copper complexes of 8,11-Oxa-dodecane-2,4-dione and 1-(Phenyl)-7,10-oxa-undecane-1,3-dione	97
3.1.6.	The preparation of the copper complexes	97
3.1.7.	The crystal structure of [Cu(POUD) ₂]	98
3.1.8.	UV / Visible spectrophotometric studies of [Cu(ODD) ₂] and [Cu(POUD) ₂]	101
3.1.9.	STA traces of [Cu(ODD) ₂] and [Cu(POUD) ₂]	105
3.1.9.1.	[Cu(ODD) ₂]	105
3.1.9.2.	[Cu(POUD) ₂]	105
3.2.0.	X-ray structural determination of [Cu(POUD) ₂]	106
3.2.0.1.	Crystallographic data	106
3.2.0.2.	Crystal Data and structure refinement for [Cu(POUD) ₂]	107
3.2.0.2.1.	Crystal data	107
3.2.0.2.2.	Atomic coordinates	108
3.2.0.2.3.	Selected bond lengths	109
3.2.0.2.4.	Bond lengths and angles	110
3.2.0.2.5.	Anisotropic displacement parameters	112
3.2.0.2.6.	Hydrogen coordinates	113

3.2.1.	Appendix	114
3.	Experimental	121
3.3.1.	The preparation of 8, 11-oxa-dodecane-2,4-dione	121
3.3.2.	The preparation of [bis{ 8,11-oxa-dodecane-2,4-dionato }barium(II)] by the dry toluene method	123
3.3.3.	The preparation of 2,2-dimethyl-9,12-oxa-tridecane-3,5-dione	125
3.3.4.	The preparation of [bis{2,2-dimethyl-9,12-oxa-tridecane-3,5-dionato }barium(II)]	127
3.3.5.	The preparation of 1-(phenyl)-7,10-oxa-undecane-1,3-dione	129
3.3.6.	The preparation of [bis{ 1-(phenyl)-7,10-oxa-undecane-1,3-dionato }barium(II)]	131
3.3.7.	The preparation of 8,11,14-oxa-pentadecane-2,4-dione	133
3.3.8.	The preparation of [bis{8,11,14-oxa-pentadecane-2, 4-dionato}barium(II)]	135
3.3.9.	The preparation of 1-(2',4',6'-trimethylphenyl)-7,10-oxa-undecane-1,3-dione	136
3.3.1.0.	The preparation of [bis{ 1-(2',4',6'-trimethylphenyl)-7,10-oxa-undecane-1,3-dionato }barium(II)]	138
3.3.1.1.	The preparation of [bis{8,11-oxa-dodecane-2,4-dionato }copper(II)]	140
3.3.1.2.	The preparation of [bis{1-(phenyl)-7,10-oxa-undecane-1,3-dionato}copper(II)]	142
3.4.	References	143

CHAPTER 4 - BARIUM MACROCYCLIC COMPLEXES

4.1.	Introduction	144
4.2.	The proposed scheme for the production of a 24-membered barium bibracchial macrocycle	149
4.2.1.	The preparation of [2- { (p-tolylsulphonyl)oxy } ethyl-p-tolylsulphonamide]	150
4.2.2.	The preparation of N-(p-tolylsulphonyl)aziridine	150
4.2.3.	The preparation and analysis of 1-amino-N,N-bis (2-toluene-p-sulphonylaminoethyl)ethyl ethanoate	151
4.2.3.1.	The preparation of 1-amino-N,N-bis (2-toluene-p-sulphonylaminoethyl)ethyl ethanoate	151
4.2.3.2.	The analysis of 1-amino-N,N-bis (2-toluene-p-sulphonylaminoethyl)ethyl ethanoate	152
4.2.3.2.1.	IR analysis	152
4.2.3.2.2.	¹ H N.M.R. analysis	152
4.2.3.2.3.	¹³ C N.M.R. analysis	153
4.2.4.	The detosylation of 1-amino-N,N'-bis (2-toluene-p-sulphonylaminoethyl)ethyl ethanoate by sodium dihydronaphthide or sodium and liquid ammonia	156
4.2.5.	The mechanism of the reduction of 1-amino-N,N'-bis(2-toluene-p-sulphonylamino ethyl)ethyl ethanoate	160
4.3.	The attempted reactions with the preformed barium macrocycle [Ba[24](Me) ₄ N ₆ (Py) ₂ (ClO ₄) ₂] and 1-bromoacetic acid / or sodium acetate	162

4.4.	The synthesis of the barium pendant arm macrocycles from the reaction of the preformed pendant arm macrocycle and barium salts	164
4.4.1.	The preparation of 7,16-bis(3-carboxypropanoyl)-1,4,10,13-tetraoxa-7,16-diazacyclooctadecane (1) and 7,16-bis(Z-3-carboxypropenoyl)-1,4,10,13-tetraoxa-7,16-diazacyclooctadecane (2) and their barium complexes	165
4.4.2.	The analysis of 7,16-bis(3-carboxypropanoyl)-1,4,10,13-tetraoxa-7,16-diazacyclooctadecane (1) and 7,16-bis(Z-3-carboxypropenoyl)-1,4,10,13-tetraoxa-7,16-diazacyclooctadecane (2) and their barium complexes	167
4.4.2.1.	IR analysis of the barium complex of macrocycle (1)	167
4.4.2.2.	¹ H N.M.R. analysis of the barium complex of macrocycle (1)	168
4.4.2.3.	¹³ C N.M.R. analysis of the barium complex of macrocycle (1)	168
4.4.2.4.	¹ H N.M.R. analysis of the barium complex of macrocycle (2)	170
4.4.2.5.	¹³ C N.M.R. analysis of the barium complex of macrocycle (2)	170
4.4.3.	The preparation and analysis of N,N'-bis(carboxymethyl)-4,13-diaza-18-crown-6 (1) and its barium complexes	171
4.4.3.1.	The preparation of macrocycle (3) and its barium complexes	171

4.4.3.2.	The analysis of the barium containing bibracchial pendant arm 4,13-diaza-18-crown-6 macrocycle	174
4.4.3.2.1.	IR analysis	174
4.4.3.2.2.	Mass spectral analysis	174
4.4.3.2.3.	¹ H N.M.R. analysis	175
4.4.3.2.4.	¹³ C N.M.R. analysis	178
4.4.3.2.5.	STA studies	181
4.4.4.	The preparation and analysis of the barium schiff-base bibracchial pendant arm macrocycles (4) and (5)	183
4.4.4.1.	The preparation of the macrocycles (4) and (5) and their barium complexes	183
4.4.2.	The analysis of the bibracchial pendant arm schiff-base macrocycles	187
4.4.4.2.1.	IR spectral analysis of macrocycle (4A)	187
4.4.4.2.2.	¹ H N.M.R. analysis of macrocycle (4A)	188
4.4.4.2.3.	¹³ C N.M.R. analysis of macrocycle (4A)	190
4.4.4.2.4.	IR analysis of macrocycle (4B)	192
4.4.4.2.5.	¹ H N.M.R. analysis of macrocycle (4B)	192
4.4.4.2.6.	¹³ C N.M.R. analysis of macrocycle (4B)	194
4.4.4.2.7.	IR spectral analysis of the pendant arm macrocycle (4)	194
4.4.4.2.8.	Mass spectral analysis	196
4.4.4.2.9.	¹ H N.M.R. analysis of macrocycle (4)	197
4.4.4.2.10.	¹³ C N.M.R. analysis of macrocycle (4)	199
4.4.4.2.11.	¹ H N.M.R. analysis of macrocycle (5)	202
4.4.4.2.12.	¹³ C N.M.R. analysis of macrocycle (5)	204

4.4.5.	The attempted metal template assisted reaction between "[Ba(TMHD) ₂]", 2,6-diacetylpyridine and 1,2-diaminoethane	206
4.5.	Experimental	210
4.5.1.	The preparation of 1-amino-N,N-bis(2-toluene-p-sulphonylaminoethyl)ethyl ethanoate	210
4.5.2.	The reductive detosylation of 1-amino-N,N-bis (2-toluene-p-sulphonylaminoethyl)ethyl ethanoate by sodium dihydronaphthylide	211
4.5.3.	The reductive detosylation of 1-amino-N,N-bis (2-toluene-p-sulphonylaminoethyl)ethyl ethanoate by the action of activated sodium metal in liquid ammonia	212
4.5.4.	The preparation of the preformed barium macrocycle [Ba [24](Me) ₄ N ₆ (Py) ₂ (ClO ₄) ₂]	213
4.5.5.	The reaction between the preformed barium macrocycle - [Ba [24](Me) ₄ N ₆ (Py) ₂ (ClO ₄) ₂], triethylamine and 1-bromoacetic acid	214
4.5.6.	The attempted reaction between the preformed barium macrocycle - [Ba [24](Me) ₄ N ₆ (Py) ₂ (ClO ₄) ₂] and sodium acetate	214
4.5.7.	The preparation of 7,16-bis(3-carboxy propanoyl)1,4,10,13-tetraoxa-7,16-diazacyclooctadecane (1)	215
4.5.8.	The preparation of [{7,16-bis(3-carboxy propanoyl)1,4,10,13-tetraoxa-7,16-diazacyclooctadecane}barium(II)]	215

4.5.9.	The preparation of 7,16-bis(Z-3-carboxy propenoyl)1,4,10,13-tetraoxa-7,16-diazacyclooctadecane (2)	217
4.5.10.	The preparation of [{7,16-bis(Z-3-carboxy propenoyl)1,4,10,13-tetraoxa-7,16-diazacyclooctadecane}barium(II)]	217
4.5.11.	The preparation of N,N'-bis(carbethoxymethyl)-4,13-diaza-18-crown-6 (3A)	219
4.5.12.	The preparation of N,N'-bis(carboxymethyl)-4,13-diaza-18-crown-6 (3)	219
4.5.13.	The preparation of [N,N'-bis(carboxymethyl)-4,13-diaza-18-crown-6 barium(II) bromide dihydrate]	220
4.5.14.	The attempted reaction between [N,N'-bis(carboxymethyl)-4,13-diaza-18-crown-6 barium(II) bromide dihydrate] and pyridine	222
4.5.15.	The attempted reaction between barium(II) hydride and N,N'-bis(carboxymethyl)-4,13-diaza-18-crown-6 (3)	223
4.5.16.	The preparation of the unsaturated macrocycle (4A)	223
4.5.17.	The preparation of the saturated macrocycle (4B)	225
4.5.18.	The preparation of the pendant arm bibracchial macrocycle (4)	226
4.5.21.	The preparation of macrocycle (5)	228
4.5.2.3.	The attempted metal template assisted reaction between "[Ba(TMHD) ₂]", 2,6-diacetylpyridine and 1,2-diaminoethane	230
4.6.	References	231

CHAPTER 5 - THE BARIUM COMPLEXES OF THE
TETRAGLYME ADDUCTS OF
 β -DIKETONES AND THE COMPLEXES
OF THIO- β -DIKETONES

5.1.	Introduction	233
5.1.1.	Barium β -diketonate tetraglyme adducts	233
5.2.	The X-ray crystal structure of [Ba(TDFND) ₂ .tetraglyme]	236
5.2.1.	STA studies	241
5.2.2.	Experimental	246
5.2.3.	Crystallographic data	246
5.2.4.	Crystal data and structure refinement for [Ba(TDFND) ₂ .tetraglyme]	247
5.2.4.1.	Crystal data	247
5.2.4.2.	Atomic coordinates	249
5.2.4.3.	Bond lengths	251
5.2.4.4.	Anisotropic displacement parameters	255
5.2.4.5.	Hydrogen coordinates	257
5.3.	The preparation and analysis of [Ba(DBM) ₂ .tetraglyme.0.25C ₇ H ₈]	258
5.3.1.	The preparation of [Ba(DBM) ₂ .tetraglyme.0.25C ₇ H ₈]	258
5.3.2.	The analysis of [Ba(DBM) ₂ .tetraglyme. 0.25C ₇ H ₈]	260
5.3.2.1.	¹ H N.M.R. analysis	260
5.3.2.2.	¹³ C N.M.R. analysis	262
5.3.2.3.	Mass spectral analysis	264

5.3.2.4.	STA studies	264
5.4.	Experimental	267
5.4.1.	The preparation of [bis{ 1,3-diphenylpropane-1,3-dionato }barium(II).tetraglyme.0.25C ₇ H ₈]	267
5.4.2.	The attempted preparation of [bis{ pentane-2,4-dionato }barium(II).tetraglyme] via Ba metal or BaH ₂	269
5.5.	Introduction	270
5.5.1.	Metal thio-β-diketonates	270
5.5.2.	The preparation and analysis of the barium and copper complexes of 2,2,6,6-tetramethyl-5-mercaptohept-4-en-3-one	272
5.5.2.1.	The preparation of [Ba(TMMHD) ₂]	272
5.5.2.3.	The preparation of [Cu(TMMHD) ₂]	273
5.5.2.4.	The analysis of [Cu(TMMHD) ₂]	274
5.5.2.4.1.	Sublimation studies	274
5.5.2.4.2.	The crystal structure of [Cu(TMMHD) ₂]	274
5.5.2.4.3.	Mass spectral analysis of [Cu(TMMHD) ₂]	281
5.5.2.4.4.	STA studies	284
5.5.3.	Appendix	286
5.5.3.1.	Crystal data and structural refinement of [Cu(TMMHD) ₂]	287
5.5.3.2.	Atomic coordinates	293
5.5.3.3.	Anisotropic displacement parameters	296
5.5.3.4.	Bond lengths	298
5.5.3.5.	Bond angles	300
5.5.3.6.	Torsion angles	303
5.5.3.7.	Non-bonded contacts	306
5.5.3.8.	Least square planes	309

5.5.4.	Experimental	313
5.5.4.1.	The preparation of [bis{ 2,2,6,6-tetramethyl-5-mercaptohept-4-en-3-oate }barium(II)] using Ba granules and gaseous ammonia	313
5.5.4.2.	The attempted preparation of [bis{ 2,2,6,6-tetramethyl-5-mercaptohept-4-en-3-oate}barium (II)] using BaCl ₂ .2H ₂ O	
5.5.4.3.	The attempted preparation of [bis{ 2,2,6,6-tetramethyl-5-mercaptohept-4-en-3-oate}barium (II)] using barium(II)acetate	314
5.5.4.4.	The preparation of [bis{ 2,2,6,6-tetramethyl-5-mercaptohept-4-en-3-oate}copper(II)]	315
5.6.	References	317

APPENDICES

Conclusions	319
Analytical equipment	321

ABBREVIATIONS

CVD	Chemical Vapour Deposition
Hacac	Acetylacetone (Pentane-2,4-dione)
HTMHD	2,2,6,6-Tetramethylheptane-3,5-dione
HDFD	1,1,1,2,2,6,6,7,7,7-Decafluoroheptane-3,5-dione
HDFHD	1,1,1,5,5,6,6,7,7,7-Decafluoroheptane-2,4-dione
HTFA (HTFAC)	1,1,1-Trifluoropentane-2,4-dione
HHFA (HHFAC)	1,1,1,5,5,5-Hexafluoropentane-2,4-dione
HTDFND	1,1,1,2,2,3,3,7,7,8,8,9,9,9-Tetradecafluoro nonane-4,6-dione
HHFOD	1,1,1,2,2,3,3-Heptafluoro-7,7-dimethyl-4,6- octanedione
HOFHD	1,1,1,5,5,6,6,6-Octafluoro-2,4-hexanedione
HHDFDD	1,1,1,2,2,3,3,4,4,5,5,6,6,10,10,10- Hexadecafluorodeca-2,4-dione
HEF3D	1,1,1,2,2,3,3,4,4,5,5,6,6,10,10,11,11,12,12,12- Eicosafluorododeca-4,6-dione
HHFDD	1,1,1,2,2,3,3,4,4,8,8,9,9,10,10,11,11,11- Octadecafluoroundeca-5,7-dione
HDTFHD	5,5-Dimethyl-1,1,1-trifluorohexane-2,4-dione
HDPFHD	6,6-Dimethyl-1,1,1,2,2-pentafluoroheptane-3,5-dione
THF	Tetrahydrofuran
DMSO	Dimethylsulphoxide
DMF	N,N-Dimethylformamide
HMPA	Hexamethylphosphorylamide
HODD	8,11-Oxa-dodecane-2,4-dione
HDOTD	2, 2-Dimethyl-9,12-Oxa-tridecane-3,5-dione
HPOUD	1-(Phenyl)-7,10-oxa-undecane-1,3-dione

HOPD	8,11,14-Oxa-pentadecane-2,4-dione
HTPOUD	1-(2',4',6'-Trimethylphenyl)-7,10-oxa-undecane-1,3-dione
18-Crown-6	1,4,7,10,13,16-Hexaoxacyclooctadecane
Tetraglyme	2,5,8,11,14-Pentaoxapentadecane
HHFIP	Hexafluoroisopropanol
HPFTB	Perfluoro-tert-butanol
TMEDA	N,N,N',N'-Tetramethylethylenediamine
DME	1,2-Dimethoxyethane
EDTA	Ethylenediaminetetraacetic acid
DBM	1,3-Diphenylpropane-1,3-dione
Sacac	2,4-mercaptopentanedione
SHFA	1,1,1,5,5,5-Hexafluoro-4-mercaptopent-3-en-2-one
TMMHD	2,2,6,6-Tetramethyl-5-mercaptohept-4-en-3-one

In reference to macrocyclic nomenclature

Priority

1	M	Metal
2	[18]	Number of member atoms in the macrocycle
3	(Me)	Methyls
4	N	Number of Nitrogen atoms
5	(Py)	Number of pyridyls
6	Cl ⁻	Counterion

CHAPTER 1

SUPERCONDUCTING MATERIALS AND

THEIR USES

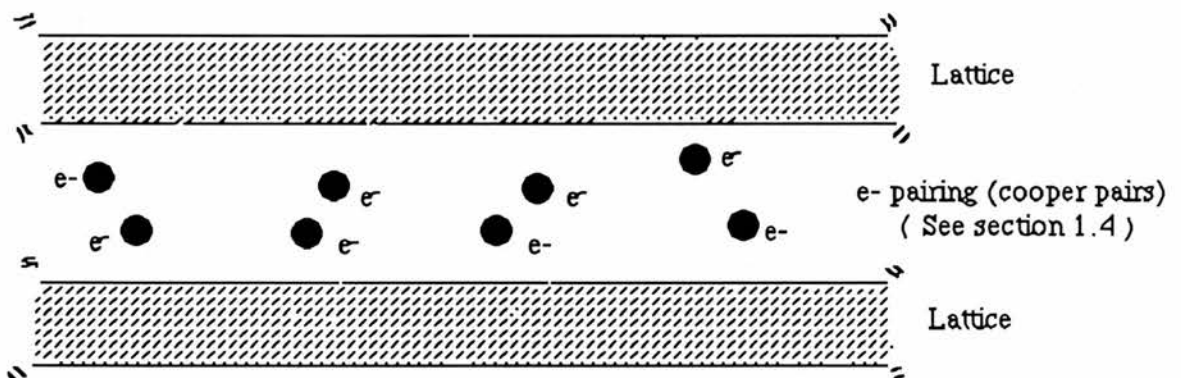
CHAPTER 1

1.1. What is superconductivity?

Superconductivity is a phenomenon which is experienced when a material conducts an electric current without resistance. Unfortunately, existing superconducting materials only superconduct well below room temperature and so the applications are very limited.

As seen in Fig 1.1., superconductivity is produced by the motion of electron pairs. Unlike a normal conductor, no resistance is produced by colliding with other particles. The temperature in which superconductivity takes place in a material is known as the T_{c_zero} value.

Fig 1.1



1.2. The different types of superconductor

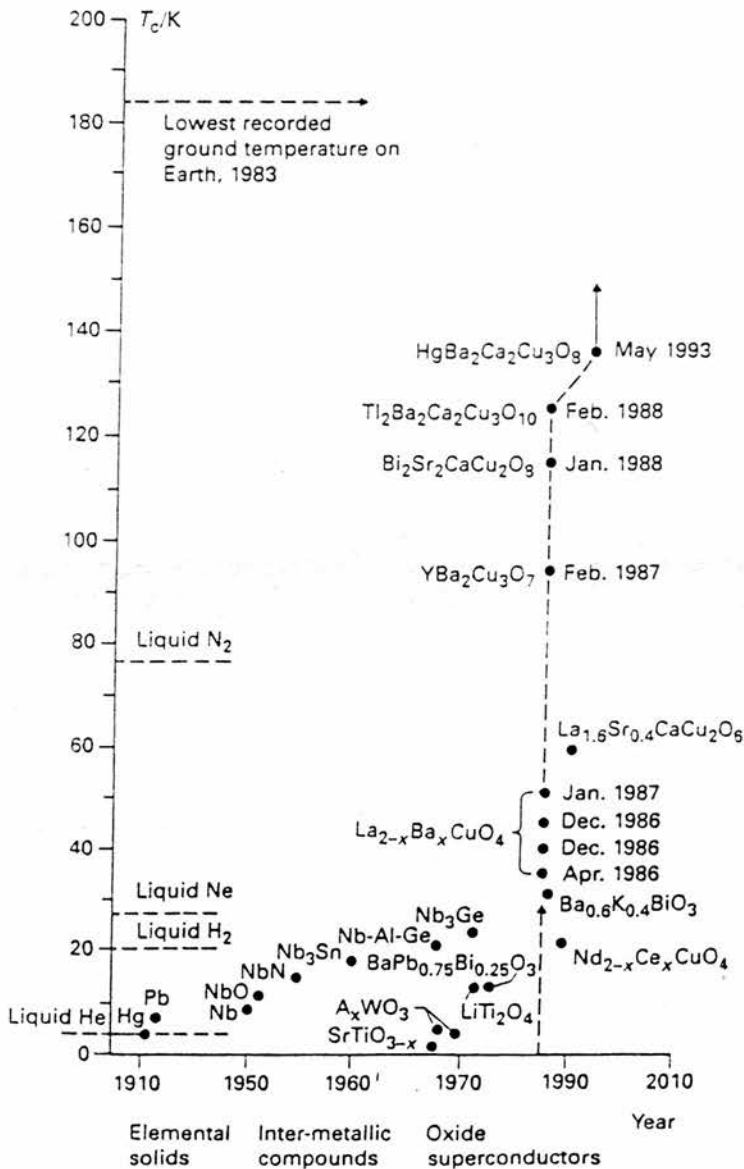
The search for a material which will superconduct at room temperature has been confined predominantly to materials of five types.

These five types are : elemental solids such as Hg^1 , Pb and Nb (known as Type 1 superconductors), intermetallic compounds such as NbN , Nb_3Sn^2 and Nb_3Ge^3 ,

(known as Type 2 superconductors), perovskite copper free oxides such as SrTiO_{3-x} , LiTi_2O_4 and $\text{Ba}_{1-x}\text{KBiO}_3$ ⁴, organic superconductors such as tetramethyltetraselenafulvalene salts (Bechgaard salts)⁵ and intercalated fullerides (K_3C_{60} ⁶, $\text{Cs}_2\text{RbC}_{60}$ ⁷ and $\text{Rb}_x\text{Tl}_y\text{C}_{60}$ ⁸) and most importantly, the perovskite cuprate superconducting materials where the majority of the recent research effort in superconducting materials is concentrated. The history of superconducting materials is summarised in Fig 1.2.a.

The graph below shows the superconducting temperature of these particular materials against time.⁹

Fig 1.2.a.



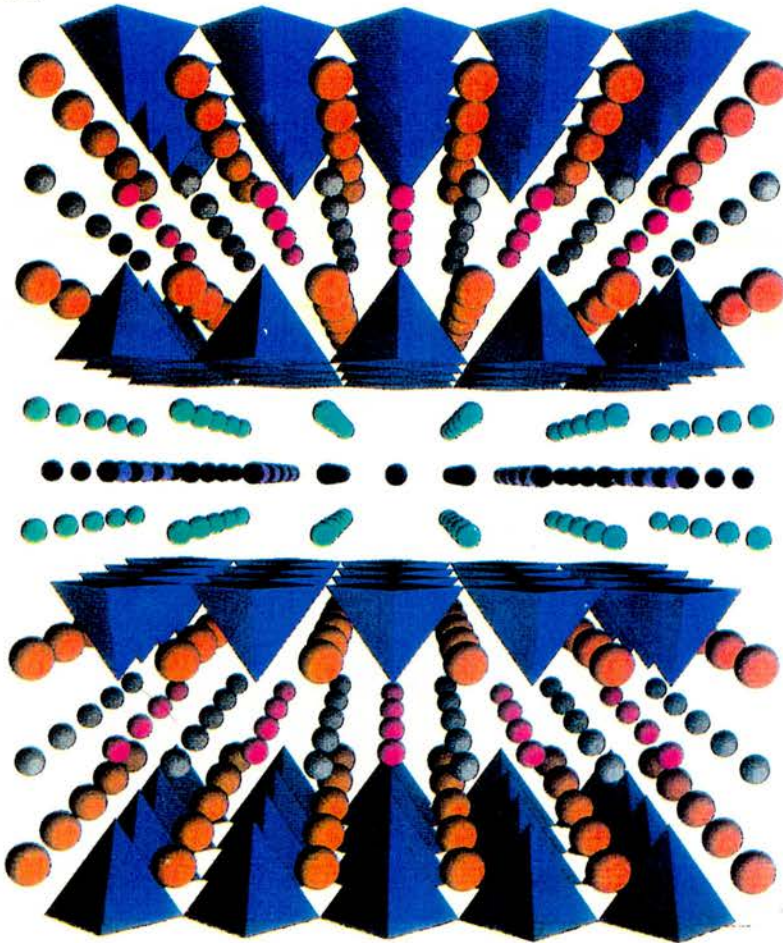
A discovery in 1986 by Bednorz and Müller¹⁰ ignited considerable research interest for the production of a new family of superconducting materials. Upon their investigations $\text{La}_{2-x}\text{Ba}_x\text{CuO}_4$ [where $x = 0.15$, and the average oxidation state of copper is 2.15, so there are some Cu^{2+} (d^9) and some Cu^{3+} (d^8)] was found to possess a $T_{c_{\text{zero}}}$ value of 30K. Not only was the value for the $T_{c_{\text{zero}}}$ the highest ever observed, but this discovery initiated investigations into other cuprate superconducting materials.

As a result, a year later, Chu discovered that $\text{YBa}_2\text{Cu}_3\text{O}_{7-x}$ ¹¹ (sometimes referred to as YBaCuO or 123) had a $T_{c_{\text{zero}}}$ value of 93K. In addition, $\text{YBa}_2\text{Cu}_3\text{O}_{7-x}$ possesses a high critical current and critical magnetic field which is extremely advantageous for commercial superconducting devices (see section 1.6). The high T_c value also meant that the material was able to superconduct above liquid N_2 temperature (77K). As a consequence, liquid nitrogen could be used as a refrigerant instead of liquid helium (4K) or liquid hydrogen (22K) which had been previously used refrigerants. Not only was the refrigerant now cheaper at 20p per litre compared to liquid helium at £8 per litre, but nitrogen makes up 78 % of the atmosphere compared to helium which makes up less than 1 %. Since 1987, various replacements have been made in some way to the YBaCuO material by changing Y for Nd, Sm, Gd or Ho or by changing the barium component. These new materials, however, did not possess the same properties as YBaCuO . Although, Maeda et al¹² found that these copper oxides could superconduct without the presence of a rare earth metal. $\text{Bi}_2\text{Sr}_2\text{Ca}_2\text{Cu}_3\text{O}_{10-x}$ was found to have a $T_{c_{\text{zero}}}$ value of 110K, although, the material was observed in three different phases with three different values of T_c - 20K, 80K and 110K. A T_c zero value of 125K was recorded by Sheng et al¹³ for a thallium containing superconductor - $\text{Tl}_2\text{Ba}_2\text{Ca}_2\text{Cu}_3\text{O}_{10-x}$. In addition to this particular phase, four other superconducting phases have been isolated (2201, 1223, 2212 and 2234 phase - referring to the number of cations present) each one difficult to isolate as a single selective phase. Recently however, perfluorinated precursors have been used in the deposition of these films to produce phase selective superconducting films of good quality (see section 1.9).

Only last year, Schilling et al¹⁴ discovered that a new mercury - containing cuprate (1223 phase) could achieve a value of T_c of 134K. This was after the initial discovery by Putlin et al¹⁵ of $HgBa_2CaCu_2O_{6+x}$ (1212 phase) - $T_{c_{zero}}$ - 121K.

Fig 1.2.b. shows the crystal structure of $HgBa_2Ca_2Cu_3O_8$ (1223 phase)

Fig 1.2.b



Key : Blue pyramids = CuO_5 , orange spheres = Ba, Pink spheres = Hg,

Green spheres = Ca, Black / Grey = O and Purple spheres = Cu

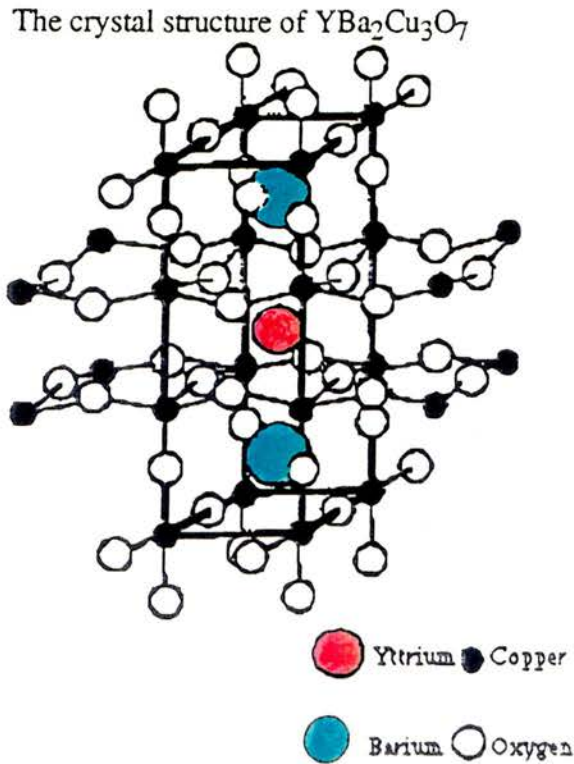
Although, $BiSrCaCuO$, $TlBaCaCuO$ and $HgBaCaCuO$ have higher T_c values than $YBaCuO$, there is evidence that $YBaCuO$ is superior in its pinning behaviour. A high J_c (critical current) relates to the flux pinning within the superconducting material.

Therefore, on the whole, YBaCuO materials give higher current and magnetic field densities than other superconducting materials, such as BiSrCaCuO, TlBaCaCuO and HgBaCaCuO.

Thus, YBaCuO is used more in existing commercial applications than the other superconducting materials.

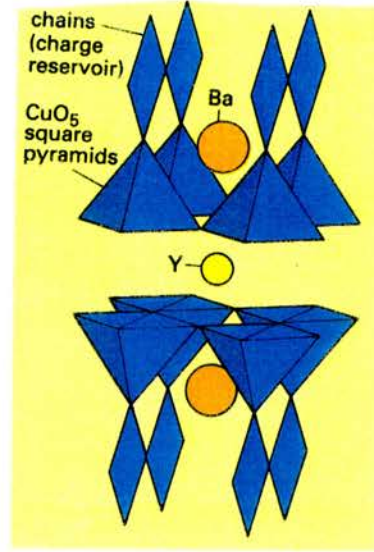
1.3. The structure of a superconductor

The structures of several superconducting cuprate oxides have been determined by X-ray crystal and powder diffraction. The structures seem to have similar geometric characteristics and thus, this section will discuss the structure of the most well known superconducting cuprate oxide $\text{YBa}_2\text{Cu}_3\text{O}_7$. An important feature of high temperature superconducting materials is the oxygen stoichiometry, determining both structural and superconducting properties. As seen in Fig 1.3.a. the oxygen deficient cuprate oxide consists of one dimensional CuO chains which run along the x axis, and two dimensional CuO sheets which lie in the z-x planes. In this particular crystal structure, there is a highly regular pattern of CuO chains and sheets. However, at annealing temperatures some oxygen atoms are displaced resulting in some disorder between the CuO chain units. As a consequence, the crystal lattice system changes from orthorhombic to tetragonal and the stoichiometric ratios of the superconducting oxide change from $\text{YBa}_2\text{Cu}_3\text{O}_7$ to $\text{YBa}_2\text{Cu}_3\text{O}_{7-x}$. It seems that a final anneal in O_2 results in the best superconducting materials¹⁶. Superconductivity, however, is observed only when $\text{YBa}_2\text{Cu}_3\text{O}_{7-x}$ is within discreet limits of $x - 0 < x < 0.5$.



It also appears that there are two distinct components of a superconducting perovskite material which both contribute to the superconducting properties. The first component consists of electronically active CuO_2 sheets in which the mechanism of superconductivity is likely to take place. These CuO_2 sheets comprise of alternating stacks which are separated by insulating block layers within the crystal lattice. Therefore, a second component which aids charge transfer between CuO_2 planes is needed, this second component is known as the charge reservoir as seen in Fig 1.3.b.

Fig 1.3.b.



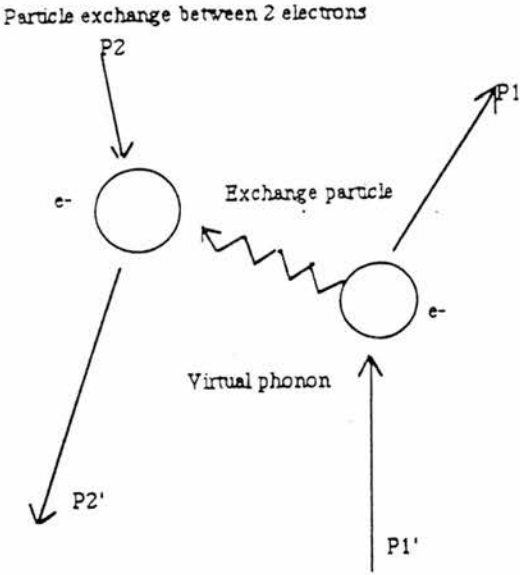
The nature and composition of the charge reservoir adjacent to the CuO₂ sheets also plays an important role in superconductivity. The charge reservoir can be highly ionic, or ionic with some covalent character. The latter, has the ability to redistribute charge effectively through the apical CuO₅ square pyramids. The charge carriers within the lattice consist of positive holes within CuO₂ sheets. The incorporation of doped ions into the insulating block layers in a controlled and continuous manner can produce positive holes. In the quest for better superconductors different charge reservoirs have been investigated. Partially replacing the CuO₅ square pyramids with CO₃²⁻ ions¹⁷ or other oxyanions¹⁸ have proved to be good replacements for the charge reservoirs. For example YSr₂Cu_{2.79}(SO₄)_{0.21}O_{6.16}¹⁹ has a T_c_{onset} value of 78K.

1.4. The mechanism of superconductivity

Unfortunately, the mechanism of superconductivity is not well understood. The only creditable mechanism was proposed by Bardeen, Cooper and Schieffer in 1957²⁰. Although, directly, the Bardeen - Cooper - Schieffer (BCS) electron - phonon mechanism is only applicable for superconductors with much lower T_c values than 40K, it can be applied to other cuprate superconductors where higher T_c values are achieved.

The BCS mechanism is based upon electron - phonon interactions in the crystal lattice which lead to electron pairing of the conduction electrons (Cooper pairs). The existence of Cooper pairs is supported by all true superconductor materials exhibiting diamagnetism.

Fig 1.4



There are several theories which go towards explaining why this electron - electron interaction should take place. The cause of the electron pairing is probably due to the polarisation of the crystal lattice. The greater the electron - electron interaction, the more thermal energy is required to destroy this interaction, therefore a higher T_c is obtained.

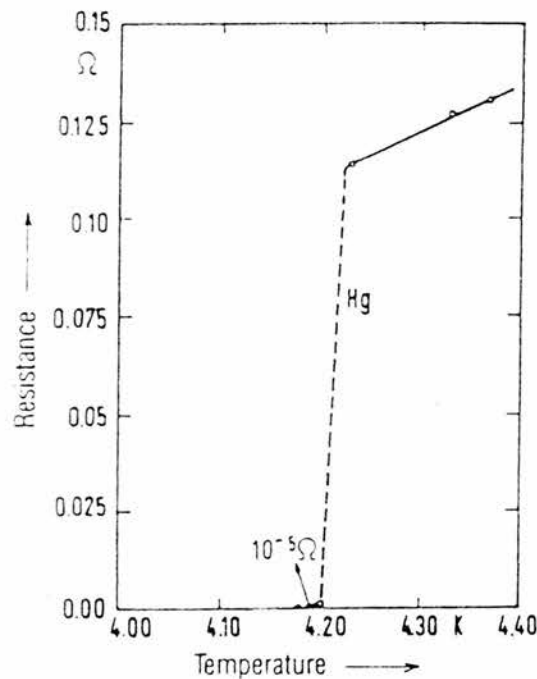
$\text{YBa}_2\text{Cu}_3\text{O}_7$ is a poor metal, but is on the metallic side of the metal - insulator transition. The area of superconduction as previously mentioned, is within the CuO sheets. As a result of Jahn - Teller distortions existing in $\text{YBa}_2\text{Cu}_3\text{O}_7$ structure, lattice vibrations (phonons) are caused which can interact with other electrons. The interaction of electrons via the vibrations of the lattice is the cause of superconductivity. The exchange of a virtual phonon, from one electron to another is shown in Fig 1.4. This interaction can also overcome the repulsion of the electrons which arise from the electrostatic interactions.

1.5. The Properties of superconductor

Temperature is not the only factor which determines superconductivity in a particular material. Several other properties such as the critical magnetic field, critical current density, diamagnetism and Josephson effects also indicate superconductivity.

The critical temperature is the temperature at which a material is truly superconducting as shown in the diagram of the first superconducting material discovered by Onnes¹.

Fig 1.5.a



Similarly, the critical current J_c and critical magnetic field H_c are parameters in which it can be determined whether a superconductor lacks all electrical resistance. The critical values of all three values are intrinsically interlinked. For example, as the temperature and magnetic field increase the critical current density decreases.

1.5.1. Meissner effect

This is as a consequence of the electron pairing (Cooper pairs) within the crystal lattice. The Meissner effect was first described in 1933 by Meissner and Ochsenfeld²¹. Because a superconductor possesses pure diamagnetism, levitation of magnets or magnetic components can take place as the superconductor can completely exclude a magnetic field from its bulk.

1.5.2. Josephson Effect

This is as a result of placing two superconducting materials between an insulator. A small current is produced without any applied voltage as a consequence of two macroscopic wavefunctions which do not overlap²². This is known as the d.c Josephson effect and has found some applications in switching devices. The a.c Josephson effect is where an applied voltage is put across the barrier. A current is produced which is directly proportional to the applied voltage. This a.c Josephson effect can be useful in SQUIDS (Superconducting Quantum Interference Devices) which measure small voltages and magnetic fields. Noge et al²³ and Yamashita et al²⁴ have prepared Josephson junctions of $\text{YBa}_2\text{Cu}_3\text{O}_7$ on $\text{MgO}(100)$ which appear to demonstrate an ideal a.c Josephson effect. DC SQUIDS were also produced by the same group.

1.6. Applications of Superconductors

The potential applications for superconductors can vary immensely from devices in computers to propulsion in ships. The estimated market size will be between \$150-200 million in 2020, with most of the market share accounted for by computer devices²⁵. The main use for superconductors in computers is by partial replacement of semiconducting devices which are used in amplifiers, modulators, valves and circuit elements. In computing, the speed of transmission of information is very important. Normal semiconducting devices tend to produce a large amount of heat which generally limits the miniaturisation of the computer and hence its speed of operation.

If superconducting / semiconducting hybrid components can be used in a computer then the speed of the transmission of information would be greater. In fact, Japan has recently produced the worlds first Josephson supercomputer²⁶ which incorporates some of these devices. As previously mentioned, superconducting materials such as SQUIDS can also be used for detecting very small voltages and magnetic fields.

Superconductors can also be used in power engineering . Values in the order of 4 Tesla must be sustained together with current densities of at least 10^6 A cm^{-2} in the usage of power applications, such as a.c and d.c motors and generators, energy storage and transport uses. The only material which is capable of reaching and sustaining these values is YBCO. The highest T_c and J_c reported for a CVD film of YBCO (123 phase) was at 92K which had a current density of $6.3 \times 10^6 \text{ A cm}^{-2}$ (77K, 0T)²⁷. This is compared to the highest T_c and J_c for BiSrCaCuO (2223 phase) at 97 K which had a current density of $3.8 \times 10^5 \text{ A cm}^{-2}$ ²⁸ . Interestingly, the highest T_c and J_c reported for TlBaCaCuO (2212 phase)²⁹ was at 108K ($J_c = 10^4 \text{ A cm}^{-2}$).

Kilometre lengths of flexible wire have actually been produced by electrophoretically depositing YBCO on Ag or Ni alloy³⁰. However, the material is untextured and hence has inadequate J_c properties.

Although, the applications for superconductors in power engineering are on the increase despite these difficulties, as shown by superconductors being used in the propulsion of ships.

In 1991, Japan built the World's first superconducting ship - Yamato 1³¹. It is powered by two engines each containing six dipole magnets which are cooled in liquid helium and gave a magnetic density of 4 Tesla.

Levitating trains such as the Japanese MAGLEV have also been produced using superconducting materials³². In fact, some of the most common applications for superconductivity involve magnetic coils. Once the magnetic field has been set up then, in principle, no further electrical power is required to maintain it. Superconducting magnets are routinely used in medium to high field nuclear magnetic resonance spectrometers.

Research experiments into particle physics and fusion can only be realistically carried out with use of superconductor coil magnets where moderate fields of 2 to 10 Tesla are produced. The world's largest superconducting solenoid is in operation at the European Centre for Nuclear Research at CERN³³.

1.7. Why CVD ?

In the next century, large scale applications of high Tc superconductors will be needed in power engineering, wires, tapes and thin films. It is apparent that most of the technological advances in the deposition of superconducting films to date does not satisfy the criterion required for high Tc superconducting appliances.. However, chemical vapour deposition (CVD) is an excellent technique to produce good quality films. Ideally, for superconducting applications, a high critical current density, magnetic field and temperature must be obtained. Thin films produced by CVD achieve extraordinary high current densities, of the order of 10^6 A cm⁻² at 77K. Furthermore, Berry et al³⁴ noticed that phase pure thin films could be produced by CVD. The surface morphologies of CVD produced films are also better than the type of films produced by other techniques such as, sintering, super-critical fluid and sol-gel techniques which may affect the superconducting properties of the film . However, as mentioned by Sievers and coworkers³⁵ CVD has one limitation ; which is that a volatile precursor is required. Volatile precursors for Y,Ba and Cu have been tried and tested in the deposition of YBa₂Cu₃O_{7-x} thin films. The Y and Cu precursors which normally comprise of [Y(TMHD)₃] (which sublimates at 120-160°C)³⁴ and [Cu(TMHD)₂]³⁶ or [Cu (acac)₂]³⁴ (which sublime at 140-155°C and 140-170°C) are excellent volatile precursors for CVD, as they are thermally stable and extremely volatile. Thus, high carry over rates are ensured and the general efficiency of using these precursors are high.

However, most of the existing barium precursors such as "[Ba(TMHD)₂]"³⁴ sublime at higher temperatures (230-240°C) and thus are likely to undergo some decomposition.

As a result, not only is the process of subliming the barium precursor inefficient with regard to time, wasted material and overheads, it also results in a variable vapour pressure at the surface of the substrate and consequently can effect the stoichiometric ratios of the $\text{YBa}_2\text{Cu}_3\text{O}_{7-x}$ type superconductor. If this happens a different phase can arise which is not only problematic but may possess no superconducting properties.

Summary of the advantages of CVD

1. Higher critical current density and magnetic field are obtained.
2. Predominantly one superconducting phase is isolated.
3. Higher growth rates are achieved with CVD.
4. Better surface morphology of films, thus, better superconducting properties are obtained.
5. For future applications, large area deposition of epitaxial films can take place.
6. The coating of complex shapes can take place using CVD.

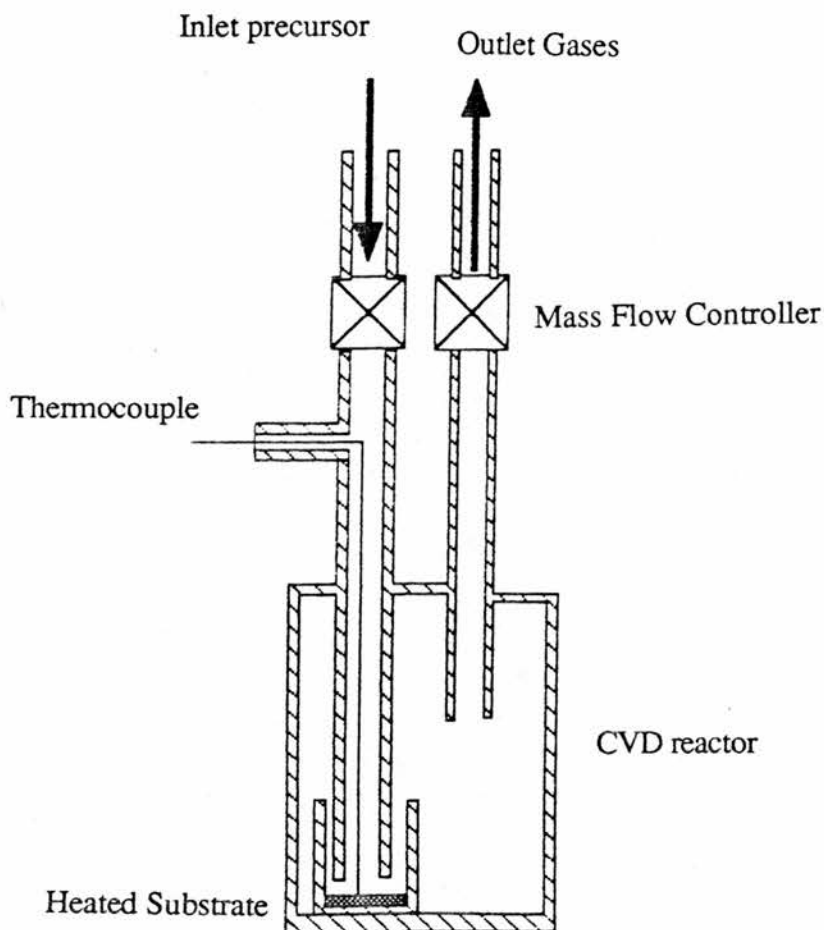
Disadvantages of CVD

1. Volatile precursor is needed.

The principle aims of this project were to develop volatile barium precursors for the deposition of high T_c superconducting films. At Strathclyde University, under the direction of Professor Michael Hitchman, precursors were to be tested using a thermal CVD apparatus similar to the one shown in Fig 1.7.

The CVD system consists of an impinging jet reactor (Archer Technicoat Ltd) with a resistive heated substrate platform (U.S inc.) and standard gas - handling facilities. The CVD process involves the heating of the precursor to sublimation temperature with the vapours in the gas phase being carried by a stream of argon to the deposition zone on the substrate. At a higher temperature the gas phase precursor decomposes to form the deposited film.

Fig.1.7



A diagram of the impinging jet CVD apparatus used at Strathclyde University.

1.8. Requirement of a CVD precursor

There are four major requirements for a CVD precursor for depositing oxide films. For CVD, the precursor has ideally to volatilise at a temperature under 200°C. A suitable CVD precursor would have to sublime intact with no decomposition. Therefore, as well as being volatile, the precursor would have to be thermally stable at subliming temperatures, but at higher substrate temperatures decompose to the corresponding oxide film. Although the above two parameters are very important, moisture and air stability are also desirable.

1.9. Non-fluorinated barium containing precursors v's fluorinated barium containing precursors

To reduce the possibility of non-superconducting phases occurring whilst in the CVD reactor, barium containing compounds incorporating fluorine were used. As discussed later (in Chapter 2), not only did the incorporation of fluorine lower the sublimation temperature of the precursor, it also reduced the amount of decomposition. Fluorine incorporation however, has the disadvantage of providing barium fluoride films instead of barium oxide in the CVD reactor. Post-annealing at 1000°C in O₂ / H₂O mixture does convert the barium fluoride to barium oxide, however, if this stage of processing can be avoided, it would be advantageous³⁷. One certain way of avoiding this is to produce a volatile barium precursor which does not contain fluorine (or silicon) and readily decomposes at higher temperatures to deposit barium oxide.

The dilemma between using the more volatile fluorine containing barium precursors and finding a volatile and thermally stable hydrocarbon containing precursor is an interesting one.

Although, it is interesting to note that when Malandrino et al³⁸ used [Ba(HFA)₂.tetraglyme] to produce a TlBaCaCuO film, not only was there an improvement in the surface morphology of the film (over that of the normal hydrocarbon containing barium precursors) but he was also able to produce a single selective phase superconducting oxide - 2223 phase - with a $T_{c_{zero}}$ value of 93K and a value of J_c of $10^4 - 10^5$ A cm⁻² at 5 Tesla.

In fact the highest J_c and H_c for a TlBaCaCuO film was obtained from fluorinated precursors by Hamaguchi et al²⁹ (see section 1.6). A similar result was noticed by Zhang³⁹, who isolated predominantly one phase of BiSrCaCuO - 2212 phase when using similar perfluorinated precursors of Sr and Ca, i.e.[Sr(HFA)₂.tetraglyme] and [Ca(HFA)₂.triglyme]. However, the $T_{c_{zero}}$ value obtained (73K) was less than that of the best BiSrCaCuO phase (110K).

1.1.0. References

1. H.K.Onnes, *Comm.Leiden.*, Suppl.Nr., 1914, **34**
2. B.T.Matthias, T.H.Gaballe, S.Geller, E.Corenzwit, *Phys.Rev.*, 1954, **95**, 1435.
3. L.R.Testardi, J.H.Wernick and W.A.Royer, *Sol State Commun.*, 1974, **15**, 1.
J.R. Gavaler, M.H.Janoko and C.K.Jones, *J.Appl.Phys.*, 1974, **45**, 7.
4. A.R.Armstrong and P.P.Edwards, *Ann.Rep.Prog.Chem.C.*, 1991, 259.
Chemistry of high temperature superconductors, C.N.R.Rao (Ed).Singapore : World Scientific, 1991.
5. K.Bechgaard, C.S.Jacobsen, K.Mortensen, K.Pedersen and M.J.Thorup, *Solid State Commun.*, 1980, **33**, 1119.
6. A.F.Hebard, M.J.Rosseinsky, R.C.Haddon, D.W.Murphy, S.H.Glarum, T.T.M.Palstra, A.P.Ramirez and A.R.Kortan, *Nature.*, 1991, **350**, 600.
K.Holczer, O.Klein, S-H.Huang, R.B.Kaner, K.J.Fu, R.L.Whetten, F.Diederich, *Science.*, 1991, **252**, 1154.
7. K.Tanigaki, T.W.Ebbesen, S.Sato, J.Mizurki, J.S.Tsai, Y.Kubo, S.Kuroshima, *Nature.*, 1991, **352**, 222.
8. Z.Iqbal, R.H.Baughman, B.L.Ramakrishna, S.Khare, N.S.Murthy, H.J.Bornemann and D.E.Morris, *Science.*, 1991, **254**, 826.
9. P.P.Edwards and C.N.R.Rao, *Chem.in.Brit.*, 1994, **30**, 9, 722.
- 10.J.G.Bednorz and K.A.Müeller, *Z.Physik.*, 1986, **B64**, 189.
11. M.K.Wu, J.R.Ashburn, C.J.Torng, P.H.Hor, R.L.Meng, L.Gao, Z.J.Huang and C.W.Chu, *Phys.Rev.Lett.*, 1987, **58**, 908.
12. H.Maeda, Y.Tanaka, M.Fukutomi and T.Asano, *Jap.J.Phys.Lett.*, 1988, 27, **L209**.
13. Z.Z.Sheng, A.M.Hermann, A.El.Ali, L.Almasan, J.Estrada, T.Datta and R.J.Matsaun, *Phys.Rev.Lett.*, 1988, **60**, 937.
14. A.M.Schilling, J.D.Cantoni and H.R.Ott, *Nature.*, 1993, **363**, 56.

15. S.N.Putilin, E.V.Antipov, O.Chmaissem and M.Marezio, *Nature.*, 1993, **362**, 226 .
16. C.Michel, B.Raveau, *Rev.Chim.Miner.*, 1984, **21**, 407.
17. C.Greaves and P.R.Slater, *J.Mater.Chem.*, 1991, **1**, 17.
18. C.Greaves and P.R.Slater, *Physica C.*, 1991, **175**, 172.
19. C.Greaves, *Tc Newsletter.*, May 1993, 10, 3.
20. J.Bardeen, L.N.Cooper and J.R.Schrieffer, *Phys.Rev.*, 1957, **108**, 1175.
21. W.Meissner and R.Ochsenfeld, *Naturwissenschaften.*, 1933, **21**, 787.
22. B.D.Josephson, *Phys.Rev.Lett.*, 1962, **1**, 251.
23. S.T.Noge, T.Yamashita, Z.Wang, T.Matsui, H.Kurosara, H.Yamane and T.Hirai, *Jpn.J.Appl.Phys.*, Part 2, 1990, **28**, L1581.
24. T.Yamashita, M.Era, S.Noge, A.Irie, H.Yamane, T.Hirai, H.Kurosawa and T.Matsui, *Jpn.J.Appl.Phys.*, Part 1, 1990, **29**, 74.
25. W.Smith (Ed), *Tc Newsletter.*, Nov 1993, 1, 10.
26. National Committee for Superconductivity, Review, January 1991, 9.
27. S.Matsuno, F.Uchikawa and K.Yoshizaki, *Jpn.J.Appl.Phys.*, 1990, **29**, 6, L947.
28. K.Endo, H.Yamasaki, S.Misawa, S.Yoshida and K.Kajimura, *Physica C.*, 1991, **185**, 1949.
29. N.Hamagushi, R.Gardiner, P.S.Kirlin, R.Dye, K.M.Hubbard and R.E.Muenchausen, *Appl.Phys.Lett.*, 1990, **57**, 2136.
30. National Committee for Superconductivity, Review, January 1991, 15.
31. W.Smith, (Ed) *Tc Newsletter.*, Jan 1992, 1.
32. Similar to ref 30, p9.
33. Similar to ref 30, p67.
34. A.D.Berry, D.K.Gaskill, R.T.Holm, E.J.Cukauskas, R.Kaplan and R.L.Henry, *Appl.Phys.Lett.*, 1988, **52**, 1743.
35. B.N.Hansen, B.M.Hybertson, R.M.Barkley and R.E.Sievers, *Chem Mater.*, 1992, **4**, 749.

36. T.Nakamori, H.Ake, T.Kanamori and S.Shibata, *Jpn.J.Appl.Phys.*, 1988, **27**, PL1265.
37. P.S.Kirlin, R.Binder, R.Gardiner and D.W.Brown, SPIE processing of films for high Tc superconducting electronics., 1989, **115**, 1187.
38. G.Malandrino, D.S.Richeson, T.J.Marks, D.C.Degroot, J.L.Schindler and C.R.Kannewurf, *Appl.Phys.Lett.*, 1991, **58**, 182.
39. J.M.Zhang, B.M.Wessels, D.S.Richeson, T.J.Marks, D.C.Degroot and C.R.Kannewurf, *J.Appl.Phys.*, 1991, **69**, 2743.

CHAPTER 2

A REVIEW OF ALL POTENTIAL VOLATILE

BARIUM COMPOUNDS

CHAPTER 2

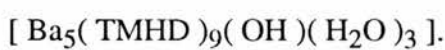
2.1. Introduction

Until recently, the chemistry of barium and its compounds has attracted little research interest. However, in the light of the development of new ferroelectric (BaTiO_3)¹ and high temperature superconducting ceramic films based on $\text{YBa}_2\text{Cu}_3\text{O}_{7-x}$ ², $\text{Bi}_2\text{Sr}_2\text{Ca}_2\text{Cu}_3\text{O}_{10-x}$ ³ and $\text{HgBa}_2\text{Ca}_2\text{Cu}_3\text{O}_8$ ⁴, an era of intense activity has ensued around the largely undeveloped area of barium chemistry and its heavy group IIA metal counterparts. Several techniques have been adopted for the deposition of these ceramic films onto substrates using laser ablation, sputtering, supercritical fluid techniques and sol-gel processes. With the exception of laser ablation, these deposition methods produce poor quality superconducting films. For large area deposition of thin films, CVD (Chemical Vapour Deposition) is ideal. This requires a volatile metal precursor to sublime into the vapour phase at a temperature of around 200°C or less. At higher temperatures the vapour phase barium compound decomposes to the corresponding oxide. Thin films of $\text{YBa}_2\text{Cu}_3\text{O}_{7-x}$ can be obtained from 3 separate precursors. With barium, several precursors have been investigated for their sublimation properties. Unfortunately, sublimation of these barium precursors is normally accompanied by decomposition. This section summarises recent research aimed at producing stable and volatile barium complexes. This chapter is divided into 7 major sub sections which cover the chemistry of barium complexes of β -diketonates and β -ketoiminates, alkoxides and siloxides, silyl amides and their related compounds, organobarium complexes and the chemistry of barium carboxylates. As a consequence of their impressive stability and volatility, barium β -diketonates have been extensively studied. This particular area has been covered by recent reviews by Sievers⁵ and Rees⁶.

2.2. BARIUM β -DIKETONATES

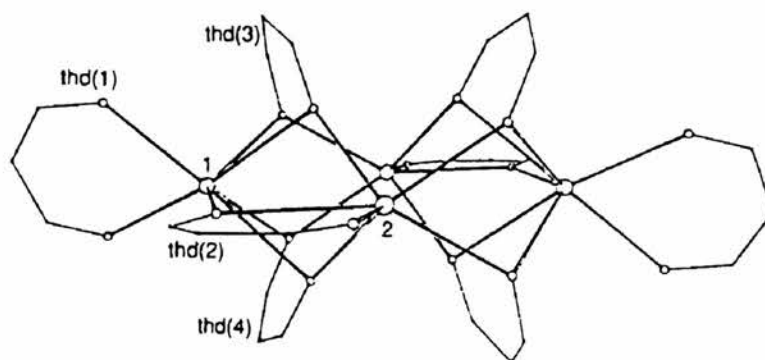
2.2.1. Non-fluorinated barium β -diketonate complexes

Several non-fluorinated barium β -diketonate complexes have been produced and analysed by X-ray, thermal and spectroscopic studies. One of the best precursors for barium oxide film formation of $\text{YBa}_2\text{Cu}_3\text{O}_{7-x}$, is "[Ba(TMHD)₂]" which has been produced by several workers⁷⁻¹⁵. "[Ba(TMHD)₂]" is not formed by normal aqueous routes, but rather by anhydrous methods using barium metal and the ligand HTMHD. The barium complex which is isolated from the anhydrous route is present in the solid state as a tetramer - [Ba₄(TMHD)₈]¹⁶⁻¹⁹. The β -diketonate complex produced by the aqueous method exists as a oxo-hydroxyl β -diketonate^{20,21} -



Glizes¹⁶ first isolated orthorhombic crystals of [Ba₄(TMHD)₈] by the sublimation of [Ba(TMHD)₂.CH₃OH]. The crystal structure shows an arrangement of centrosymmetric cyclic tetramers which contained 4 barium atoms in a rhombus which are 7 coordinate with bridging β -diketonate ligands. Volatile oligomeric species - [Ba₂TMHD₃]⁺ and [Ba₃TMHD₅]⁺ are detected in the EI mass spectrum of [Ba₄(TMHD)₈] which seems to indicate that the β -diketonate complex is oligomeric in the solid as well as the gas state. Drozdov¹⁸ obtained triclinic crystals of [Ba₄(TMHD)₈] by reacting barium metal with HTMHD in pentane. A crystal structure is shown in Fig.2.2.1.a

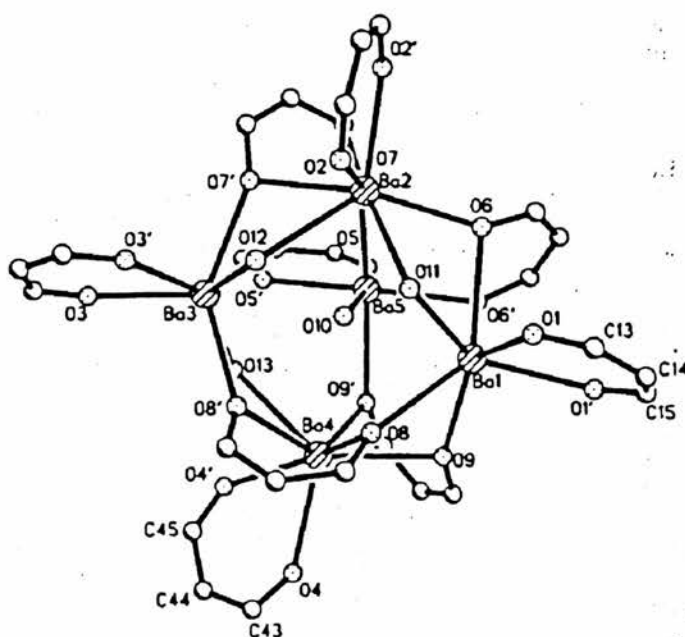
Fig. 2.2.1.a



According to Drake¹⁹, $[\text{Ba}_4(\text{TMHD})_8]$ sublimes intact with virtually no decomposition between 190-210°C / 10^{-3} Torr. Interestingly, the melting point of the anhydrous β -diketonate is at a higher temperature than that of the hydrated form of $[\text{Ba}_5(\text{TMHD})_9(\text{OH})(\text{H}_2\text{O})_3]$ - m.p = 171-172°C, $\text{Ba}_4[\text{TMHD}]_8$ - m.p = 194-197°C. STA thermal analysis shows volatilisation occurring between 260-410°C with 10% weight residue. This is in contrast with other workers who found their % weight residue much higher for the $[\text{Ba}_5(\text{TMHD})_9(\text{OH})(\text{H}_2\text{O})_3]$. The reason for this discrepancy is due to the method of preparing and storing of the barium β -diketonate. The reduction in % weight residue remaining was attributed to the absence of intermolecular interactions which are present in the hydrated form of $[\text{Ba}_5(\text{TMHD})_9(\text{OH})(\text{H}_2\text{O})_3]$.

The oxo-hydroxyl species of the barium β -diketonate - $[\text{Ba}_5(\text{TMHD})_9(\text{OH})(\text{H}_2\text{O})_3]$ was isolated by Sievers^{20,21}. The penta-barium cluster was produced by reacting barium hydroxide octahydrate with HTMHD, similar to the procedure described by Hammond⁷. Single crystals of $[\text{Ba}_5(\text{TMHD})_9(\text{OH})(\text{H}_2\text{O})_3]$ were grown in warm pentane. The X-ray crystal structure is shown below. In the negative ion EI mass spectrum of $[\text{Ba}_5(\text{TMHD})_9(\text{OH})(\text{H}_2\text{O})_3]$, $[\text{Ba}_5(\text{TMHD})_9(\text{OH})]^-$ was observed in the mass spectrum. This indicates that the barium complex is pentanuclear in the solid, as well as, the gas phase.

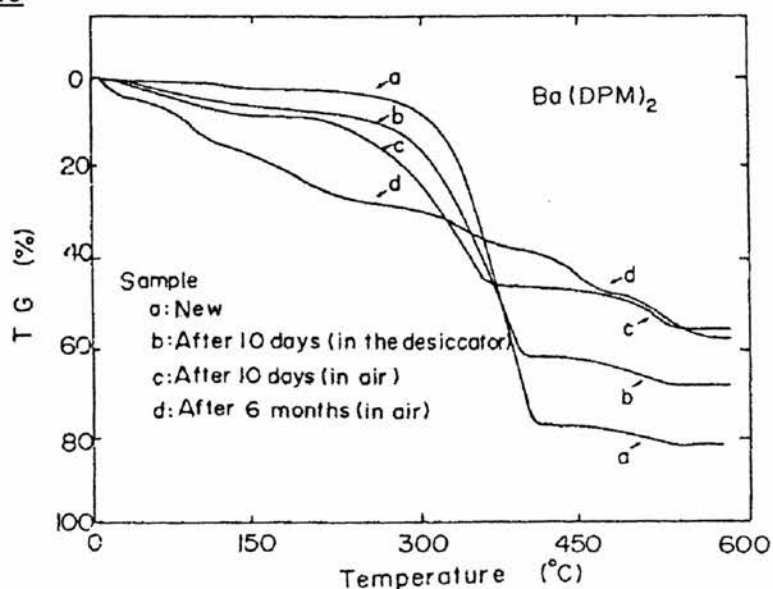
Fig 2.2.1.b



Although, the precursor $[Ba_5(TMHD)_9(OH)(H_2O)_3]$ is volatile, the precursor also suffers from decomposition whilst volatilising. This creates a difference in vapour pressure in the CVD reactor and consequently can affect the stoichiometry of $YBa_2Cu_3O_{7-x}$ superconducting film. It also precludes the repeated use of a single sample of precursor.

It is apparent from several studies that $[Ba_5(TMHD)_9(OH)(H_2O)_3]$ and $[Ba_4(TMHD)_8]$ also undergo slow decomposition^{22,23}. It appears that this decomposition is accelerated by air (CO_2)²⁴, moisture²⁴ and light²⁵. STA experiments conducted by Sato²⁴ found that a freshly prepared sample of "[Ba(TMHD)₂]" had a % weight residue of 14% after heating to 600°C. In contrast the same sample that was exposed to air for six months was found to have a 35% weight residue. Drozdov¹⁷ also noticed a similar phenomenon with "[Ba(TMHD)₂]". This is shown in the thermogram below, Fig 2.2.1.c.

Fig.2.2.1.c

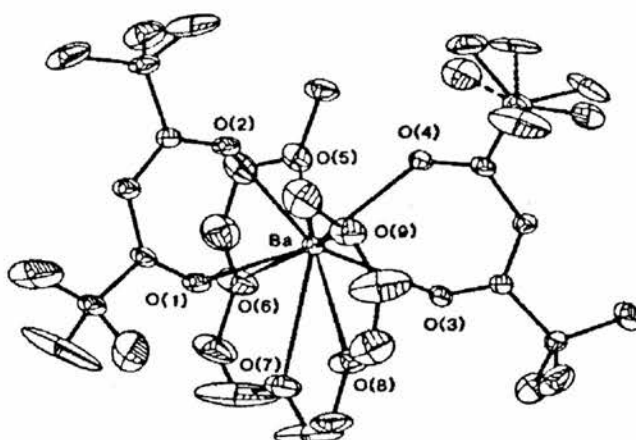


2.2.2. Non-fluorinated polyether barium β -diketonate complexes

A notable feature of barium is its strong Lewis acidity, which ensures in the absence of Lewis based solvents, a polymeric network would assemble once a barium β -diketonate complex had formed. The molecular architecture of these complexes can therefore be altered by adding polydentate Lewis bases, such as polyglymes, crown ethers, and polydentate amines. This causes the saturation of the barium centre by filling in the vacant coordination sites. An ability to maximise barium's coordination number (10-12) would effectively produce a monomeric, volatile complex. This phenomenon was demonstrated by Thompson²⁶, Gardiner²⁷, Drozdov¹⁷ and Drake²⁸, who synthesised a volatile polyether barium β -diketonate complex.

[Ba(TMHD)₂.tetraglyme] was produced from the reaction between HTMHD, tetraglyme and a hydrocarbon soluble barium ethoxide [Ba(OEt)₂(EtOH)₄] or from the reaction of [Ba₅(TMHD)₉(OH)(H₂O)₃] and tetraglyme in a toluene solvent. [Ba(TMHD)₂.tetraglyme] is a volatile monomeric complex which sublimes between 320-410°C at 1 atm under STA conditions. It was noticed that the tetraglyme adduct had obtained a greater volatility and stability over the tetraglyme free hydrated compound - [Ba₅(TMHD)₉(OH)(H₂O)]. Thermal studies demonstrate that [Ba(TMHD)₂.tetraglyme] dissociates the tetraglyme ligand at 98°C prior to sublimation of [Ba(TMHD)₂]_n under STA conditions. The corresponding sublimation results in either 6% or 4% weight residue^{28,29}. This difference in weight residue may be due to carbanaceous impurities in Drakes compound. The reason that the tetraglyme dissociates prior to sublimation is due to relatively weak coordination of the tetraglyme to the barium centre which is rendered electron rich as a part of the electron donating ^tbutyl groups of β-diketonate ligand. The X-ray crystal structure was deduced by Drake and coworkers²⁸, showing a 9 coordinate monomeric crystalline solid. The 5 oxygen atoms in the tetraglyme ligand are essentially coplanar and bisect the plane of the 2 β-diketonate ligands which lie above and below the plane of the tetraglyme. The β-diketonate moieties bond symmetrically with the metal centre. However, as a result of the steric bulk of the ^tbutyl group, the β-diketonate ligands deviate from being coplanar by 22.9°. A similar structural characteristic is noticed in the crystal structure of Ba[TDFND]₂.tetraglyme in which the β-diketonate ligands deviate from being coplanar by 26° (see chapter 5)³⁰.

Fig.2.2.2.a

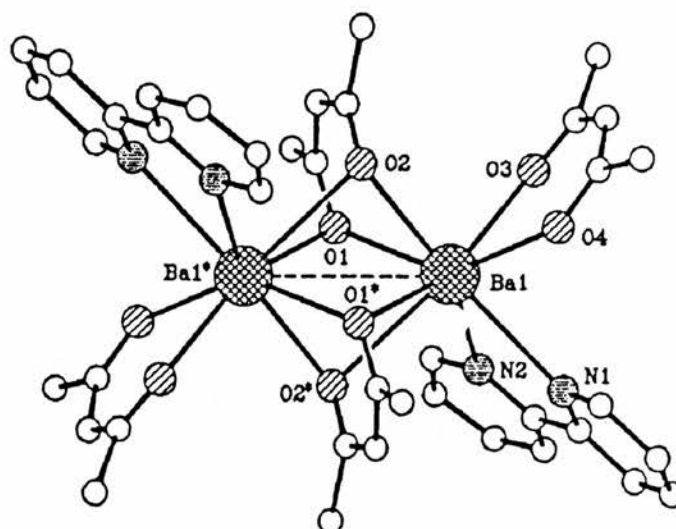


Cook³¹, Okazaki³² and Timmer³³ also reported on the volatility of the 18-crown-6 ether complex of $[Ba(TMHD)_2]$. It appears again that the polydentate ligand dissociates from the complex before sublimation. $[Ba(TMHD)_2 \cdot 18\text{-crown-6}]$ melts at 155°C ³¹, $\{ [Ba(TMHD)_2 \cdot 18\text{-crown-6} \cdot 0.5\text{H}_2\text{O}] \}$ melts at $130\text{-}135^\circ\text{C}$ ³³ which is higher than the tetraglyme complex at 103°C (STA). Indeed, $[Ba(TMHD)_2 \cdot 18\text{-crown-6}]$ complex also has a lower volatility than the tetraglyme complex which may be as a result of crystal packing. Timmer did not observe sublimation, probably because the conditions to see sublimation were not obtained. Interestingly, Norman and co workers³⁴ attempted to synthesise $[Ba(acac)_2 \cdot 18\text{-crown-6}]$ and $[Ba(TMHD)_2 \cdot 18\text{-crown-6}]$. However, these compounds were never isolated.

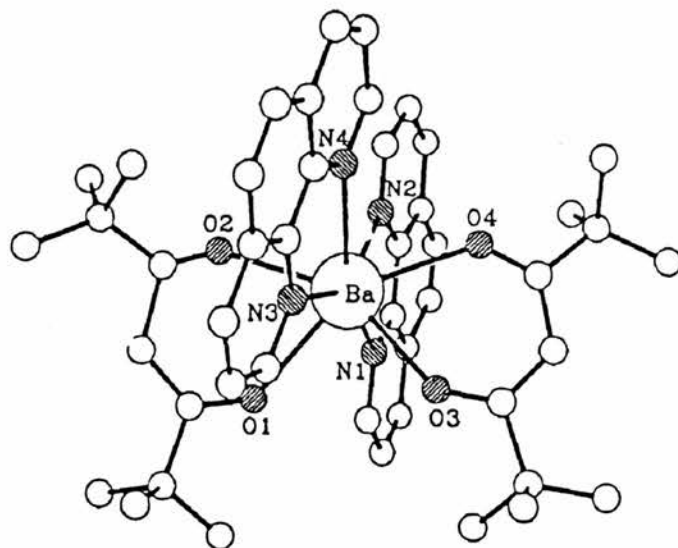
A number of nitrogen lewis donor molecules were complexed to $[Ba_5(TMHD)_9(OH)(H_2O)_3]$ in the search for enhanced volatilisation without the dissociation of the Lewis base. Rees³⁵, attempted to isolate a nitrogen Lewis base adduct of $[Ba_5(TMHD)_9(OH)(H_2O)_3]$ in the solid state - $[Ba_2(TMHD)_4 \cdot (NH_3)_4]$. The ammonia adduct was synthesised and then characterised by thermal and crystallographic studies. It has a lower volatility [sublimates at $213\text{-}224^\circ\text{C} / 5 \times 10^{-4} \text{ mmHg}$ for 2hrs] than the Lewis base free compound leaving a large %Wt residue of 16% when studied by STA.

The search for this kind of adduct was driven by the observations made by Barron³⁶ who saturated the carrier gas stream with ammonia gas and other amines whilst subliming $[Ba_5(TMHD)_9(OH)(H_2O)_3]$. Enhanced volatility of $[Ba_5(TMHD)_9(OH)(H_2O)_3]$ was obtained through this method with a range of N-donors. Depending on the amine used, $[Ba_5(TMHD)_9(OH)(H_2O)_3]$ could become volatile at temperatures as low as 130°C using triethylamine vapour in the carrier gas stream. This strongly suggests that the ammonia gas is used as a mass transport agent which forms donor adducts in the gas phase. (Several other workers noticed that injecting donor base solvents such as, tetraglyme³⁷, THF^{38,39}, HTMHD⁴⁰ or H_2O ⁴¹ into the carrier gas stream also enhanced the volatility or / and stability of $[Ba_5(TMHD)_9(OH)(H_2O)_3]$).

Other nitrogen Lewis base adducts of $[Ba_5(TMHD)_9(OH)(H_2O)_3]$ have also been produced with either bipyridyl⁴² or 1,10-phenanthroline^{43,44}. These adducts have both been characterised by thermal and X-ray analysis. The X-ray crystal structure of $[Ba_2(TMHD)_4(bipy)_2]$ shows a highly symmetrical dimer. It appears that the bipyridyl ligand breaks down the oligomerisation which is present in the tetrameric structure of $[Ba_4(TMHD)_8]$. Under STA conditions the nitrogen Lewis base is shown to dissociate from the complex prior to sublimation. In the case of $[Ba_2(TMHD)_4(bipy)_2]$ the loss of bipyridyl occurs between 80-90°C and is followed by the sublimation of $Ba_4(TMHD)_8$.

Fig.2.2.2.b

The 1,10-phenanthroline adduct was also investigated by X-ray and thermal analysis. By comparison the 1,10-phenanthroline adduct of $[Ba_5(TMHD)_9(OH)(H_2O)_3]$ - $[Ba(TMHD)_2(Phen)]$ is an 8 coordinate, monomeric complex. The compound dissociates to the free base prior to sublimation of $[Ba_4(TMHD)_8]$ at $200^\circ C / 0.01 Torr$.

Fig.2.2.2.c

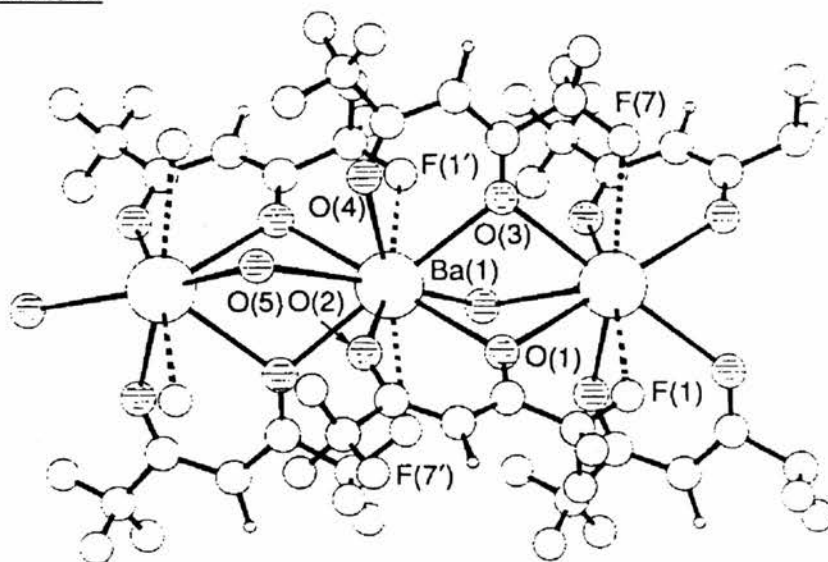
2.2.3. Fluorinated barium β -diketonates

Without fluorination intermolecular hydrogen bonding can occur within the barium β -diketonate complex, thus, leading to oligomerisation and decreased volatility.

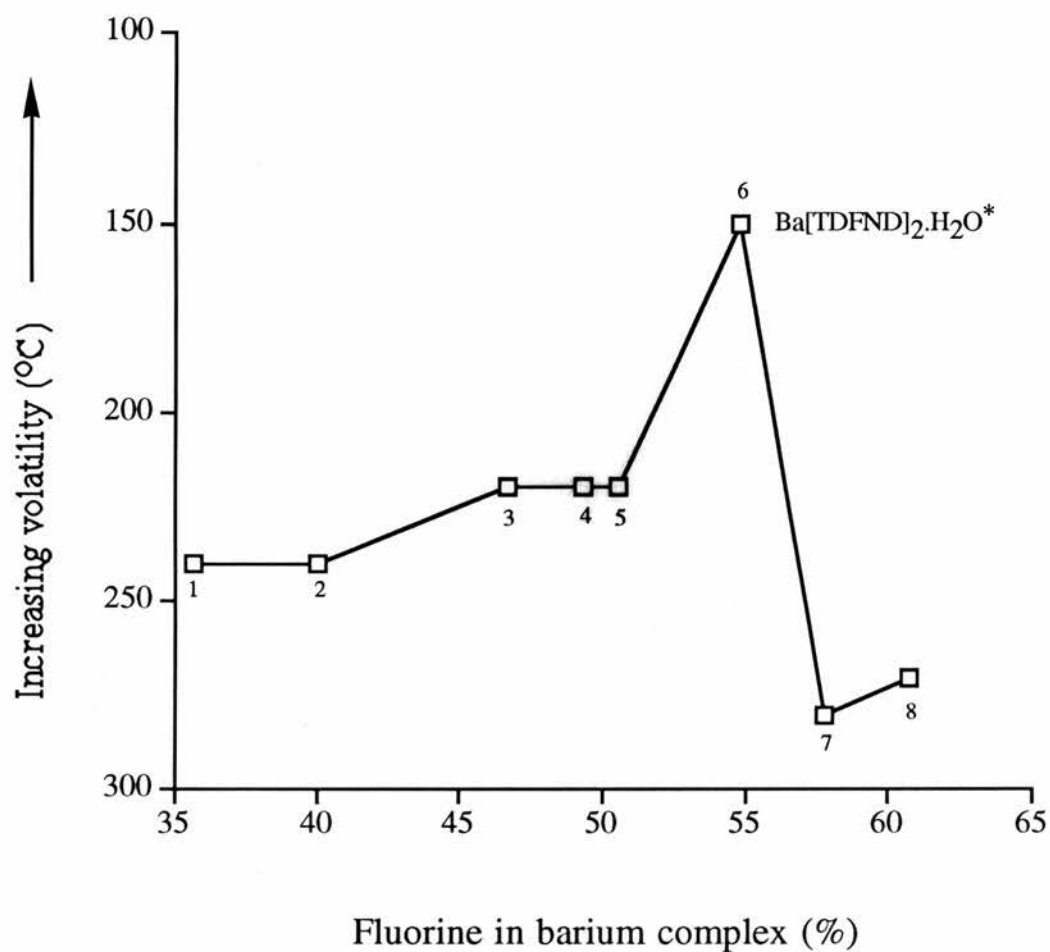
Replacing the hydrogen atom with a highly electronegative atom, such as fluorine, seems to lower the van der Waals interactions leading to a decrease in the oligomerisation and hence, an increase in volatility.

The anhydrous form of [Ba(HFA)₂] was prepared by Purdy et al⁴⁵, by the reaction between barium chips and the free β -diketone. The anhydrous form is soluble in THF and ether suggesting that monomeric adducts may form with these coordinating solvents. Again, as with [Ba(TDFND)₂.H₂O] polymeric fragments are observed in the EI mass spectrum for [Ba(HFA)₂]. The presence of [Ba₂(HFA)F₂⁺], [Ba₂(HFA)₂F⁺] and [Ba₂(HFA)₃⁺], also suggests that [Ba(HFA)₂] must exist at least as dimers in the gas phase. The hydrated form of [Ba(HFA)₂] sublimes at 205-220°C / 10⁻⁵ mmHg, with simultaneous decomposition. STA studies conducted at 1 atm illustrate that the compound sublimes between 240-255°C. The X-ray crystal structure of the hydrated form shows infinite polymeric chains with bridging HFA and H₂O ligands⁴⁶. The presence of C-F-Ba bridges is also observed (Ba-F 2.92-2.97Å) with the barium atom being 10 coordinate.

Fig.2.2.3.a



Thompson et al²⁶ synthesised a series of volatile perfluorinated β -diketonates for Ba, Sr, Ca, Y and Cu^{47,8}. The ligand systems which they examined were TDFND ($R=R'=C_3F_7$) and DFHD ($R=CF_3$, $R'=C_3F_7$). The hydrated barium complex of TDFND melts at 187°C and volatilises under STA conditions at 150°C, 200°C. (It appears that volatilisation takes place in two stages). After the initial loss of water the complex sublimes intact at 1 atm without any weight residue. Surprisingly, the anhydrous form, has a lower volatility and a higher melting point at 196°C than the hydrated form. The anhydrous form can be prepared by either dehydrating the hydrated form⁴⁸ or by preparing the anhydrous complex in the absence of moisture⁴⁷. The volatility of $[Ba(TDFND)_2 \cdot H_2O]$ is also observed in the FAB or EI mass spectra, which detects molecular fragments containing up to 4 Ba atoms - $[Ba_4F_4(TDFND)]^+$, suggesting that the molecule sublimes at least partially as tetramers⁴⁹. In a methanol solution, molecular weight studies on the barium complex seem to indicate that the complex is monomeric and that coordinating solvents may breakdown the polymeric structure. A range of other fluorinated β -diketonate complexes of barium have been synthesised and their volatilities examined. A plot of sublimation temperature against % fluorine of these particular complexes are shown in Fig 2.2.3.b.

Fig 2.2.3.b.The volatility of perfluorinated barium β -diketonates

Barium complex	Ref	Barium complex	Ref
1. $[\text{Ba}(\text{HFOD})_2 \cdot \text{H}_2\text{O}]$	50	5. $[\text{Ba}(\text{OFHD})_2]$	51
2. $[\text{Ba}(\text{HFA})_2 \cdot \text{H}_2\text{O}]$	45	6. $[\text{Ba}(\text{TDFND})_2 \cdot \text{H}_2\text{O}]$	50
3. $[\text{Ba}(\text{DFHD})_2]$	51	7. $[\text{Ba}(\text{HDFDD})_2]$	47
4. $[\text{Ba}(\text{DFHD})_2 \cdot \text{H}_2\text{O}]$	50	8. $[\text{Ba}(\text{EF3D})_2]$	47

All sublimation temperatures are quoted at 1 atm using STA conditions (with the only exception being [Ba(HFA)₂H₂O] which was sublimed at CVD conditions at 1 atm). The heating rate of the STA for the barium complexes [Ba(TDFND)₂.H₂O], [Ba(DFHD)₂.H₂O], [Ba(EF3D)₂], [Ba(HDFDD)₂] was at 20° / min. This is compared with a heating rate of 10° / min for the barium complexes [Ba(DFHD)₂] and [Ba(OFHD)₂], respectively.

For compounds (1-6), the level of volatility increases with the level of fluorination in the β-diketonate. In optimising, the volatility of the barium β-diketonate, it is apparent that the greatest volatility is achieved for [Ba(TDFND)₂.H₂O] where R=R'= C₃F₇. By increasing the level of fluorination beyond 55% there seems to be a decrease in the volatility and an increase in the chance of decomposition within the complex.

Sugawara and Sato⁵² developed a series of volatile perfluorinated barium precursors, the most volatile being [Ba(HFDD)₂] where R=C₃F₇, R'=C₄F₉. Under plasma enhanced CVD conditions [Ba(HFDD)₂] volatilised at 157°C at 1 Torr. This volatilising temperature is lower than [Ba(TDFND)₂] which sublimed at 175°C at 1 Torr, but as the data was given at 1Torr, it was not possible to correlate this sublimation temperature to the graph in Fig 2.2.3.b (In Fig 2.2.3.b, all temperatures are quoted at 1 atm). This observation seems to support suggestions that the longer the perfluorinated chain the greater the volatility. This may be attributed to the lower van der Waal's interactions or as a consequence of crystal packing.

With all the perfluorinated β-diketonates studied so far there has been evidence either from X-ray, thermal or mass spectroscopic studies to show that these barium compounds exist as polymeric species. [Ba(HFOD)₂.2H₂O] is no exception.

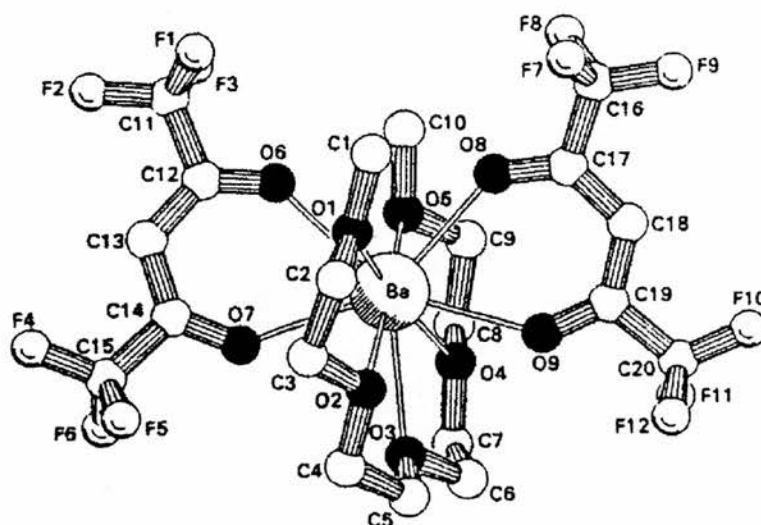
Belcher et al⁵³ undertook a series of thermal investigations using mass spectroscopic, STA, and sublimation studies on a series of perfluorinated β-diketonates ([Ba(DTFHD)₂.2H₂O] R=^tBu, R'=CF₃; [Ba(DPFHD)₂.2H₂O] R=^tBu, R'=CF₃CF₂ and [Ba(HFOD)₂.2H₂O] R=^tBu, R'=C₃F₇).

These particular compounds were sublimed between 190-220°C at 0.1 Torr. STA studies concluded that [Ba(HFOD)₂.H₂O] gave the greatest volatility around 300°C at 1 atm and the % weight residue was less than 5%. Sublimation accompanies decomposition in this particular complex. Higher % residues (9.0%wt residue) were obtained by Thompson et al⁸ who also observed a melting point of 175°C. However, this difference in % weight residue is probably due to some impurity, such as barium bromide which has not decomposed. This is indicated by an endotherm in the STA analysis of [Ba(HFOD)₂.H₂O] at around 920°C which probably corresponds to the BaBr₂ melt.

2.2.4. Polyether adducts perfluorinated barium β-diketonate

Similar to the non-fluorinated tetraglyme adducts of barium β-diketonates, the fluorinated analogues are more thermally stable and more volatile than the tetraglyme free compounds. For example, [Ba(HFA)₂.tetraglyme] sublimes at 150°C / 0.03 Torr⁵⁴ compared to [Ba(HFA)₂.H₂O] which sublimes at 240°C / 1 atm. As with most tetraglyme adducts of barium β-diketonates, the tetraglyme ligand lies between the plane of the two β-diketonate ligands. [Ba(HFA)₂.tetraglyme] is no exception, with the tetraglyme ligand saturating the coordination sites on the barium centre, resulting in a 9 coordinate, monomeric solid⁵⁵.

Fig.2.2.4.a



It is interesting to note that $[\text{Ba}(\text{HFA})_2 \cdot \text{tetraglyme}]$ also seems to possess a higher thermal volatility and thermal stability than $[\text{Ba}(\text{TMHD})_2 \cdot \text{tetraglyme}]$. Under STA conditions, $[\text{Ba}(\text{HFA})_2 \cdot \text{tetraglyme}]$ sublimes at 125°C and decomposes at around 275°C . This is compared to $[\text{Ba}(\text{TMHD})_2 \cdot \text{tetraglyme}]$ which dissociates the tetraglyme ligand at 98°C and volatilises the readily formed $[\{ \text{Ba}(\text{TMHD})_2 \}_n]$ at 320°C . The higher thermal stability and volatility of $[\text{Ba}(\text{HFA})_2 \cdot \text{tetraglyme}]$ seems to be as a result of the stronger electron withdrawing groups on the β -substituents of the β -diketonate moiety. To compensate for the flow of electron density away from the barium centre (caused by the strongly electron withdrawing groups - CF_3), the tetraglyme ligand pushes electron density towards the barium centre resulting in the tetraglyme ligand being more strongly bound to the barium centre. Thus, dissociation of the tetraglyme might not take place under STA conditions.

As previously described, $[\text{Ba}(\text{TMHD})_2 \cdot \text{tetraglyme}]$ does dissociate the tetraglyme ligand prior to sublimation which leads to premature decomposition.

The highest volatility ever achieved by a barium compound is $[\text{Ba}(\text{TDFND})_2 \cdot \text{tetraglyme}]^{30}$. This will be discussed in detail in chapter 5. It volatilises at 160°C (under STA conditions) and melts at 70°C .

Interestingly, the hexaglyme analog - [Ba(TDFND)₂.hexaglyme] melts at 40°C⁵⁶, although no other thermal details have been published.

However, for the tetraglyme adducts of higher perfluorinated β-diketonates such a relationship between the electron withdrawing effects of the β substituents and the higher volatility and stability breaks down. Apparently for the barium complexes - [Ba(HDFDD)₂.tetraglyme] and [Ba(EF3D)₂.tetraglyme], the tetraglyme dissociates in advance of sublimation which leaves a residue due to some decomposition. As suggested with the polyether free perfluorinated β-diketonates, there must be a limit of fluorination which can be incorporated into the β-diketonate complex before a higher molecular mass results in partial decomposition of the complex.

Timmer³³, Norman³⁴ and Thompson⁴⁷ have all synthesised the 18-crown-6 adducts of perfluorinated barium β-diketonates. [Ba(TFA)₂] and [Ba(HFA)₂] adducts of 18-crown-6 ether were prepared by Timmer in which in both cases the volatility of the barium compounds did not match up to the tetraglyme compounds. The former compound volatilised at 150-170°C / 0.01- 0.5 mmHg with extensive decomposition and [Ba(HFA)₂.18-crown-6] volatilised at 165°C / 0.03 mmHg.

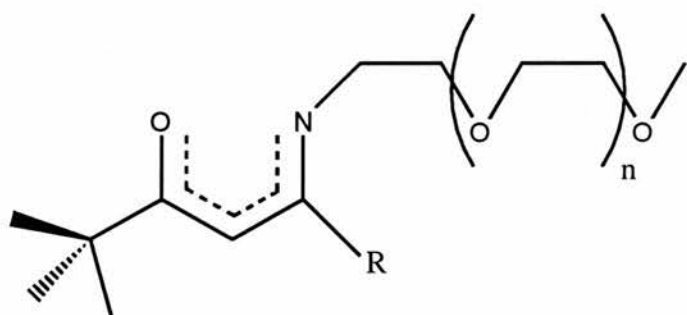
[Ba(HFA)₂.18-crown-6] is a ten coordinate, volatile, monomeric solid.

Interestingly, the 18-crown-6 ether adduct of [Ba(TDFND)₂] was also found to have a lower volatility and lower thermal stability than the tetraglyme complex. Thompson et al⁴⁷, found that [Ba(TDFND)₂.18-crown-6] melted at 165°C and volatilised between 210-340°C leaving a moderate residue.

2.3. BARIUM β -KETOIMINATE COMPLEXES

Initial studies by Rees⁵⁷ and Nash²⁹ (see Chapter 3) into designing and synthesising molecular bound polyether appendages onto β -diketonate functionalities gave involatile barium compounds which were polymeric in the solid state. However, in solution the molecular aggregates disassemble in the presence of coordination solvents to give what may appear to be monomeric species. Building on this molecular strategy of minimising molecular oligomerisation, and hence to produce smaller lattice cohesive energies, Marks and co workers^{58,59} made a series of barium β -ketoiminates which could be sublimed with some decomposition. These compounds were found to be air sensitive, as in the case of Nash and Rees, and were found to decompose to their corresponding ligand. [Ba(diki)₂] and [Ba(triki)₂] were found to be volatile, 8 coordinate solids.

Fig 2.3.a.



Where R = Me₃
 [Ba(miki)₂] = n = 0
 [Ba(diki)₂] = n = 1
 [Ba(triki)₂] = n = 2

Where R = ^tBu
 [Ba(dpmiki)₂] = n = 0
 [Ba(dpdiki)₂] = n = 1
 [Ba(dpatriki)₂] = n = 2

They were produced by the direct synthesis from BaH₂ and the ligand to produce the corresponding barium complex. Bis [5-(2'-methoxyethoxyethyl) imino-2,2-dimethyl-3-hexaneato] barium (II), [Ba(diki)₂] and bis [5-(2'-methoxybisethoxyethyl) imino-2,2-dimethyl-3-hexaneato] barium (II), [Ba(triki)₂] sublime between 80-120°C.

The major ion in the EI mass spectrum in both complexes $[Ba(diki)_2]$ and $[Ba(triki)_2]$ is BaL^+ which is also accompanied by the observation of polymeric fragments (where $L = triki$ or $diki$). The N-derivation offers an appendage point for additional intramolecular coordination and saturation of the Ba^{2+} ion. From the STA analysis, the coordinated compounds shown in Fig 2.3.b. demonstrate a lower volatility than

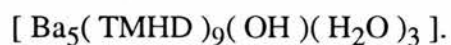


Fig 2.3.b.

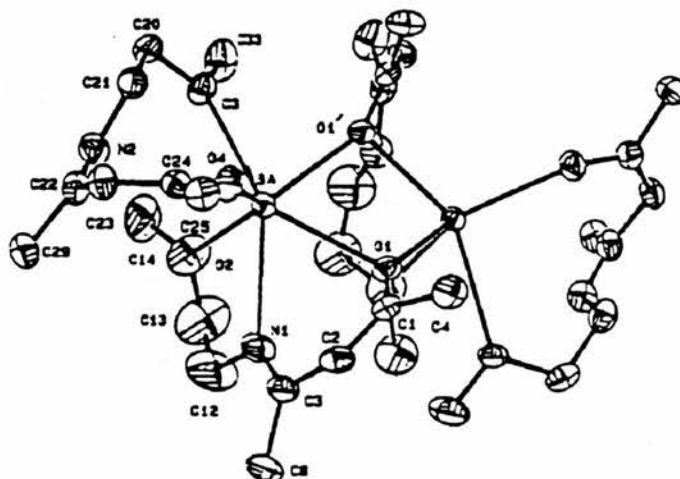
Barium complex	% Residue after STA	M.P. / °C
$[Ba(Miki)_2]$	39	138-40
$[Ba(Diki)_2]$	39	170-1
$[Ba(Triki)_2]$	29	80-2
$[Ba(Dpmiki)_2]$	33	165-8
$[Ba(Dpdiki)_2]$	26	137-9
$[Ba(Dptriki)_2]$	23	127-8

It is interesting to note that $[Ba(miki)_2]$ and $[Ba(dpmiki)_2]$ are isolated as six coordinate dimeric barium compounds, in contrast to, $[Ba(diki)_2]$ and $[Ba(triki)_2]$ which are 8 coordinate monomeric solids.

The crystal structure of $[\text{Ba}(\text{dpmiki})_2]_2$ shows two symmetrically equivalent - O(ketoiminate) atoms with both barium atoms being six coordinate.

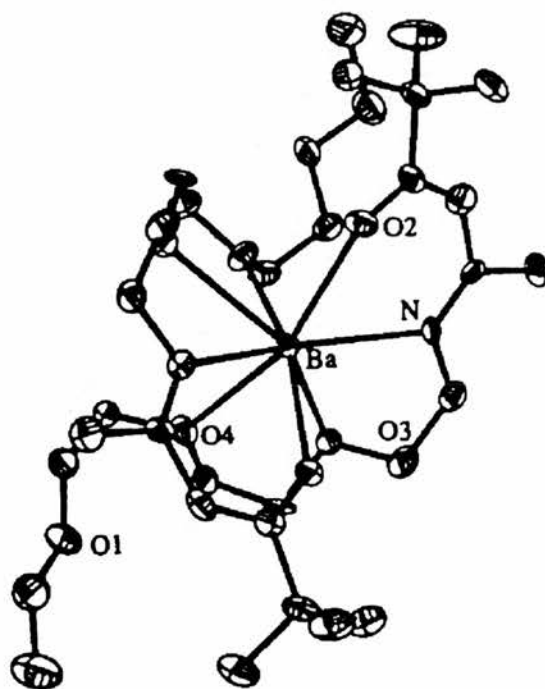
$[\text{Ba}(\text{dpmiki})_2]_2$ is shown in Fig 2.3.c.

Fig.2.3.c.



$[\text{Ba}(\text{triki})_2]$ is a 8 coordinate, monomeric solid with the terminal lariat ether oxygen atoms uncoordinated. The compound, $[\text{Ba}(\text{triki})_2]$ is shown in Fig 2.3.d.

Fig. 2.3.d.



[Ba(triki)₂] have been utilised to grow BaPbO₃ films. However, residual BaO has been a contaminant in the resulting dielectric film.

Other ketoimines have also been produced. In particular, Mazurenko⁶⁰ developed a series of H₂O, DMF and DMSO adducts of [Ba(NAA)₂] where NAA is 4-iminopentan-2-one. Sublimation of the DMSO and DMF adducts occurred between 210-250°C under STA conditions. Decomposition to barium carbonate took place at temperatures greater than 300°C, a 7% weight residue was left after some decomposition. Volatile copper(II) non perfluorinated and fluorinated β-ketoimines have been synthesised by Norman^{61,62}. However, the corresponding barium compounds have not been produced.

2.4. BARIUM ALKOXIDES AND SILOXIDES

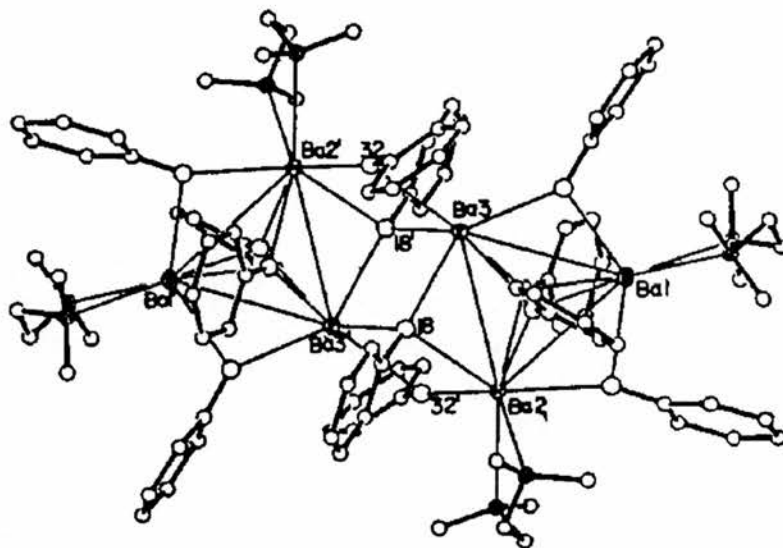
2.4.1. Barium monodentate, monofunctional alcoholates

The first barium alkoxides to be prepared were simple alkoxides $[Ba(OR)_2 (R=Me,Et)]^{63,64}$ where the complexes possessed low solubility and volatility. These solid alkaline earth methoxides and ethoxides were shown to be polymeric with a CdI_2 structure (powder X-ray diffraction). Mazdiasni⁶⁵ also prepared barium isopropoxide, but found this had a limited solubility and volatility. In an attempt to increase the volatility, a range sterically hindered barium alkoxides were synthesised. The barium alkoxides $[Ba(OEt)_2]$, $[Ba(OCMeEtPr)_2]$, $[Ba(OCMe_3)_2]$, $[Ba(OCH(CMe_3)_2)_2]$, $[Ba(HFIP)_2]$ and $[Ba(PFTB)_2]$ were all found to sublime between $230-280^\circ C < 10^{-5}$ Torr⁶⁶. However, some notable decomposition accompanied sublimation. These compounds were insoluble in saturated hydrocarbons but soluble in THF. Oxo free barium tert-butoxide complexes have been isolated by Purdy⁶⁶ and Borup⁶⁷. STA studies undertaken by Borup show that the complex, $[Ba(OBu^t)_2(tBuOH)_4]$, decomposes with the loss of free butanol at $20^\circ C$ and $100^\circ C$. Further heating causes the complex to decompose to BaO and $BaCO_3$ after $360^\circ C$. This result is very interesting as a similar compound produced by Purdy⁶⁶ sublimes at $270^\circ C$ but decomposes rapidly at $320^\circ C$. Borup also examined the X-ray crystal structure of $[Ba(OBu^t)_2(tBuOH)_4]$ in which a distorted Ba_4O_4 tetranuclear cube was found at its centre.

In an similar attempt to obtain barium t-butoxide, Caulton synthesised a multinuclear hydrido oxo barium alkoxide - $[H_3Ba_6(O)(OBu^t)_{11}(OEt_2CH_2O)(THF)_3]^{68}$ Thermal studies on this particular multinuclear hydrido oxo barium alkoxide - $[H_3Ba_6(O)(OBu^t)_{11}(OEt_2CH_2O)(THF)_3]$ showed that it was involatile.

In fact, the formation of all oxo barium alkoxides results in involatile complexes (a list of some other oxo alkoxides species that have been produced are shown Fig.2.4.1.b). To demonstrate that homoleptic barium phenoxides can be produced without the presence of oxo or hydrido species, Caulton and co workers⁶⁹ complexed Ba metal to phenol in the presence of toluene and TMEDA to produce a hexanuclear aggregate $[\text{Ba}_6(\text{OPh})_{12}(\text{TMEDA})_4 \cdot \text{C}_7\text{H}_8]$ which melts at 96-99°C. The structure consists of 2 linked $\text{Ba}_3(\text{OPh})_6(\text{TMEDA})_2$ units which result in 6 and 7 coordinate barium atoms. This centrosymmetric dimer however, has not been analysed for its sublimation properties.

Fig.2.4.1.a



Non oxo alkoxide species were also isolated by Hitchcock⁷⁰, Tesh⁷¹ and Drake⁷². $[\text{Ba}(\text{OC}_6\text{H}_2\text{Bu}^t_{2-2,6-\text{Me}-4})_2(\text{THF})_4]$ was formed by the cocondensation of barium metal vapour and the alcohol in a solution of toluene and THF^{70,71}. This barium compound was analysed by ¹H and ¹³C NMR and later by X-ray crystal analysis. A five coordinate barium species is isolated where 3 THF molecules bind datively to the barium centre in a distorted trigonal bipyramidal monomer. However, no volatility studies were undertaken on this monomeric barium alkoxide.

Interestingly, the reaction between barium metal and 2,6-^tBu₂C₆H₃OH in the presence of a saturated ammoniacal solution of THF in HMPA also gave a monomeric, moisture sensitive solid. However, no STA studies were undertaken, although, the complex has a low melting point of 94-97°C⁷³. A similar reaction was undertaken by Thompson et al²⁶ who refluxed barium metal with 2,6-^tBu₂C₆H₃OH. As a consequence of its lack of stability it was not isolated from solution. Ammonical solutions of activated barium metal have again been used to react with the more sterically hindered phenols, such as 2,4,6-^tbutylphenol, to give [Ba(OC₆H₂Bu^t₃)₂]₂⁷². This particular complex sublimes at 250°C / 10⁻⁴ Torr with some decomposition. In conclusion, it was found that the reaction between barium metal and some sterically hindered ligands such as ^tBuCOH, PhOH and 2,6-^tBuPhOH still results in barium compounds which are oligomeric or polymeric and do not achieve the appropriate volatility to be used in CVD applications.

The presence of the oxo species in barium alkoxides is more likely to be due to decomposition of the complex through water or O₂ contamination. If this is the case it then remains to question whether the volatility of the barium alkoxide complex produced from 2-methoxyethanol would be even higher with less decomposition if the oxo species was absent from the reaction system (see section 2.4.2.).

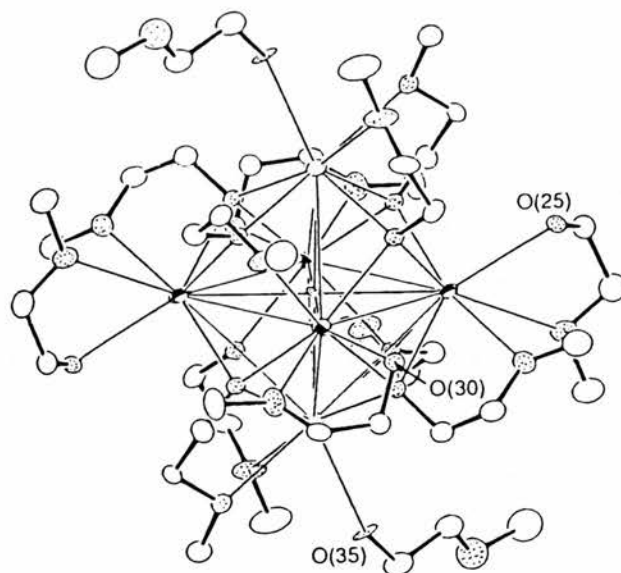
Fig 2.4.1.b.

Barium complex	M.P ^a / Volatility ^b °C	Ref
Oxo containing barium alkoxides		
[Ba(2,6- ^t Bu ₂ C ₆ H ₃ O) ₂ (HOCH ₂ CH ₂ NMe ₂) ₄ .2C ₇ H ₈]	94-97 ^a	73
[Ba ₄ O(2,4,6-NMe ₂ -CH ₂ -C ₆ H ₂ O) ₆]	Decomp. at 135 ^c	74
[HBa(O)(OPh) ₉ (THF) ₈]	-	68
[H ₂ Ba(μ ⁵ O) ₂ (OPh) ₁₄ (HMPA) ₆]	217-220 ^a	75
[Ba ₅ (μ ⁵ OH)(μ ³ -OAr) ₄ (μ ² -OAr) ₄ (OAr)(THF) ₅]	Decomp. at 100 ^d	76
[H ₃ Ba ₆ (O)(O ^t Bu) ₁₁ (OCe ₂ t ₂ CH ₂ O)(THF) ₃]	> 340 ^a	68
Non-oxo homoleptic barium alkoxides		
[Ba ₆ (OPh) ₁₂ (TMEDA) ₄ .4C ₇ H ₈]	96-99 ^a	69
[Ba(2,6- ^t Bu ₂ -4-Me-C ₆ H ₂ O) ₂ (THF) ₄]	-	70
[Ba(2,4,6- ^t Bu ₃ -C ₆ H ₂ O) ₂	180-183 ^a / Sublimes 250 ^b	72
[Ba(O ^t Bu) ₂ (^t BuOH) ₂] ₄	Decomp. 360 ^e	67
[Ba(O ^t Bu) ₂] _n	Sublimes 270 ^b / Decomp. 320	66

2.4.2. Barium oligoether alcoholates

The direct reaction between 2-methoxyethanol and barium granules results in a multinuclear hydrido-oxo barium alkoxide - $[H_4Ba_6(\mu^6-O)(OCH_2CH_2OCH_3)_{14}]$ (μ^6-O refers to the oxygen atom in the complex being bridged to six barium atoms). This particular complex is hydrocarbon soluble and is volatile at $160^\circ C / 10^{-1}$ Torr⁷⁷. Sublimation occurs with continuing decomposition (30% sublimation occurs). The crystal structure of $[H_4Ba_6(\mu^6-O)(OCH_2CH_2OCH_3)_{14}]$ shows the oxo ligand to be totally encapsulated by 6 barium atoms. The molecule has a centre of inversion with each Ba atom obtaining 8 coordination. It seems likely that the volatility of the hexanuclear barium oxo alkoxide would also be increased if the interaggregate O--H--O bonding were not present. Thompson et al²⁶, isolated a similar complex which showed slight volatility. However, no further characterisation was undertaken on this complex.

Fig.2.4.2.a



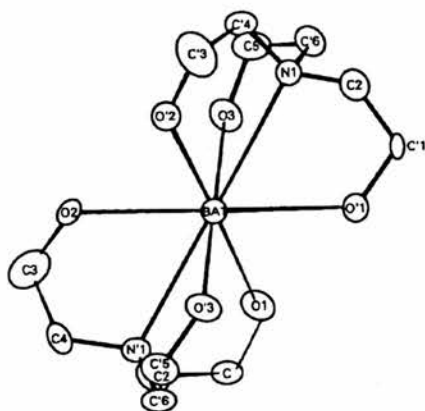
In an attempt to capture the barium centre with a higher coordinating alcohol, Rees et al⁷⁸, synthesised a series of barium compounds containing oligoether alcohols. Unlike Caulton's multinuclear hydrido-oxo barium alkoxide species $[H_4Ba_6(\mu^6-O)-(OCH_2CH_2OCH_3)_{14}]$ which was isolated in the solid state, Rees 'Clam Shell' barium compound was liquid at room temperature. The oligoether alcohols $[HO(CH_2CH_2O)_nCH_3]$ $n=2,3$ were complexed to barium in order to optimise the encapsulation of the barium centre. Both the 6 and 8 coordinate barium oils are supposed to be monomeric in solution and mononuclear species are found in the EI mass spectrum. However, contrary to the monomeric status of these barium compounds, they appear to be involatile. This appears to be in direct contrast with Caulton's multinuclear oligomeric barium alkoxides species which appears to be volatile at 160°C / 0.01Torr⁷⁷.

Interestingly, $[Ba(OC_2H_4OCH_3)_2]$ and $[Ba(OC_2H_4OC_2H_4OC_4H_9)_2]$ were also isolated as hydrocarbon soluble oils by Hampson⁷⁹ and Fahrnholtz⁸⁰. These, however, were not fully characterised and no thermal analysis was given on these compounds.

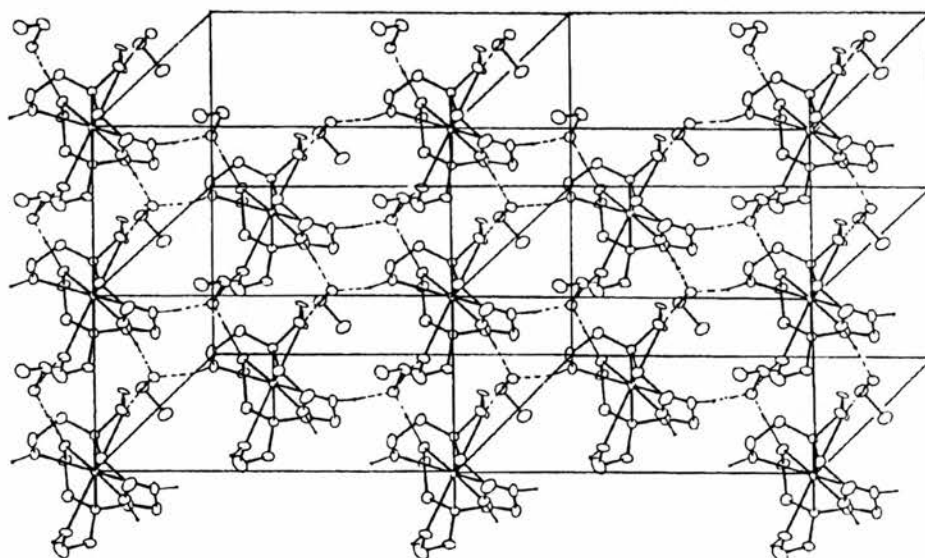
2.4.3. Barium polyfunctional alcoholates

In spite of the surge in current interest in barium alkoxides for precursors in the formation of materials for electronic and ferromagnetic devices, not much research has covered the barium chemistry of polyfunctional alcohols. Barium salts of certain coordinated triethanolamines have been structurally characterised by X-ray crystallographic means^{81,82,83}. The salts display a high coordination to the barium centre and thus attempts were made to make a high coordinate, volatile, covalent bonded barium containing complex.

Direct reaction of barium metal and triethanolamine produces an 8 coordinate barium complex, as shown in fig.2.4.3.a.^{84,85}.

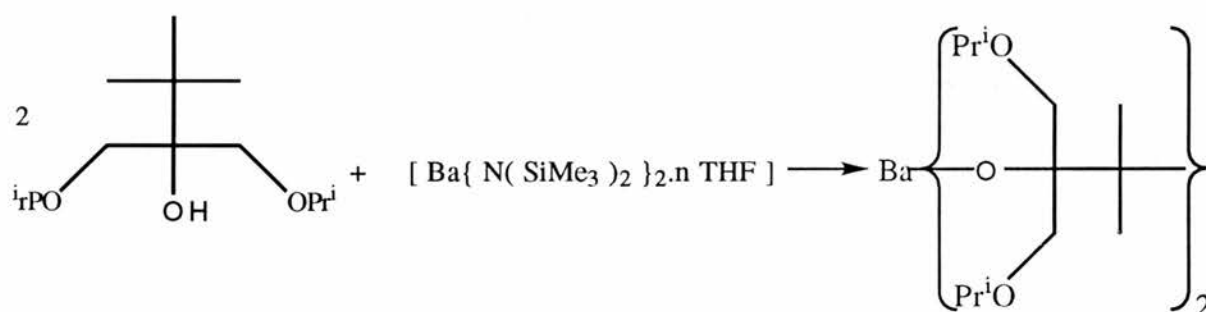
Fig.2.4.3.a

Incorporation of ethanol molecules into the molecular framework results in a two dimensional intermolecular hydrogen bonded barium complex which is shown in Fig 2.4.3.b.

Fig.2.4.3.b.

The barium centre is encapsulated by two tetradentate amino alcohol units which may contribute to the compounds extra stability by blocking the coordination sites of barium. Fragmentation in the mass spectrum shows some barium containing species - $\text{Ba}(\text{OH})(\text{OHC}_2\text{H}_4)_3\text{N}^+$ which may indicate slight volatility at the EI mass spectrum conditions. Although, volatility tests show that the barium complex is unsuitable for CVD applications. A lack of volatility could be attributed to intermolecular H-bonding which exists between monomeric units. Similar extensive hydrogen bonding is noticed in the crystal structure of $[\text{Ba}(\text{TEA})_2(\text{OC}_6\text{H}_4\text{O-NO}_2)_2]$ (TEA = triethanolamine) where the intermolecular interactions occur via the anions. Hermann et al⁸⁶ also isolated a series of barium trifunctional alcoholates which could be sublimed between 150-185°C / 10^{-2} mbar. Fig.2.4.3.c. shows the preparation of the isopropyl derivative.

Fig 2.4.3.c.



Sublimation studies indicate that the barium compound ($\text{R} = \text{iPr}$) sublimes at 600°C / 6 mbar with virtually no decomposition

(3% weight residue). This increase in volatility is attributable to the steric bulk and the extra donor functionalities. In spite of this, dimeric species are detected in the gas phase, and the X-ray structures of the Ca and Cd alcohol derivatives show dimer formation.

2.4.4. Crown ether adducts of barium alkoxides

Drake¹⁹, Drozdov¹⁷, Timmer³³ and Cook³¹ produced a series of polyether adducts of barium β -diketonates. These polyether adducts gave monomeric, volatile complexes as opposed to the less volatile aggregates of their parent β -diketonates.

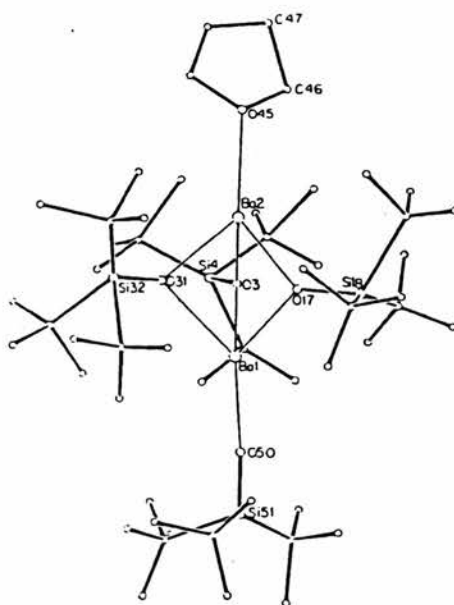
Encouraged by these observations, Miele et al⁸⁷, complexed Ba metal to a sterically hindered alcohol (3,5-di-*t*-butylphenol) in the presence of 18-crown-6 to produce the barium alkoxide polyether complex. Indeed, as seen with the β -diketonates, the barium alkoxide polyether complex was a 8 coordinate monomeric solid. However, this is where the comparison ends, as volatility studies showed that the barium complex decomposed to 18-crown-6 and the alcohol at 10^{-1} mmHg.

A similar barium alkoxide polyether complex- $\{ [\text{Ba}(\text{Picrate})_2 \text{ dibenzo-24-crown}] \}$ where picrate = $2,4,6\text{-C}_6\text{H}_2(\text{NO}_2)_3\text{O}^-$ } was prepared and studied by Hughes et al⁸⁸. $[\text{Ba}(\text{Picrate})_2 \text{ dibenzo-24-crown}]$ is a 10 coordinate, H-bonded complex which melts at 104°C. Unfortunately, no further thermal data was given.

2.5. Barium siloxides

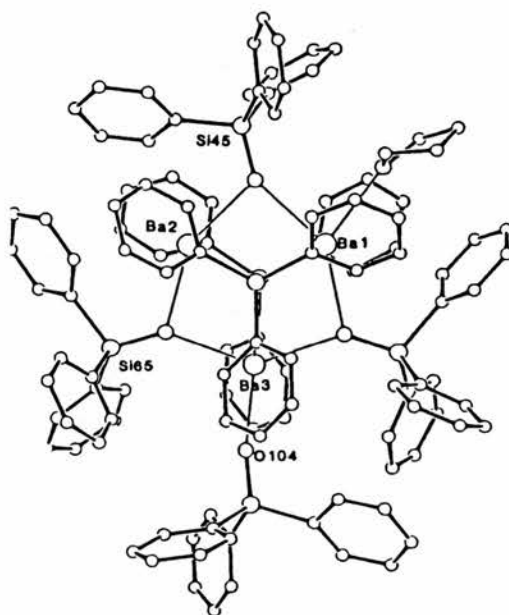
Large sterically hindered siloxides such as $[\text{Ba}_2(\text{OSi}^t\text{Bu}_3)_4(\text{THF})]$ were also isolated⁸⁹. This particular compound sublimed at 80°C / at 1 Torr. Its high volatility is probably as a consequence of the barium complex existing as a discrete dimer with no intermolecular bonding present between dimeric units. Each barium atom is 4 coordinate and this seems to be typical of the low coordination exhibited by sterically hindered alkoxides, siloxides and silyl amides. No other thermal data has been published on this particular compound. An X-ray crystal structure is shown below.

Fig.2.5.1.a



[Ba₃(OSiPh₃)₆(THF).0.5 THF] was synthesised by a facile reaction with Ph₃SiOH in an ammoniacal solution of barium metal in THF⁹⁰. X-ray analysis of the barium complex shows a Ba₃ core with 2 μ³-OSiPh₃ ligands and 3 μ²-OSiPh₃ moieties. The coordination number of the barium in this complex is relatively low, with coordination numbers of 4 and 5 being achieved. The barium complex sublimes at 230-245°C, but decomposes at higher temperatures >250°C. Surprisingly, no oxo or hydroxy species are detected as in the complexes with phenoxide, t-butoxide and methoxyethoxide derivatives. This is probably due to the difference in strength of Si-O bond compared to the strength of the C-O bond in other barium alkoxide compounds and probably due to the unlikely possibility of a siloxide undergoing β- hydrogen abstraction to form an unstable silylene. On the other hand a normal alkoxide can undergo β-hydrogen abstraction to form an alkene and oxo species.

Fig 2.5.1.b.



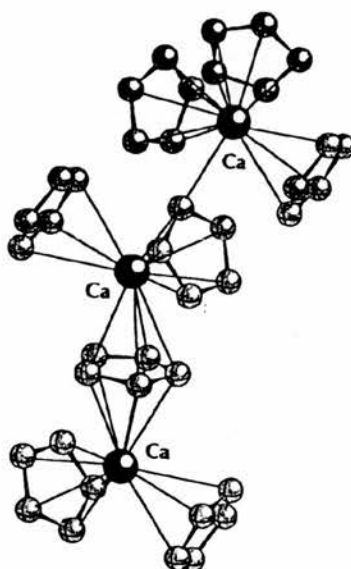
2.6. ORGANOMETALLIC BARIUM COMPOUNDS

A series of organometallic barium compounds have been made for a wide range of applications including new Grignard reagents [$\text{Ba}(\text{C}_2\text{H}_5)_2$]⁹¹⁻⁹⁵, polymer initiators for anionic polymerisation [$\text{Ba}(\text{Ph}_3\text{C})_2(\text{THF})_2$], [$\text{Ba}(\text{H}_2\text{C}=\text{CPh}_2)$]^{96,97}, and recently, compounds potentially useful for CVD technology { [$\text{Ba}(\text{Cp}^*)_2$], [$\text{Ba}(\text{Cp}^{4i})_2$] where Cp^* = pentamethylcyclopentadienyl, Cp^{4i} =tetraisopropylcyclopentadienyl]^{98,99}. Unfortunately, the pyrophoric nature of barium metallocenes makes them unsuitable for CVD application. A comprehensive review of all organometallic barium compounds has been undertaken by Hanusa¹⁰⁰.

2.6.1. Simple barium metallocenes

Barium metallocenes have been produced by several synthetic pathways which either include metal vapour techniques¹⁰¹, solution studies using halide exchange reactions^{102,98}, mixed liquid and gaseous ammonia solvent reactions¹⁰³, activated metal powders¹⁰⁴ or by the reaction between barium hydride and cyclopentadiene¹⁰⁵. The latter method was adopted to produce the first bariocene¹⁰⁵. However, due to very low yields, other synthetic strategies had to be adopted. Solution reactions using barium iodide and the alkali metal salts of cyclopentadiene produced bariocenes in good yields. Although, due to their limited solubility, purification was a problem. The limited range of solubility of bariocene stems from the coordinative unsaturation of the metal centre, which leads to intermolecular interactions. These intermolecular interactions can be noticed in the calcium derivative¹⁰⁶ in Fig 2.6.1.a.

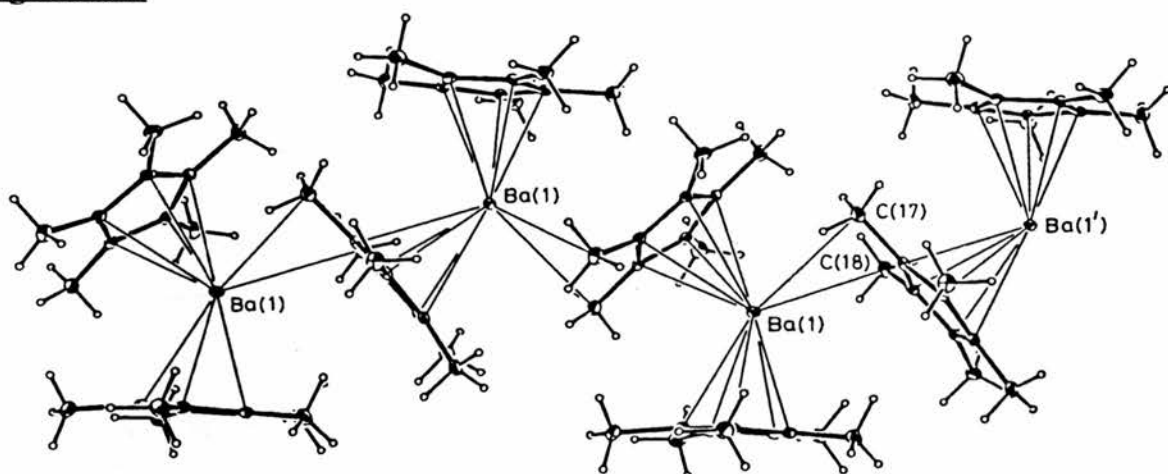
Fig.2.6.1.a.



However, incorporating methyl groups on to the ring centroid has a dramatic effect on the solubility and volatility of the compound^{107,108}. The change in physical properties arises from the weaker intermolecular barium-cyclopentadienyl (Cp^{M}) interactions from other molecules.

An X-ray crystallographical structure of $[\text{Cp}^*_2\text{Ba}]$ shows a 6 coordinate^{1†}, polymeric solid. The metallocene units pack so that, in addition to the two Cp* rings directly bonded to the barium centre, the face of the third Cp* ring, on of those coordinated to an adjacent Ba atom, is in close proximity to the metal. The shortest intermolecular Ba-CH₃ distance within this complex is at 3.349(5) Å. Apart from $[\text{Cp}^*_2\text{Ba}]$ existing in a “quasi-polymeric” network, it appears the complex sublimes at 130-140°C / 0.01 mm Hg. The “quasi-polymeric” structure is represented in Fig.2.6.1.b.

Fig.2.6.1.b

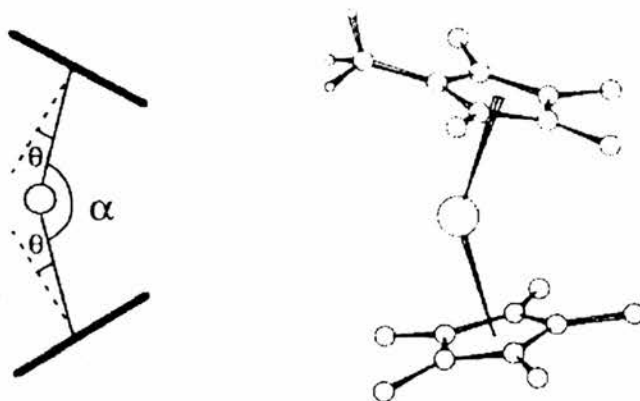


All barium metallocenes are air and moisture sensitive and adopt a structure with C_{2v} symmetry in the gas^{109,110} or solid state^{107,108}. It appears that this is in direct contrast to electrostatic and molecular considerations which would predict the ring centroid having a D_{5h} or D_{5d} symmetry.

† The cyclopentadienyl anion is a 6 electron donor and in theory can form 3 coordinative bonds which can occupy 3 coordination sites. Therefore, a classical $d\pi-\pi$ interaction will take place giving a η^5 6 coordinate system.

The bending of the cyclopentadienyl rings is a result of several effects: d orbital participation, intermolecular interactions, polarisation effects of the Ba^{2+} ion by the cyclopentadienyl anions and stereochemical influence of the solvent molecules competing for coordination sites. Barium metallocenes also exhibit a smaller ligand to ligand repulsion from the cyclopentadienyl rings in comparison with other alkali or alkaline metallocenes. $[Cp^*_2Mg]$ has a D_{5d} or D_{5h} idealised symmetry. Furthermore, gas electron diffraction studies on BaI_2 also show that BaI_2 is bent¹¹¹ where the Ca and SrI_2 ¹¹² are linear.

Fig. 2.6.1.c



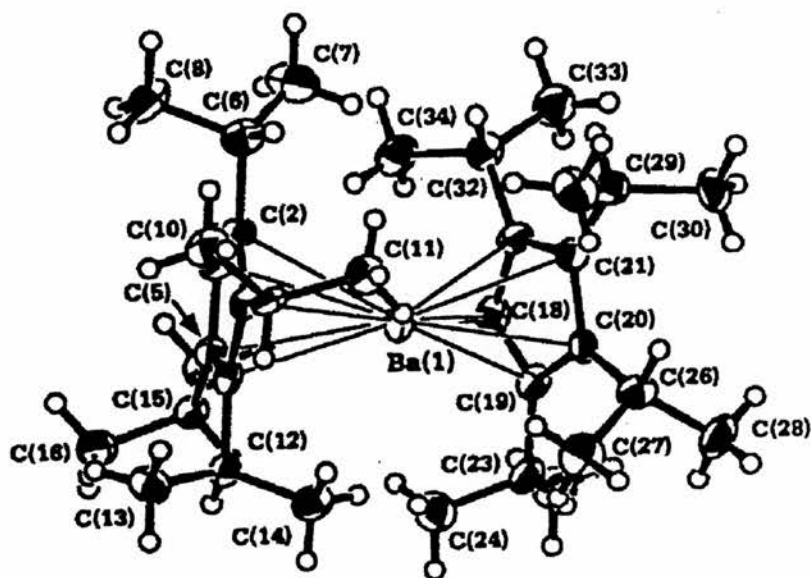
In fact, for barium metallocenes, the larger the angle α , the greater the volatility of the compound (see Fig.2.6.1.d). For instance, $[Cp^*_2Ba]$ consists of a polymeric network and volatilises at $130-140^\circ C / 10^{-3} \text{ mm Hg}$ ¹⁰⁷. As a consequence of increasing the steric bulk attached to the cyclopentadienyl ring, the electronic differences between the tetraisopropylcyclopentadienyl anion (Cp^{4i}) and other cyclopentadienyl anions (Cp^{ni}) results in different angles of α . This results in a decrease in oligomerisation and an increase in volatility. This is demonstrated for $[\text{bis}(\text{tetraisopropylcyclopentadienyl})\text{barium}(\text{II})]$ which has the largest angle of α and volatilises at $90^\circ C / 0.01\text{Torr}$ ⁹⁹.

Fig.2.6.1.d

Barium Metallocene	Aggregation	M.P. °C	Sublimation °C	α °	Ref
[Cp ₂ Ba]	Polymeric	-	420-60	-	105
[{(tBu)C ₅ H ₄ } ₂ Ba]	Aggregate	320	320	-	113
[Cp* ₂ Ba]	1 D polymer	265-8	135	131	107
[{(iPr) ₃ C ₅ H ₂ } ₂ Ba]	Unknown	93-4	120	-	114
[{(iPr) ₃ C ₅ H ₂ } ₂ Ba.(THF) ₂]	Monomeric	107-20	110	131.7	114
[{(Me ₃ Si) ₂ C ₅ H ₃ } ₂ Ba]	Aggregate	222	340	-	115
[{(iPr) ₄ C ₅ H } ₂ Ba]	Monomeric	149-50	90	154.3	99
[{ Cp* ₂ Ba. (μ -C ₄ H ₄ N ₂) }]	Bridged Dimer	226-7	-	138.0	116
[{(Fluorenyl) ₂ Ba.4NH ₃ }]	Monomeric	-	-	112	117
[{(N-Carbazoyl) ₂ Ba.3DME }]	Monomeric	-	-	98.1	118

Williams and coworkers prepared [bis (tetraisopropylcyclopentadienyl) barium (II)]⁹⁹ by reacting the K⁺ salt of Cp⁴ⁱ with BaI₂ in THF. Its enhanced volatility is attributed to the isopropyl groups interlocking and forming "cages" around the barium centre. It is a monomeric, 6 coordinate, thermally stable, solid and has the ability to form adducts, but is air and moisture sensitive. The structure is shown in Fig.2.6.1.e.

Fig.2.6.1.e



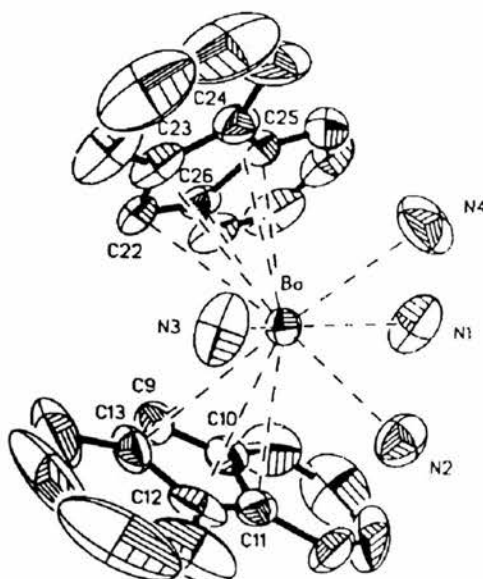
Two conformational forms are isolated in the triclinic unit cell. Two conformers are observed in all of the structurally characterised barium metallocenes. Within the crystal structure of $[(Cp^{4i})_2Ba]$, the average Ba-C distance is 2.94 Å, which is much shorter than the average Ba-C distance experienced in $[Cp^*_2Ba]$ at 2.99 Å. It also has a larger ring centroid-Ba-ring centroid angle α of 154.3° . This is compared to $[Cp^*_2Ba]$ at 131.0° (solid state). It is quite interesting that the barium derivative of Cp^{4i} has a higher volatility than the calcium derivative. This may be explained by the different crystal packing arrangements of the barium derivative.

As mentioned previously, adducts of barium metallocenes play an important role in this particular area of chemistry. McCormick, Williams, and Burns, have all synthesised a series of $[Cp^*_2Ba]$ adducts of THF⁹⁸, 2,6-xylylcyanide⁹⁸, bipyridine⁹⁸, pyrazine¹¹⁶ and PEt_3 ⁹⁸. The extra solubility and volatility expected for these adducts have not been experimentally observed. At first, this observation is puzzling. It seems that the adducts decompose to their corresponding base free compounds when heat is applied. The role of the donor adduct molecules is to break down the oligomerisation, and as a result of this, saturation of the barium centre is obtained.

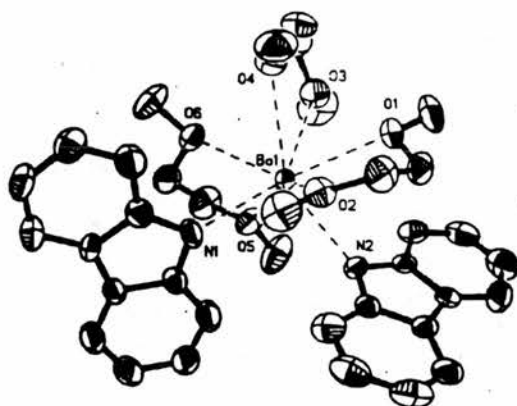
It appears that the overriding factor is the lower charge density of the Ba^{2+} ion which results in a weaker binding of the Lewis base.

2.6.2. Other Arenes and larger metallocenes

Other Arenes and larger metallocenes have also been of great research interest, whether in solution for their electronic, spectroscopic and conductance properties^{119,120,121}, or in the solid state^{122,117,91,101}. Investigations by Drake¹²² have shown that barium metal can react in mixed ammonia-ethereal solutions at $-40^{\circ}C$ with triphenylmethane, fluorene and indene to produce the associated barium complexes (previous work involving metal vapour techniques had produced similar base free compounds^{91,101}). Electron Impact (EI) Mass spectroscopic and FAB studies have detected monomeric species in the gaseous state. It seems that Drake's observations of monomeric species in the gas phase may be as a consequence of the compound being coated with tetraglyme (a coordinating polyether) prior to the sample being tested in the mass spectrometer and not essentially due to the barium fluorenyl compound being monomeric and / or volatile. Furthermore, the Et_2O , THF and DME adducts of bis(fluorenyl) barium (II) were shown to decompose between $60-90^{\circ}C$ which would indicate the presence of a polymeric network. However, to support Drake's observations a monomeric, 10 coordinate, ammonia adduct of bis(fluorenyl) barium (II) - $[Ba(Fluorenyl)_2 \cdot 4NH_3]$ was isolated in the solid state by Mösges¹¹⁷. The structure is shown below in Fig.2.6.2.a. It is interesting to note that the angle α is 112.3 and 116.4° . The small angle may be as a result of the ammonia molecules competing for coordination sites on the barium. Thus, the fluorenyl groups are pushed further together. No thermal data is given on this compound.

Fig. 2.6.2.a

The bent conformation of barium metallocenes is also observed with N-carbazoyl barium compounds. $[\text{Ba}(\text{N-carbazoyl})_2 \cdot 3\text{DME}]$ is a 8-coordinate, monomeric crystalline solid¹¹⁸. Unfortunately, no thermal data was published on this compound. However, the ligand does possess extraordinary $\eta^1 \sigma$ coordination to the barium via the ring N atoms. This is in direct contrast to most barium metallocenes which have multi $\eta \pi$ coordination to the barium. 3 DME molecules complete the saturation of the barium centre as shown in Fig.2.6.2.b.

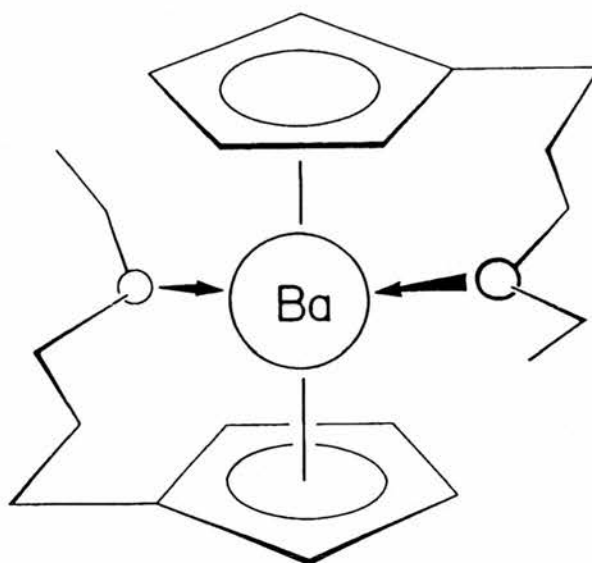
Fig.2.6.2.b.

[Ba(COT)₂] (where COT = cyclooctatetraene) compounds have also been synthesised by reacting barium metal vapour and the COT ligand in THF at -196°C¹²³. [Ba(COT)₂] is a involatile, air sensitive, pyrophoric solid. Its relatively high melting point (>300°C), low solubility and high ionic character suggests that it exists in a polymeric network of poly η COT ligands.

2.6.3. Polyether "scorpion tail" metallocenes

In an attempt to enhance the volatility and stability of barium metallocenes further, pendant polyether appendages were incorporated into the η⁵ carbocyclic π bound units of cyclopentadiene. Rees^{124,6}, isolated these particular barium compounds as oils. They are also air and moisture sensitive. As a consequence of the barium compound being poorly characterised, no thermal studies were undertaken.

Fig. 2.6.3.a



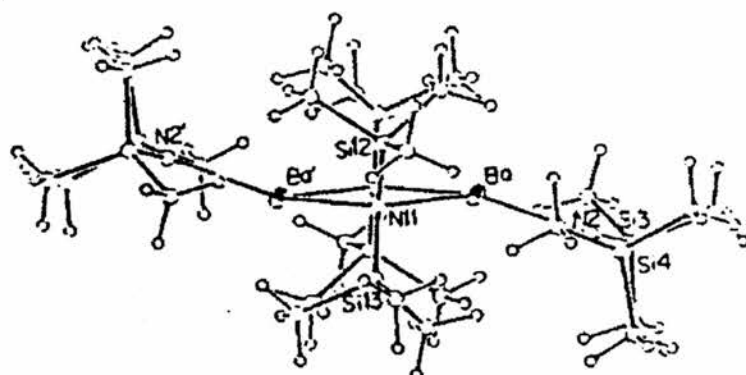
It is interesting to note that the postulated structure of these polyether "scorpion tail" metallocenes by Rees illustrates a D_{5d} symmetry (staggered conformation) or D_{5h} symmetry (eclipsed conformation), whereas all other structurally characterised barium metallocenes in the gas and solid state adopt a bent C_{2v} or C_s symmetry.

Analogous complexes were also reported by Rees - $[\text{Ba}[\text{C}_5\text{H}_4\{(\text{CH}_2)_n\text{ER}\}]_2]$ where $n=2,3$ and $\text{ER} = \text{OMe}, \text{OEt}$ or NMe_2

2.7. BARIUM SILYL AMIDES

Barium silyl amides are made by various synthetic methods including transmetalation reactions with $[\text{Sn}\{\text{N}(\text{SiMe}_3)_2\}_2]^{125}$ or $[\text{Hg}\{\text{N}(\text{SiMe}_3)_2\}_2]^{126}$ or by the reaction between Ba metal and Hexamethyldisilazane in THF with ammonia gas as a catalyst¹²⁷. The first barium silyl amide was prepared by Bradley et al¹²⁶. Barium silyl amides are normally isolated as the THF¹²⁷, DME¹²⁵, 4-*t*-butylpyridine or bipyridyl adducts¹²⁹. The base free complex $[\{\text{Ba}[\text{N}(\text{SiMe}_3)_2]_2\}_2]$ was obtained from the sublimation of $[\text{Ba}[\text{N}(\text{SiMe}_3)_2]_2(\text{THF})_2]$ at approximately 50 mTorr using heat from an infra-red lamp ($[\{\text{Ba}[\text{N}(\text{SiMe}_3)_2]_2\}_2]$ was found to sublime at $160^\circ\text{C} / 10^{-3} \text{ Torr}$)⁶⁷. Surprisingly, the observed melting point for $[\{\text{Ba}[\text{N}(\text{SiMe}_3)_2]_2\}_2]$ is $186\text{-}188^\circ\text{C}$ as observed by Vaartstra¹²⁷. By comparison, Westerhausen saw the same complex decompose at 150°C ¹²⁵. The high resolution mass spectrum shows dimeric species in the vapour phase - $(\text{Ba}_2\text{N}_3\text{Si}_6\text{C}_{18}\text{H}_{54})^+$. The latter observation is supported by $[\{\text{Ba}[\text{N}(\text{SiMe}_3)_2]_2\}_2]$ existing as a dimer in the solid state as shown in Fig.2.7.a. The crystal structure shows that the molecule is perfectly centrosymmetrical with an inversion centre. This low coordinate barium complex is stabilised by the bulky $\text{N}(\text{SiMe}_3)_2$ groups which effectively block out any competing molecules which may coordinate to the barium centre. It appears in a solution of benzene, the barium complex $[\text{Ba}\{\text{N}(\text{SiMe}_3)_2\}_2]$ is also dimeric.

Fig.2.7.a

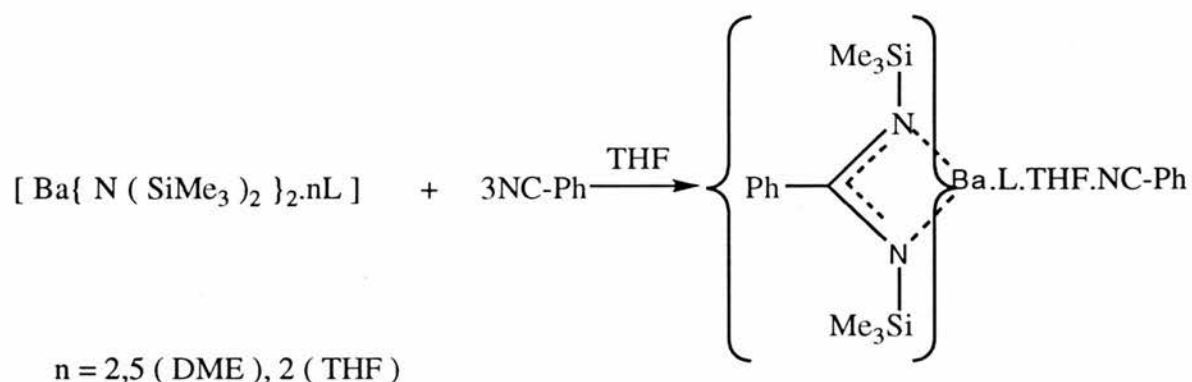


In spite of this, coordinating solvents such as THF break down the oligomerisation and a monomeric, 4 coordinate THF adduct is observed in the solid state. The DME adduct of $[Ba\{N(SiMe_3)_2\}_2]^{125}$ shows extensive fragmentation in the mass spectrum $-(BaNSi_2Me_6)^+$ and therefore it is no surprise that the complex decomposes near to its melting point ($76^\circ C$). This suggests that the compound is involatile and is oligomeric. Yttrium, copper and barium oxides have been produced by the sol-gel techniques using the hydrolysis of the associated metal silyl amide compounds. However, no metal oxides have been deposited using volatile metal silyl amide precursors.

2.7.1. Other barium trimethylsilyl compounds

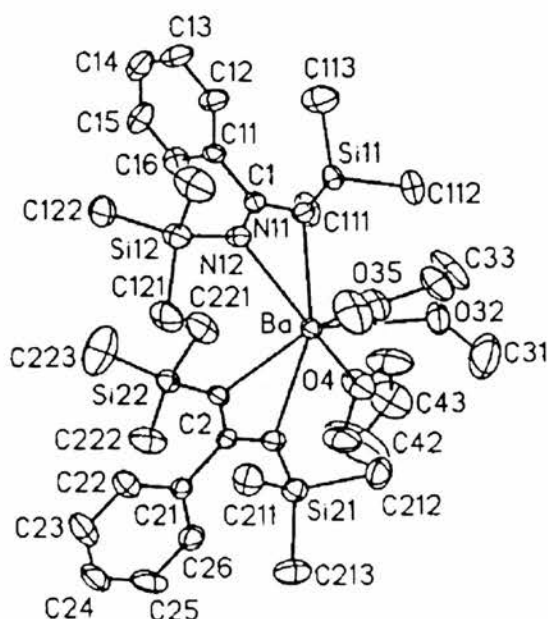
The utility of barium silyl amides is also demonstrated by their addition reactions with benzonitrile in THF to produce [barium (II) bis{ N,N-bis(trimethyl silyl) benzamidate }]¹²⁹ as shown in Fig 2.7.1.a.

Fig 2.7.1.a.



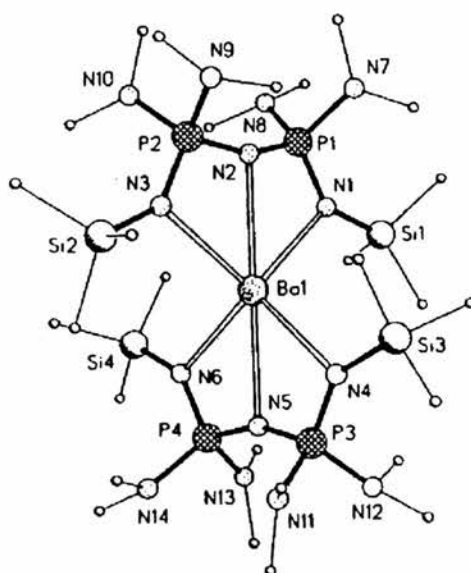
It seems that the corresponding DME and THF adducts decompose on melting - DME adduct - 86°C (decompose), THF adduct - 70-71°C (decompose). Treatment of the THF adduct with DME in toluene results in a new complex. The crystal structure of the THF.DME adduct is shown in Fig.2.7.1.b¹³⁰.

Fig. 2.7.1.b



2.7.2. BARIUM CYCLOPHOSPHAZENE COMPLEXES

The first barium cyclophosphazene compound was produced by Pardey et al¹³¹. The reaction between $[Ba\{N(SiMe_3)_2\}_2 \cdot 2THF]$ and a phosphazene produces the barium cyclophosphazene complex. As a consequence of the exceptionally attractive leaving group, $N(SiMe_3)_2$, in barium bis(trimethyl silyl amide), reactions with phosphazenes take place with relative ease to produce barium cyclophosphazene compounds. The barium complex is a white, moisture sensitive, involatile solid. In spite of the lack of volatility, it is a monomeric 6 coordinate crystalline solid. Attempted sublimation resulted in decomposition to the parent phosphazene ligand at $110^\circ C / 0.01 \text{ bar}$ (m.p. = $220^\circ C$).

Fig.2.7.2.a

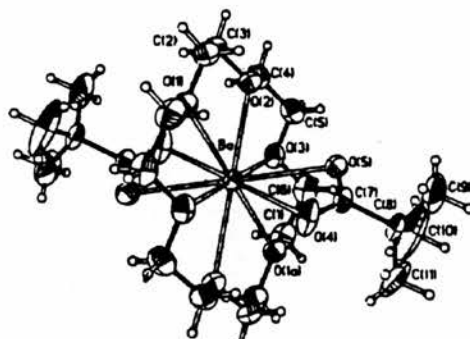
However, this particular cyclophosphazene compound, along with a similar low coordinate cubane cyclophosphazene has been under investigation for sol-gel preparations of $[\text{Ba}(\text{OH})_2 \cdot x\text{H}_2\text{O}]$ in the hope they can serve as precursors for high temperature superconductors.

Although most trimethylsilyl, benzamidate and cyclophosphazene complexes of barium are dimeric, or even monomeric, decomposition occurs very readily. This is probably as a consequence of the ease with which rupture of the Ba-N bond occurs when heat is applied. Relatively low melting points are achieved for these particular compounds suggesting that there is an absence of intermolecular bonding between the molecules. The former statement rationalises the inability of these compounds to be used as precursors for CVD applications.

2.8. METAL CARBOXYLATES

A recent survey of the literature concerning barium carboxylates, has found that most exist as polymeric networks of coordinating bidentate and monodentate carboxylate ligand moieties. Most of these carboxylates were found to be involatile either by sublimation studies or STA analysis.

Generally, most barium containing carboxylates optimise the saturation of the barium centre by bridging interactions which raise the coordination numbers to 9 and 10¹³²⁻¹³⁴. This is different from some bulky siloxides⁸⁹, alkoxides⁶⁹ and silyl amides¹²⁷ which have lower coordination numbers, such as 4 and 6. Most carboxylates are polymeric, but there are some cases of monomeric 10 coordinate systems. The 18-crown 6 ether adduct of barium bis (trimethylacetate) was investigated by X-ray analysis¹³⁵. It is a 10 coordinate, monomeric, solid with two carboxylate ligands, bidentate in coordination. However, no thermal studies have been reported.

Fig.2.8.a

Similar polyether carboxylate compounds have been made by Timmer et al³³, but they were found to be involatile, colourless solids.

In fact, the only known reported volatile barium carboxylate is barium neodecanoate (ethyldipropylacetato)¹³⁶

It seems steric hinderence from bulky side groups prevents extensive oligomerisation in this particular barium carboxylate. Bis (ethyl dipropylacetato)₂ barium(II) is made from the free acid and barium metal in benzene. The evidence of the mass spectrum seems to suggest that it exists as a oligomeric species in the vapour phase. (BaL⁺ and Ba₂L₃⁺ seen). It is isolated as a pale viscous liquid and it appears to have a higher 'thermal stability than

[Ba₅(TMHD)₉(OH)(H₂O)₃]. The barium carboxylate sublimes to give a white solid sublimate which was not analysed.

2.9. REFERENCES

1. Q.X.Jia, J.Yi, Q.Z.Shi, K.K.Ho, C.H.Chang and W.A.Anderson, *Mater.Res.Soc.Symp.Proc.*, 284, 523, 1993.
2. M.K.Wu, J.R.Ashburn, C.J.Torng, P.H.Hor, R.L.Meng, L.Gao, Z.J.Huang and C.W.Chu, *Phys.Rev.Lett.*, 58, 908, 1987.
3. H.Maeda, Y.Tanaka, M.Fukutomi, and T.Asano, *Jap.J.Phys.Lett.*, 27, L209, 1988.
4. A.M.Schilling, J.D.Cantoni and H.R.Ott, *Nature.*, 56, 356.
5. R.E.Sievers, S.B.Turnipseed, L.Huang and A.F.Lagalante, *Coord.Chem.Rev.*, 128, 285, 1993.
6. W.S.Rees.Jr and A.Barron, *Adv.Mat.Opt.Electron.*, 6, 2, 271, 1993.
7. G.S.Hammond, D.C.Nonhebel and C.H.S.Wu, *Inorg.Chem.*, 2, 73, 1963.
8. S.C.Thompson, D.J.Cole-Hamilton, D.D.Gilliland, M.L.Hitchman and J.C.Barnes, *Adv.Mater.Opt.Electron.*, 1, 81, 1992.
- 9.H.Zama and S.Oda, *Jap.J.Appl.Phys.*, 29, 1072, 1990.
- 10.A.Drozdov, N.Kuzmina, S.Troyanov and L.Martynenko, *Mater.Sci.Engin.*, B18, 139, 1993.
11. J.Eisentraut and R.E.Sievers, *J.Am.Chem.Soc.*, 87, 22, 5255, 1965.
12. E.W.Berg and J.J.Chiang Acosta, *Anal.Chim.Acta.*, 40, 101, 1968.
13. T.Ozawa, *Thermochimica Acta.*, 174, 185, 1991.
14. J.E.Schwarzberg, R.E.Sievers, R.W.Moshier, *Anal.Chem.*, 42, 19, 18282, 1970.
15. E.W.Berg and N.M.Herrera, *Anal.Chim.Acta.*, 60, 117, 1972.
16. A.Gleizes, S.Sans-Lenain and D.Medus, *C.R.Acad. Sci.Paris.*, 313, 2, 761, 1991.
17. A.Drozdov, N.Kuzmina, S.Troyanov and L.Martynenko, *Mater.Sci.Engin.*, B18, 139, 1993.
18. A.Drozdov and S.I.Troyanov, *Polyhedron.*, 11, 22, 2877, 1992.

19. S.R.Drake, M.B.Hursthouse, K.M.Abdul Malik and D.J.Otway, *J.Chem.Soc.Dalton.Trans.*, 2883, 1993.
20. S.B.Turnipseed, R.M.Barkley and R.E.Sievers, *Inorg.Chem.*, 30, 1164, 1991.
21. L.Huang, S.B.Turnipseed, C.Haltiwanger, R.M.Barkley and R.E.Sievers, *Inorg.Chem.*, 33, 798, 1994.
22. Z.Hideaki and O.Shunri, *Jpn.J.Appl.Phys.*, 29, 1072, 1990.
23. N.Kuzmina, I.Zaytsera, M.Checernikora, L.Martynenko, A.Cherednichenko and V.Vorna, *Zh.Neorg.Khim.*, 36, 2739, 1990.
24. R.Sato, K.Takahashi, M.Yoshino, H.Kato and S.Ohshima, *Jpn.J.Appl.Phys.*, 32, 1, 4, 1590, 1993.
25. H.Harmina, H.Ohnishi, K.Hanaoka, K.Tachibana and Y.Goto, *Jpn.J.Appl.Phys.*, 1946, 1991.
26. S.C.Thompson, Ph.D. Thesis, *University of St.Andrews.*, 1991.
27. R.Gardiner, D.W.Brown and P.S.Kirlin, *Chem Mater.*, 3, 1053, 1991.
28. S.R.Drake, S.A.S.Miller, M.B.Hursthouse and K.M.Abdul Malik, *Polyhedron.*, 12, 13, 1621, 1993.
29. J.A.P.Nash, S.C.Thompson, D.F.Foster, D.J.Cole-Hamilton and J.C.Barnes, *J.Chem.Soc.Dalton.Trans.*, in press, 1994.
30. J.A.P.Nash, J.C.Barnes, D.J.Cole-Hamilton, B.C.Richards, S.L.Cook and M.L.Hitchman, *Adv.Mat.Opt.Electron.*, in press 1994.
31. S.Cook, Private Communication, 1994.
32. T.Okazaki, K.Tokutone and S.Nakai, *Jpn.Kokai.Tokkyo.Koho.*, J.P.04 257 592, 1992.
33. K.Timmer and H.A.Meinema, *Inorg.Chim.Acta.*, 187, 99, 1991.
34. J.A.T.Norman and G.P.Pez, *J.Chem.Soc.Chem.Commun.*, 971, 1991.
35. W.S.Rees Jr, M.W.Carris and W.Hesse, *Inorg.Chem.*, 30, 4481, 1991.
36. A.Barron, Strem Chemiker, Strem Chemicals, Newburyport, M.A., U.S.A., 13, 1, 1990.

37. C.I.M.A.Spee, A.Mackor, In Science and Technolgy of thin film superconductors; Mc.Connell, R.D.Wolf, Eds; Plenum: New York., 1989, 281.
38. S.Matsuno, F.Uchikawa and K.Yoshizaki, *Jpn.J.Appl.Phys.*, 1990, **29**, L947.
39. F.Uchikawa, S.Matsuno, K.Equara and K.Yoshizaki, Extended Abstracts of the 50th Autumn meeting of the Japanese Society of Applied Physics, 1989, 158.
40. P.H.Dickenson, T.H.Geballe, A.Sanjurjo, D.Hildenbrand, G.Craig, M.Zisk, J.Collman, S.A.Banning and R.E.Sievers, *J.Appl.Phys.*, 1989, **66**, 444.
41. F.Schmaderer, R.Huber, H.Detzman and G.Wahl, VIIIth EURO CVD Conference, *J.Physique II.*, 1992, **C2**, 1.
42. A.Drozdov and S.Troyanov, *Polyhedron.*, 1993, **12**, 24, 2973.
43. A.Drozdov, S.Troyanov, N.P.Kuzmina, L.I.Martynenko, A.S.Alikhanyan and I.P.Makerova, *J.Physique IV Colloque.*, 1993, **C3**, 3, 379.
44. R.Sato, K.Takahashi, M.Yoshino, H.Kato and S.Ohshima, *Jpn.J.Appl.Phys.*, 1993, **1**, **4**, 32, 1590.
45. A.Purdy, A.D.Berry, R.T.Holm, M.Fatemi and D.K.Gaskill, *Inorg.Chem.*, 1989, **28**, 2799.
46. D.C.Bradley, M.Hasein, M.B.Hursthouse, M.Motevalli, O.F.Z.Khan, R.G.Pritchard and J.O.Williams, *J.Chem.Soc.Chem.Commun.*, 1992, **7**, 575.
47. S.C.Thompson, D.J.Cole-Hamilton, S.L.Cook and D.Barr, Eur.Pat.Appl., 92307390, February 1993.
48. M.L.Hitchman, S.H.Shamlan, D.D.Gilliland, D.J.Cole-Hamilton, J.A.P.Nash, S.C.Thompson and S.L.Cook, *J.Mater.Chem.*, in press, 1994.
49. M.L.Hitchman, S.H.Shamlan, D.D.Gilliland, D.J.Cole-Hamilton, S.C.Thompson, S.L.Cook and B.C.Richards, *Mat.Res.Soc.Symp.Proc.*, 1994, 335, 249.
50. D.D.Gilliland, M.L.Hitchman, S.C.Thompson and D.J.Cole-Hamilton, *J.Phys III France.*, 1992, **2**, 1381.
51. H.Sato and S.Sugawara, *Inorg.Chem.*, 1993, **32**,10,1941.

52. K.Sato, S.Sugawara, K.Fujiura, Jpn.Kokai.Tokkyo.Koho., J.P.05 192 565, 92 / 1, 330.
53. R.Belcher, G.R.Cranby, J.R.Mayer, W.I.Stephen and P.C.Uden, *Anal.Chim.Acta.*, 1972, **60**, 109.
54. K.Timmer, C.I.M.A.Spee, A.Mackor and H.A.Meinema, Eur.Pat.Appl., 1991, 405 634, A2.
55. P.Van der Sluis, A.L.Spek, K.Timmer and H.A.Meinema, *Acta.Cryst.*, 1990, **C46**, 1741.
56. S.H.Shamlan, M.L.Hitchman, S.L.Cook and B.C.Richards, *J.Mater.Chem.*, 1994, **4**, 1, 81.
57. W.S.Rees.Jr, C.R.Caballero and W.Hesse, *Angew.Chem.Int.Ed.Engl.*, 1992, **31**, 735.
58. D.L.Schulz, B.L.Hinds, C.L.Stern and T.J.Marks, *Inorg.Chem.*, 1993, **32**, 249.
59. D.L.Schulz, B.J.Hinds, D.A.Neumayer, C.L.Stern and T.J.Marks, *Chem.Mater.*, 1993, **5**, 1605.
60. E.A.Mazurenko, O.S.Pozil'skii and V.Ya.Zub, *Ukr.Khim.Zh.* (Russ Edd), 1990, **57**, 8, 795.
61. S.M.Pine, P.N.Dyer, J.A.T.Norman, B.A.Muratore and R.L.Iampietro, *Mat.Res.Soc.Symp.Proc.*, 204, 415, 1990.
62. J.A.T.Norman, U.S.Patent No 4, 950,790, 1990.
63. H.D.Lutz, *Z.Anorg.Allg.Chem.*, 1967, **207**, 353.
64. H.D.Lutz, *Z.Anorg.Allg.Chem.*, 1968, **132**, 356.
65. J.S.Smith II, R.T.Doloff and K.S.Mazdiasni, *J.Am.Ceram.Soc.*, 1970, **53**, 91.
66. A.P.Purdy, C.F.George and J.H.Callahan, *Inorg.Chem.*, 1991, **30**, 2812.
67. B.Borup, J.A.Samuels, W.E.Streib and K.G.Caulton, *Inorg.Chem.*, 1994, **33**, 994.
68. K.G.Caulton, M.H.Chisholm, S.R.Drake and K.Folting, *J.Chem.Soc.Chem.Commun.*, 1990, 1349.

69. K.G.Caulton, M.H.Chisholm, S.R.Drake, K.Folting, J.C.Huffman and W.E.Streib, *Inorg.Chem.*, 1993, **32**, 1970.
70. P.B.Hitchcock, M.F.Lappert, G.A.Lawless and B.Royo, *J.Chem.Soc.Chem.Comm.*, 1990, 1141.
71. K.Tesh, T.P.Hanusa, J.C.Huffmann and C.J.Huffman, *Inorg.Chem.*, 1992, **31**, 5572.
72. S.R.Drake, D.J.Otway, M.B.Hursthouse and K.M.Abdul Malik, *Polyhedron.*, 1992, **11**, 16, 1995.
73. K.G.Caulton, M.H.Chisholm, S.R.Drake and K.Folting, *Inorg.Chem.*, 1991, **30**, 1500.
74. K.Tesh and T.P.Hanusa, *J.Chem.Soc.Chem.Comm.*, 1991, 879.
75. K.G.Caulton, M.H.Chisholm, S.R.Drake, K.Folting and J.C.Huffman, *Inorg.Chem.*, 1993, **32**, 816.
76. P.Miele, J.D.Foulon and N.Hovnanian, *Polyhedron.*, 1993, **12**, 2, 209.
77. K.G.Caulton, M.H.Chisholm, S.R.Drake and J.C.Huffman, *J.Chem.Soc.Chem.Comm.*, 1990, 1498.
78. W.S.Rees.Jr.and D.A.Moreno, *J.Chem.Soc.Chem.Comm.*, 1991, 1759.
79. P.J.Hampson and T.J.Leedham, *Chemtronics.*, 1991, **5**, 115.
80. W.G.Fahranholtz, D.M.Millar and D.A.Payne, Research Update 1988, Ceramic Superconductors II, American Ceramic Society, Westerville, OH, 1988, 141.
81. J.A.Kanters, W.J.J.Smeets, K.Ventatasubramanian and N.S.Poonia, *Acta.Crystallogr.*, 1985, **C40**, 1701.
82. J.A.Kanters, A.Dekoster, A.Schouten, K.Venkatasubramanian and N.S.Poonia, *Acta.Crystallogr.*, 1985, **C41**, 1585.
83. J.A.Kanters, W.J.J.Smeets, A.J.M.Dusenborg, K.Ventatasubramanian and N.S.Poonia, *Acta.Crystallogr.*, 1984, **C40**, 1699.
84. O.Poncelet, L.G.Hubert-Pfalzgraf, L.Toupet and J.C.Duran, *Polyhedron*, 1991, **10**, 17, 2045.

85. L.G.Hubert-Pfalzgraf, M.C.Massiani, J.C.Duran and J.Vaissermann, *Mat.Res.Soc.Symp.Proc.* Better ceramics through Chemistry., 1992, **271**, 135.
86. W.A.Hermann, N.W.Huber and T.Priermeir, *Angew.Chem.Int.Ed.Engl.*, 1994, **33**, 1, 105.
87. P.Miele, J.D.Foulon, Hovmanian and L.Cot, *Polyhedron*, 1993, **12**, 3, 267.
88. D.L.Hughes and J.N.Wingfield, *J.Chem.Soc.Chem.Commun.*, 1977, 804.
89. S.R.Drake, W.E.Streib, K.Folting, M.H.Chisholm and K.G.Caulton, *Inorg.Chem.*, 1992, **31**, 3205.
90. K.G.Caulton, M.H.Chisholm, S.R.Drake and W.E.Streib, *Angew.Chem.Int.Ed.Engl.*, 1990, **29**, 12, 1483.
91. P.West and M.C.Woodville, *Ger.Offen.* 2132955 , 1972 ; U.S.Patent 3718703, 1973.
92. I.E.Paleeva, N.I.Sheverdina and K.A.Kocheshkov, *Zh.Obshch.Khim.*, 1974, **44**, 1133.
93. I.E.Paleeva, N.I.Sheverdina, M.A. Zemlyanichenko and K.A.Kosheshkov, *Dokl.Akad.Neuk.SSSR.*, 1973, **210**, 1134.
94. L.Miginiac, *J.Organomet.Chem.*, 1982, **235**, 238.
95. C.L.Raston and G.Salem, Chemistry of the Metal Carbon bond (Ed., F.R.Hartley), J.Wiley., 1987, 412.
96. L.C.Tang, C.Mathis and B.Francois, *J.Organomet.Chem.*, 1983, **243**, 356.
97. W.E.Lindsell, F.C.Robertson and I.Soutar, *Eur.Polymer.J.*, 1983, **19**, 115.
98. C.J.Burns and R.A.Andersen, *J.Organmet.Chem.*, 1987, **31**, 325.
99. R.A.Williams, K.F.Tesh and T.P.Hanusa, *J.Am.Chem.Soc.*, 1991, **113**, 4843.
100. T.P.Hanusa, *Polyhedron.*, 1990, **9**, 11, 1345. Report No 31.
101. B.G.Gowenlock, W.E.Lindsell and B.Singh, *J.Chem.Soc.Dalton.Trans.*, 1978, 657.
102. M.J.Mc.Cormick, R.A.Williams, L.J.Levine and T.P.Hanusa, *Polyhedron.*, 1988, **7**, **9**, 725.
103. S.R.Drake and D.J.Otway, *J.Chem.Soc.Chem.Commun.*, 1991, 517.

104. M.J.Mc.Cormick, K.B.Moon, S.R.Jones and T.P.Hanusa, *J.Chem.Soc.Chem.Commun.*, 1990, 778.
105. E.O.Fischer and G.Stölzle, *Chem.Ber.*, 1961, 2187.
106. R.Zerger and G.Stucky, *J.Organomet.Chem.*, 1974, 7,80.
107. R.A.Williams, T.P.Hanusa and J.C.Huffman, *J.Chem.Soc.Chem.Commun.*, 1988, 1045.
108. R.A.Williams, T.P.Hanusa and J.C.Huffman, *Organometallics.*, 1990, 9, 1128.
109. R.A.Anderson, R.Blom, C.J.Burns and H.V.Volden, *J.Chem.Soc.Chem.Commun.*, 1987, 769.
110. R.Blom, K.Faegri Jr and H.V.Volden, *Organometallics.*, 1990, 9, 372.
111. V.P.Spiridonov, A.G.Gershikov, A.B.Altmen, G.V.Romanov and A.A.Ivanov, *Chem.Phys.Lett.*, 1981, 41, 77.
112. V.V.Kasporov, S.Yu and N.G.Rambidid, *J.Struct.Chem.*, 1979, 20, 285.
113. M.G.Gardiner, C.L.Raston and C.H.L.Kennard, *Organometallics.*, 1991, 10, 3680.
114. D.J.Burkey, R.A.Williams and T.P.Hanusa, *Organometallics.*, 1993, 12, 1331.
115. L.M.Engelhardt, P.C.Junk, C.L.Raston and A.H.White, *J.Chem.Soc.Chem.Commun.*, 1988, 1500.
116. R.A.Williams, T.P.Hanusa and J.C.Huffman, *J.Organomet.Chem.*, 1992, 429, 143.
117. G.Mösger, F.Hampel and P.von Ragué Schleyer, *Organometallics.*, 1992, 11, 1769.
118. G.Mösger, F.Hampel, M.Kaupp and P.von Ragué Schleyer, *J.Am.Chem.Soc.*, 1992, 114, 10880.
119. T.E.Hogen-Esch and M.J.Plodinec, *J.Phys.Chem.*, 1976, 10, 80, 1085.
120. D.H.O'Brien, C.R.Russell and A.J.Hart, *J.Am.Chem.Soc.*, 1979, 101, 633.
121. C.Mathis, B.Francois and J.Smid, *J.Organomet.Chem.*, 1981, 217, 291.
122. S.R.Drake and D.J.Otway, *Polyhedron.*, 1992, 7, 745.

123. D.S.Hutchings, P.C.Junk, W.C.Patalinghug, C.L.Raston and A.H.White, *J.Chem.Soc.Chem.Commun.*, 1989, **15**, 973.
124. W.S.Rees Jr and K.Dippel, *Chem.Process.Adv.Mater.*, 1992, 327.
125. M.Westerhausen, *Inorg.Chem.*, 1991, **30**, 96.
126. D.C.Bradley, M.B.Hursthouse, A.A.Ibrahams, K.M.A.Malik, M.Motevalli, R.Moseler, H.Powell, J.D.Runnacles and A.C.Sullivan, *Polyhedron.*, 1990, **9**,24, 2959.
127. B.A.Vaarstra, J.C.Huffman, W.E.Streib and K.G.Caulton, *Inorg.Chem.*, 1991, **30**, 121.
128. J.M.Boncella, C.J.Coston and J.K.Cammack, *Polyhedron.*, 1991, **10**, 7, 769,.
129. M.Westerhausen, H.D.Hausen and W.Schwarz, *Z.Anorg.Allg.Chem.*, 1992, 618, 121.
130. M.Westerhausen and W.Schwarz, *Z.Anorg.Allg.Chem.*, 1993, **619**, 1455.
131. S.K.Pardey, A.Steiner, H.W.Roesky and D.Stalke, *Angew.Chem.Int.Ed.Engl.*, 1993, **4**, 32, 596.
132. S.I.Troyanov and N.P.Kuzmina, *Koord.Khim.*, 1992, **18**, 9, 992.
133. I.Gautier-Luneau and A.Mosset, *J.Solid.State.Chem.*, 1988, **73**, 473.
134. D.A.Edwards, J.F.Keily, M.F.Mahon, K.C.Molloy and D.Thompsett, *J.Chem.Soc.Dalton.Trans.*, 1993, 3471.
135. A.L.Rheingold, C.B.White and B.S.Haggerty, *Acta.Crysallogr.*, 1993, **C49**, 808.
136. V.M.Vorotyntsev, D.A.Shamrakov and L.G.Suslova, *Vysoko.Veshch.*, 1991, **5**, 113, .

CHAPTER 3

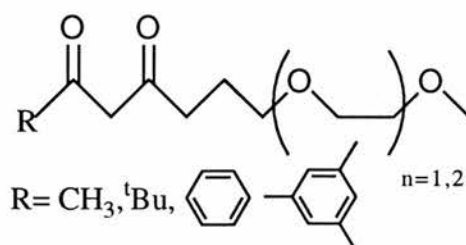
SCORPION-TAIL BARIUM β -DIKETONATES

CHAPTER 3

3.1. Introduction

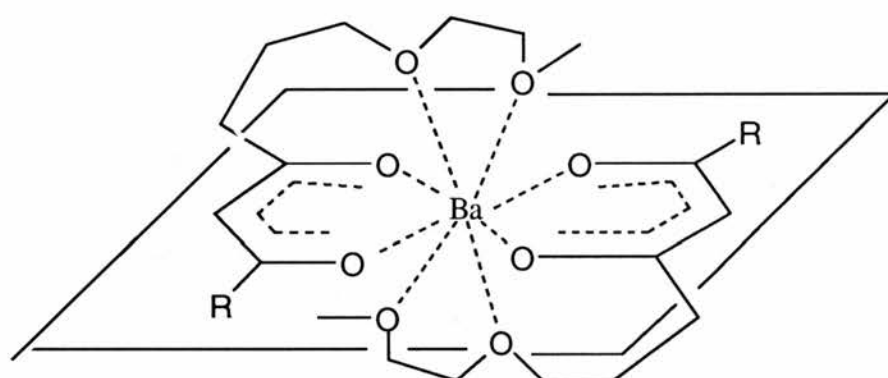
Although, $[\text{Ba}(\text{TMHD})_2 \cdot \text{tetraglyme}]^1$ has an increased volatility and stability over its tetraglyme free counterpart - " $[\text{Ba}(\text{TMHD})_2]$ " " $[\text{Ba}_5(\text{TMHD})_9(\text{OH})(\text{H}_2\text{O})_3]^{2,3}$, it also encounters some decomposition. Thermal studies on $[\text{Ba}(\text{TMHD})_2 \cdot \text{tetraglyme}]$ show that the tetraglyme ligand dissociates prior to sublimation, so in fact, sublimation is totally due to the readily formed $[\text{Ba}(\text{TMHD})_2]_n$ where n can be between 1-4. Although, almost complete evaporation occurs under the conditions of the STA experiment, bulk sublimation is not possible because of concomitant decomposition and hence $[\text{Ba}(\text{TMHD})_2 \cdot \text{tetraglyme}]$ is not a suitable CVD precursor. Obtaining volatility in barium compounds requires the encapsulation of the barium centre with a ligand set that contains two anionic ligands to give a monomeric complex. Thus, in order to prevent the dissociation of the polyether that occurs for $[\text{Ba}(\text{TMHD})_2 \cdot \text{tetraglyme}]$, it was decided to design and synthesise a series of non-fluorinated barium β -diketonates in which the β -diketone and the polyether appendage are incorporated into one individual ligand.

Fig 3.1.a



Although, dissociation of polyether ligand might take place, the polyether used will be unable to leave the environment of the barium atom. Molecular modelling aids show that the polyether chain might be able to encapsulate the barium centre by giving extra coordination through the polyether oxygen atoms. It was hoped that encapsulation of the barium centre would take place with the 2 anionic ligands, giving a neutral 8-10 coordinate, monomeric, volatile solid. Fig 3.1.b shows the possible binding in these particular barium compounds. As a consequence of the possible binding to the barium centre, the ligands are referred to as "scorpion tail" β -diketonates.

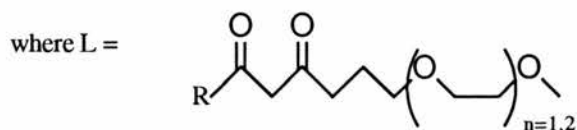
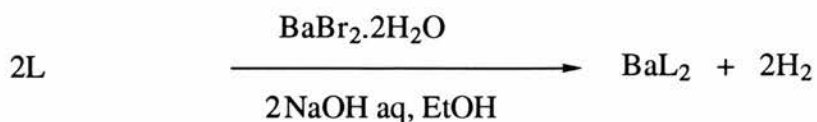
Fig 3.1.b.



In the z plane

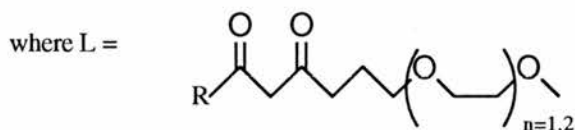
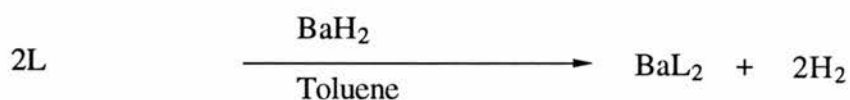
Two methods of complexing the β -diketonate ligand to the barium centre were adopted; firstly by reacting the β -diketone with barium (II) bromide in an aqueous medium, as shown in

Fig 3.1.c.

Fig 3.1.c.

This method produced non-volatile, hygroscopic solids which were insoluble in most organic solvents. It was thought that the aqueous method caused polymerisation through hydrogen bonding, and therefore, made the barium complex involatile.

The second method of complexation involved the reaction between barium hydride and the β -diketone in dry toluene (i.e. in the absence of water).

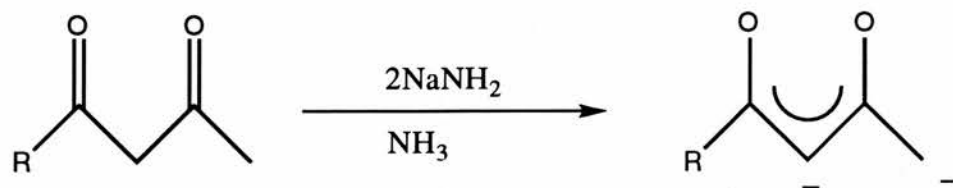
Fig 3.1.d.

The reason for changing from a hydrated method to an anhydrous method was two fold; it was considered that using the water method caused some water molecules to compete for coordination sites on the barium centre and secondly, the elimination of water would reduce the intermolecular H-bonding, and therefore, reduced the polymerisation within the structure.

The barium complexes prepared by the toluene method are generally air sensitive oils which are soluble in most organic solvents. Similar clear oils were obtained by Rees and coworkers⁴ with "satisfactory %C and %H analysis" (i.e.the C and H analysis were not published). My studies conclude that the presence of any residual ligand in the barium complex gives oils. The attempted removal of the strongly H-bonded ligand from the barium complex, by washing the complex with petrol seems to purify the barium complex to a certain degree. Sublimation studies show that all the barium complexes investigated so far, decompose before they sublime.

3.2. Ligand Preparation

This involves a two stage reaction, where a sodium dianion of β -diketone is produced as an intermediate. The reaction involves the deprotonation of a β -diketone by two moles of sodium amide in freshly distilled liquid ammonia, to produce the sodium dianion. In situ, the sodium dianion is reacted further with a bromoether in the presence of liquid ammonia. After four hours, concentrated hydrochloric acid is added. The ligand is then isolated following extraction with ether. It is believed that the presence of ammonia in the reaction system when reacting the bromoether is, necessary for a successful reaction to take place. This may be due to the solvation effects of the dianion, or may be due to the temperature control (-33°C). The reaction sequence is shown in Fig 3.2.

Fig 3.2

(i) $\text{CH}_3 (\text{OCH}_2\text{CH}_2)_n \text{Br}$, $n = 2, 3$
(ii) H^+



3.3. Keto-enol Tautomerism

Like any other β -diketone, the ligands synthesised experience keto-enol tautomerism, where an equilibrium is produced in neat solution to give a particular keto-enol mixture.

Fig 3.3.



Keto-Enol Tautomerism

Different β -diketones will give different keto-enol ratios. The proportion of the keto-enol mixture in neat solution is affected by several parameters. These parameters include temperature, solvent effects, the presence of a species that is capable of H-bonding, α -substituents, deuteration and β -substituents (α -substituents are defined as groups positioned at the methylene carbon).

For instance, the effect of altering the steric bulk and / or electron withdrawing power of a β -substituent can change the % enol form in solution. In fact, 8,11-oxa-dodecane exists as 76% in the enol form, compared to the phenyl analog which exists as 92% in the enol form. This is due to the increase in delocalisation caused by the phenyl β -substituent which favours the enol form.

3.4. IR Data for the ligands

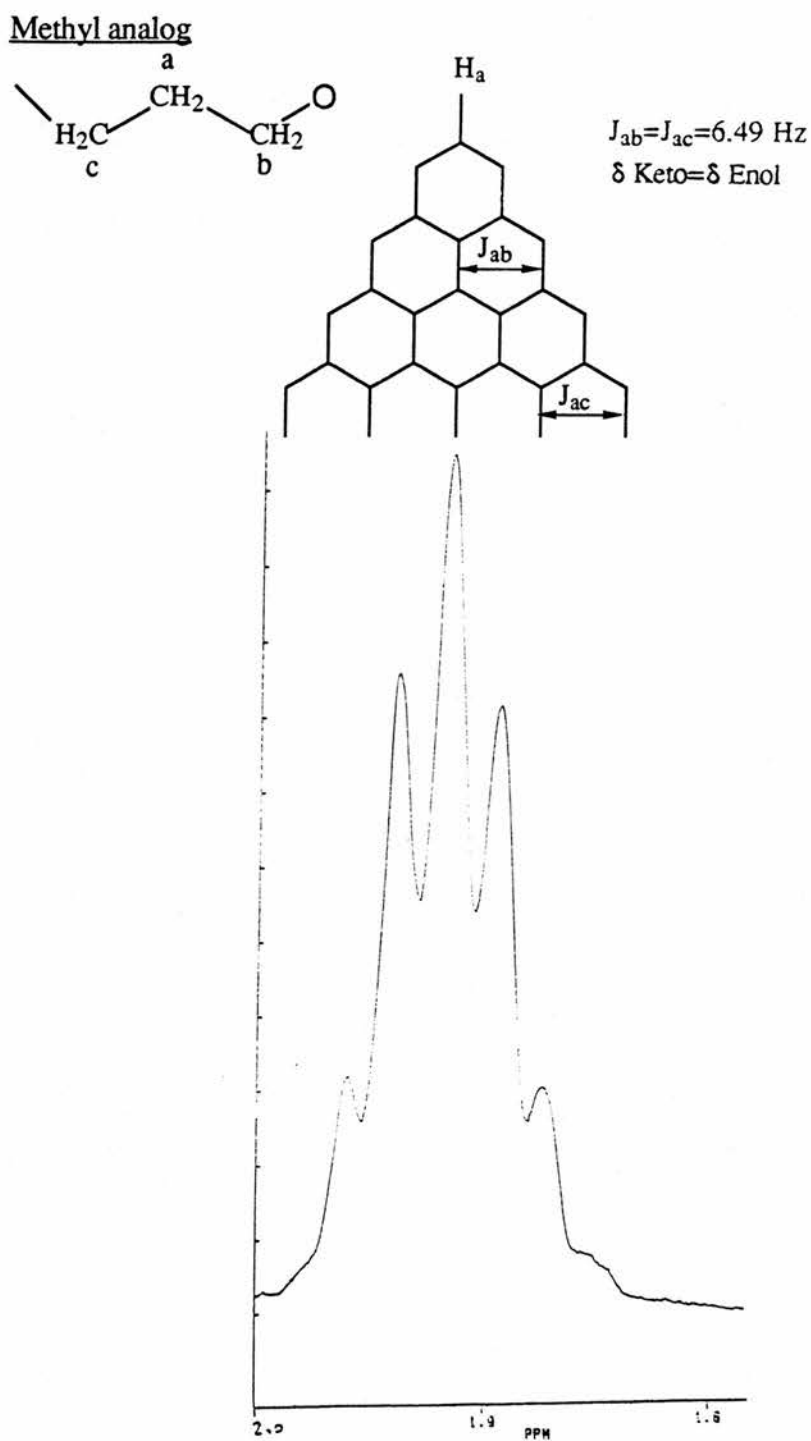
There are four characteristic absorptions in the spectra. These absorptions correspond to $\nu(\text{O-H})$, $(\text{C=O})_{\text{sym}}$, $(\text{C=O})_{\text{asym}}$ and (C=C) . The $\nu(\text{O-H})$ occurs as a broad absorption between the ranges of $3370\text{-}3533\text{ cm}^{-1}$. This gives an indication of the enol form in solution. Similarly, $\nu(\text{C=C})$ at $1619\text{-}1603\text{ cm}^{-1}$ shows the presence of the enol form. The $\nu(\text{C=O})_{\text{sym}}$ and $\nu(\text{C=O})_{\text{asym}}$ occur in the ranges $1727\text{-}1670\text{ cm}^{-1}$. The characteristic absorptions have been investigated in detail by several workers interpreting the IR spectra of simple acac derivatives⁵. (On the basis of the current literature the assignments are given).

3.5. ¹H N.M.R. Data for the ligands

A better technique to observe the keto-enol tautomerism is by using ¹H N.M.R. In many cases the chemical shifts for the keto form differs significantly from that of the enol form so the two tautomers can more easily be identified. In fact, in the cases of all the ligands so far discussed, a single peak corresponding to the enolic methyne group occurs between δ 5.15 and 6.14. This is characteristic of the enol form of the β -diketone. Similarly, a broad OH peak is found between δ 15.47 and 16.18. It is interesting to note, that in the spectrum of 1-(phenyl)-7,10-oxa-undecane the corresponding peaks for the enol methyne and OH groups occur further downfield in the ¹H N.M.R. spectrum than the ^tbutyl, methyl and the mesityl analogs. This may be accounted for by the greater electron-withdrawing effect offered by the phenyl β -substituent. ¹H and ¹³C N.M.R. spectra of the phenyl analog are shown in figs 3.5.c-d, respectively. The ether chain of the ligand gives rise to a series of triplets in the spectrum between δ 3.25-3.57. In this particular case, the resonances from the keto and enol forms overlap due to similar chemical shift. A multipet is observed for the two protons (on C_a in fig 3.5.a) which are sandwiched between two other CH₂ groups.

An expansion of this multiplet at δ 1.91 for the methyl analog shows a quintet, which represents equal coupling to the two adjacent CH_2 groups and equal chemical shifts of the keto and enol forms.

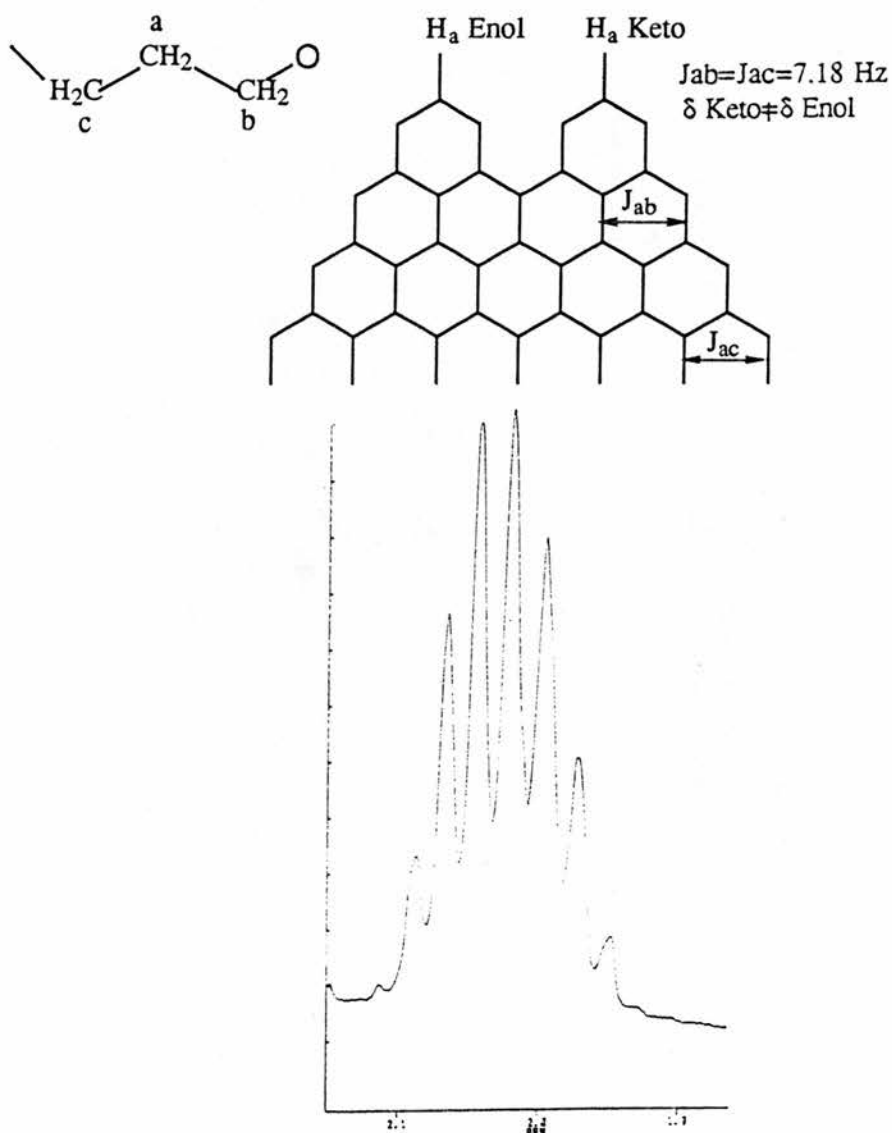
Fig 3.5.a



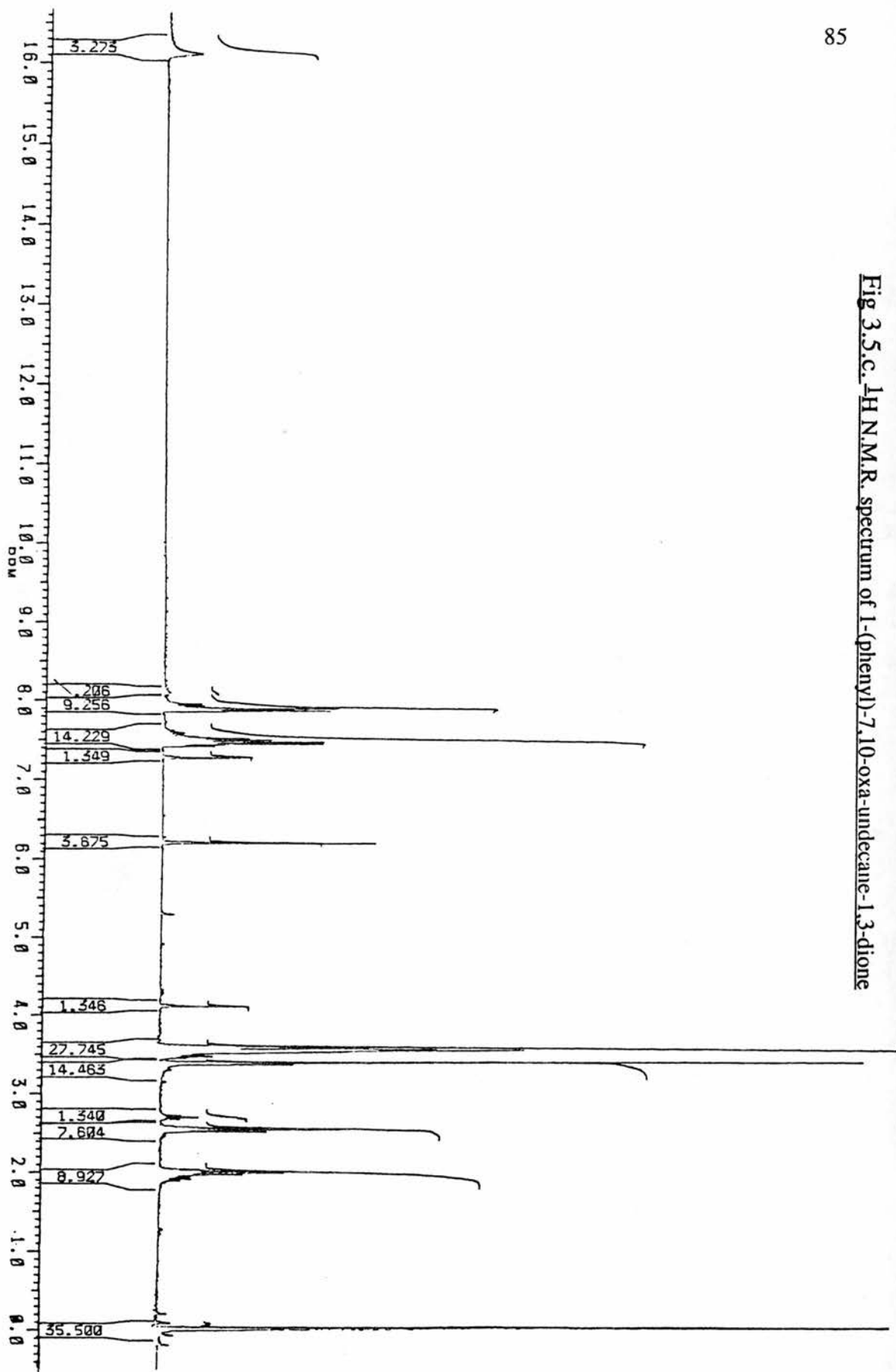
However, seven lines are observed at δ 1.76 (see Fig 3.5.b.) for the same protons in the mesityl analog showing that these hydrogen atoms for the keto and enol forms have slightly different chemical shifts. In this case, the β -diketone exists in 46 % enol form. The chemical shifts of the two protons on carbon atom Cc are different for the keto and enol forms of all scorpion β -diketonate which were examined.

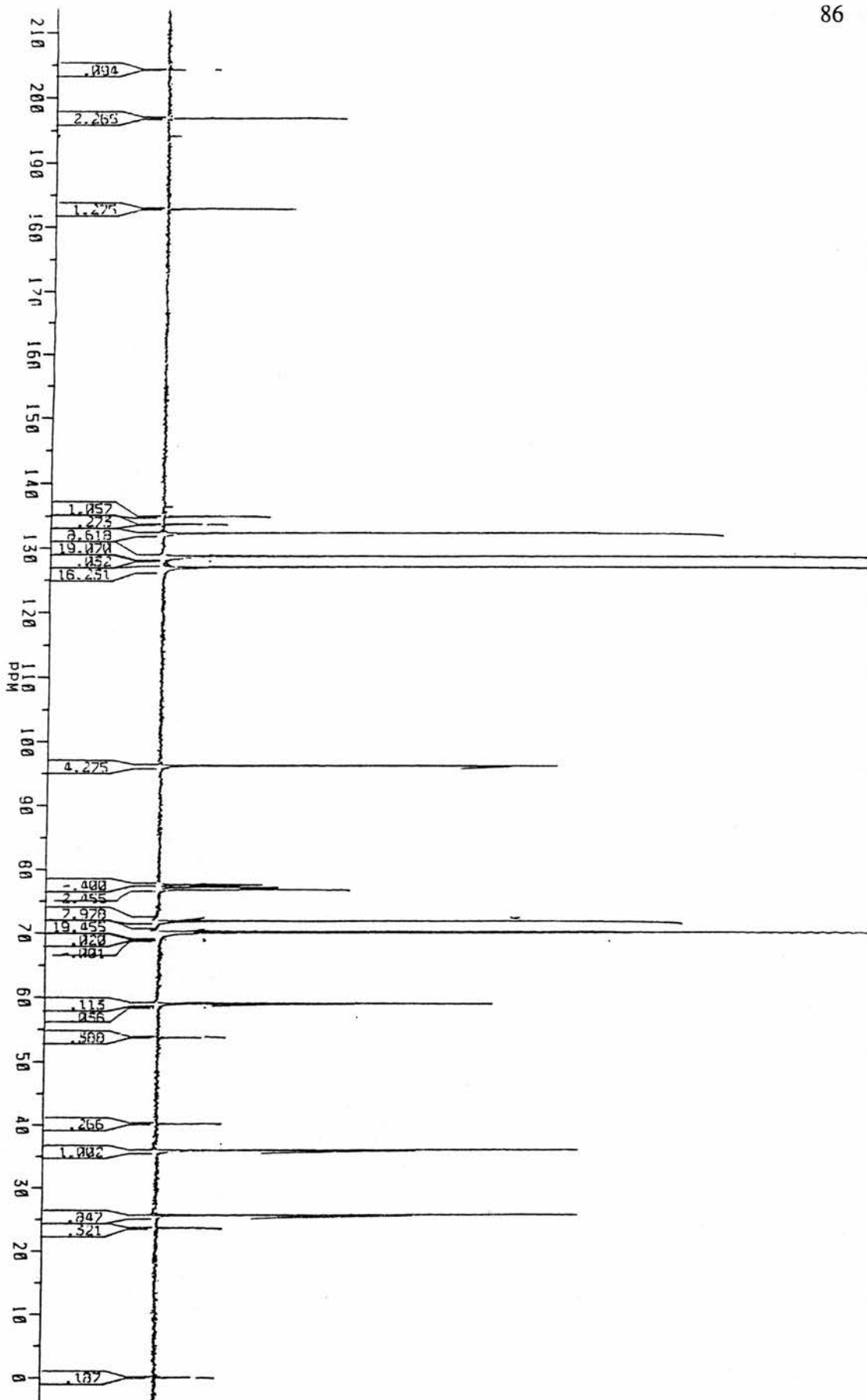
Fig 3.5.b

Mesityl analog



The majority of the other peaks correspond to β -substituent groups which do not need to be discussed in any detail.

Fig 3.5.c. ^1H N.M.R. spectrum of 1-(phenyl)-7,10-oxa-undecane-1,3-dione



3.6. ^{13}C N.M.R Data for the ligands

In the majority of the spectra, the ^{13}C N.M.R shows two peaks for each carbon in the ligand corresponding to keto and enol forms. In the ligands, four peaks are observed in the carbonyl region (δ 182.90-210.42). The methylene carbon between the two carbonyls occurs in a range between δ 95.15 and 102.34. The ether chain carbons resonate between δ 70.02 and 71.96, and the terminal carbon atoms (11C and 14C) at δ 58.98 and 59.04. The most shielded carbon, as with the proton, is the carbon sandwiched between the two CH_2 groups. This occurs at δ 23.39 and 25.55 for the keto and enol forms.

3.7. Microanalysis of the ligands

The microanalysis of the β -diketone ligands are all within experimental error of the proposed empirical formula or of its hemi-hydrate (0.25 - 0.5 H_2O).

3.8. Reactions of the Scorpion tail β -diketones with BaH_2 in toluene

Under anhydrous conditions, HODD, HDOTD, HPOUD, HOPD and HTPOUD were added separately to stirred suspensions of barium (II) hydride in dry toluene. On addition of the ligand some effervescence was observed. After stirring overnight, the suspension was filtered to give a white solid and an orange solution. The toluene was removed from the orange solution to leave an oil (A). The orange oil was dissolved in a minimum amount of methylene chloride, which was then transferred to a stirred solution of petrol. After several washings the excess solvent was then removed to leave oils, in the case of [$\text{Ba}(\text{ODD})_2$], [$\text{Ba}(\text{DOTD})_2$] and [$\text{Ba}(\text{OPD})_2$]; a yellow oily / sticky solid in the case of [$\text{Ba}(\text{POUD})_2$] and a white solid for [$\text{Ba}(\text{TPOUD})_2$].

3.9. IR Data for the barium complexes

Apart from the different β -substituent vibrations, nearly all the barium complexes produced by the toluene method have similar spectra. These include ν (O-H), ν (C-O)_{sym}, ν (C-C)_{sym} and ν (Ba-O). The ν (Ba-O) occurs in the range 460-407 cm^{-1} . This band is absent in the IR spectra of the free ligands, which tell us that a complexation reaction between the ligand and the barium centre has taken place. Strong absorptions in the IR are also observed for ν (C-O)_{sym} in the range 1607-1569 cm^{-1} . The perturbed ν (C-C)_{sym} occurs at 1510-1501 cm^{-1} , respectively. These bands are also absent in the free ligand at this frequency range. The presence of the perturbed C=O and C=C bonds at absorption frequencies lower than those observed for ν (C=O) and ν (C=C) in the free ligand, seem to indicate that complexation has taken place. The frequency shifts are due to the replacement of C=O and C=C bond character by more delocalised character upon chelation. The presence of any excess ligand within the barium complex will be noticed by the absorption frequencies between the ranges of 3533-3370 cm^{-1} . This corresponds to intermolecular H-bonded OH from the enol form of the free ligand which occurs as a broad absorption. No absorption is noticed for [Ba(TPOUD)₂], which was extensively washed with methylene chloride and petrol to remove any excess ligand.

3.1.0. ^1H N.M.R. Data for the barium complexes

The ^1H N.M.R. spectra of all the barium complexes show broad peaks which may be due to the exchange with the free ligand. Low temperature studies have been performed on $[\text{Ba}(\text{POUD})_2]$ in CDCl_3 at -30°C , however the peaks only become broader. The investigation of the barium complexes at room temperature by ^1H N.M.R. seemed to indicate that upon complexation the peaks moved upfield in the spectra relative to the corresponding peaks in the free ligand. This was also noticed in the ^{13}C N.M.R. spectra of the complexes. Apart from the slight upfield shift, the corresponding peaks in the barium complexes occur in similar regions to those of the free ligands. The ^1H and ^{13}C N.M.R. spectra of $[\text{Ba}(\text{POUD})_2]$ are shown in Figs 3.1.0.a-b, respectively.

3.1.1. ^{13}C N.M.R. Data of the barium complexes

As already discussed the peaks in the ^{13}C N.M.R. spectra of the barium complexes seem to move upfield of those of the corresponding free ligand. Furthermore, due to the elimination of keto-enol tautomerism, which exists in the free ligand only, one resonance occurs for each C atom rather than the two for the corresponding free ligand.

Fig 3.1.0.a. ^1H N.M.R. spectrum of [bis(1-(phenyl)-7,10-oxa-undecane-1,3-dionato) barium (II)]

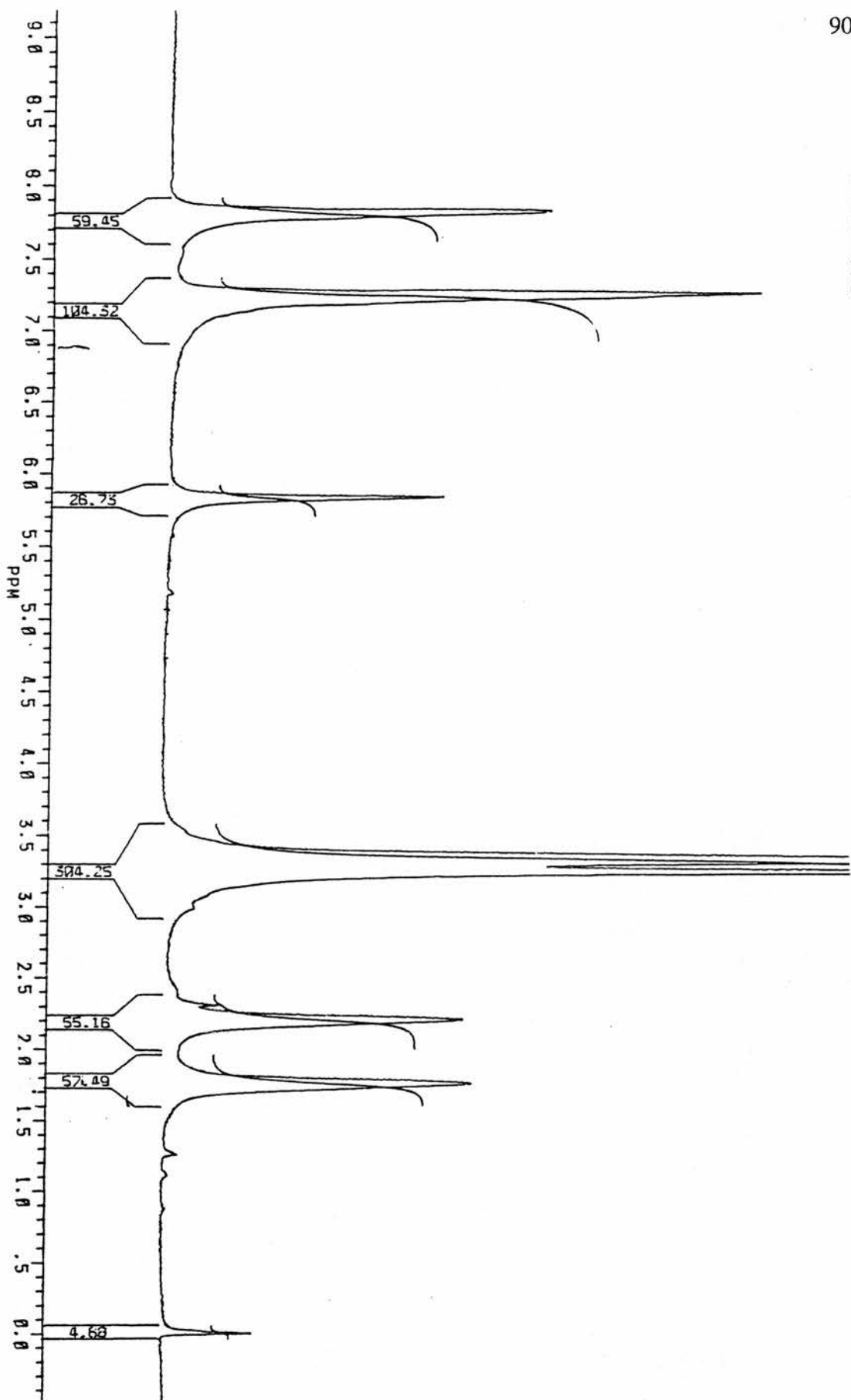
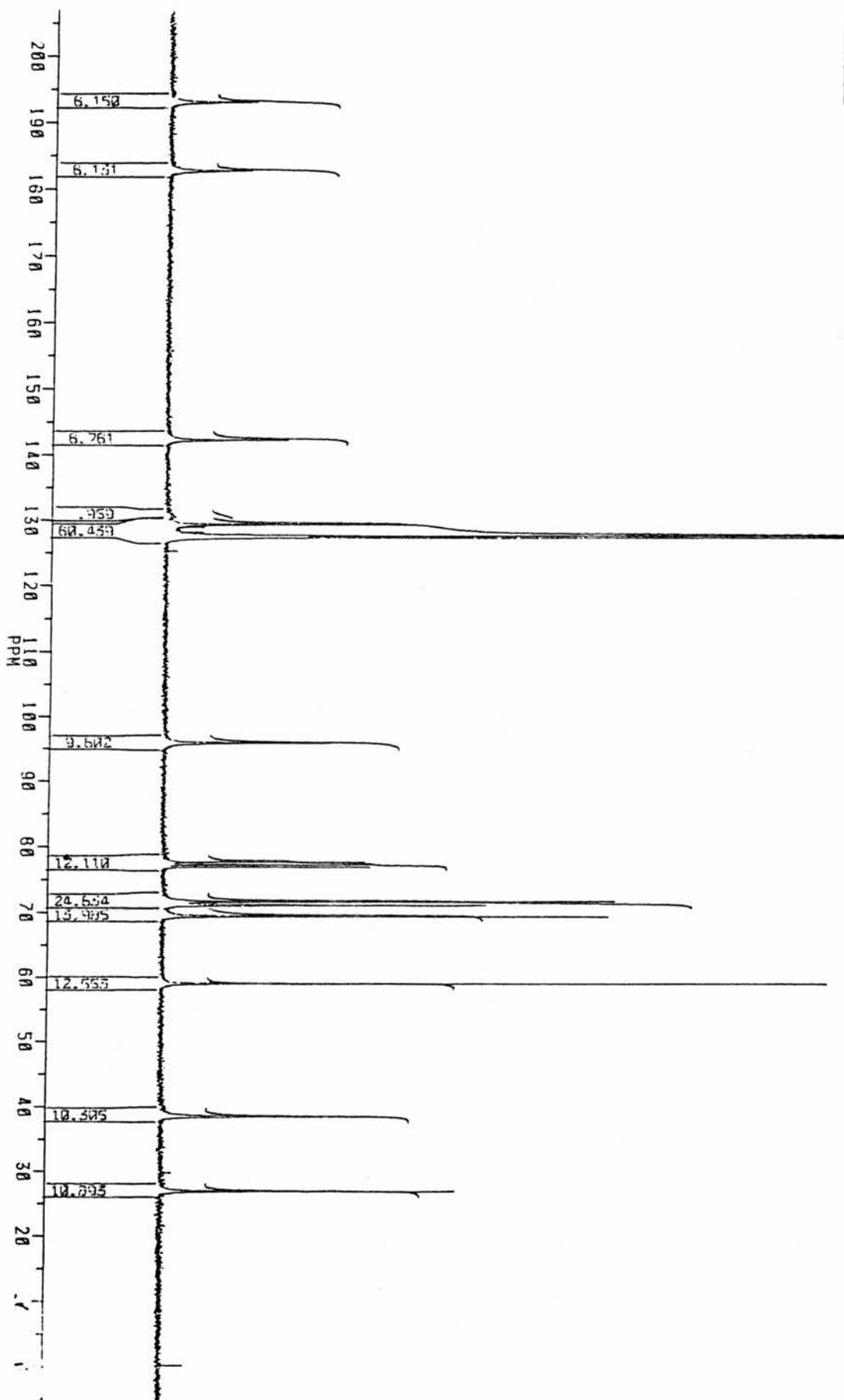


Fig 3.1.0.b. ^{13}C N.M.R. spectrum of [bis[1-(phenyl)-7,10-oxa-undecane-1,3-dionato]barium (II)]



3.1.2. Microanalysis of the barium complexes

The microanalysis seems to suggest that the barium complex has been formed in all cases, but some residual ligand is left behind in most of the complexes. Washing with methylene chloride and petrol seemed to purify the barium complexes. The removal of the free ligand by distillation was not attempted due to the decomposition of the barium complex

The %C and %H analysis of the barium complexes [Ba(TPOUD)₂] and [Ba(POUD)₂] are found to be higher than expected, seeming to indicate the presence of residual ligand. This suggestion seems to be supported by the presence of a broad ν (O-H) between 3465 and 3375 cm^{-1} . However, the IR spectrum of the barium complex, [Ba(TPOUD)₂], shows no peaks corresponding to ν (O-H) or ν (C=O)_{asym} mode, which would be characteristic of the presence of the free ligand. [Ba(DOTD)₂] has the correct microanalysis. Furthermore, for the barium complex, [Ba(ODD)₂] the values for the microanalysis are low compared to the expected values. [Ba(ODD)₂] - (Found %C: 42.53, %H: 6.13, Expected %C: 44.40, %H: 6.30, the free ligand %C: 59.39, %H: 8.96).

3.1.3. STA Analysis

Simultaneous Thermal Analysis (STA) consists of 2 analytical procedures. These are Thermogravimetric Analysis (TGA) and Differential Thermal Analysis (DTA). Thermogravimetric Analysis is where a sample is heated over a temperature range (40-1000°C) and the % mass loss is recorded.

Differential Thermal Analysis monitors any exothermic or endothermic processes taking place whilst the sample is heated over this temperature range. Together they provide a useful tool in investigating the thermal processes taking place within the barium complexes.

In the DTA trace exothermic events are observed as peaks and endothermic events are observed as troughs. Exothermic processes are normally associated with bond-breaking within a compound, such as decomposition. Endothermic processes are normally associated with changes of state, such as melting, boiling and sublimation.

Therefore, sublimation is shown by a trough in the DTA trace accompanied by a % loss of mass in the STA. Decomposition is usually represented by a peak in the DTA trace accompanied by a loss of mass (In the DTA trace of [Cu(POUD)₂] and [Cu(ODD)₂] decomposition is represented by a trough). A discussion about the thermal properties of the barium complexes that were synthesised now follows. Copies of the STA's are shown in the Appendix (section 3.2.1).

3.1.3.1. [Ba(ODD)₂]

Two major exotherms are observed in the DTA trace. These occur at 245°C and 555°C, respectively. The barium complex slowly decomposes when heated from 40-1000°C. The inflexion in the TGA trace at 335°C corresponds to 34% mass loss. The loss of one molecule of ligand would account for 37.45% mass loss. The start of the inflexion in the curve, however, occurs at 29% mass loss which corresponds to the loss of 6,9-oxa-decane-2-one.

In fact, the loss of 6,9-oxa-decane-2-one is supported by ^1H N.M.R. studies on a clear liquid sublimate from $[\text{Ba}(\text{ODD})_2]$ obtained from a sublimation test. The other product in this sublimate is acetone (10.75% mass loss). Unfortunately, the data accumulated from the STA and the sublimation test would tend to show that $[\text{Ba}(\text{ODD})_2]$ is unsuitable for the use in CVD precursor applications because it decomposes before subliming.

3.1.3.2. [Ba(DOTD)₂]

In the DTA of the t butyl analog, six major exotherms are seen at 230, 285, 434, 510, 535 and 725°C. Unfortunately, the six major exotherms all experience an associated mass loss in the TGA trace. The DTA trace shows a small endotherm at 515°C which may be due to slight sublimation. However, there are also two peaks in the DTA trace corresponding to exotherms in this region, so any sublimation may be accompanied by decomposition. On the evidence accumulated, as with the methyl analog, the t butyl analog seems to be unsuitable as a potential CVD precursor.

3.1.3.3. [Ba(POUD)₂]

Three major exotherms are shown in the DTA trace which are accompanied by corresponding mass losses. These exotherms occur at 315, 468 and 632°C. The first recorded mass loss is at 240°C which is accompanied by large exothermic event with a peak at 315°C. Therefore, partial decomposition has taken place. The loss of the ligand would correspond to 39.80% mass loss. Interestingly, the first recorded mass loss at 240°C corresponds to 32% mass loss. The ^1H N.M.R spectrum of liquid sublimate of $[\text{Ba}(\text{POUD})_2]$ seems to indicate the presence of 6,9-oxa-decane-2-one and acetophenone. This would correspond to 24.12 and 42.20% mass loss.

By the presence of these species in the sublimate we can conclude that [Ba(POUD)₂] undergoes decomposition by a similar pathway to that of [Ba(ODD)₂]. The residual mass left at 1000°C is approximately 18%. This is within moderately close agreement with the barium complex decomposing to the barium oxide (23.11%).

From the STA and sublimation test on [Ba(POUD)₂] we can conclude that the barium complex decomposes upon heating and therefore, is not suitable for CVD precursor applications.

3.1.3.4. [Ba(TPOUD)₂]

Two major endotherms are seen in the DTA trace. These occur at 132 and 615°C. At 132°C an endothermic process occurs with no corresponding mass loss, which therefore indicates melting has taken place. This in good accordance with the observed melting point at 137-8°C. Slow decomposition then follows.

The loss of the mesityl ligand corresponds to 40.95% mass loss. Surprisingly, the TGA trace shows 39.22% mass loss at 540°C. After the endotherm at 615°C the barium complex decomposes.

3.1.4. Why are the barium complexes decomposing?

The thermal properties of the barium complexes so far investigated seem to show that they slowly decompose, or decompose near to their melting point. The main reason we think that the barium compounds are not volatile is because the polyether appendages attached to the β - diketone function are simply not coordinating intramolecularly to the barium centre.

The reasons for this :

1 . There may be too much strain generated if the polyether chain were to encapsulate the barium. This is supported by the X-ray crystal structure of [Cu(POUD)₂]; where the ethereal chain is fairly rigid and indeed binds to an adjacent copper atom rather than chelates. - see section 3.1.7.

2 . The terminal polyether oxygen or oxygens may be too far away from the barium centre. In fact, this theory is supported by the findings of Schulz⁶, where the X-ray crystal structure of

[Ba(triki)₂] gave an 8 coordinate barium complex instead of 10 coordinate barium complex. The remote oxygen atom does not bind to the barium atom.

3.1.5. The copper complexes of 8,11-oxa-dodecane-2,4-dione and 1-(phenyl)-7,10-oxa-undecane-1, 3-dione

In order to characterise the ligands fully and investigate the coordination that the ligand exhibits around a metal centre, copper derivatives of 8, 11-oxa-dodecane-2,4-dione and 1-(phenyl)-7,10-oxa-undecane-1,3-dione were synthesised.

3.1.6. The preparation of the copper complexes

The copper complexes were produced by reacting an aqueous solution of copper(II) nitrate with the ligand in an ethanolic / ammoniacal solution. The corresponding copper derivatives were isolated as solids.



Where L = bis-1-(phenyl)-7,10-oxa-undecane-1,3-dione

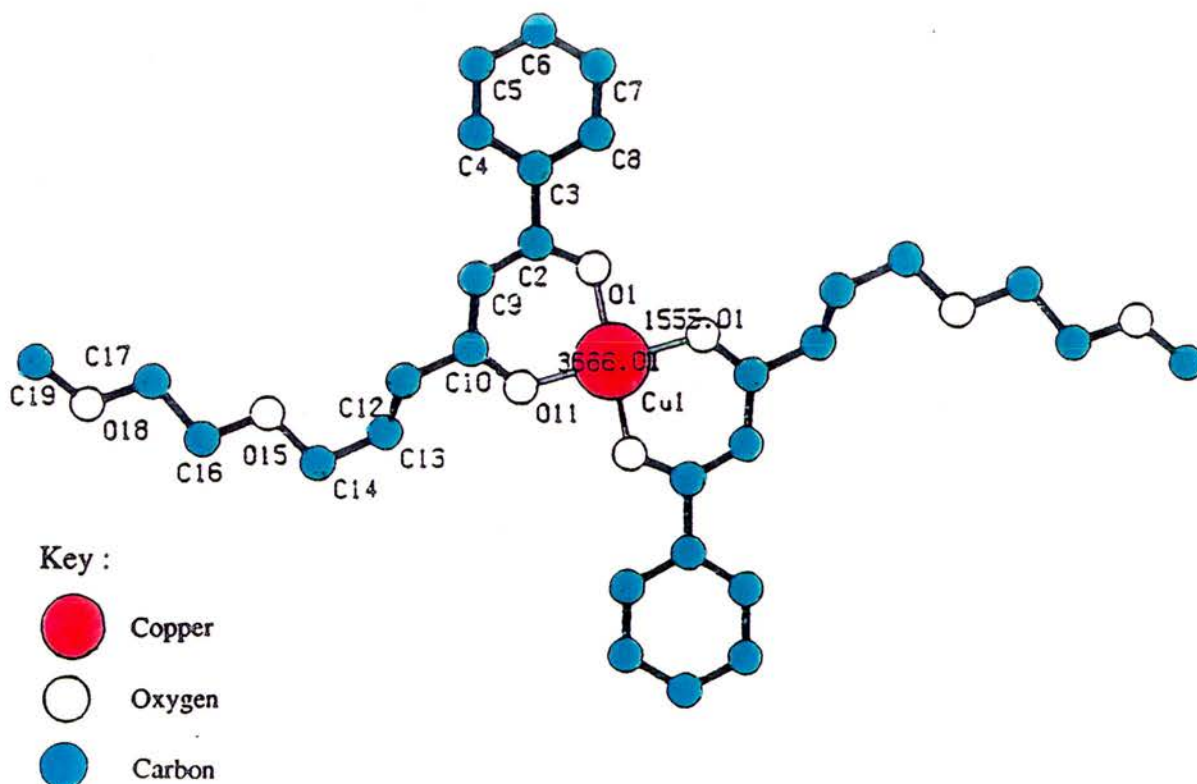
The X-ray crystal structure of [bis{ 1-(phenyl)-7,10-oxa-undecane-1,3-dionato} copper(II)] has been solved. The various parameters, atomic coordinates, bond angles, anisotropic and isotropic displacement parameters are shown in tables 1-6 (section 3.2.0.2). The crystal structure is discussed in section 3.1.7.

3.1.7. The crystal structure of [Cu(POUD)₂]

The X-ray crystal structure of [bis{ 1-(phenyl)-7,10-oxa-undecane-1,3-dionato } copper(II)] was deduced with the help of Dr. John Barnes and Mr John Paton, University of Dundee, Tayside.

Fig 3.1.7.d. shows that [Cu(POUD)₂] is a 1-dimensional, 4+2 Jahn-Teller distorted polymeric solid. A coordination number of 6 is achieved by each copper atom being surrounded by 6 oxygen atoms. 4 oxygen atoms from the two β-diketonate moieties coordinate to give a square planar arrangement. However, two axial coordination sites are taken up by the terminal oxygen atoms from two neighbouring ethereal chains from different molecules within the unit cell. In the structure factor tables (see section 3.2.0.2) the terminal oxygens are represented by O*(18). The length of these Cu(1)-O(18)* ethereal oxygen interactions is quite long at 3.065 Å. However, the O(1)*- Cu(1) - O(18)*2 [85.0° (2)] and the O(11)*- Cu(1) - O(18)*2 [96.6° (2)] bond angles show that the oxygen atoms occupy the axial positions.

Fig 3.1.7.a. Crystal structure of [Cu(POUD)₂] (in the z plane)



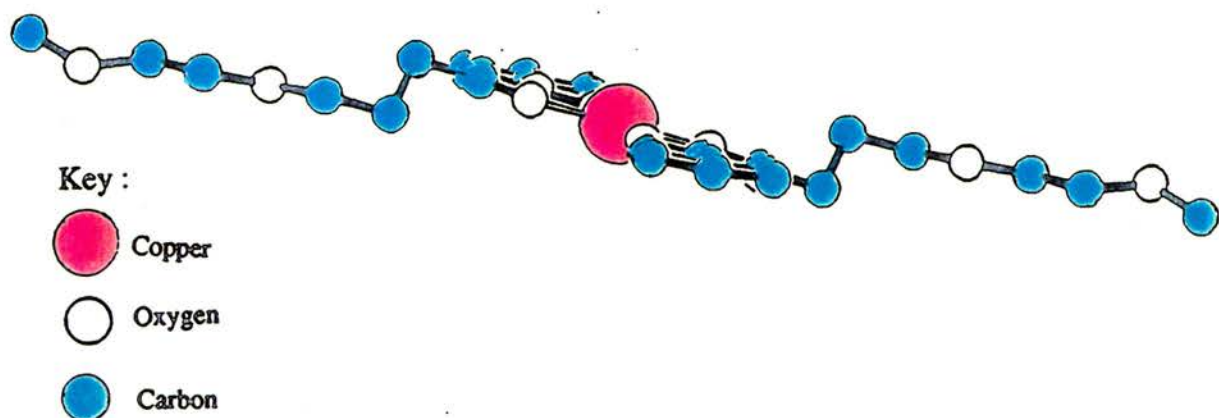
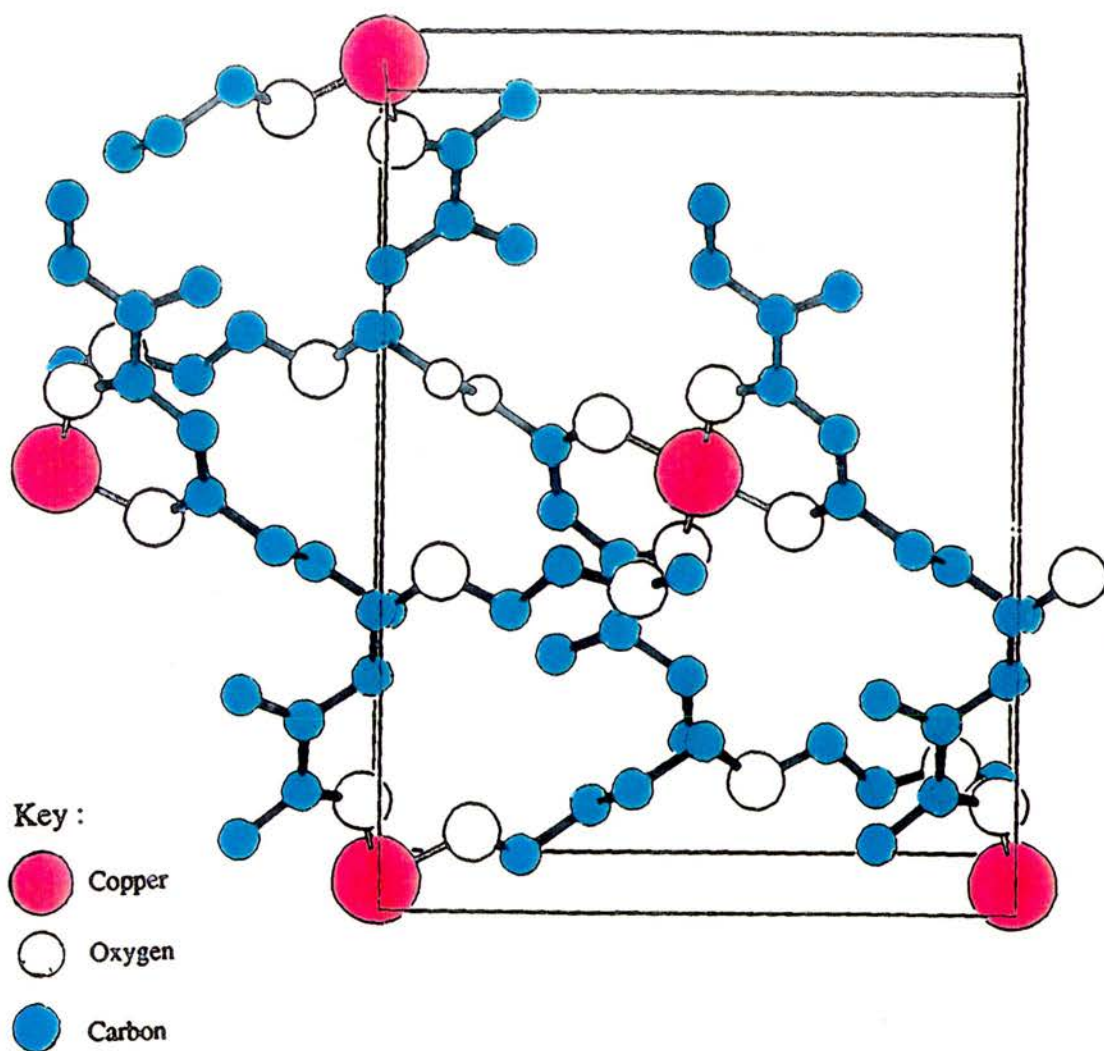


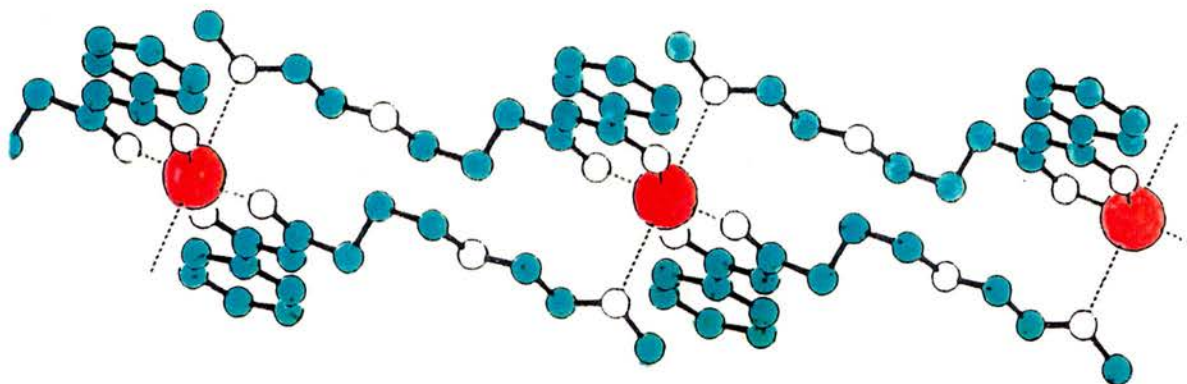
Fig 3.1.7.c. Crystal structure of [Cu(POUD)₂] shown through the unit cell



The restriction in rotation about the C12-C13 (see fig 3.1.7.a) means that no extra intramolecular binding can exist and thus a planar polymeric network exists. In fact, the isotropic displacement parameters show that thermal motion for the ethereal chain is quite small (table 6, section 3.2.0.2.). The smaller the value for $U(\text{eq})$, the more rigid it is. The ethereal chain is fairly rigid with a value of 38 (5). However, the terminal CH_3 groups are fairly flexible with a value of 146 (26).

This unusual polymeric structure is probably the main reason for the decomposition rather than sublimation of not only $[\text{Cu}(\text{POUD})_2]$, but all the barium complexes with scorpion-tails. The intermolecular bonding which arises in $[\text{Cu}(\text{POUD})_2]$ is probably best demonstrated in Fig 3.1.7.d.

Fig 3.1.7.d.



Surprisingly, in the copper complex the phenyl ring does not appear to participate to any great extent in conjugation with the β -diketonate moiety. This is shown by the C-C bond lengths of C2-C3 occurring at 1.510 \AA (8) indicating single bond formation (table 3, section 3.2.0.2.).

A similar copper complex was produced by Rees⁴, who obtained a five coordinate species where the lariat ethereal oxygen is at 2.987 \AA away from the central copper atom of the neighbouring molecule.

The Cu - O distances for Rees copper complex from the β -diketonate moiety are very similar to those experienced in [Cu(acac)₂] and [Cu(POUD)₂].

The Cu-O β -diketonate bond lengths for [Cu(acac)₂]⁷ are at 1.92 Å and the Cu-O β -diketonate bond lengths for [Cu(POUD)₂] are as follows - Cu(1) - O(1),(1)* - 1.919 Å (4), Cu(1) - O(11),(11)* - 1.923 Å (4).

3.1.8. UV / Visible spectrophotometric studies of [Cu(ODD)₂] and [Cu(POUD)₂]

It is known that the symmetry of some copper (II) complexes can be deduced by taking into consideration the UV / visible spectrometric observations of these complexes in solution. The purpose of undertaking UV / visible spectrometric studies on [Cu(POUD)₂] and in particular, [Cu(ODD)₂] was to obtain information regarding the coordination geometry of [Cu(ODD)₂] in solution. Hall and coworkers⁸ reported the correlation between the colour of certain copper(II) complexes and their increased coordination. Belford⁹ reported that the visible absorption bands of copper(II) β -diketonates are more intense and located at lower energy (longer wavelength) in coordinating solvents than non-coordinating solvents. Interestingly, [bis(8,11-oxa-dodecane-2,4-dionato)copper(II)] shows visible d-d transitions at 661.5 nm - $\epsilon_{\max}=38.29 \text{ M}^{-1} \text{ cm}^{-1}$ and 560.2 nm - $\epsilon_{\max}=33.46 \text{ M}^{-1} \text{ cm}^{-1}$ (toluene solution - 0.15 mM) this compared to the phenyl analog with transitions at 652.9 nm - $\epsilon_{\max}=94.92 \text{ M}^{-1} \text{ cm}^{-1}$ and 546.8 nm - $\epsilon_{\max}=91.67 \text{ M}^{-1} \text{ cm}^{-1}$ (toluene solution - 16.94 mM) (see Figs 3.1.8. a-b).

The corresponding copper β -diketonates, [Cu(acac)₂]¹⁰, [Cu(TFAC)₂]¹⁰, [Cu(HFAC)₂]^{10,11}, [Cu(TMHD)₂]¹² and [Cu(ethyl acetoacetate)₂]¹⁰ have been studied for their UV / visible spectrophotometric properties by several workers. In the visible spectrum of [Cu(ethyl acetoacetate)₂] there are 2 broad peaks at 560 and 650 nm (CHCl₃ solution, 10 mM).

In the literature this copper complex is described as a distorted octahedral structure (4+2) with 4 oxygens lying in a plane at 1.89-1.92 Å and the C atoms of the CH₂ group in the adjacent molecule lying at a distance of 3.10 Å from the copper centre. It is a green solid.

By comparison the visible spectrum of [Cu(acac)₂], exhibits two bands at 552 and 660 nm (CHCl₃ solution, 10 mM). However, this is a blue solid. The X-ray crystal structure of [Cu(acac)₂] shows that there is a square planar arrangement of oxygen atoms at 1.92 Å.

Clearly, the above correlations between the colour of the copper complex and geometry around the copper centre are only indicative because the absorption bands for different coordination geometries overlap.

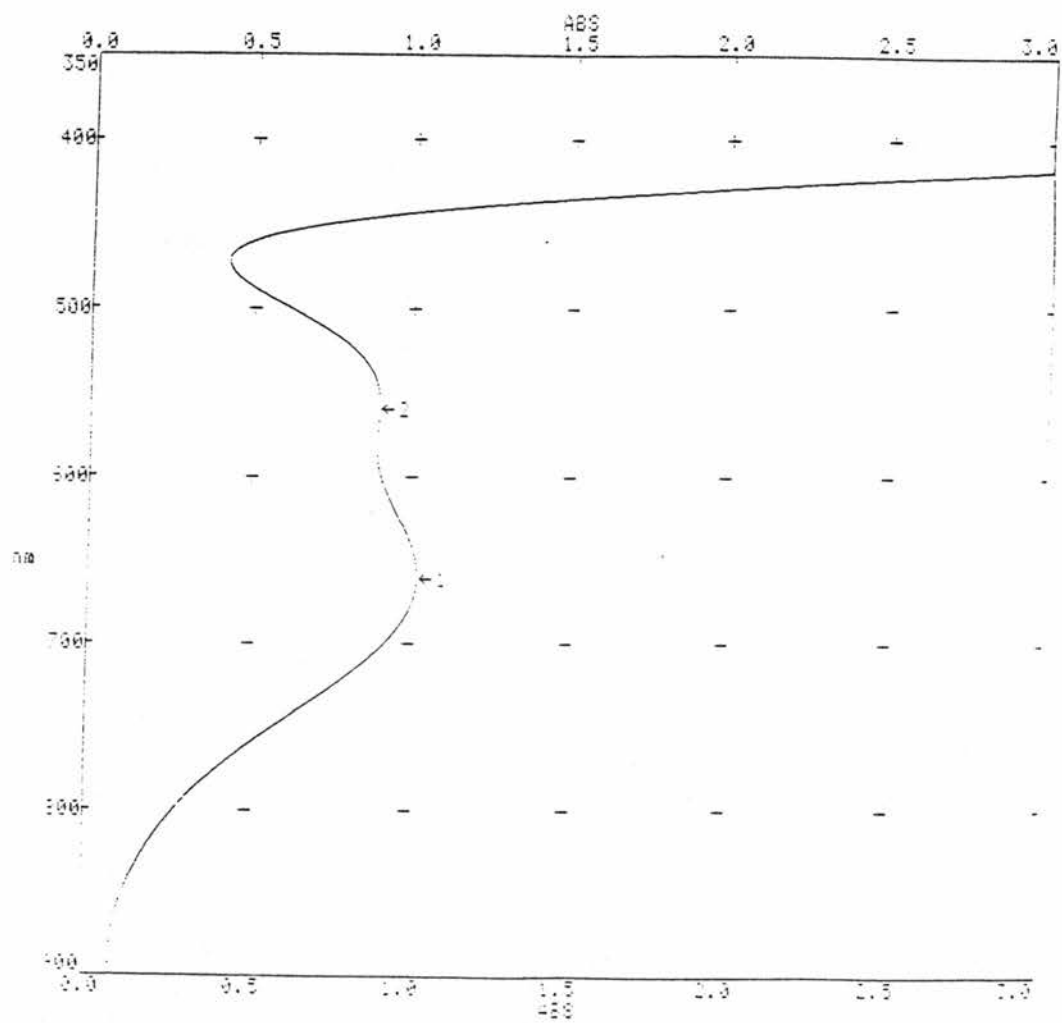
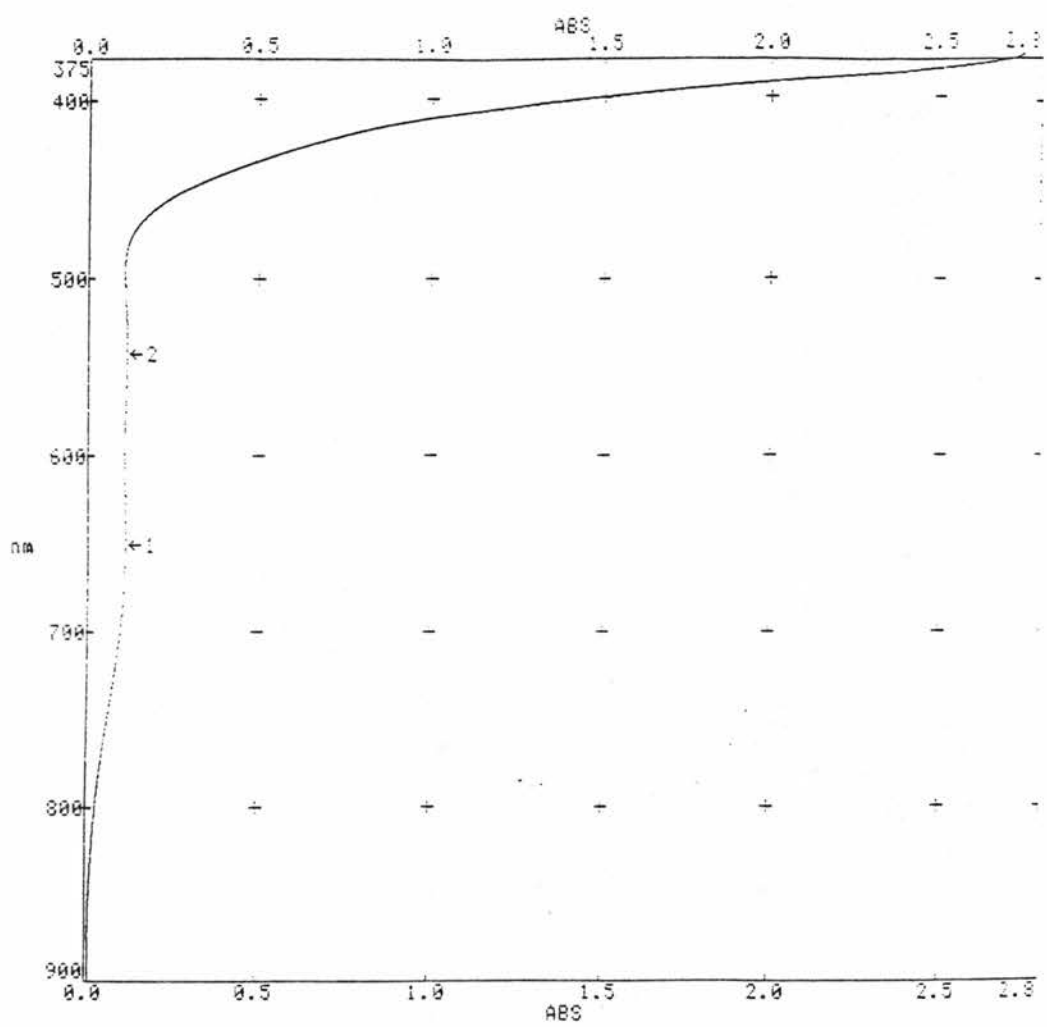


Fig 3.1.9.a. UV/visible spectrum of $[Cu(ODD)_2]$

Fig 3.1.9.b. UV/visible spectrum of $[Cu(POUD)_2]$

3.1.9. STA traces of [Cu(ODD)₂] and [Cu(POUD)₂]

The STA traces for [Cu(ODD)₂] and [Cu(POUD)₂] are contained in the Appendix (section 3.2.1.) .

3.1.9.1. [Cu(ODD)₂]

There are two endotherms at 89°C and 285°C. The first endotherm occurs at 89°C with no associated mass loss which would indicate the melting point of the solid. Indeed this is confirmed by observation of the bulk melting point (85-86°C). The second endotherm at 285°C shows a considerable mass loss with a trough in the DTA trace. After the second endotherm the solid slowly decomposes to its corresponding oxide, (CuO residue 16.68 %) (17.06 % calculated). Sublimation tests conducted at 200°C / 40 Torr (dynamic vacuum) seemed to confirm these results in that no copper complex could be sublimed intact.

3.1.9.2. [Cu(POUD)₂]

Whilst heating from 40°C to 1000°C two major endotherms are observed in the DTA trace. These occur at 70°C and 289°C, respectively.

The TGA at 70°C shows no associated mass loss which must represent the melting point of the solid. The second endotherm at 289°C shows a considerable mass loss and slow decomposes to the corresponding CuO residue 14.09 %, (13.47 % calculated).

Sublimation tests using a woods metal bath to 200°C / 40 Torr (dynamic vacuum) confirmed that this complex was also involatile.

3.2.0. X-ray Structural Determination of [Cu(POUD)₂]

Green platelet crystals were obtained by the slow evaporation of a solution of the [Cu(POUD)₂] in DMSO. After 4 days, sharply defined crystals, fit for X-ray crystallographic studies, were produced. Twinning occurred in 50 % of the crystals. These crystals were air and moisture stable.

From the preliminary X-ray studies using rotation and oscillation photographs and Weissenberg methods we were able to calculate the value of the unit cell volume V, the number of molecules per unit cell, the density of the complex, the size of a (unit cell parameter) and determine the space group.

A crystal of [Cu(POUD)₂] measuring 0.5 x 0.3 x 0.3 mm was sealed in a lindemann glass capillary. Using an Enraf-Nonius CAD 4 diffractometer (SERC service at U.W., Cardiff), 4841 total and 2587 independent reflections [$R_{(int)} = 0.0820$] were collected. The final R indices [$I > 2 \sigma(I)$] $R_1 = 0.0648$, $wR_2 = 0.1541$. R indices (all data) $R_1 = 0.1246$, $wR_2 = 0.2208$.

The data was collected from $2.30^\circ < \theta < 26.83^\circ$ for the index ranges $-10 \leq h \leq 9$, $-13 \leq k \leq 8$, $-16 \leq l \leq 14$.

3.2.0.1. Crystallographic data

Formula = C₃₀H₃₈CuO₈ $M_r = 590.14$. Monoclinic, $P2_1/C$, $a = 9.109(9) \text{ \AA}$, $b = 11.189(8) \text{ \AA}$, $c = 14.453(6) \text{ \AA}$, $\beta = 103.64^\circ(9)$. $V = 1432(2) \text{ \AA}^3$, $Z = 2$, $D = 1.369 \text{ Mgm}^{-3}$, $(MoK\alpha) = 0.71069 \text{ \AA}$, $\lambda = 0.812 \text{ mm}^{-1}$, $F(000) = 622$, $T = 293(2) \text{ K}$.

3.2.0.2.1.

Identification code	jn69
Empirical formula	C30 H38 Cu O8
Formula weight	590.14
Temperature	293(2) K
Wavelength	0.71069 Å
Crystal system	Monoclinic
Space group	P2 ₁ /C
Unit cell dimensions	a = 9.109(9) Å alpha = 90 deg. b = 11.189(8) Å beta = 103.64(9) de c = 14.453(6) Å gamma = 90 deg.
Volume	1432(2) Å ³
Z	2
Density (calculated)	1.369 Mg/m ³
Absorption coefficient	0.812 mm ⁻¹
F(000)	622
Crystal size	0.5 x 0.3 x 0.3
Theta range for data collection	2.30 to 26.83 deg.
Index ranges	-10<=h<=9, -13<=k<=8, -16<=l<=14
Reflections collected	4841
Independent reflections	2587 [R(int) = 0.0820]
Refinement method	Full-matrix least-squares on F ²
Data / restraints / parameters	2587 / 0 / 182
Goodness-of-fit on F ²	0.554
Final R indices [I>2sigma(I)]	R1 = 0.0648, wR2 = 0.1541
R indices (all data)	R1 = 0.1246, wR2 = 0.2208
Largest diff. peak and hole	0.857 and -0.294 e.Å ⁻³

3.2.0.2.2. Atomic coordinates ($\times 10^4$) and equivalent isotropic displacement parameters ($\text{\AA}^2 \times 10^3$) for 1. $U(\text{eq})$ is defined as one third of the trace of the orthogonalized U_{ij} tensor.

	x	y	z	$U(\text{eq})$
Cu(1)	5000	0	0	47(1)
O(1)	3348(5)	236(3)	-1086(3)	41(1)
C(2)	2528(6)	1184(5)	-1257(4)	33(1)
C(3)	1379(6)	1168(5)	-2200(4)	33(1)
C(4)	497(8)	2160(6)	-2563(4)	54(2)
C(5)	-566(9)	2121(6)	-3429(4)	59(2)
C(6)	-747(7)	1058(6)	-3954(4)	49(2)
C(7)	163(7)	67(5)	-3630(4)	40(1)
C(8)	1219(7)	118(5)	-2765(4)	34(1)
C(9)	2629(7)	2165(5)	-649(4)	41(1)
C(10)	3696(7)	2288(5)	229(4)	41(1)
O(11)	4711(5)	1506(3)	573(3)	49(1)
C(12)	3638(6)	3382(5)	836(4)	36(1)
C(13)	5132(7)	4015(5)	1136(4)	41(1)
C(14)	5093(7)	5130(5)	1718(4)	38(1)
O(15)	4037(4)	5967(3)	1166(3)	37(1)
C(16)	4026(8)	7074(5)	1626(4)	47(2)
C(17)	2819(9)	7871(6)	1003(5)	60(2)
O(18)	3035(6)	9041(4)	1288(4)	83(2)
C(19)	1768(9)	9791(6)	1008(7)	74(2)

Cu(1)-O(1)	1.919(4)
Cu(1)-O(1)#1	1.919(4)
Cu(1)-O(11)#1	1.923(4)
Cu(1)-O(11)	1.923(4)
Cu(1)-O(18)#2	3.065(7)
Cu(1)-O(18)#3	3.065(7)
O(1)-C(2)	1.287(6)
C(2)-C(9)	1.396(8)
C(2)-C(3)	1.510(8)
C(3)-C(4)	1.397(8)
C(3)-C(8)	1.419(7)
C(4)-C(5)	1.391(9)
C(5)-C(6)	1.400(9)
C(6)-C(7)	1.398(8)
C(7)-C(8)	1.387(8)
C(9)-C(10)	1.412(8)
C(10)-O(11)	1.285(7)
C(10)-C(12)	1.514(7)
C(12)-C(13)	1.504(8)
C(13)-C(14)	1.510(7)
C(14)-O(15)	1.442(6)
O(15)-C(16)	1.408(6)
C(16)-C(17)	1.532(9)
C(17)-O(18)	1.373(7)
O(18)-C(19)	1.406(8)
O(18)-Cu(1)#4	3.065(7)
O(1)-Cu(1)-O(11)#1	85.9(2)
O(1)-Cu(1)-O(11)	94.1(2)
O(1)-Cu(1)-O(18)#2	95.0(2)
O(1)#1-Cu(1)-O(18)#2	85.0(2)
O(11)#1-Cu(1)-O(18)#2	96.6(2)
O(11)-Cu(1)-O(18)#2	83.4(2)
C(2)-O(1)-Cu(1)	125.3(4)
O(1)-C(2)-C(9)	125.3(5)
O(1)-C(2)-C(3)	114.3(5)
C(9)-C(2)-C(3)	120.4(5)
C(2)-C(9)-C(10)	124.9(6)
O(11)-C(10)-C(9)	124.2(5)
O(11)-C(10)-C(12)	116.5(5)
C(9)-C(10)-C(12)	119.3(5)
C(10)-O(11)-Cu(1)	126.1(4)
C(13)-C(12)-C(10)	113.2(5)
C(12)-C(13)-C(14)	114.3(5)
O(15)-C(14)-C(13)	109.1(4)
C(16)-O(15)-C(14)	112.9(4)
O(15)-C(16)-C(17)	108.6(5)
O(18)-C(17)-C(16)	110.3(5)
C(17)-O(18)-C(19)	115.6(6)
C(17)-O(18)-Cu(1)#4	102.3(5)
C(19)-O(18)-Cu(1)#4	100.0(4)

Symmetry transformations used to generate equivalent atoms:

#1 -x+1, -y, -z #2 x, y-1, z #3 -x+1, -y+1, -z

#4 x, y+1, z

3.2.0.2.4. Bond lengths [Å] and angles [deg] for [Cu(POUD)₂]

Cu(1)-O(1)	1.919(4)
Cu(1)-O(1)#1	1.919(4)
Cu(1)-O(11)#1	1.923(4)
Cu(1)-O(11)	1.923(4)
Cu(1)-C(2)	2.863(6)
Cu(1)-C(2)#1	2.863(6)
Cu(1)-C(10)	2.874(6)
Cu(1)-C(10)#1	2.874(6)
Cu(1)-O(18)#2	3.065(7)
Cu(1)-O(18)#3	3.065(7)
O(1)-C(2)	1.287(6)
C(2)-C(9)	1.396(8)
C(2)-C(3)	1.510(8)
C(3)-C(4)	1.397(8)
C(3)-C(8)	1.419(7)
C(4)-C(5)	1.391(9)
C(5)-C(6)	1.400(9)
C(6)-C(7)	1.398(8)
C(7)-C(8)	1.387(8)
C(9)-C(10)	1.412(8)
C(10)-O(11)	1.285(7)
C(10)-C(12)	1.514(7)
C(12)-C(13)	1.504(8)
C(13)-C(14)	1.510(7)
C(14)-O(15)	1.442(6)
O(15)-C(16)	1.408(6)
C(16)-C(17)	1.532(9)
C(17)-O(18)	1.373(7)
O(18)-C(19)	1.406(8)
O(18)-Cu(1)#4	3.065(7)
O(1)-Cu(1)-O(1)#1	180.0
O(1)-Cu(1)-O(11)#1	85.9(2)
O(1)#1-Cu(1)-O(11)#1	94.1(2)
O(1)-Cu(1)-O(11)	94.1(2)
O(1)#1-Cu(1)-O(11)	85.9(2)
O(11)#1-Cu(1)-O(11)	180.0

O(1)-C(2)-C(9)	125.3(5)
O(1)-C(2)-C(3)	114.3(5)
C(9)-C(2)-C(3)	120.4(5)
O(1)-C(2)-Cu(1)	33.2(2)
C(9)-C(2)-Cu(1)	92.2(4)
C(3)-C(2)-Cu(1)	147.3(4)
C(4)-C(3)-C(8)	118.0(5)
C(4)-C(3)-C(2)	123.0(5)
C(8)-C(3)-C(2)	119.0(5)
C(5)-C(4)-C(3)	121.9(6)
C(4)-C(5)-C(6)	118.9(6)
C(7)-C(6)-C(5)	120.5(6)
C(8)-C(7)-C(6)	120.0(5)
C(7)-C(8)-C(3)	120.5(5)
C(2)-C(9)-C(10)	124.9(6)
O(11)-C(10)-C(9)	124.2(5)
O(11)-C(10)-C(12)	116.5(5)
C(9)-C(10)-C(12)	119.3(5)
O(11)-C(10)-Cu(1)	32.7(2)
C(9)-C(10)-Cu(1)	91.4(4)
C(12)-C(10)-Cu(1)	149.2(4)
C(10)-O(11)-Cu(1)	126.1(4)
C(13)-C(12)-C(10)	113.2(5)
C(12)-C(13)-C(14)	114.3(5)
O(15)-C(14)-C(13)	109.1(4)
C(16)-O(15)-C(14)	112.9(4)
O(15)-C(16)-C(17)	108.6(5)
O(18)-C(17)-C(16)	110.3(5)
C(17)-O(18)-C(19)	115.6(6)
C(17)-O(18)-Cu(1)#4	102.3(5)
C(19)-O(18)-Cu(1)#4	100.0(4)

Symmetry transformations used to generate equivalent atoms:

#1 -x+1,-y,-z #2 x,y-1,z #3 -x+1,-y+1,-z
 #4 x,y+1,z

3.2.0.2.5.

Anisotropic displacement parameters ($A^2 \times 10^3$)
 The anisotropic displacement factor exponent takes the form:
 $-2 \pi^2 [h^2 a^2 U_{11} + \dots + 2 h k a^* b^* U_{12}]$

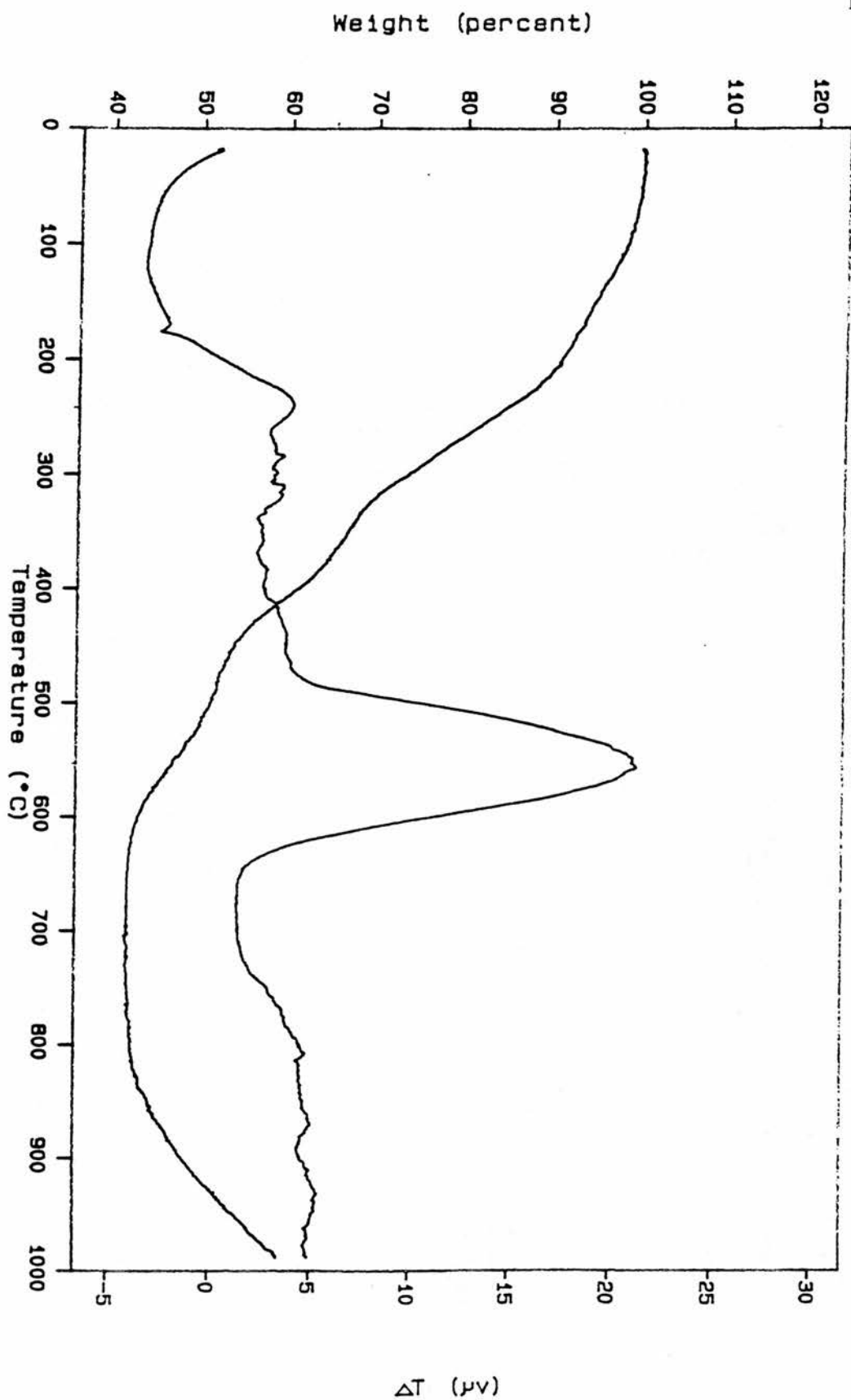
	U11	U22	U33	U23	U13	U12
Cu(1)	53(1)	32(1)	46(1)	-8(1)	-12(1)	11(1)
O(1)	45(2)	35(2)	38(2)	-7(2)	-3(2)	10(2)
C(2)	39(3)	26(3)	36(3)	4(2)	11(2)	-7(2)
C(3)	38(3)	28(3)	34(3)	8(2)	9(2)	-9(2)
C(4)	83(5)	40(4)	31(3)	-4(3)	-5(3)	14(3)
C(5)	80(5)	56(5)	33(4)	1(3)	-5(3)	21(4)
C(6)	55(4)	59(4)	28(3)	1(3)	0(3)	-3(3)
C(7)	46(4)	37(4)	35(3)	-7(2)	3(2)	1(3)
C(8)	41(3)	28(3)	31(3)	-3(2)	4(2)	6(2)
C(9)	55(4)	30(3)	33(3)	0(2)	0(3)	2(3)
C(10)	52(4)	33(4)	31(3)	2(2)	-2(3)	0(3)
O(11)	58(3)	38(3)	40(2)	-6(2)	-11(2)	9(2)
C(12)	38(3)	34(3)	39(3)	-4(2)	11(2)	15(2)
C(13)	63(4)	32(3)	22(3)	4(2)	1(2)	4(3)
C(14)	52(4)	36(3)	22(3)	-3(2)	1(2)	12(3)
O(15)	54(3)	26(2)	33(2)	-2(2)	12(2)	2(2)
C(16)	68(4)	29(3)	40(3)	-5(3)	7(3)	-4(3)
C(17)	74(5)	35(4)	61(4)	-13(3)	-6(4)	-9(3)
O(18)	68(4)	50(3)	108(5)	-6(3)	-21(3)	12(3)
C(19)	63(5)	70(6)	93(6)	20(4)	27(5)	27(4)

3.2.0.2.6. Hydrogen coordinates ($\times 10^4$) and isotropic displacement parameters ($\text{\AA}^2 \times 10^3$) for $[\text{Cu}(\text{POUD})_2]$

	x	y	z	U(eq)
H(4)	624(8)	2867(6)	-2214(4)	55(8)
H(5)	-1146(9)	2790(6)	-3655(4)	55(8)
H(6)	-1479(7)	1011(6)	-4523(4)	55(8)
H(7)	61(7)	-627(5)	-3994(4)	55(8)
H(8)	1826(7)	-542(5)	-2553(4)	55(8)
H(9)	1941(7)	2783(5)	-836(4)	44(17)
H(12A)	2893(6)	3934(5)	482(4)	38(5)
H(12B)	3311(6)	3142(5)	1401(4)	38(5)
H(13A)	5471(7)	4228(5)	570(4)	38(5)
H(13B)	5867(7)	3466(5)	1504(4)	38(5)
H(14A)	4788(7)	4929(5)	2298(4)	38(5)
H(14B)	6092(7)	5485(5)	1892(4)	38(5)
H(16A)	5009(8)	7452(5)	1723(4)	38(5)
H(16B)	3800(8)	6957(5)	2243(4)	38(5)
H(17A)	2874(9)	7801(6)	343(5)	38(5)
H(17B)	1824(9)	7610(6)	1050(5)	38(5)
H(19A)	2029(9)	10585(6)	1240(7)	146(26)
H(19B)	961(9)	9494(6)	1267(7)	146(26)
H(19C)	1451(9)	9804(6)	326(7)	146(26)

3.2.1. APPENDIX

a) STA data on the barium and copper complexes

Fig 3.2.1.1.a. STA - [Ba(ODD)₂]

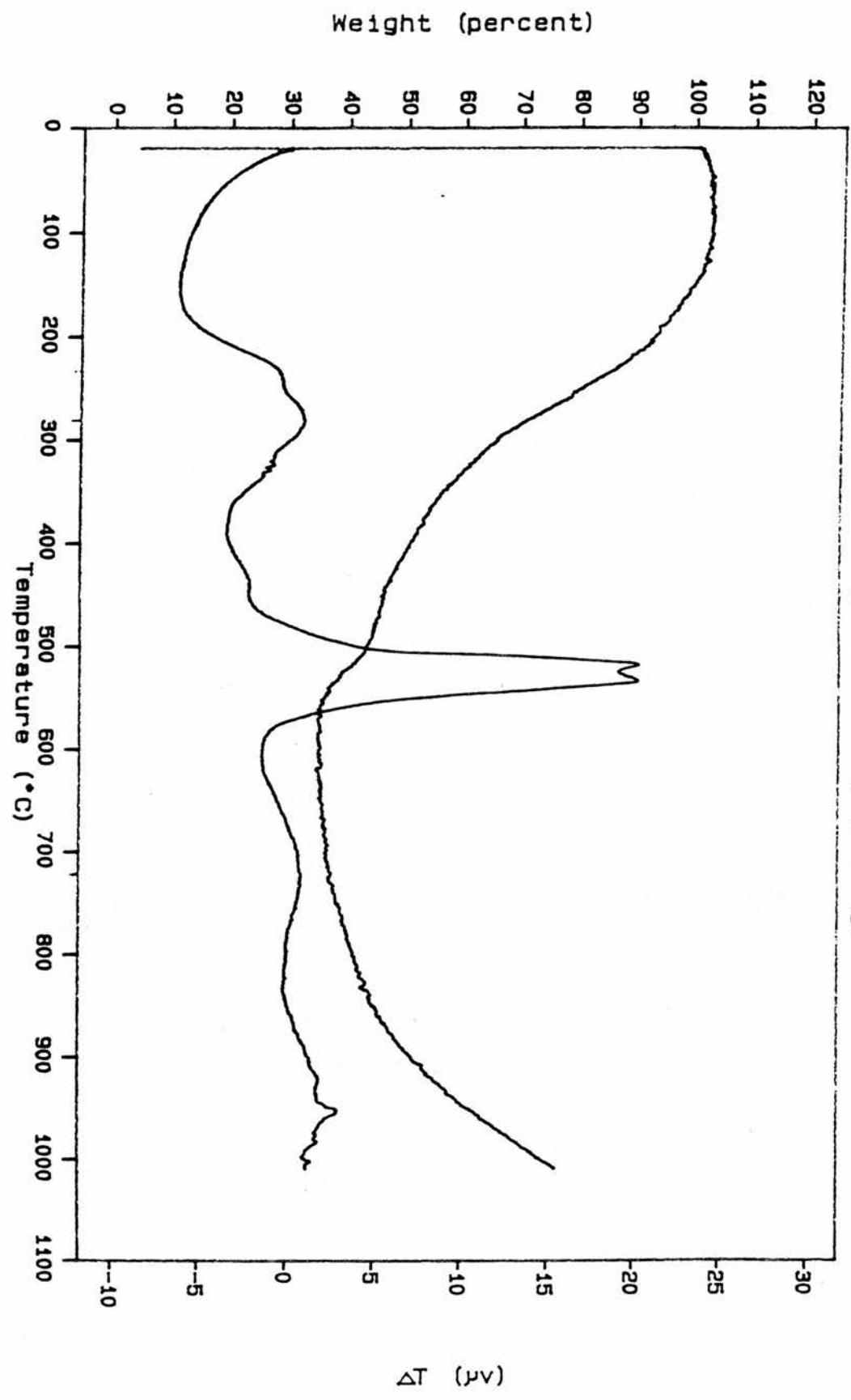


Fig 3.2.1.2.a. STA - [Ba(DOTD)₂]

Weight (percent)

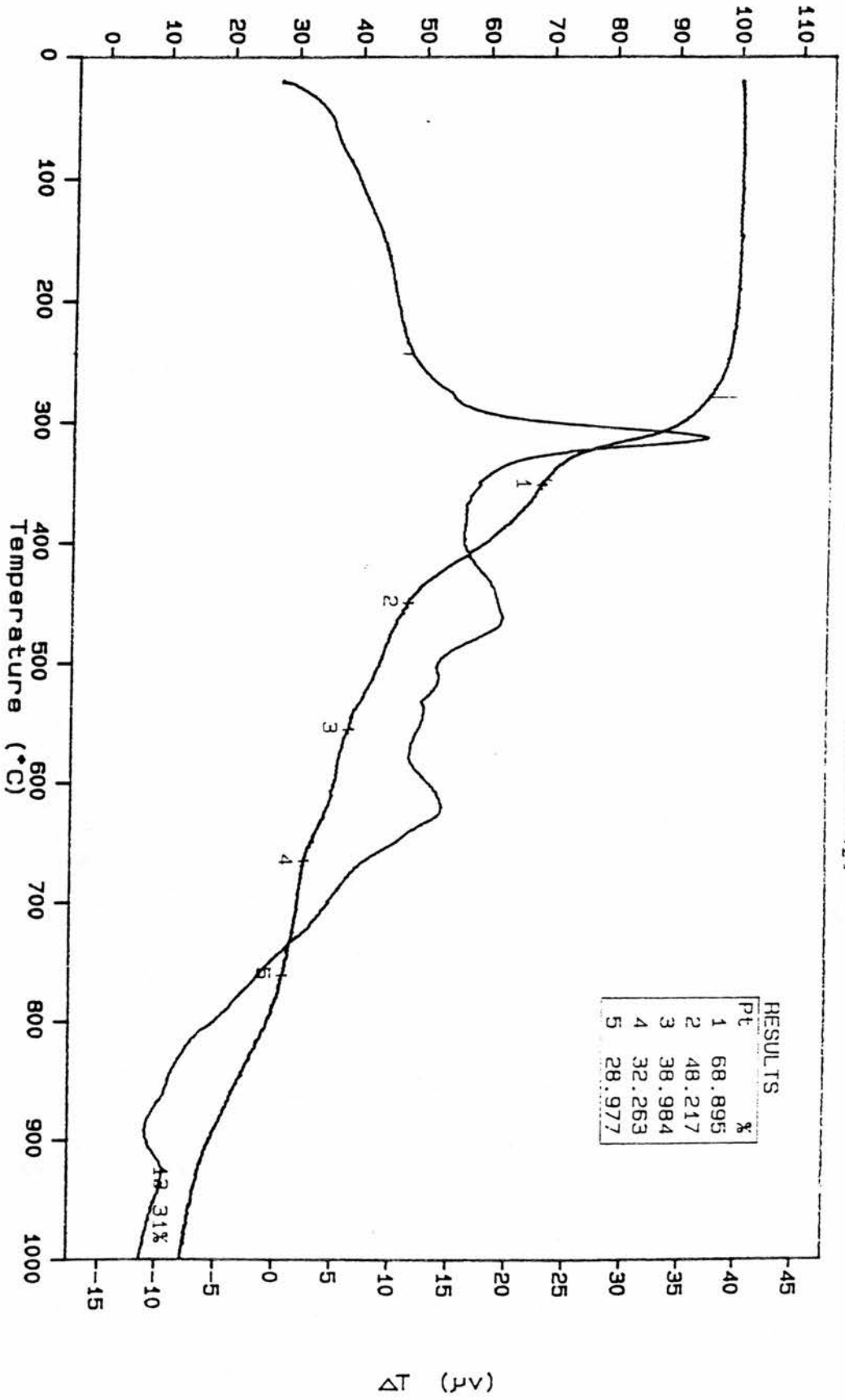
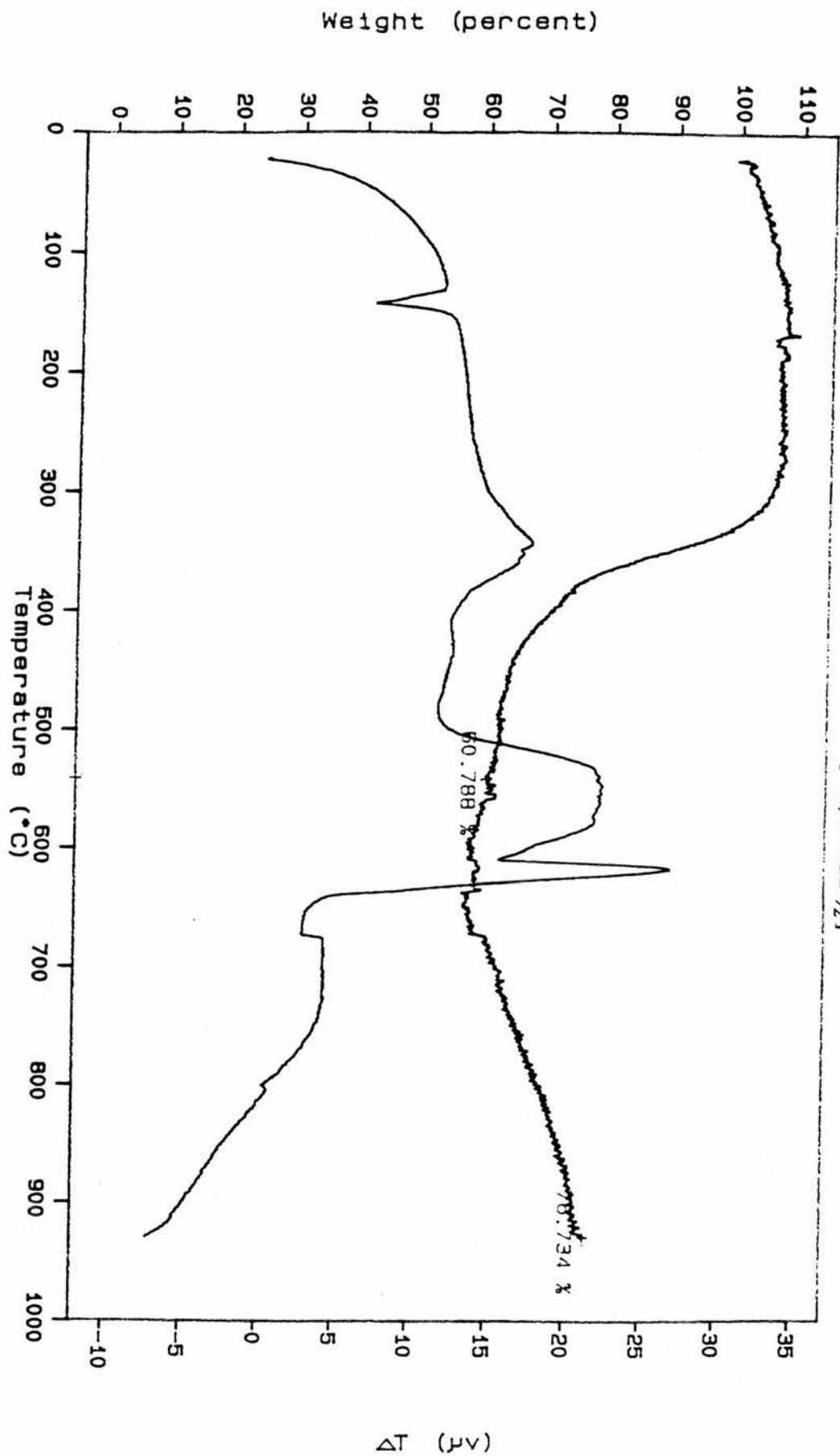


Fig.3.2.1.3.a. STA - [Ba(POUD)₂]

Fig 3.2.1.4.a. STA - [Ba(TPOUD)₂]

Weight (percent)

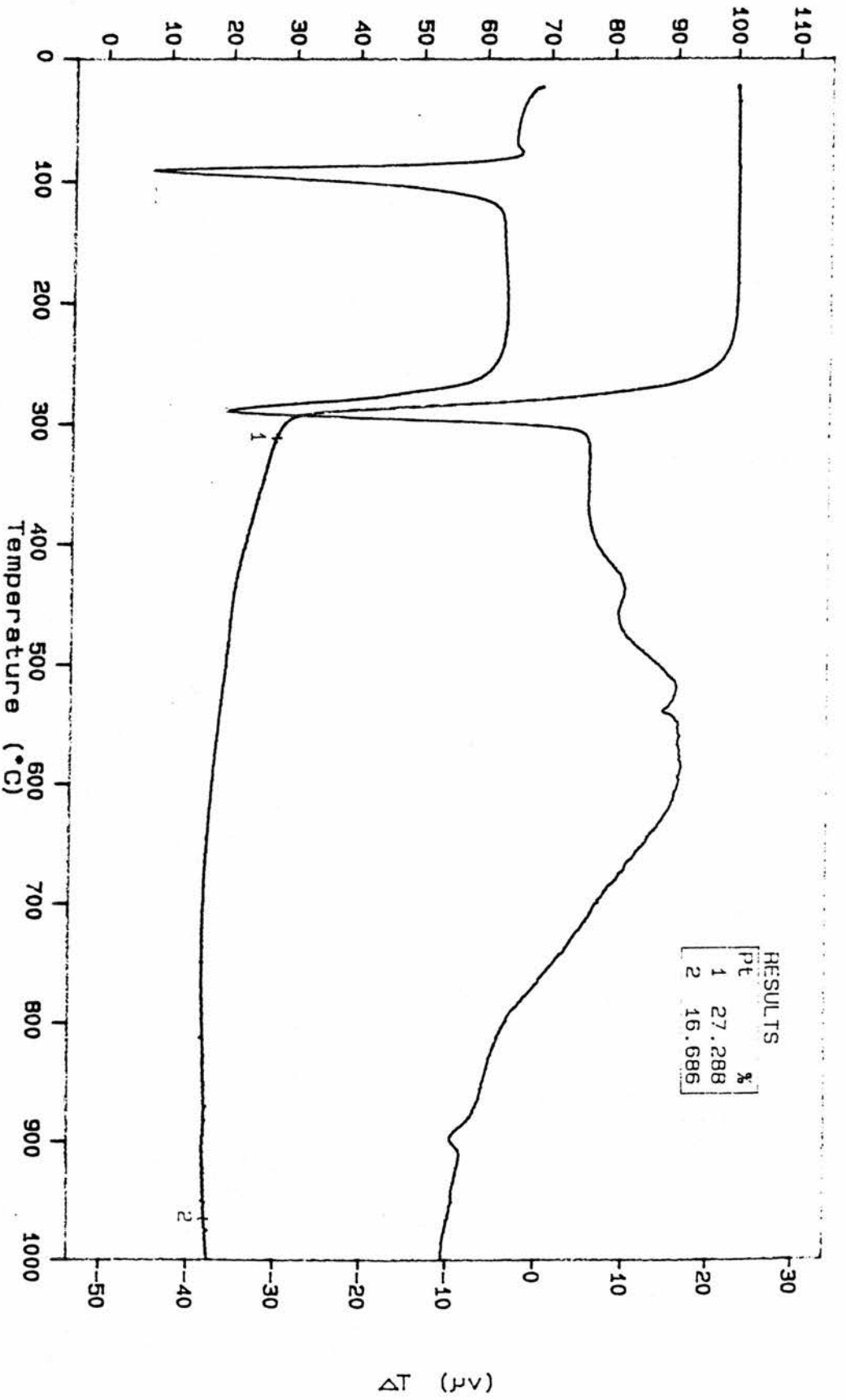


Fig 3.2.1.5.a. STA - [Cu(ODD)₂]

Weight (percent)

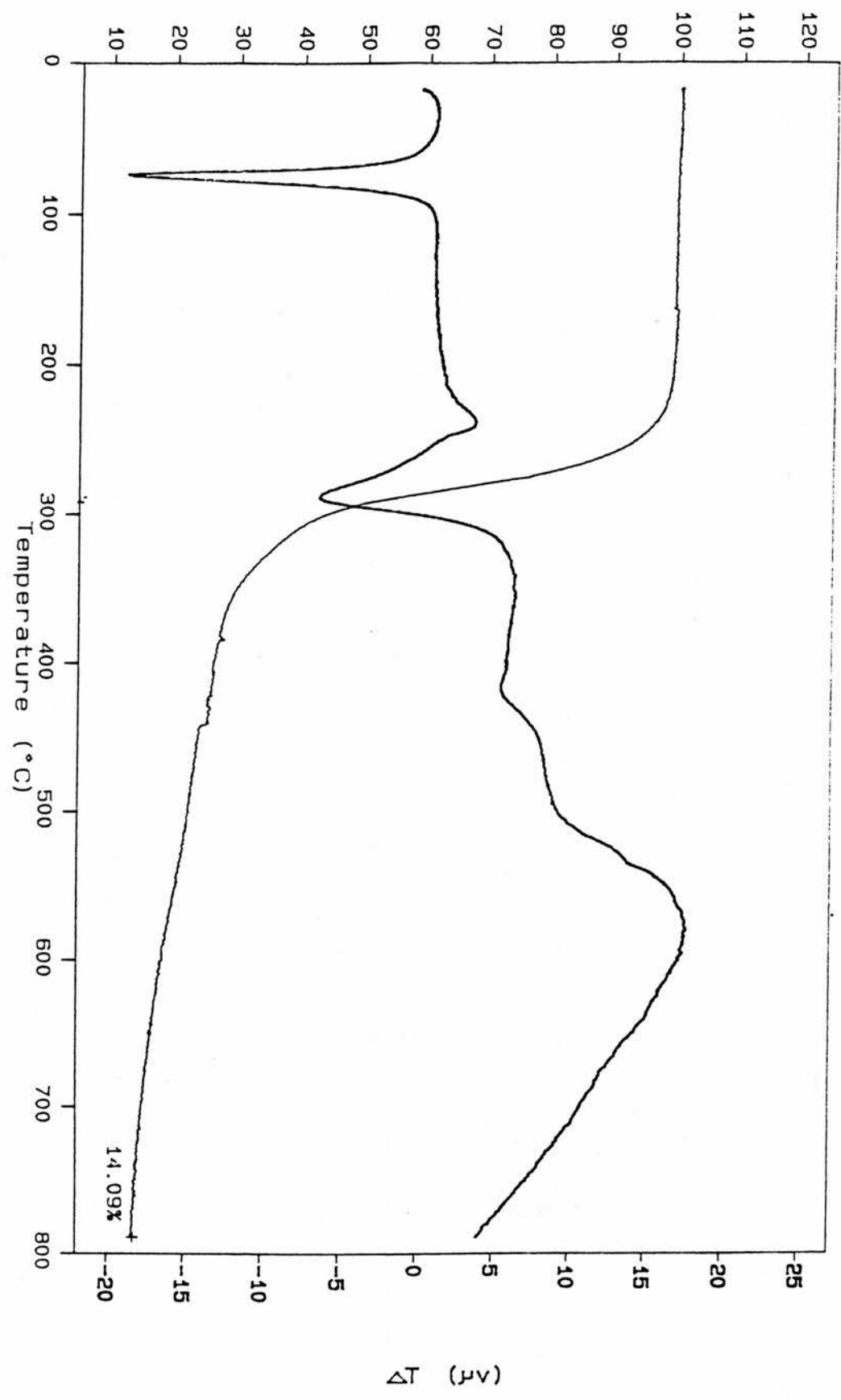


Fig 3.2.1.6.a STA - Cu[POUD]2

ΔT (mV)

3.3. EXPERIMENTAL

3.3.1. The preparation of 8,11-oxa-dodecane-2,4-dione

Sodium metal (3.77 g, 16.39 mmol) was chopped into small pieces and added to freshly distilled ammonia (400 cm³) containing iron (III) chloride (40 mg). The resulting grey suspension at -78°C (cardice/acetone bath) was treated with pentane-2,4-dione (9.96 g, 9.96 mmol) in diethyl ether (30cm³). The low temperature bath was removed, and the reaction mixture was allowed to return to reflux for 1 hour.

1-bromo-2-(2-methoxyethoxy)ethane (15.78 g, 8.62 mmol) in diethyl ether (30cm³) was added to the reaction mixture to give a pale orange solution. After 4 hours of stirring, a cream precipitate was produced. The cream suspension was refluxed whilst warming for 5 minutes and was then cooled for a further 15 minutes in a ice-water bath. A few chips of ice were added to the suspension followed by a mixture of ice (40 g) and concentrated hydrochloric acid (30 cm³). This resulted in the production of two orange layers. The aqueous layer was separated and washed three times with diethyl ether (50 cm³). The combined ethereal extracts were dried using anhydrous magnesium sulphate, which was filtered and evaporated in a vacuum at room temperature. A yellow liquid remained which was purified by distillation under reduced pressure.

The yellow liquid was fully characterised as 8,11-oxa-dodecane-2,4-dione.

B.p.= 113-4°C / 3.5 mmHg. Yield = 0.91g, 54.68%. Found% : C 58.53, H 8.35 ; C₁₀H₁₈O₄ requires C 59.39, H 8.96 %

3.3.1.1. IR Data

λ_{\max} : 3490 (w, b), 2933 (s, sp), 2873 (s, sp), 1723 (s, sp), 1706 (s, sp), 1619 (s, sp), 1453 (s, sp), 1360 (s, sp), 1310 (m, sp), 1201 (m, sp), 1116 (s, sp), 950 (m, sp), 874 (w, sp), 782 (m, sp) and 527 (s, sp) cm^{-1} , respectively.

3.3.1.2. ^1H N.M.R.Data

Resonance peaks are observed at δ 1.91 (tt, 2H), 2.07 (s, 3He), 2.27 (s, 3Hk), 2.39 (t, 2He), 2.63 (t, 2Hk), 3.40 (s, 3He), 3.41 (s, 3Hk), 3.52 (m, 2H), 3.57 (m, 2H), 3.58 (m, 2H), 5.54 (s, 0.3H) and 15.55 (b, OH).

76% enol form was observed for the ligand. This in comparison with 79% enol form observed in the parent β -diketone. No parent β -diketone was seen in the spectrum for the ligand.

3.3.1.3. ^{13}C N.M.R.Data

Peaks are observed at δ 23.52(5C^e), 24.73 (Me^e), 25.43(5C^k), 30.85 (Me^k), 34.92 (4C^e), 40.44 (4C^k), 57.83 (2C^k), 59.03 (11C), 70.02 (6C), 70.24 (9C), 71.92 (8C), 99.85 (2H^e), 190.70 (3C^e), 194.14 (1C^e), 203.10 (3C^k) and 204.60 (1C^k).

3.3.1.4. Electron Impact Mass Spectrum

M/e : 202, 176, 170, 161, 143, 127, 126, 113, 111, 103, 100, 85, 69, 59, 58, 45, 43, 29 and 28 respectively. The molecular ion is present at 202 mass units.

3.3.2. The preparation of [bis(8,11-oxa-dodecane-2,4-dionato)barium(II)] by the the dry toluene method

In a dry box, barium (II) hydride (0.71 g, 5.10 mmol) was weighed into a flask. The flask was sealed and transferred to the nitrogen manifold. Toluene (30 cm³) was added to the barium (II) hydride to form a white suspension.

8,11-oxa-dodecane-2,4-dione (2.17 g, 10.74 mmol) was added to the suspension whereupon some effervescence was noticed. The suspension was stirred overnight. After several filtrations, a yellow solution remained. The solvent was removed to leave an orange oil (A). Dichloromethane (10 cm³) was added to the orange oil (A). The resulting solution was transferred into a large excess of petroleum ether (150 cm³) which formed a clear solution. However, with the reduction in solvent volume, an orange oil was observed. Washings with an excess amounts of petrol were undertaken. After several decantations the solvent was removed again to leave an orange oil. It was characterised as the barium complex.

Yield = 1.20 g, 43.73 %. Found% : C 42.53, H 6.13 ;C₂₀H₃₄O₈Ba requires C 44.40, H 6.30 %.

3.3.2.1. IR Data

λ_{\max} : 3465 (w, br), 2942 (s, sp), 2873 (s, sp), 1710 (s, sp), 1607 (s, sp), 1510 (s, sp), 1419 (m, sp), 1358 (s, sp), 1242 (s, sp), 1200 (m, sp), 1118 (s, sp), 1022 (s, sp), 915 (m, sp), 871 (m, sp), 762 (s, sp), 734 (w, sp), 653 (w, sp), 527 (m, sp) and 460 (w, sp) cm⁻¹.

3.3.2.2. Mass spectrum

M / e : 458, 457, 335, 323, 319, 305, 280, 278, 270, 264, 258, 257, 236, 212, 198, 176, 167, 154, 148, 135, 127, 126, 111, 107, 103, 85, 69, 59, 58, 45, 43, 41, 29 and 28 mass units. The spectrum shows some barium containing peaks but , the molecular ion is not observed . The proposed formula weight of the barium complex occurs at 540 amu .

3.3.2.3. ¹H N.M.R. Data

Broad peaks are observed at δ 1.82, 2.12, 3.41, 3.60 and 5.14.

3.3.2.4. ¹³C N.M.R Data

Peaks are found at δ 26.47 (5C), 28.32 (Me), 37.81 (4C), 58.92 (11C), 69.45 (6C), 71.12 (9C), 71.79 (8C), 99.94 (2C), 189.00 (3C)and 194.30 (1C).

3.3.2.5. Sublimation test

The yellow oil was heated in a stream of dry nitrogen at 40 Torr from room temperature to 270°C. Partial decomposition was observed at 125°C and full decomposition was seen at 210°C.

3.3.3. The preparation of 2,2-dimethyl-9,12-oxa-tridecane-3,5-dione

A similar procedure for 8,11-oxa-dodecane-2,4-dione was adopted for the ^tbutyl analog. In the preparation of 2,2-dimethyl-9,12-oxa-tridecane-3,5-dione, sodium metal (1.58 g, 68.70 mmol), 5,5-dimethylhexane-3,5-dione (4.14 g, 29.23 mmol) and 1-bromo-2-(2-methoxyethoxy)ethane (6.23 g, 34.07 mmol) were used in the reaction. The resulting red oil was fractionally distilled under reduced pressure to give a clear liquid.

It was characterised as 2,2-dimethyl-9,12-oxa-tridecane-3,5-dione.

B.p = 143-145°C / 3.5 mmHg. Yield = 4.20 g, 59.07 %. Found % :

C 63.66, H 10.40 ; C₁₃H₂₄O₄ requires C 63.91, H 9.90 %.

3.3.3.1. IR Data

λ_{\max} : 3444 (w, br), 2966 (s, sp), 2930 (s, sp), 2873 (s, sp), 1727 (m, sp), 1699 (w, sp), 1607 (s, sp), 1481 (m, sp), 1458 (m, sp), 1363 (s, sp), 1275 (m, sp), 1199 (m, sp), 1119 (s, sp), 1029 (m, sp), 915 (m, sp), 734 (s, sp), 538 (w, sp) and 477 (w, sp) cm^{-1} .

3.3.3.2. Mass spectrum

M / e: 215, 214, 200, 190, 188, 187, 168, 167, 156, 154, 147, 142, 127, 125, 112, 111, 103, 88, 87, 72, 69, 59, 57, 55, 43, 41, 32, 31, 29, 28 and 27 mass units. Proposed formula weight of the ligand is at 244. The molecular ion was not observed.

3.3.3.3. ^1H N.M.R.Data

Peaks are observed at δ 1.1 (s, 9H), 1.85 (tt, 2H), 2.34 (t, 2H^e), 2.60 (t, 2H^k), 3.33 (s, 3H^e), 3.34 (s, 3H^k), 3 triplets from 3.52-3.60, 5.54 (s, 1H) and 15.71 (b, OH). The ligand exists in a 71% enol form. The parent 5,5-dimethylhexane-2,4-dione exists in 78% enol form.

3.3.3.4. ^{13}C N.M.R Data

Peaks are observed at δ 23.50 (5C^e), 25.51 (5C^k), 25.92 (t_{bu}), 27.24 (t_{bu}), 32.35 (4C^e), 35.43 (4C^k), 38.88, 39.12, 40.06, 44.96, 51.38 (2C^k), 58.98 (11C), 70.01 (9C), 70.28 (8C), 71.89 (6C), 95.15 (2C^e), 195.41 (1C^e), 196.71 (3C^e), 199.67 (1C^k) and 200.86 (3C^k).

3.3.4. The preparation of [bis(2,2-dimethyl-9,12-oxa-tridecane-3,5-dionato)barium(II)]

Under identical conditions to the method that produced the methyl analog, a toluene suspension of barium (II) hydride (0.52 g, 3.74 mmol) was stirred overnight in the presence of 2,2-dimethyl-9,12-oxa-tridecane-3,5-dione (2.07 g, 8.50 mmol). The procedure followed a similar path to the methyl analog. An orange oil was produced. Yield = 1.89 g, 81.14 %. Found % : C 49.69, H 8.16 ; $C_{26}H_{46}O_8Ba$ requires : C 50.04, H 7.43 %.

3.3.4.1. IR Data

λ_{max} : 3420 (w, br), 2950 (s, sp), 2875 (s, sp), 1710 (w, sp), 1597 (s, sp), 1510 (s, sp), 1435 (s, sp), 1359 (s, sp), 1224 (s, sp), 1201 (m, sp), 1120 (m, sp), 1027 (s, sp), 954 (m, sp), 870 (m, sp), 756 (m, sp), 732 (m, sp), 697 (w, sp), 550 (w, sp) and 460 (s, sp) cm^{-1} .

3.3.4.2. Mass spectrum

M / e : 542, 298, 213, 187, 168, 152, 142, 128, 111, 85, 69, 59, 57, 43, 41, 31 and 29 mass units. The molecular ion was not seen. The proposed formula weight of the barium complex is 624 amu.

3.3.4.3. ^1H N.M.R. Data

Broad peaks are observed at δ 1.10, 1.85, 2.20, 2.35, 3.38 and 5.38.

3.3.4.4. ^{13}C N.M.R. Data

Carbon signals are seen at δ 25.68 (5C), 26.49 (^tbu), 27.70 (^tbu), 39.88 (4C), 58.35 (11C), 69.02 (6C), 70.55 (9C), 71.27 (8C), 93.15 (2C), 190.54 (3C) and 198.32 (1C).

3.3.4.5. Sublimation test

The yellow oil was heated from room temperature to 292°C at 40 Torr. Partial decomposition occurs at 180°C. The barium complex undergoes full decomposition at 250-260°C.

3.3.5. The preparation of 1-(phenyl)-7,10-oxa-undecane-1,3-dione

In a similar procedure to that of the ^tbutyl and methyl analogs, sodium amide was produced in situ by reacting sodium metal (3.24 g, 140.98 mmol) in liquid ammonia (350 cm³) in the presence iron (III) chloride (40 mg) as a catalyst.

The suspension was cooled using a cardice / acetone bath. A yellow ethereal solution of 1-(phenyl)hexane-1,3-dione (10.66 g, 65.73 mmol) was transferred to the suspension.

After the suspension had stirred for 1 hour, the temperature bath was removed. An ethereal solution of 1-bromo-2-(2-methoxyethoxy)ethane (11.28 g, 61.63 mmol) was added slowly to give a green suspension. A similar reaction and isolation procedure then followed to give a brown oil. The brown oil was fractionally distilled under pressure to leave a clear liquid.

The clear yellow liquid was fully characterised as 1-(Phenyl)-7,10-oxa-undecane-1,3-dione. Yield = 10.49 g, 64.46%. B.p. = 166°C / 3.5 mmHg. Found % : C 68.26, H 8.23 ; C₁₅H₂₀O₄ requires C 68.16, H 7.63.

3.3.5.1. IR Data

λ_{\max} : 3503 (s, br), 3064 (s, sp), 2925 (s, sp), 2873 (s, sp), 1710 (m, sp) ,
1670 (w, sh), 1603 (s, sp), 1583 (s, sp), 1450 (s, sp), 1352 (s, sp), 1272 (s, sp),
1103 (s, sp), 956 (m, sp), 850 (m, sp), 769 (s, sp), 698 (s, sp), 619 (w, sp),
572 (w, sp) and 492 (w, sp) cm^{-1} .

3.3.5.2. Mass spectrum

M / e : 264, 232, 229, 219, 206, 205, 190, 189, 188, 187, 186, 175, 174, 173, 171,
170, 169, 163, 162, 161, 160, 158, 157, 131, 133, 120, 115, 111, 106, 105, 103,
92, 88, 83, 78, 77, 76, 69, 65, 59, 58, 55, 51, 45, 43, 41, 29, 28 and 27 mass units,
respectively. The molecular ion is observed at 264 mass units.

3.3.5.3. ^1H N.M.R. Data

Proton signals are found at δ 1.93 (tt, 2H), 2.65 (t, 2H^e), 2.85 (t, 2H^k),
3.32 (s, 3H^e), 3.33 (s, 3H^k), 3 triplets from 3.46-3.49, 4.04 (s, 2H^k),
6.14 (s, 1H^e), 7.40 (m, 3H) and 7.84 (m, 2H).

The % enol existing in solution is found to be 92%. In comparison the parent β -diketone is 91% enol.

3.3.5.4. ^{13}C N.M.R.data

Peaks are observed at δ 23.58 (5C^e), 25.55 (5C^k), 35.86 (4C^e), 40.08 (4C^k), 53.71 (2C^k), 58.98 (11C), 69.93 (9C), 70.21 (8C), 71.90 (6C), 96.18 (3H^e), 126.92, 128.56, 132.19, 133.64, 134.83, 137.00 - phenyl ring, 182.90 (1C^e), 194.00 (3C^e), 196.77 (1C^k) and 204.5 (3C^k).

3.3.6. The preparation of [bis{1-(phenyl)-7,10-oxaundecane-1,3-dionato }barium(II)]

In a similar method the barium complex was synthesised by reacting 1-(phenyl)-7,10-oxa-undecane-1,3-dione (4.99 g, 18.90 mmol) in a toluene suspension of barium (II) hydride (1.37 g, 9.83 mmol). The general procedure follows a similar pathway to obtain the barium complex. A yellow sticky solid / oil was characterised as the barium complex. Yield = 5.10 g, 81.34 %. Found % : C 55.18, H 6.01 ; $\text{C}_{30}\text{H}_{38}\text{O}_8\text{Ba}$ requires C 54.27, H 5.77 %.

3.3.6.1. IR Data

λ_{max} : 3375 (w, br), 3060 (s, sp), 2927 (s, sp), 1603 (s, sp), 1569 (s, sp), 1501 (s, sp), 1340 (s, sp), 1300 (s, sp), 1256 (s, sp), 1179 (s, sp), 1119 (s, br), 1028 (m, sp), 957 (m, sp), 869 (m, sp), 850 (m, sp), 802 (m, sp), 619 (w, sp), 573 (m, sp), 502 (m, sp) and 407 cm^{-1} (m, sp).

3.3.6.2. Mass spectrum

M / e : 335, 294, 277, 267, 264, 232, 205, 190, 189, 188, 161, 162, 147, 120, 106, 105, 92, 91, 89, 85, 83, 78, 77, 76, 68, 65, 63, 59, 58, 55, 52, 50, 45, 44, 43, 39, 29, 28 and 27 mass units. The molecular ion is not observed, but the ligand molecular ion is observed at 264.

3.3.6.3. ^1H N.M.R.data

Broad peaks are seen at δ 1.78, 2.20, 3.23, 3.36, 5.83, 7.20 and 7.80.

3.3.6.4. ^{13}C N.M.R.data

The carbon signals occur at δ 26.74 (5C), 38.34 (4C), 58.79 (11C), 69.23 (6C), 70.95 (9C), 71.51 (8C), 95.78 (2C), 127.29, 127.57, 128.13, 128.90, 129.20, 142.20 -Phenyl ring, 182.61 (1C) and 192.97 (3C).

3.3.6.5. Sublimation test

The yellow sticky solid / viscous oil was heated from room temperature to 250°C at 40 Torr. Melting of the barium complex occurred at < 80°C. However, partial decomposition occurred at 175°C and full decomposition at 250°C.

3.3.7. The preparation of 8,11,14-oxa-pentadecane-2,4-dione

A similar procedure was adopted for the preparation of 8,11,14-oxa-pentadecane-2,4-dione to that used for the ligands previously described in this report. Sodium amide (69.66 mmol) was prepared insitu from adding sodium metal (1.6 g, 69.66 mmol) to liquid ammonia (400 cm³). Under low temperature conditions pentane-2,4-dione (2.92 g, 29.2 mmol) was added to the suspension. Following 1 hour of stirring, in which the temperature bath was removed, an ethereal solution of 1-bromo-2-(2-methoxyethoxy)ethane (5.68 g, 25.02 mmol) was added. The work-up followed the same method as for with the other ligands. A yellow oil was produced. B.p = 139-141°C / 3.0 mmHg. Yield = 3.86 g, 62.66 %. Found % : C 59.15, H 9.47 ; C₁₂H₂₂O₅ requires C 58.52, H 9.00 %.

3.3.7.1. IR Data

λ_{\max} : 3533, 2927, 1717, 1619, 1457, 1356, 1247, 1200, 1117, 852 and 533 cm⁻¹, respectively.

3.3.7.2. Mass spectra

M / e : 169, 155, 147, 144, 139, 138, 128, 127, 125, 116, 114, 112, 104, 102, 100, 99, 95, 89, 87, 85, 73, 71, 69, 60, 59, 58, 56, 44, 43, 38, 32, 31, 29, 28 and 27 mass units. The molecular ion was not found. The proposed formula weight of the ligand is 246 amu.

3.3.7.3. ^1H N.M.R.data

Peaks were observed at δ 1.90 (tt, 2H), 2.09 (s, 3H^e), 2.27 (s, 3H^k), 2.38 (t, 2H^e), 2.61 (t, 2H^k), 3.40 (3H^e), 3.42 (3H^k), 3.52 (t, 2H), 3.57 (t, 2H), 3.58 (t, 2H), 5.54 (s, 1H^e) and 15.47 (b, OH). 62% enol form was observed for the ligand. Pentan-2,4-dione exists 79% in the enol form.

3.3.7.4. ^{13}C N.M.R.data

Carbon signals were found at δ 23.58 (5C^e), 24.81 (Me^e), 25.49 (5C^k), 30.91 (Me^k), 34.94 (4C^e), 40.47 (4C^k), 57.89 (2C^k), 59.04 (14C), 70.13 (6C), 70.20 (12C), 70.56 (11C), 70.62 (9C), 71.96 (8C), 99.90 (2C^e), 190.81 (3C^e), 194.16 (3C^k, 1C^e) and 204.01 (1C^k).

3.3.8. The preparation of [bis(8,11,14-oxa-pentadecane-2,4-dionato)barium(II)]

Under dry conditions, 8,11,14-oxa-pentadecane-2,4-dione (0.92 g, 3.74 mmol) was added to a stirred toluene suspension of barium (II) hydride (0.21 g, 1.51 mmol). As described previously the barium complex was produced and characterised by a similar method. At room temperature it was an orange oil. Yield = 0.68 g, 71.97 %.

3.3.8.1. IR Data

λ_{\max} : 3410 (w, br), 3063 (w, sp), 2873 (s, sp), 2246 (w, sp), 1725 (w, sp), 1603 (s, sp), 1510 (s, sp), 1462 (s, sp), 1354 (s, sp), 1299 (s, sp), 1245 (s, sp), 1201 (m, sp), 1111 (s, sp), 1029 (w, sp), 919 (s, sp), 875 (w, sp), 733 (s, sp), 528 (w, sp) and 411 cm^{-1} (w, sp).

3.3.8.2. Mass spectrum

M/e : 330, 320, 317, 302, an accumulation of peaks between 296 and 147, 127, 126, 113, 112, 103, 100, 89, 85, 83, 71, 69, 67, 59, 58, 57, 55, 45, 44, 41, 31, 29, 28 and 27 mass units. No molecular ion is observed. The proposed formula weight of the barium complex is at 632 gmol^{-1} .

3.3.8.3. ^1H N.M.R.data

Broad peaks are observed at δ 0.90, 1.90, 2.24, 3.34, 3.50, 3.60 and 5.25.

3.3.8.4. ^{13}C N.M.R.data

Peaks are observed at δ 26.08 (5C), 30.35 (Me), 38.71 (4C), 58.98 (14C), 69.85 (6C), 70.41 (12C), 70.53 (11C), 70.72 (9C), 71.88 (8C), 99.20 (2C), 189.88 (3C) and 192.86 (1C).

3.3.8.5. Sublimation test

The yellow viscous oil was heated to 295°C at 1 Torr at static vacuum. Partial decomposition occurs at 170°C and full decomposition at 182-190°C to give a brown residue and a clear sublimate. However, the clear sublimate did not give a positive barium flame test.

3.3.9. The preparation of 1-(2',4',6'-trimethylphenyl)-7,10-oxa-undecane-1,3-dione

Sodium amide(~100.43 mmol) was prepared from reacting sodium metal (2.31 g, 100.43 mmol) in liquid ammonia (400 cm³) in the presence of FeCl₃ (30 mg). Under low temperature conditions , 1-(2',4',6'-trimethylphenyl)butane-1,3-dione (9.26g , 45.3 mmol) was added to the grey suspension. After an hour of refluxing at room temperature, 1-bromo-2-(2-methoxyethoxy)ethane (8.31 g, 45.39 mmol) was added to the suspension. The method then followed the general preparation for these ligands. A clear liquid was obtained. Yield = 2.84 g, 20.81. B.p. = 106°C / 3.5 mmHg. Found % : C 71.03, H 8.94 ; C₁₈H₂₆O₄ requires C 70.56, H 8.55 %.

3.3.9.1. IR Data

λ_{\max} : 3370 (w, sp), 2925 (s, sp), 2873 (s, sp), 1699 (s, sp), 1613 (s, sp), 1452 (m, sp), 1379 (m, sp), 1356 (m, sp), 1255 (m, sp), 1199 (m, sp), 1117 (s, sp), 1033 (m, sp), 987 (w, sp), 851 (s, sp), 599 (w, sp) and 535 (w, sp) cm^{-1} .

3.3.9.2. Mass spectrum

M / e : 306, 292, 291, 289, 288, 265, 264, 249, 238, 231, 217, 204, 190, 189, 188, 186, 175, 173, 171, 166, 162, 160, 148, 147, 145, 133, 128, 127, 120, 119, 117, 115, 105, 104, 103, 91, 79, 78, 77, 69, 59, 55, 53, 51, 45, 43, 41, 38, 31, 29, 28 and 27 mass units. The molecular ion was observed at 306 mass units.

3.3.9.3. ^1H N.M.R.data

Peaks were observed at δ 1.74 (tt, 2H), 1.91 (s, 3H), 2.02 (s, 6H), 2.22 (2H^e), 2.53 (2H^k), 3.06 (s, 3H^e), 3.07 (s, 3H^k), 3.25 (m, 9H), 5.15 (s, 1H) and 6.29 (d, 2H).

The % enol in solution is 46%.

3.3.9.4. ^{13}C N.M.R.data

Peaks are observed at δ 19.01(Mesityl Me^k), 19.57(Mesityl Me^e), 21.01 (Mesityl Me^k), 21.08 (Mesityl Me^e), 23.39 (5C^e), 25.30 (5C^k), 36.02 (4C^e), 41.17 (2C^k), 59.03 (11C), 70.01 (6C), 70.08 (6C), 70.18 (8C), 70.28 (8C), 71.93 (9C), 102.34 (2C^e), 128.36, 128.43, 132.42, 133.98, 134.70, 138.17, 138.78, 139.73 - phenyl ring, 187.07 (1C^e), 197.43 (1C^k,3C^e) and 210.42 (3C^k).

3.3.1.0. The preparation of [bis{1-(2',4',6'-trimethylphenyl)-7,10-oxa-undecane-1,3-dionato}barium(II)]

The barium complex was produced by reacting a toluene suspension of barium (II) hydride (0.13 g, 0.93 mmol) with 1-(2',4',6'-trimethylphenyl)-7,10-oxa-undecane-1,3-dione (0.58 g, 1.88 mmol) to produce a white solid. The general procedure for producing the barium complex was adopted. The white solid was then characterised. Yield = 0.52 g, 74.29. M.p. = 137.5 - 138°C. Found % : C 59.80, H 7.21 ; C₃₆H₅₀O₈Ba requires C 57.80, H 6.74 %.

3.3.1.0.1. IR Data

λ_{max} : 1590 (s, sp), 1507 (m, sp), 1319 (m, sp), 1203 (m, sp), 1164 (s, sp), 1114 (s, sp), 1090 (s, sp), 1057 (s, sp), 954 (m, sp), 849 (m, sp), 764 (w, sp), 737 (m, sp), 583 (w, sp), 524 (w, sp) and 452 cm⁻¹ (w, sp).

3.3.1.0.2. Mass spectrum

M / e : 264, 190, 189, 187, 175, 162, 160, 149, 148, 147, 146, 133, 120, 119, 118, 117, 105, 103 , 91, 78, 77, 69, 65, 60, 59 , 55, 51, 45, 44, 43, 41, 33, 31, 29, 28 and 27 mass units. No molecular ion is observed.

3.3.1.0.3. ¹H N.M.R.data

Relatively broad peaks are observed at δ 1.28, 1.80, 2.09, 2.16, 2.60, 3.34, 3.51, 5.11, 6.70 and 6.83 .

3.3.1.0.4. ¹³C N.M.R.data

Peaks are observed at δ 20.30 (Mesityl Me), 21.80 (Mesityl Me), 27.76 (5C), 38.27, 38.35 (4C), 59.84 (11C), 69.95, 70.09 (6C), 71.19 (9C), 72.37 (8C), 101.07 (2C), 128.46, 134.32, 136.41, 143.45- Phenyl ring, 179.15 (1C) and 191.60 (3C).

3.3.1.0.5. Sublimation test

The white solid was heated from room temperature to 242°C at 40 Torr. The barium complex melted at <145-146°C. However, decomposition occurred near to its melting point.

3.3.1.1. The preparation of [bis (8,11-oxa-dodecane-2,4-dionato)copper(II)]

In an open beaker, a solution of copper (II) nitrate (1.30 g, 5.38 mmol) was added to a made up solution of 8,11-oxa-dodecane-2,4-dione (2.00 g, 9.89 mmol) in 95% ethanol (20 cm³). On addition a green solution was produced which seemed to effervesce. At the bottom of the beaker a cloudy white precipitate formed. Upon the addition of aqueous ammonia (5 mol dm⁻³), the solution turned to dark blue.

A further 8 cm³ of aqueous ammonia was added. A blue precipitate formed at the bottom of the beaker, suggesting the complex had formed and was not particularly soluble in aqueous media. A blue solution was extracted using diethyl ether (3 x 50 cm³). The combined ethereal extracts were dried using anhydrous magnesium sulphate and filtered. The blue solution was then evaporated to dryness to leave a blue residue. The blue residue was then recrystallised from a minimum amount of ether. Yield = 0.82 g, 35.77 %. M.p. = 85-86°C. Found % : C 51.12, H 7.07 ; C₂₀H₃₄O₈Cu requires C 51.55, H 7.35 %.

3.3.1.1.1. IR Data

λ_{\max} : 1574 (s, sp), 1552 (m, sp), 1523 (s, sp), 1275 (w, sp), 1168 (w, sp), 1104 (m, sp), 956 (w, sp), 880 (w, sp), 781 (m, sp), 723 (w, sp) and 476 (w, sp) cm⁻¹.

3.3.1.1.2. Mass spectrum

M / e : 472, 468, 466, 465, 460, 458, 452, 442, 424, 412, 410, 395, 383, 372, 356, 307, 288, 269, 258, 249, 225, 205, 202, 191, 181, 157, 141, 127, 126, 112, 100, 85, 72, 59, 54, 45, 44, 43, 41, 29, 28 and 27 mass units. Molecular ion is seen at 466 mass units.

3.3.1.1.3. UV / visible spectrum

8 peaks are observed at 299.4 (33400 cm^{-1}), 280.5 (35650 cm^{-1}), 263.2 (37993 cm^{-1}), 259.1 (38491 cm^{-1}), 248.5 (40241 cm^{-1}), 245.4 (40749 cm^{-1}), 240.3 (41614 cm^{-1}) and 237 nm (42158 cm^{-1}) at a concentration of 0.15 mM. At a concentration of 26.82 mM, 2 broad peaks were seen at 661.5 (15117 cm^{-1}) - $\epsilon_{\text{max}}=38.29 \text{ M}^{-1} \text{ cm}^{-1}$ and 560.2 nm (17850 cm^{-1}) - $\epsilon_{\text{max}}=33.46 \text{ M}^{-1} \text{ cm}^{-1}$ (toluene solution).

3.3.1.2. The preparation of [bis { 1-(phenyl)-7,10-oxaundecane-1,3-dionato }copper (II)]

A similar procedure was adopted for the phenyl analog except a green solid was recovered.

Yield = 1.65 g, 74.35 %. M.p = 67.5-68°C. Found % : C 61.05, H 6.45 ; C₃₀H₃₈O₈Cu requires C 61.06, H 6.49 %.

3.3.1.2.1. IR Data

λ_{\max} : 1590 (s, sp), 1557 (s, sp), 1510 (s, sp), 1201 (m, sp), 1102 (s, sp), 975 (m, sp), 865 (w, sp), 767 (s, sp), 709 (s, sp), 689 (w, sp), 670 (w, sp), 554 (w, sp) and 448 cm⁻¹ (w, sp) .

3.3.1.2.2. UV / visible spectrum

Peaks are at 201.5, 218.7, 233.1, 249.7, 282.4, 324.8 nm at a concentration of 0.0763 mM. At a concentration of 16.94 mM, 2 broad peaks are observed at 652.9 (15377 cm⁻¹) - ϵ_{\max} =94.92 M⁻¹ cm⁻¹ and 546.8 nm (18429 cm⁻¹) - ϵ_{\max} = 91.67 M⁻¹ cm⁻¹ (toluene solution).

3.4. References

1. S.C.Thompson, Ph.D Thesis, University of St.Andrews., 1991.
2. L.Huang, S.B.Turnipseed, C.Haltiwanger, R.M.Barkley and R.E.Sievers, *Inorg.Chem.*, 1994, **33**, 798, 803.
3. J.B.Turnipseed, R.M.Barkley and R.E.Sievers, *Inorg.Chem.*, 1991, **30**, 1164.
4. W.S.Rees.Jr, C.R.Caballero and W.Hesse, *Angew.Chem., Int.Ed.Engl.*, 1992, **31**, 735.
5. Metal β -diketonates and Allied derivatives, R.C.Mehrotra, R.Bohra and D.P.Gaur, Academic Press, 1978, 109-119.
6. D.L.Schulz, B.J.Hinds, C.L.Stern and T.J.Marks, *Inorg.Chem.*, 1993, **32**, 249.
7. P.C.Le Brun, W.D.Lyon and H.A.Kuska, *J.Crystallogr. and Spectr.Res.*, 1986, **16**, 889.
8. G.Hall and T.S.Piper, *Mol.Phys.*, 1962, **5**,169.
9. R.L.Belford, M.Calvin and G.Belford, *J.Chem.Phys.*, 1957, **26**, 1165.
10. R.L.Belford, A.E.Martell and M.Calvin, *J.Inorg & Nucl. Chem.*, 1956, **2**, 11.
11. J.A.Bertrand and R.I.Kaplan, *Inorg.Chem.*, 1966, **5**, 489.
12. F.A.Cotton and J.J.Wise., *Inorg.Chem.*, 1967, **6**, 5.

CHAPTER 4

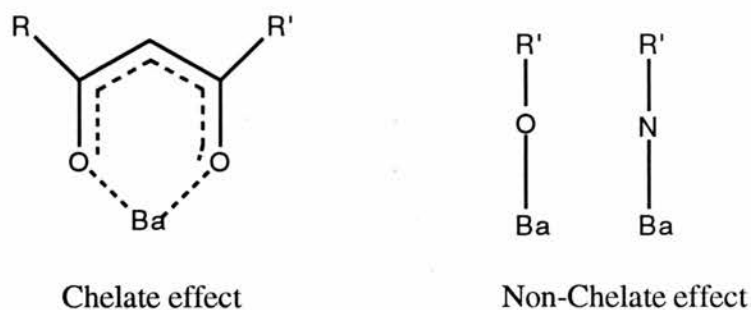
BARIUM MACROCYCLIC COMPLEXES

CHAPTER FOUR

4.1 Introduction

The stability and volatility of barium complexes are determined by many effects, such as the degree of oligomerisation in the complex, the strength of the Ba-X bond ($X = O, S, N$) and, probably and most importantly the "chelate effect" which exists in some barium complexes. The "chelate effect" refers to the enhanced stability obtained through compounds containing chelate rings. Hence, the stability of most barium β -diketonates is greater than that of barium alkoxides, siloxides and silyl amides. Despite the extra stability, non-fluorinated barium β -diketonates still undergo some decomposition whilst volatilising under STA conditions. Their volatility is also low because the ability of Ba^{2+} to expand its coordination sphere to 8-10 means that in most cases they are polymeric.

Fig.4.1.a

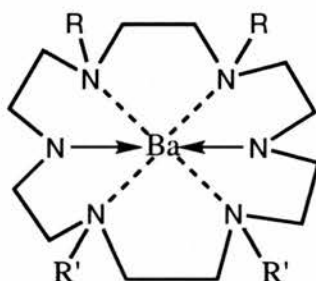


To produce a neutral barium complex with extra stability (no decomposition in the STA) and hence volatility, would require total encapsulation of the barium centre.

A greater thermodynamic stability than that of barium β -diketonates should be obtained with complexes containing cyclic polydentate ligands. This extra stability is a consequence of the "macrocyclic effect"¹.

Since these ligands also occupy many more donor sites, the chances of polymerisation are greatly reduced and it is anticipated that they may be monomeric.

Fig 4.1.b

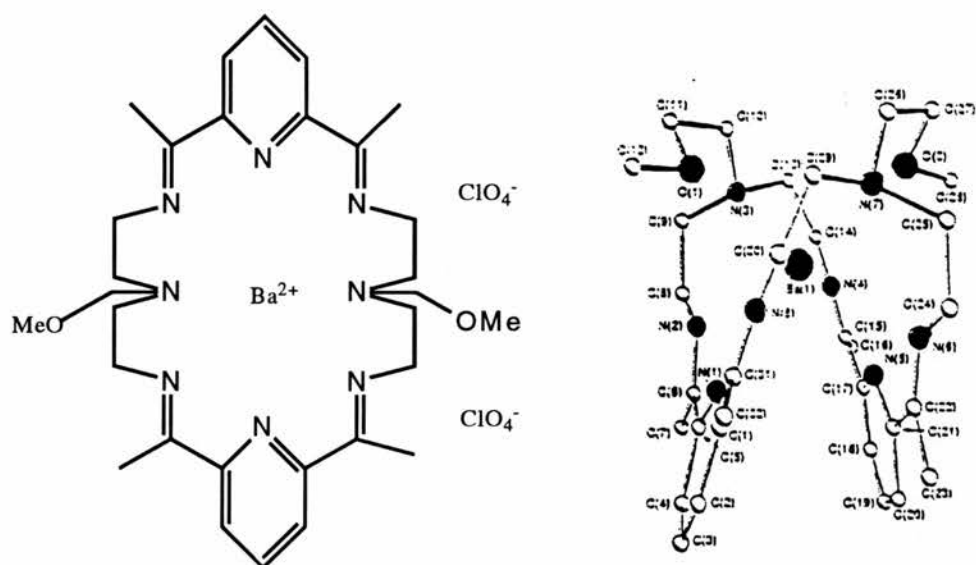


The 'Macrocyclic effect'

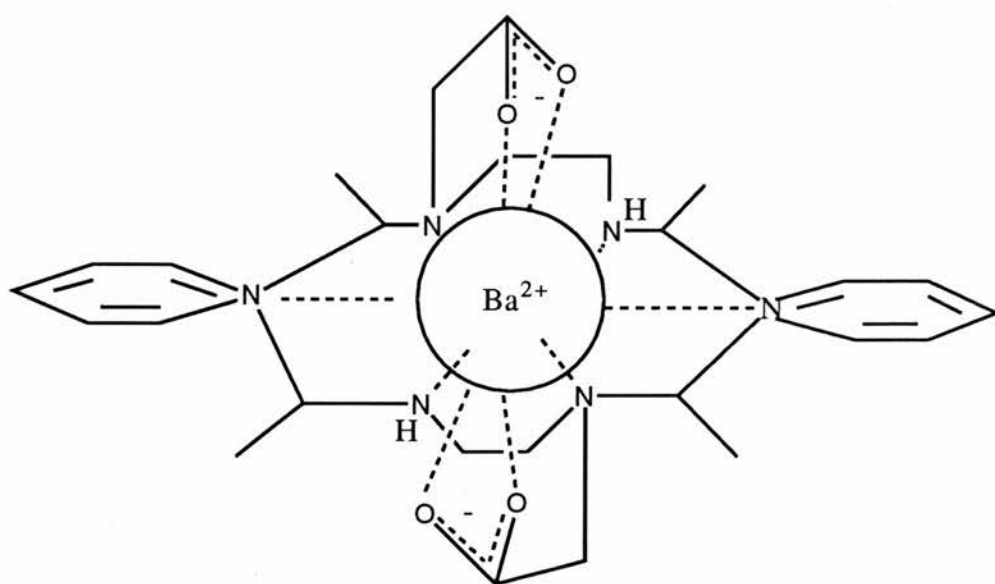
It has been known for a long time that podands (polydentate glymes) and coronands (crown ethers) add to the stability of metal complexes. As a result of this observation, enhanced volatility and stability are obtained for non-fluorinated barium β -diketonate complexes with coordinated podands and coronands^{2,3}. However, as with the base free barium β -diketonates, slight decomposition is noticed whilst volatilising (see chapter 2).

In an attempt to obtain 100% volatilisation of a neutral non fluorinated barium complex, further strategies were adopted. The design and synthesis of a series of multidentate neutral pendant arm barium macrocycles has been under investigation. It was hoped that some of the barium macrocycles would be monomeric and volatile.

Investigations by Bailey⁴, Adams⁵ and Nelson⁶ using Ba²⁺ as a metal template in the synthesis of macrocycles have shown that monomeric barium macrocycles can be synthesised and isolated. However, the barium macrocycle has always been isolated as the perchlorate salt. Not only are perchlorate salts potentially explosive but because the barium compounds are ionic, they are unlikely to be volatile. A schematic diagram and an X-ray crystal structure of one of the monomeric barium macrocyclic complexes is shown in Fig.4.1.c.

Fig.4.1.c

In spite of this if the Ba^{2+} cationic charge is neutralised by two pendant arms each having a negative charge, then a monomeric volatile barium precursor would presumably result. The pendant arms are attached to the macrocyclic framework via the bridgehead N-atoms.

Fig 4.1.d.

A proposed schematic diagram of a pendant arm barium macrocycle is shown in Fig 4.1.d. However, the macrocyclic framework may be folded as shown in Fig 4.1.c.

Several synthetic pathways were employed to produce a neutral barium bibracchial pendant arm macrocycle. The synthetic strategies that were adopted are described as follows:

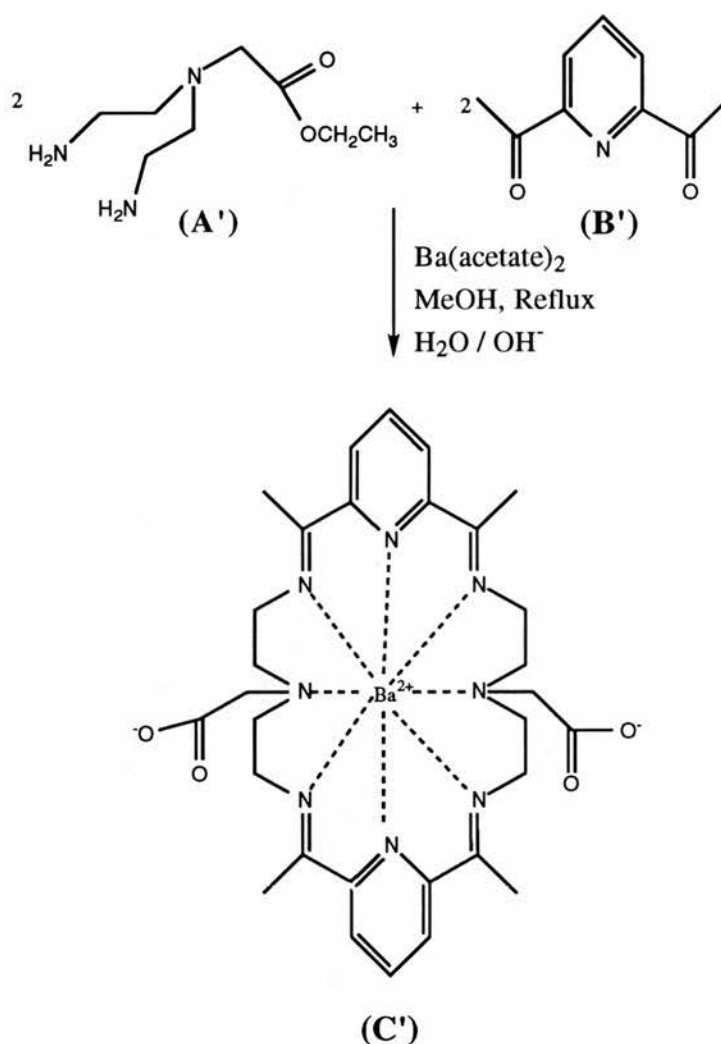
1. To prepare a pendant arm barium macrocycle from the cyclocondensation reaction between a N-functionalised amine and 2,6-diacetylpyridine in the presence of a barium template (**SYNTHETIC STRATEGY 1**).
2. To react a preformed barium macrocycle with a synthon which contains a pendant arm appendage (including naked anion exchange reactions with the preformed barium macrocycle) (**SYNTHETIC STRATEGY 2**).
3. To produce the pendant arm barium macrocycle by reacting the preformed macrocycle with a barium salt (**SYNTHETIC STRATEGY 3**).

This chapter details all the synthetic strategies to form a neutral barium pendant arm macrocycle, as well as an attempted synthesis of a barium macrocycle from the reaction between $[Ba_4(TMHD)_8]$, 2,6-diacetylpyridine and 1,2-diaminoethane (**SYNTHETIC STRATEGY 4**).

Applying the proposed synthetic routes as described in Fig 4.2.a., attempts were made to prepare and isolate a series of intermediates which would finally result in the production of a barium macrocycle via a 2+2 Schiff base cyclocondensation reaction between a N-functionalised amine and 2,6-diacetylpyridine in the presence of a barium template (**SYNTHETIC STRATEGY 1**).

4.2. The proposed scheme for the production of a 24-membered barium bibracchial macrocycle

Fig 4.2.a

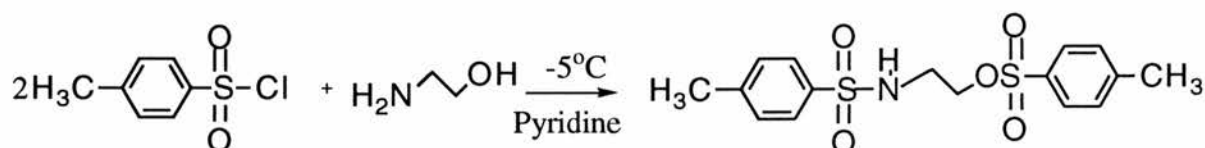


The attempted synthesis of (A') involved the preparation of several intermediates. The intermediates that were prepared are described in sections 4.2.1-4.2.4. The intermediates which have been produced before are referenced (7-8).

4.2.1. The preparation of [2- { (p-tolylsulphonyl)oxy } ethyl]-p-tolylsulphonamide]⁷

The first intermediate to be produced was [2- { (p-tolylsulphonyl)oxy } ethyl]-p-tolylsulphonamide]. This compound is produced by the reaction between two equivalents of p-toluenesulphonyl chloride and one equivalent of ethanolamine at -5°C in pyridine.

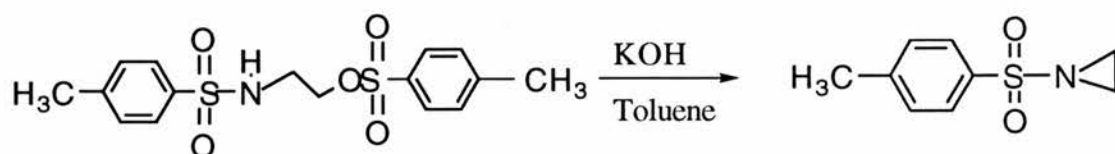
Fig.4.2.1.a.



4.2.2. The preparation of N-(p-tolylsulphonyl)aziridine⁸

The isolated cream solid was then treated with potassium hydroxide in toluene. As a result of this reaction, a white solid, N-(p-tolylsulphonyl)aziridine was isolated.

Fig.4.2.2.a.



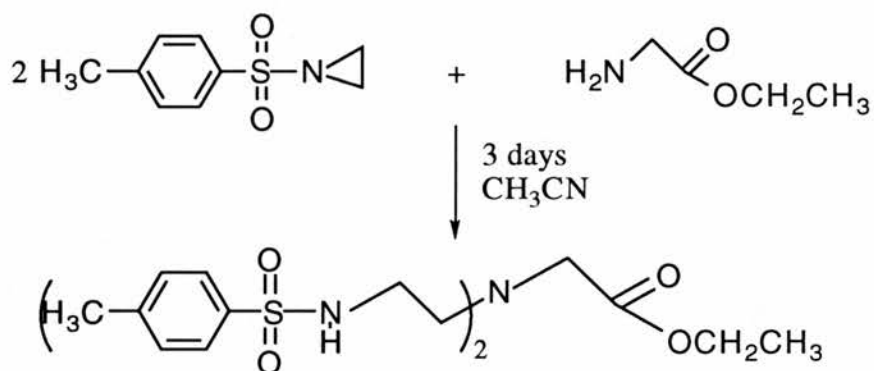
4.2.3. The preparation and analysis of 1-amino-N,N-bis(2-toluene-p-sulphonylaminoethyl)ethyl ethanoate

4.2.3.1. The preparation of 1-amino-N,N-bis(2-toluene-p-sulphonylaminoethyl)ethyl ethanoate

Nucleophilic attack on the strained C-N bond of N-(toluene-p-sulphonyl)aziridine by ethylglycinate resulted in the production of a protected amine -

1-amino-N,N-bis(2-toluene-p-sulphonylaminoethyl)ethyl ethanoate.

Fig.4.2.3.a.



4.2.3.2. The analysis of 1-amino-N,N-bis(2-toluene-p-sulphonylaminoethyl)ethyl ethanoate

4.2.3.2.1. IR analysis

A neat film of 1-amino-N,N-bis(2-toluene-p-sulphonylaminoethyl)ethyl ethanoate gave several high intensity absorptions in the IR spectrum. The peaks in fingerprint region are of very large intensity compared to the peaks observed between the wavenumbers 4000-1400 cm^{-1} .

However, a strong absorption was observed at 3272 cm^{-1} which was due to a ν (N-H). The absorption frequencies at 2979, 1597, 909 and 817 cm^{-1} are attributable to the phenyl ring vibrational modes of - ν (C-H), ν (C-C) and δ (C-C). A strong absorbance is shown at 1729 cm^{-1} which is attributable to ν (C=O) of the ester function. Although, the ν (C-O) from the ester part of the molecule seems to be superimposed on by the strong absorptions for ν (SO₂R) and ν (SO₂R) at 1350 and 1154 cm^{-1} .

4.2.3.2.2. ¹H N.M.R. analysis

The ¹H N.M.R. spectrum strongly indicates that the proposed compound has been formed. The triplet at δ 1.23 and the quartet at δ 4.12 correspond to the ethyl grouping on the ester function. Two triplets are observed at δ 2.71 and 2.91 due to the inequivalent protons which exist in the ethylene part of the molecule adjacent to the 2 nitrogen atoms. The singlet at δ 3.20 is attributable to the protons of the CH₂ adjacent to the C=O function. Interestingly, the CH₂ which originates from the ethyl glycinate occurs more downfield in the ¹H N.M.R. spectrum at δ 3.41.

The N-H protons are found to resonate at δ 5.81 and occur as a broad singlet. The other peaks at δ 2.44, 7.34, 7.81 are attributable to the tosyl signals.

4.2.3.2.3. ^{13}C N.M.R. analysis

The carbon resonance peaks seem to support the ^1H N.M.R. spectrum in that the proposed compound has been formed.

The tosyl carbons resonate at δ 22.03, 127.68, 130.24, 137.26, 143.81. The C atom of the ester function resonates at δ 172.36. The peaks at δ 14.65 and 41.49 are attributable to the ethyl carbons of the ester function. The peaks of ethylene carbons resonate at δ 54.40 and 54.87.

The CH_2 from the ester function that originated from the ethyl glycinate resonates at δ 61.40. The ^1H and ^{13}C N.M.R. spectra of 1-amino-N,N-bis(2-toluene-p-sulphonylaminoethyl)ethyl ethanoate are shown in Figs 4.2.3.2.3.b-c.

Fig 4.2.3.2.2.a. ^1H N.M.R. spectrum of 1-amino-N,N-bis(2-Toluene-p-sulphonylaminoethyl)ethyl ethanoate

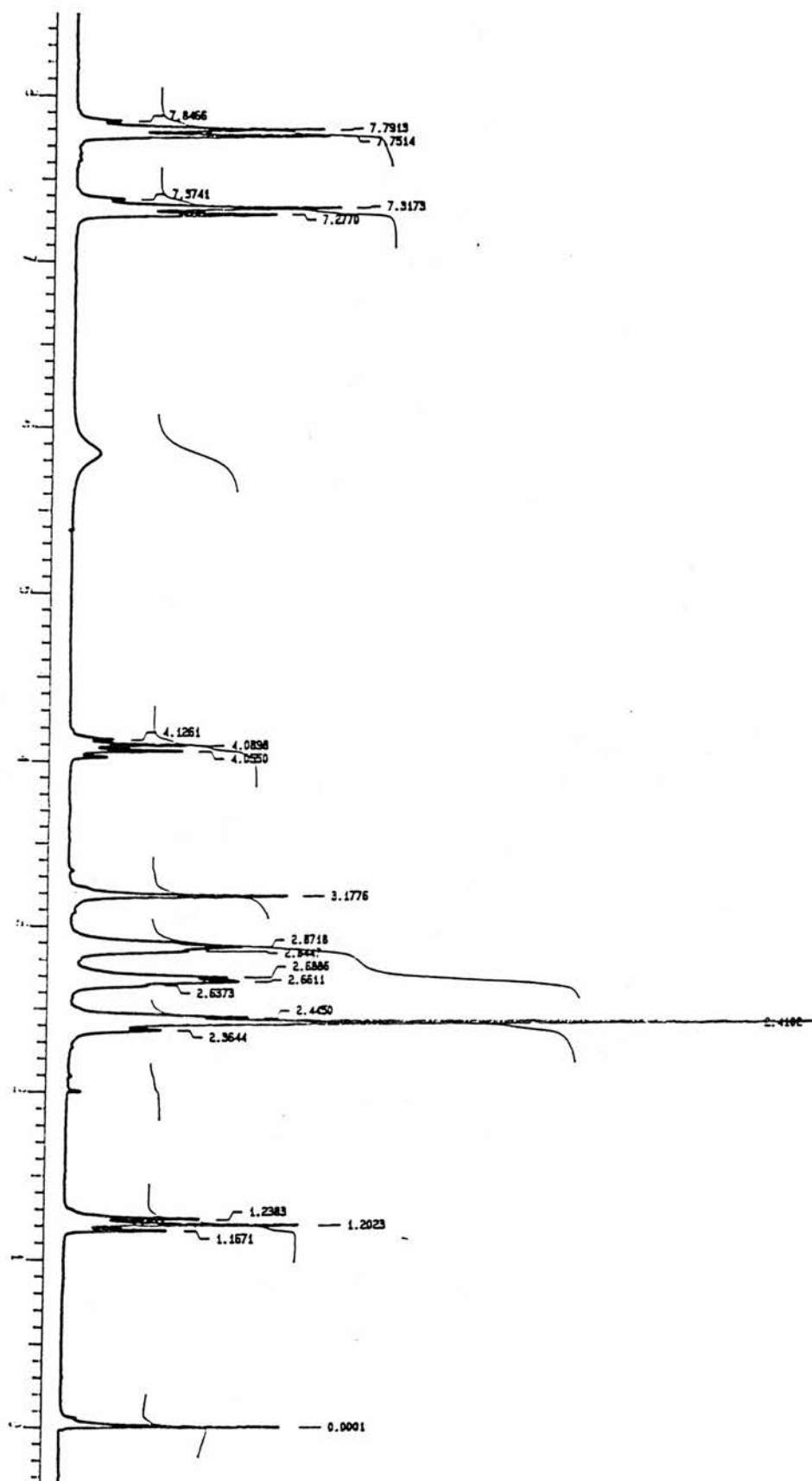
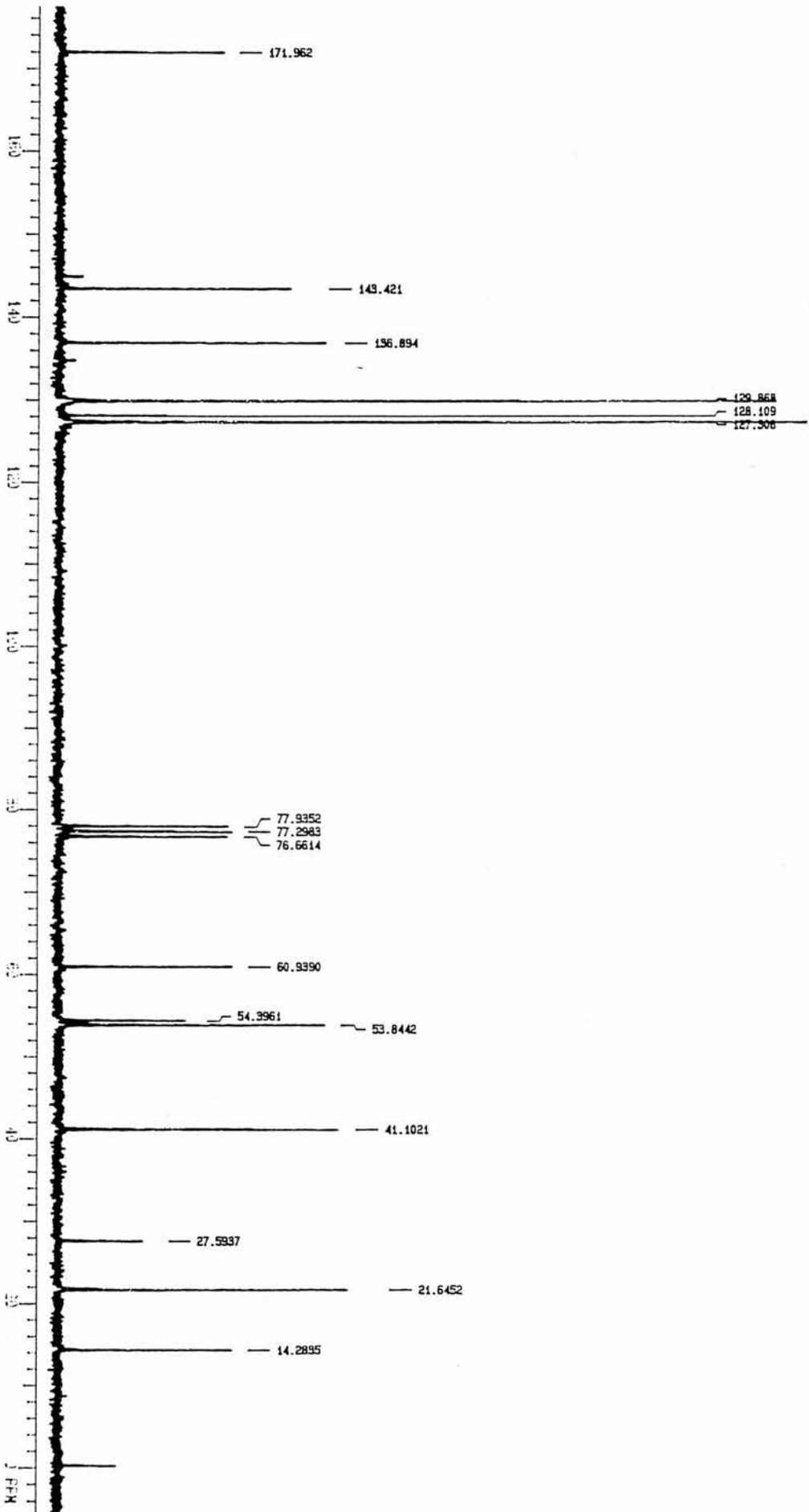


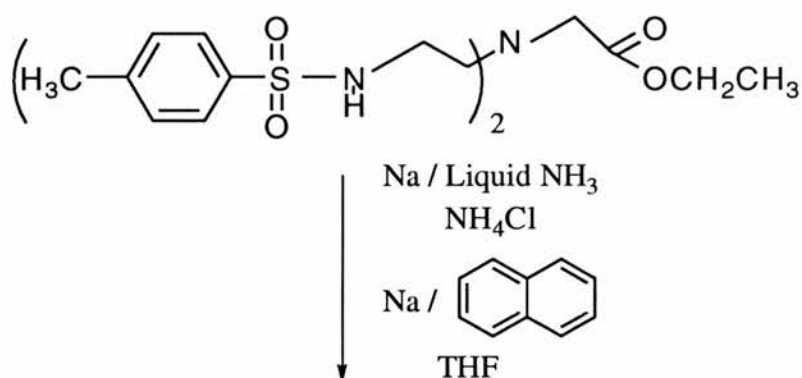
Fig 4.2.3.2.3.a. ^{13}C N.M.R. spectrum of 1-amino-N,N-bis(2-Toluene-p-sulphonylaminoethyl)ethyl ethanoate



4.2.4. The detosylation of 1-amino-N,N-bis(2-toluene-p-sulphonylaminoethyl)ethyl ethanoate using sodium dihydronaphthide or sodium and liquid ammonia

The isolated yellow oil was then reductively detosylated either by using a solution of sodium dihydronaphthide or by the action of sodium in liquid ammonia. Two different reduction routes were attempted to see whether or not the free amine could be isolated without hydrolysis or cyclisation. If the N-functionised amine could be isolated without hydrolysis or cyclisation, then the amine could have been electronically neutral. The amine could have then be purified easily by extracting with organic solvents.

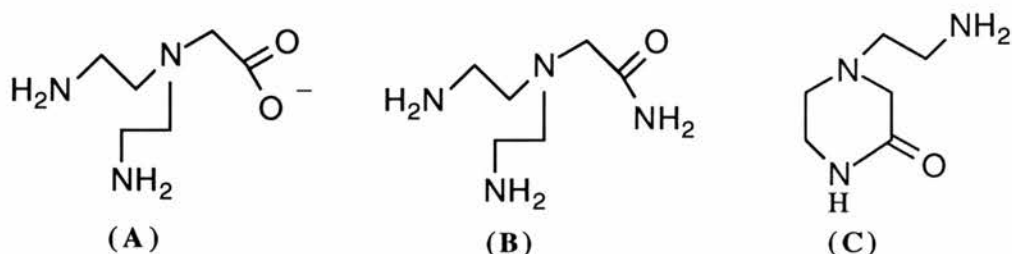
Fig.4.2.4.a



Water soluble detosylated products
 +
 Organic soluble tosylated products

However, when trying to extract the corresponding reaction mixture with organic solvents, the detosylated product remained in the aqueous phase. This observation would suggest that hydrolysis of the ester function had taken place, thus, producing a highly charged zwitterionic water soluble species (A in Fig.4.2.4.b.). However, a reaction with ammonia or cyclisation could have also take place to produce a branched chained amide (B in Fig.4.2.4.b.) or a stable 6-membered cyclic amide (C in Fig.4.2.4.b.) which would also likely to be water soluble.

Fig.4.2.4.b.



All detosylated products would have an affinity for water and not necessarily have any solubility in organic solvents.

The difficulty in purifying the detosylated product in the aqueous phase arises from the amount of sodium salts produced in the reaction.

Several purification procedures such as the recrystallisation from boiling water, extraction of the aqueous layer at different pH's with CH₂Cl₂ including that of the measured isoelectric point (4) resulted in the detosylated species remaining unpurified.

Surprisingly, no tosyl signals were seen in the ¹H and ¹³C N.M.R spectrum of the reaction mixture in D₂O which is shown in Figs 4.2.4.c-d. Apparently, no water soluble sodium salts of the tosyl group were isolated possibly because of the prior reduction of the tosyl group to toluene, sulphur dioxide and p-thiocresol.

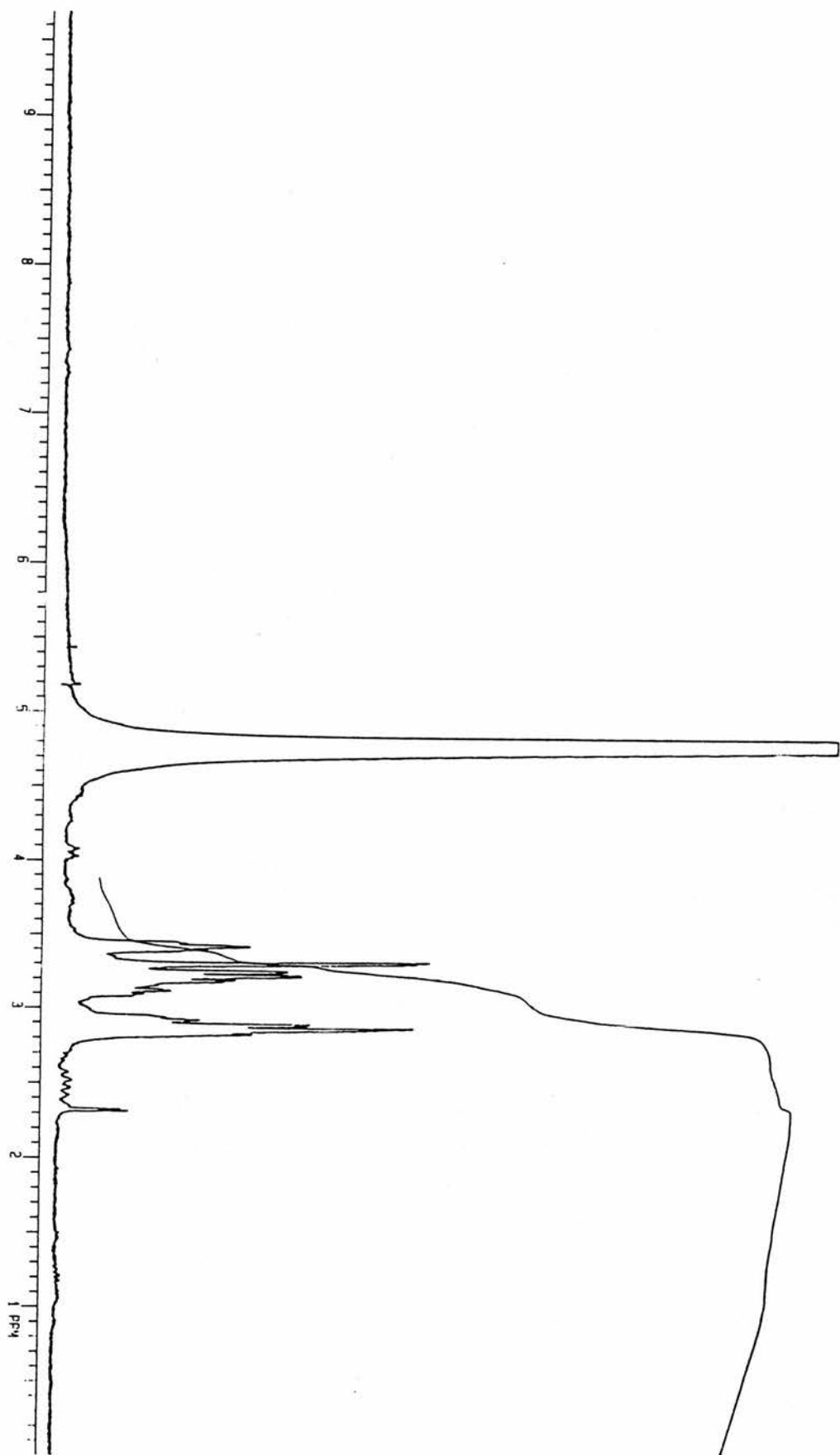
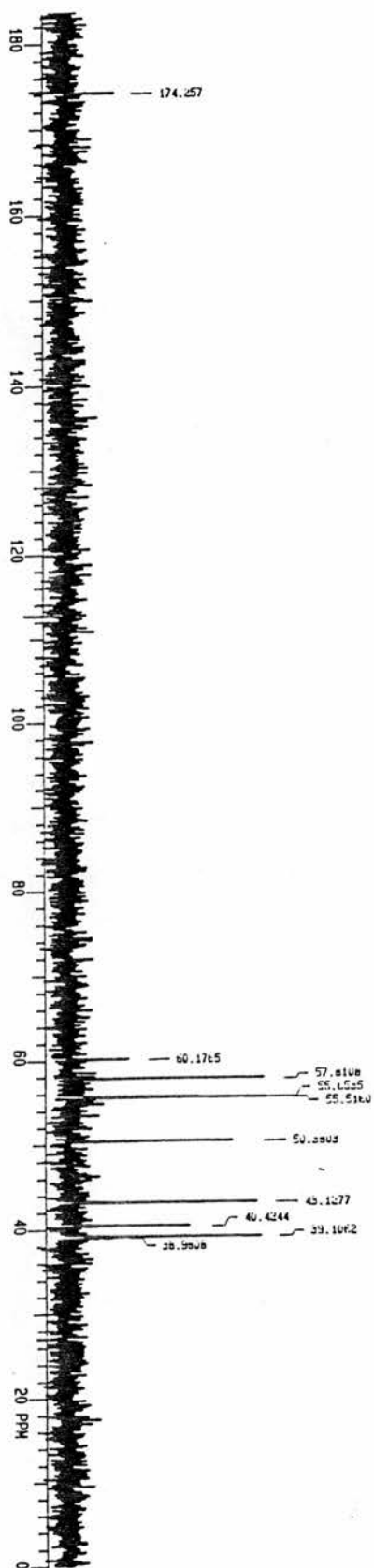
Fig 4.2.4.c. ^1H N.M.R. spectrum of the detosylated product in the aqueous phase

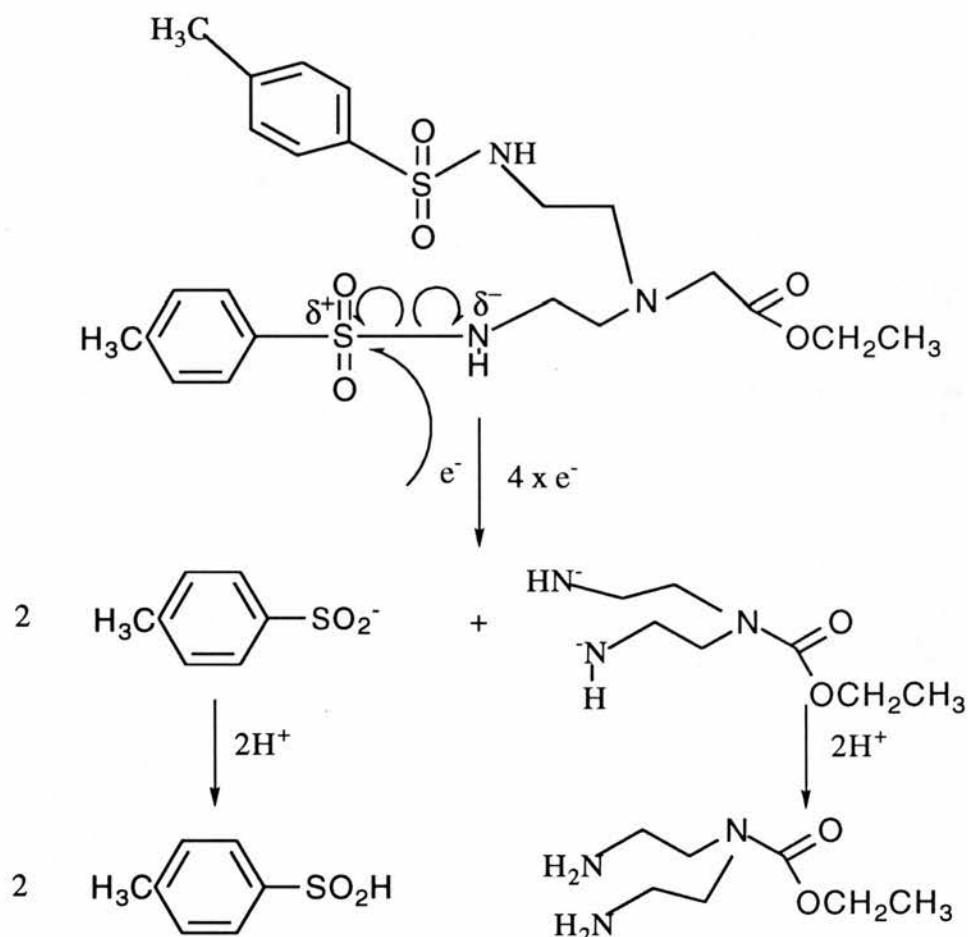
Fig 4.2.4.d. ^{13}C N.M.R. spectrum of the detosylated product in the aqueous phase

4.2.5. The mechanism of the reduction of 1-amino-N,N-bis(2-toluene-p-sulphonylaminoethyl)ethyl ethanoate

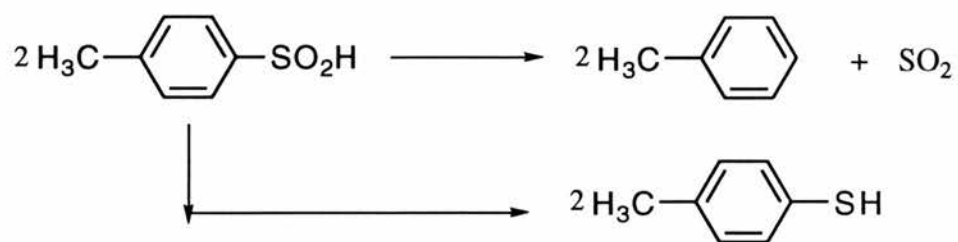
The reductant is either produced by the action of sodium and liquid ammonia or sodium and naphthalene. The reaction produces electrons.



The reduction involves the attack of solvated electrons (produced by the sodium / NH_3) on the δ^+ sulphur atom of the tosyl group in a classical Birch reduction.



p-toluenesulphonic acid produced from the reduction can also react further.



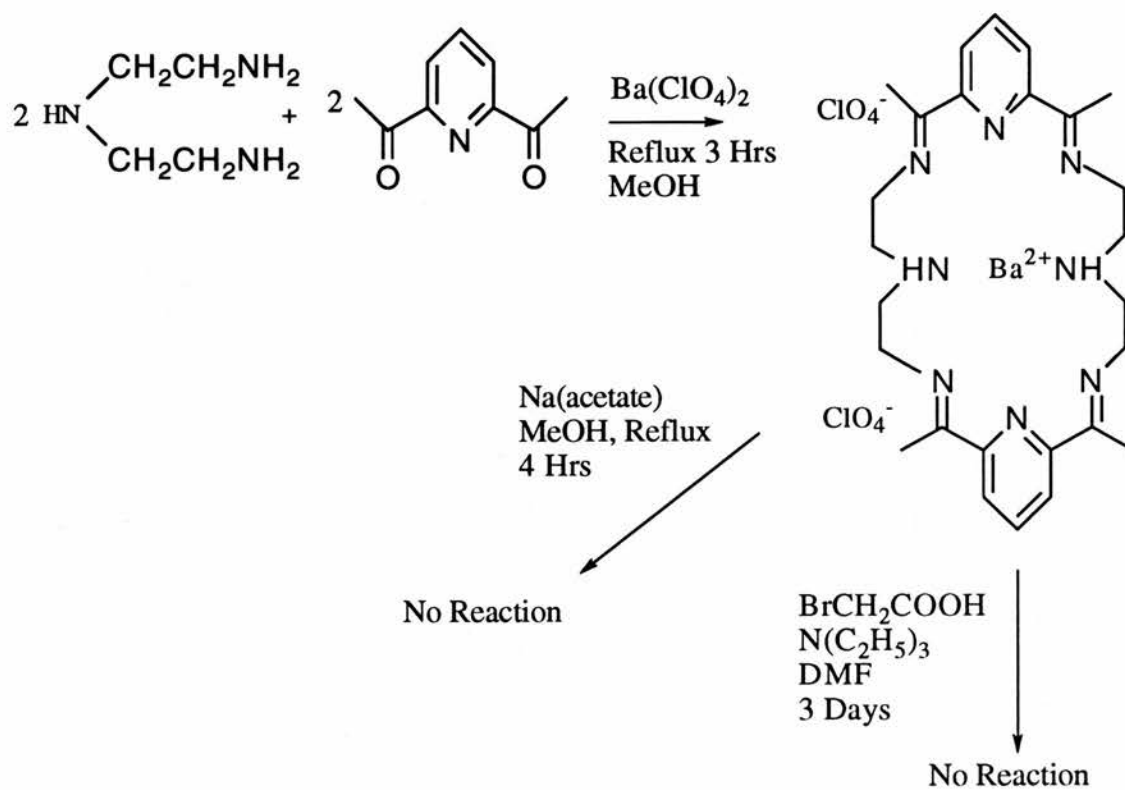
Unfortunately, the desulphated product remained unpurified, although the ¹H and ¹³C NMR definitely showed signals which could only result from the desulphated product. Countless difficulties in isolating the N-functionalised carboxylate pendant armed amine in a purified state meant that further strategical routes concerning the production of a 2+2 Schiff-base pendant arm barium macrocycle via a N-functionalised amine were not undertaken.

4.3. The attempted reactions with the preformed barium macrocycle [Ba[24](Me)₄N₆(Py)₂(ClO₄)₂] and 1-bromoacetic acid / or sodium acetate (naked anion exchange reactions)

As a consequence of the difficulties encountered in isolating the N-functionalised amine, other synthetic strategies were adopted in an attempt to produce a monomeric neutral barium macrocycle. With the preformed barium perchlorate macrocycle - [Ba[24](Me)₄N₆(Py)₂(ClO₄)₂], attempts were made to incorporate pendant arms into the macrocyclic framework in the hope of neutralising the Ba²⁺ cationic charge. Naked anion exchange reactions were also undertaken with the preformed barium macrocycle - [Ba[24](Me)₄N₆(Py)₂(ClO₄)₂] in an attempt to replace the perchlorate anion with acetate anions (see Fig 4.3.a.)(**SYNTHETIC STRATEGY 2**).

However, functionalisation of the macrocycle ring and the naked anion exchange did not take place. The preformed macrocycle - [Ba[24](Me)₄N₆(Py)₂(ClO₄)₂] was first isolated by Nelson⁹.

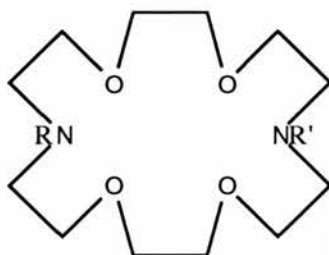
Fig 4.3.a



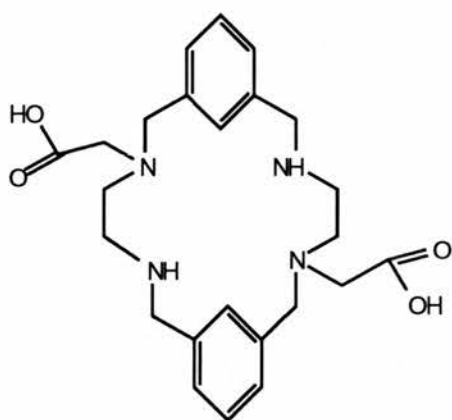
4.4. The synthesis of the barium pendant arm macrocycles from the reaction of the preformed pendant arm macrocycle and barium salts

In **SYNTHETIC STRATEGY 3** it was decided to make a series of barium pendant arm macrocycles by reacting the preformed macrocycle with barium salts. The following macrocycles shown in Fig 4.4.a., were produced and complexed to barium.

Fig.4.4.a.

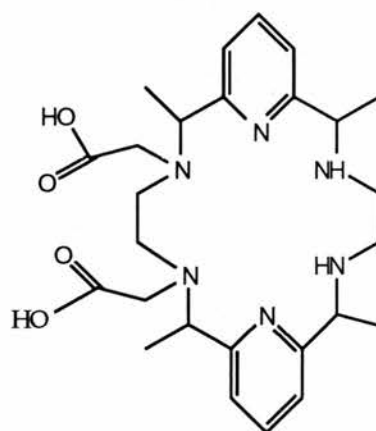


- (1) $R = R' = \text{COCH}_2\text{CH}_2\text{COOH}$
 (2) $R = R' = \text{COCH}=\text{CHCOOH}$
 (3) $R = R' = \text{CH}_2\text{COOH}$



(4)

(Exists as 2 isomers)



(5)

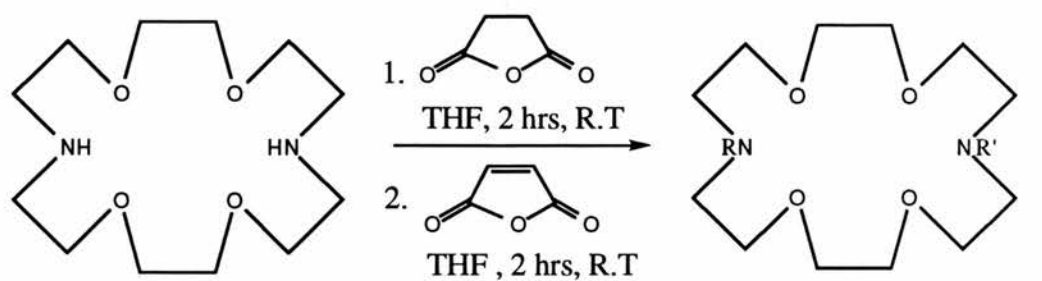
4.4.1. The preparation of 7,16-bis(3-carboxypropanoyl)-1,4,10,13-tetraoxa-7,16-diazacyclooctadecane (1) and 7,16 - bis(Z-3-carboxypropenoyl)-1,4,10,13-tetraoxa-7,16-diazacyclooctadecane (2) and their barium complexes

Whilst investigating the complexation properties of certain anionic pendant arm macrocycles, De Jong synthesised 7,16-bis(3-carboxypropanoyl)-1,4,10,13-tetraoxa-7,16-diazacyclooctadecane (1) and 7,16 - bis(Z-3-carboxypropenoyl)-1,4,10,13-tetraoxa-7,16-diazacyclooctadecane (2). In an attempt to solubilise Barium(II) sulphate into an aqueous medium, De Jong added (1) and (2) to a lithium hydroxide / barium(II) sulphate mixture in water. De Jong indicated that the barium complex precipitated in both cases. For our purposes these two compounds were thought to be ideal, as it was hoped that a monomeric volatile barium complex would result. However, our investigations showed that the barium complex of (1) and (2) remained in a solution of distilled water, as a result of refluxing an aqueous solution of (1) and (2) with an aqueous solution of barium(II) hydroxide.octahydrate. Consequently, the barium complex of (1) and (2) was isolated and characterised from the aqueous solution.

Both barium complexes of (1) and (2) are very soluble in protic solvents such as water and methanol, but insoluble in dichloromethane and diethyl ether. The solubility of these barium complexes would tend to indicate that intramolecular and intermolecular hydrogen bonding is taking place between the residual water molecule(s) and the barium complex.

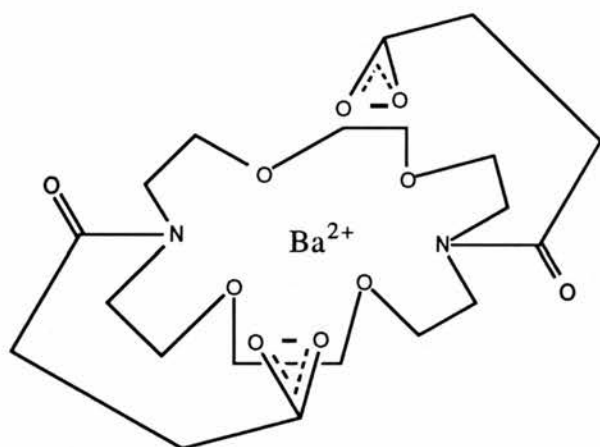
As a result of this hydrogen bonding which takes place within the complexes, the compounds do not sublime but decompose to their corresponding ligand at 225°C under vacuum.

Fig 4.4.1.a.



1. $R = R' = \text{COCH}_2\text{CH}_2\text{COOH}$
2. $R = R' = \text{COCH}=\text{CHCOOH}$

$\text{Ba}(\text{OH})_2 \cdot 8\text{H}_2\text{O}$
 Reflux, 13 hrs
 H_2O



1 and 2

The barium complex exists in 2 isomeric forms with the orientation of the pendant arms producing cis and trans isomers. The intra or / and inter-molecular hydrogen bonding is not shown in Fig 4.4.1.a.

4.4.2. The analysis of 7,16-bis(3-carboxypropanoyl)-1,4,10,13-tetraoxa-7,16-diazacyclooctadecane (1) and 7,16-bis(Z-3-carboxypropenoyl)-1,4,10,13-tetraoxa-7,16-diazacyclooctadecane (2) and their barium complexes

4.4.2.1. IR analysis of the barium complex of macrocycle (1)

The major difference in the IR spectrum of the ligand and the barium complex is a strong, broad absorbance at 1625 cm^{-1} . As a result of the greater electron density in the carboxylic acid function and therefore the greater the double bond character (C=O), the $\nu(\text{C=O})$ for the ligand occurs at 1739 cm^{-1} . Once the ligand is complexed to the barium centre, the $\nu(\text{C=O})$ shifts to 1625 cm^{-1} as a result of the reduced double bond character in the carboxylate function. As the barium complex was isolated in the hydrated state, an $\nu(\text{O-H})$ is observed at 3397 cm^{-1} . Intermolecular H-bonding is probably present within the barium complex due to the peaks broadness. This is supported by the microanalysis of the barium complex which suggests one molecule of water is bound to the complex.

The other absorbances at 1297 , 1212 and 1112 cm^{-1} are attributable to the $\nu(\text{C-O})$ and $\nu(\text{C-N})$.

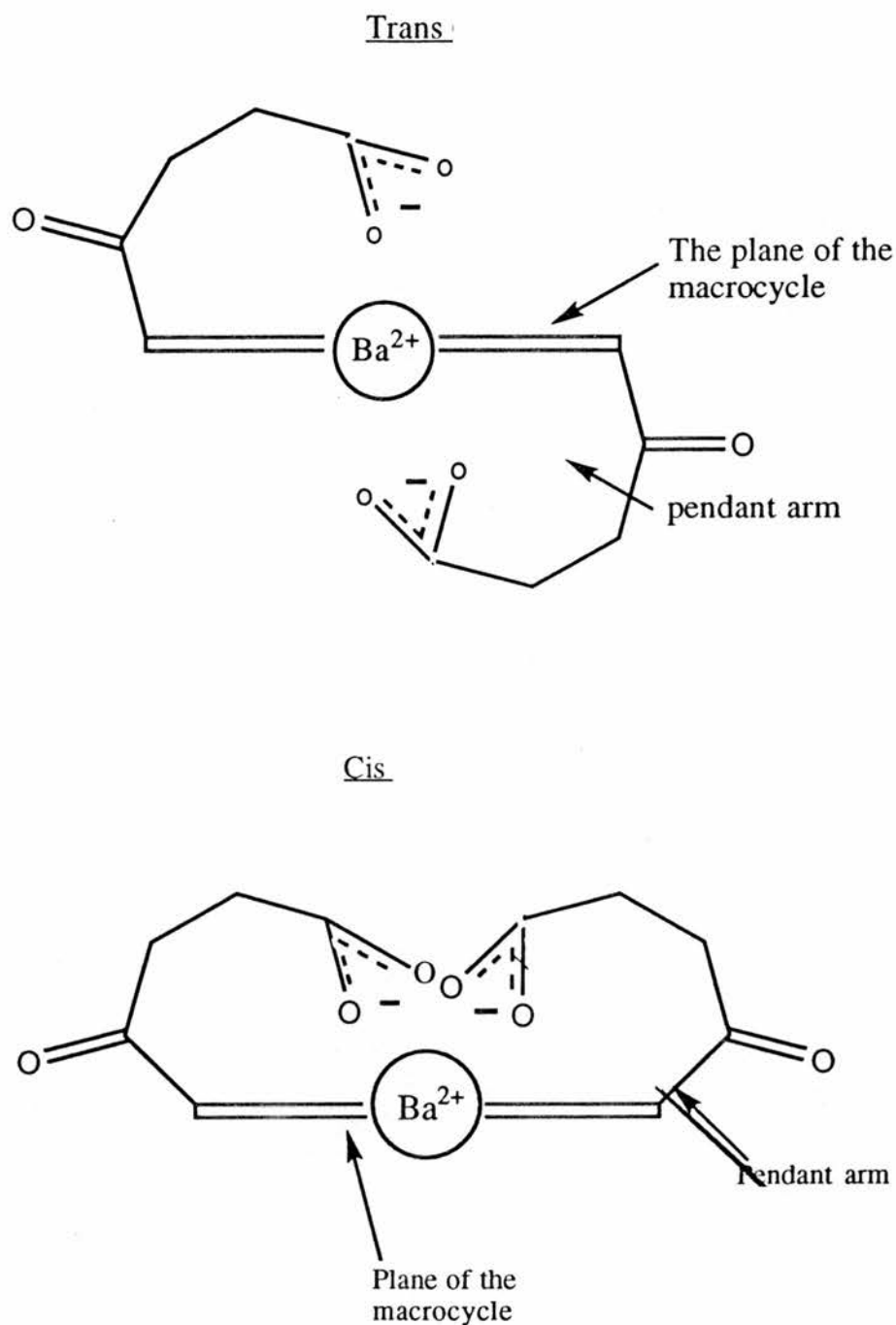
4.4.2.2. ^1H N.M.R. analysis of the barium complex of macrocycle (1)

Two triplets at δ 2.46 and 2.67 correspond to the four CH_2 's on the pendant arms of the barium macrocyclic complex. It is interesting to note that the triplets in the ligand occur at a chemical shift more downfield at δ 2.61 and 2.71.

There is also a greater difference in chemical shift between the two triplets in the barium complex compared to the ligand. A series of triplets amounting to 24 protons occur between the region of δ 3.68-3.80. The series of triplets are as a consequence of the protons resonating in the diaza-18-crown-6 ether ring.

4.4.2.3. ^{13}C N.M.R. analysis of the barium complex of macrocycle (1)

The ^{13}C N.M.R. analysis shows the presence of two isomeric forms of the barium complexes. The barium complex exists in solution as both cis and trans isomers.



The two peaks at δ 27.45 and 30.67 correspond to four carbons of the ethylene groups on the pendant arm. The cis and trans isomer are particularly evident in the carbon resonances attributed to the ethylene carbons on the macrocyclic ring. The ethylene carbons adjacent to the nitrogen atom occur upfield at δ 45.30 and 46.94 to the other ethylene carbons adjacent to oxygen atoms. (δ 68.59 - 68.09).

4.4.2.4. ¹H N.M.R. analysis of the barium complex of macrocycle (2)

The ¹H N.M.R. spectrum shows predominantly 3 peaks at δ 3.59, 5.95 and 6.60.

These peaks all occur upfield to that of their corresponding resonances observed in the ligand at δ 3.56, 6.05 and 6.74.

Two sets of doublets at δ 5.95 and 6.60 are attributable to the cis coupling along the C=C double bond in the pendant arm chain. The multiplet at δ 3.59 represents the presence of 24 hydrogen atoms resonating in the barium complex. These protons are a part of the 4,13-diaza-18-crown-6-ether ring.

4.4.2.5. ¹³C N.M.R. analysis of the barium complex of macrocycle (2)

The ¹³C N.M.R. spectrum of the barium complex of macrocycle (2) also shows the existence of two isomers. The carbonyl resonances are observed at δ 173.12 and 172.64. Interestingly, the peaks at δ 139.68 and 137.66 are attributable to the C=C double bond resonances. Finally, several peaks are observed in the region between δ 72.21 - 49.91 which are attributable to the carbon atoms resonating in the 4,13-diaza-18-crown-6-ether ring.

4.4.3 The preparation and analysis of N,N'-bis(carboxymethyl)-4,13-diaza-18-crown-6 (3) and it's barium complexes

4.4.3.1. The preparation of macrocycle (3) and it's barium complexes

The copper¹⁰ and zinc (II)¹¹ complexes of N,N'-bis(carboxymethyl)-4,13-diaza-18-crown-6 (3) have been investigated in the solid state by X-ray analysis. In the solid state, both complexes are monomeric with both metal cations in the centre of the macrocyclic 4,13-diaza-18-crown-6 ring. In the X-ray crystal structure of the Copper complex the Cu atom is coordinated to the 2 ring N atoms. Furthermore, two of the crown ether oxygens are weakly bound. The Cu²⁺ cationic charge is neutralised by two monodentate carboxylate pendant arms which overall leads to a 6-coordinate Jahn-Teller distorted octahedral structure. The barium complex has not previously been isolated in the solid state, but solution studies have been undertaken with a variety of cations (Ca²⁺, Mg²⁺, Zn²⁺, Co²⁺, Ni²⁺, Cu²⁺, most of the lanthanides and some actinides M³⁺ ions - Am³⁺ and Cm³⁺)¹²⁻¹⁶, including Ba²⁺¹⁷⁻¹⁸.

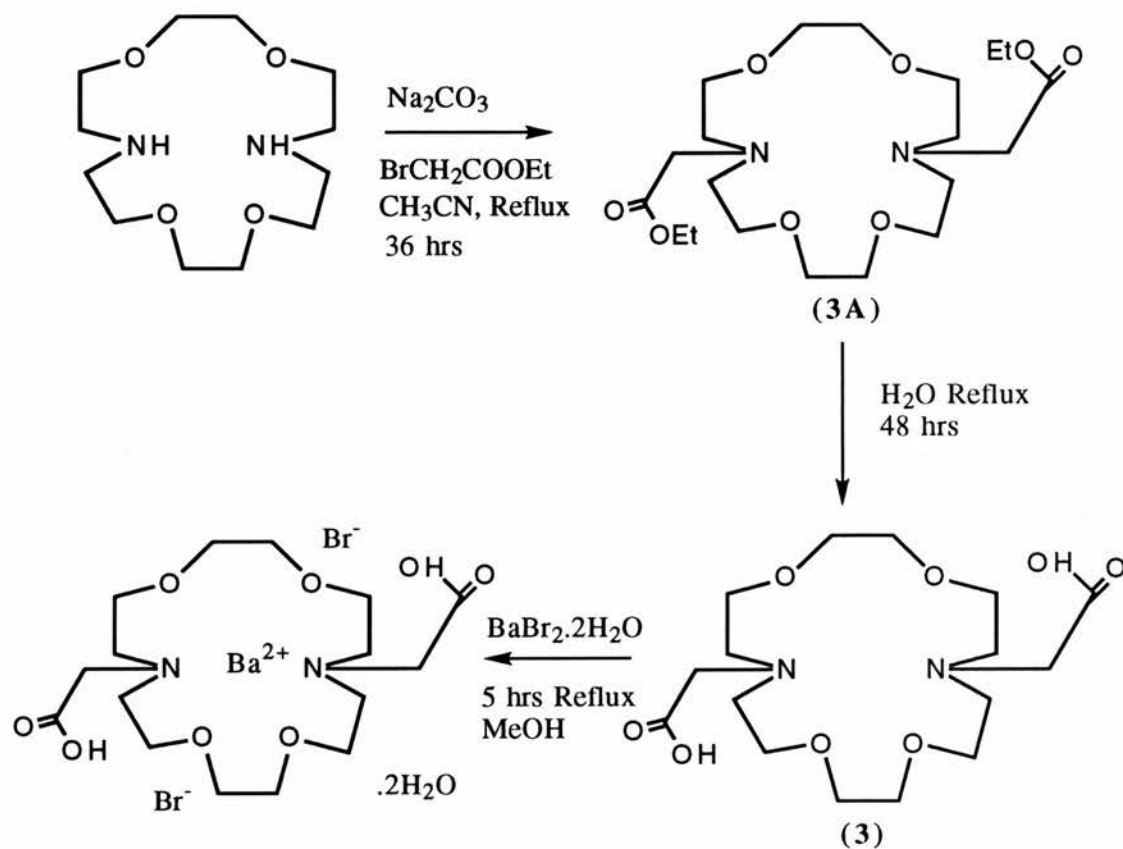
The complexing properties of this particular ligand have been of considerable research interest. Stability constants in solution have also been compared with other complexants, such as, kryptofix 2,2, 18-crown-6 and EDTA.

It seems that the stability constant value for the barium complex of EDTA in solution is slightly larger at $\log K_{\text{BaL}}^{2-} = 7.80$ than that of the stability constant value for the barium complex of N,N'-bis(carboxymethyl)-4,13-diaza-18-crown-6 (3) in solution at $\log K_{\text{BaL}} = 7.63$. As a consequence, [Ba(EDTA)²⁻] has a similar but marginal increase in the stabilisation in solution compared to that of (3).

Although, as a result of this extra stabilisation, an attempt to synthesise and isolate the barium complex of N,N'-bis(carboxymethyl)-4,13-diaza-18-crown-6 (3) in the solid

state was undertaken. It was hoped that the barium complex would be monomeric and volatile.

Fig.4.4.3.1.a.



The preparation of a bibracchial macrocyclic ligand utilises the N-alkylation reaction of the bridgehead N atom of the 4,13-diaza-18-crown-6 ligand. In an acetonitrile suspension, 4,13-diaza-18-crown-6, ethyl bromoacetate and sodium carbonate were reacted for 24 hours at reflux to produce N,N'-bis(carbethoxymethyl)-4,13-diaza-18-crown-6 (**3A**). The carboxylate macrocyclic ligand was prepared from the hydrolysis of the ester pendant arm macrocycle (**3A**). The preparation follows similar procedures by Kulstad, Malmsten¹⁹, Gatto and Gokel²⁰.

Attempts to make the neutral barium pendant arm macrocyclic complex were plagued with difficulty. No reaction occurred when barium hydride was refluxed with N,N'-bis(carboxymethyl)-4,13-diaza-18-crown-6 (**3**). A barium bromide salt of the macrocycle (**3**) was produced by direct reaction with barium(II) bromide dihydrate and the parent macrocycle (**3**). The preparation of the macrocycle (**3**) and it's barium complexes are shown schematically in fig.4.4.3.1.a. It was hoped that, once the barium metal cation was in the centre of the macrocycle, it would be possible to deprotonate the carboxylate pendant arms, and thus, produce a monomeric neutral barium complex.

Reactions with [N,N'-bis(carboxymethyl)-4,13-diaza-18-crown-6 barium(II) bromide dihydrate] and pyridine and triethylamine at reflux resulted in precipitation of neither the neutral barium complex nor the amine hydrobromide salt.

4.4.3.2. The analysis of the barium containing bibracchial pendant arm 4,13-diaza-18-crown-6 macrocycle

4.4.3.2.1. IR analysis

As a consequence of the carboxylic acid function remaining protonated, the absorption peak at 1733 corresponds to ν (C=O). The barium complex is shown to have extensive hydrogen bonding as shown by the strong broad absorbance at 3377 cm^{-1} . Whether this absorbance is due to the intermolecular or intramolecular hydrogen bonding with residual water molecules or with pendant arms is not clear. However, the stretching frequency for a carbonyl hydrogen bonded dimeric carboxylic acids normally occur between 1740 and 1650 cm^{-1} . Evidence of further carboxylic acid interaction is observed at 938 cm^{-1} attributable to δ (OC-OH). As predicted from the literature this absorbance peak is quite broad. In the fingerprint region two other characteristic peaks are observed at 1295 and 1118 cm^{-1} which are attributable to ν (C-O) and ν (C-C).

4.4.3.2.2. Mass spectral analysis

The EI mass spectrum of the barium(II) bromide dihydrate complex shows extensive fragmentation and does not show the molecular ion. The highest fragment registered is at 231 which would suggest that the barium complex is involatile. This would strongly support the STA and thermal studies that were undertaken.

4.4.3.2.3. ^1H N.M.R. analysis

It seems from the ^1H N.M.R. spectrum of [(N,N'-carboxymethyl-4,13-diaza-18-crown-6) barium(II) bromide dihydrate] that two isomers are present in solution.

The isomers arise from the different orientation of the pendant arms about the plane of the macrocycle. Inequivalent intensities in the proton peaks seems to suggest that one isomer is favoured to the other isomer. In addition, the proton resonance peaks attributable to cis configuration or the trans configuration cannot be evaluated on the basis of this ^1H N.M.R. spectrum.

The broad triplets at δ 2.55 and 2.90 are attributable to the ethylene carbons adjacent to the nitrogen atoms in the macrocyclic framework. (Carbon atoms. 3,5,12 and 14)

It appears on complexation with the barium cation that the ethylene carbons resonate upfield to that observed in the free ligand (N,N'carboxymethyl)-4,13-Diaza-18-crown-6 at δ 3.55.

As a result of the inequivalent chemical environment experienced by the protons adjacent to carbons 2,3,5,6,11,12,14 and 15, two other triplets are observed at δ 23.10 and 3.32 for the two different isomers.

The CH_2 pendant arm protons resonate at δ 3.45 and 3.50 and are represented by two singlets for the two isomers.

The protons which are adjacent to both oxygen atoms occur downfield of the other ethylene protons in barium macrocycle, by resonating at δ 3.73 and 3.75. As a consequence of being in an equal magnetic environment the ethylene protons at atom positions 8,9,17 and 18 appear as singlets (no coupling).

As a consequence of obtaining the spectrum in CD_3OD , exchange with the protons of the carboxylic acid appendages will take place and thus no peak for the COOH is observed.

Fig 4.4.3.2.3.a. ^1H N.M.R. spectrum of $\text{N,N}'$ -bis (carboxymethyl)-4,13-diaza-18-crown-6 (1)

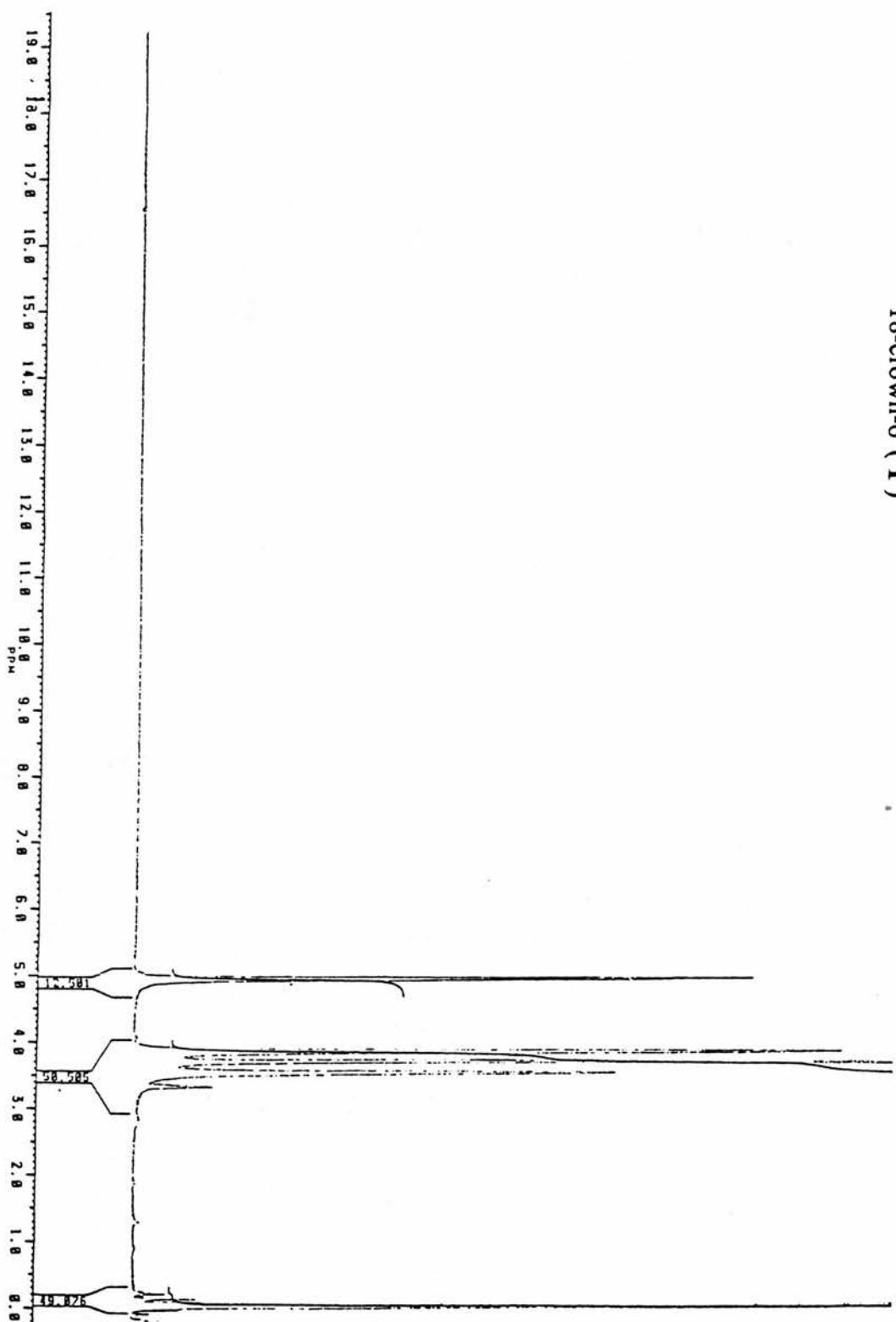
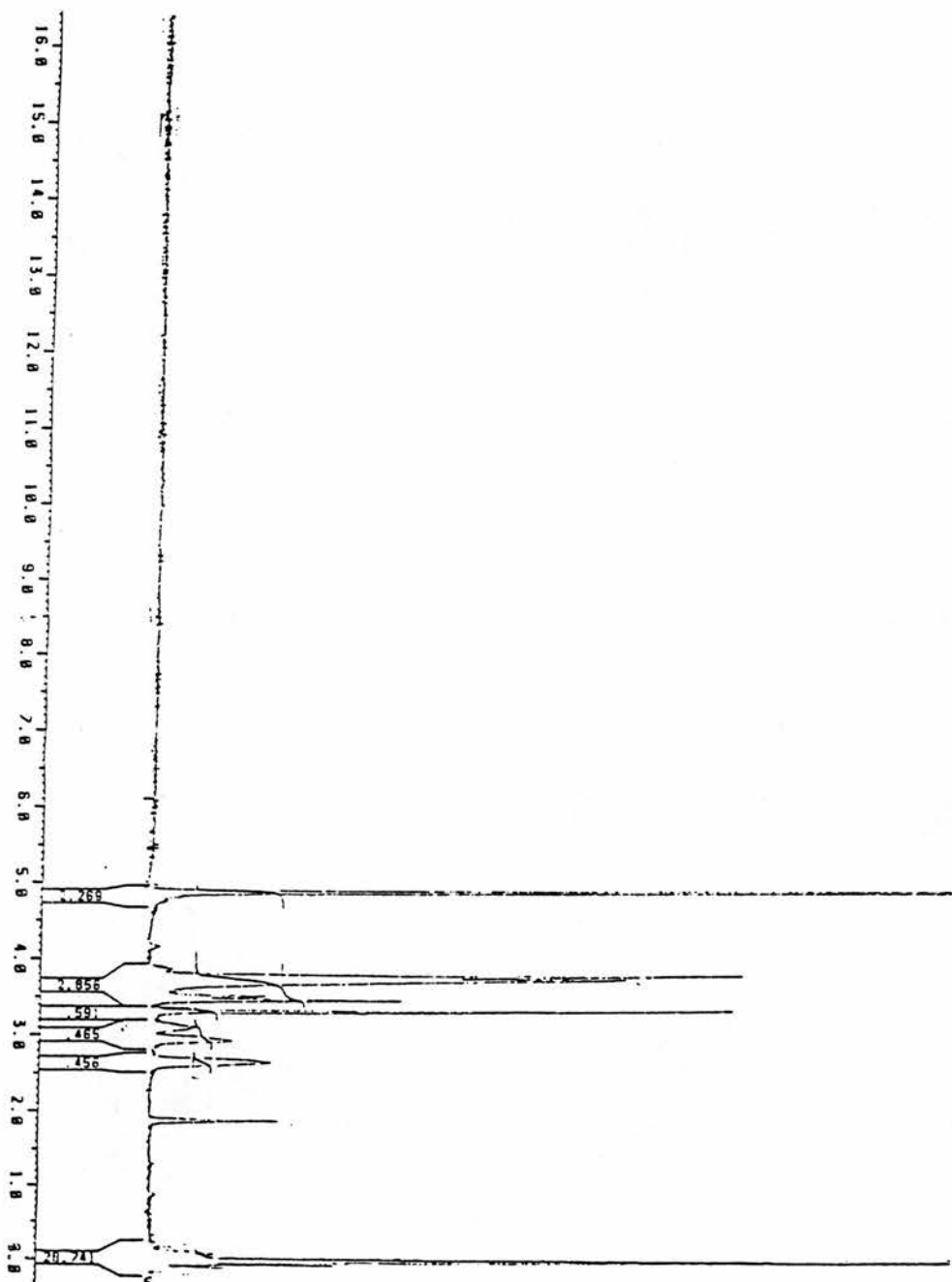


Fig 4.4.3.2.3.b. ^1H N.M.R. spectrum of [N,N'-bis (carboxymethyl)-4,13-diaza-18-crown-6]barium (II) bromide dihydrate



4.4.3.2.4. ^{13}C N.M.R. analysis

The ^{13}C N.M.R spectrum of N,N'bis (carboxymethyl)-4,13-diaza-18-crown-6 barium (II) bromide dihydrate seems to support the presence of two isomers in solution. 10 peaks are shown in the spectra, which is twice as many as expected. The isomers arise from the different orientation of the pendant arms about the plane of the macrocycle.

It appears that the pendant arms are either syn or trans to the plane of the macrocycle. The carbon peaks are also inequivalent in their intensities which suggests that one particular isomer is favoured to the other. The two carbonyl resonances at δ 179.10 and 178.66 occur upfield to the single carbonyl resonance of the parent ligand (N,N-carboxymethyl-4,13-diaza-18-crown-6) which is probably a cause of anisotropic effects.

The carbon peaks observed at δ 71.35 and 70.98 are attributable to the ethylene carbons situated adjacent to both oxygen atoms at atom positions 8,9,17 and 18. The CH_2 carbon resonance from the pendant arms on the macrocycle occurs at δ 69.60 and 69.51. This appears to occur downfield of the single carbon resonance observed for the CH_2 in pendant arm of the parent ligand at δ 66.21. Carbon atom positions 2, 6,11,15 have two peaks attributable to two isomeric forms of the barium(II) bromide salt at δ 58.66 and 58.38. Interestingly, the carbon peaks at δ 56.26 and 57.03 occur upfield to all the other ethylene carbons in the barium macrocycle ring. These ethylene carbons experience a lower electron-withdrawing effect than the ethylene carbons adjacent to the oxygen atoms. It appears that the carbon atom positions 3,5,12 and 14 give rise to these upfield resonances.

Fig 4.4.3.2.4.a. ^{13}C N.M.R. spectrum of N,N'- bis (carboxymethyl) -4,13-diaza-18-crown-6 (1)

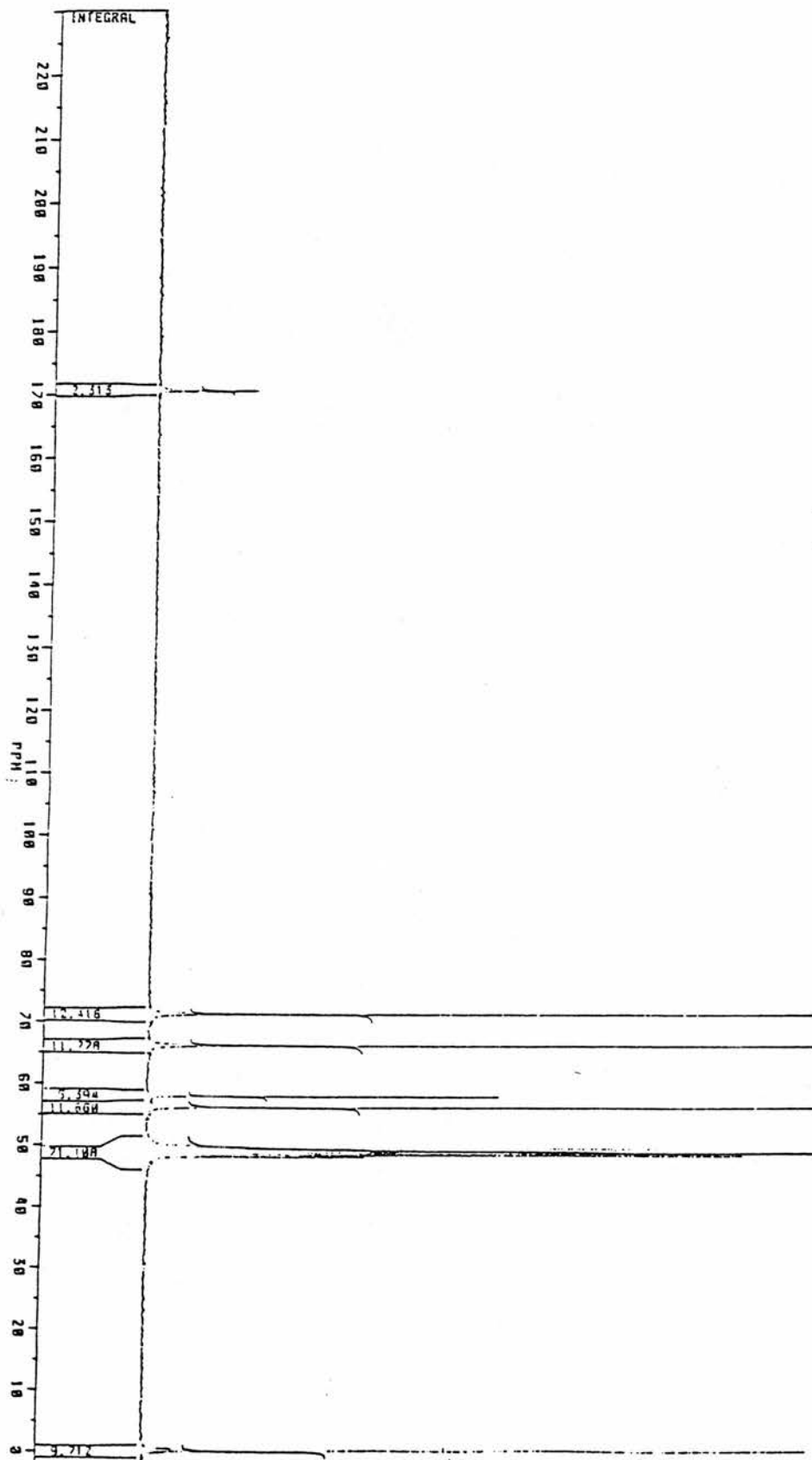
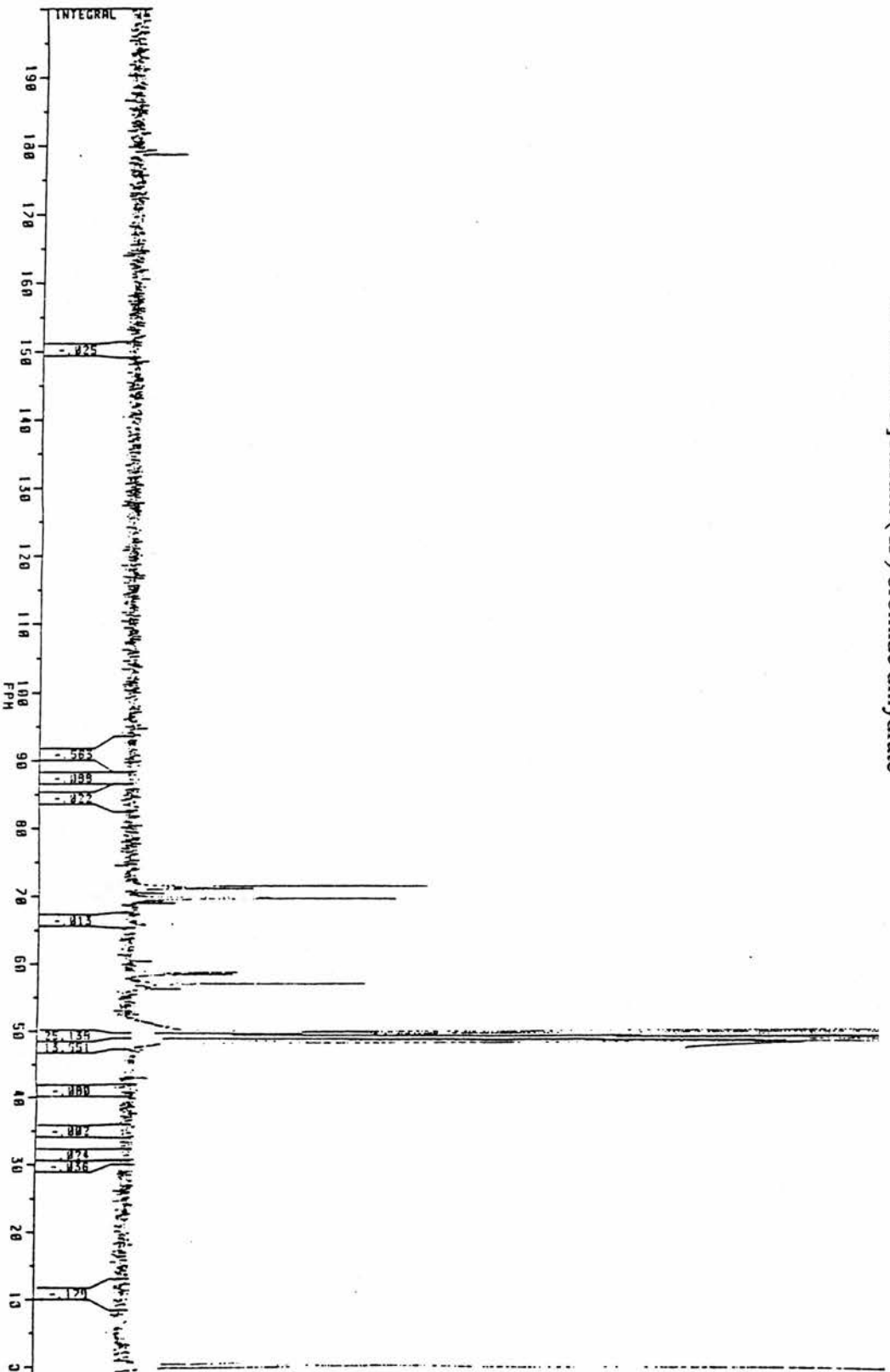


Fig.4.4.3.2.4.b. ^{13}C N.M.R. spectrum of [N,N'-bis (carboxymethyl)-4,13-diaza-18-crown-6]barium (II) bromide dihydrate



4.4.3.2.5. STA Studies

The STA studies of [(N,N'- carboxymethyl-4,13-diaza-18-crown-6)barium(II) bromide] show 3 major endotherms at 95°C, 208°C, and 320°C. The endotherm at 95°C corresponds to the loss of two water molecules from the barium hydrated complex (5.06 % of the hydrated complex). The second endotherm corresponds to broad melting point at 208°C. This is supported by the observed melting point determination which showed slight discoloration at 180°C and decomposition / melting point at 210°C.

The presence of another endotherm at 320°C seems to indicate that after melting the complex fully decomposes. The subsequent decomposition leaves a % weight residue of 30 %.

The observed % weight residue is far too high for the residue to exist as BaO, as that would require a % weight residue of 21.55 % at 1000°C. The residue obtained at 1000°C may be attributable to the formation of a barium oxybromide - 0.5 Ba₂OBr₂ which would leave a calculated, 31.66% weight residue at 1000°C.

Another possibility is that the barium macrocycle has not fully decomposed to barium oxide and some carbon residue is left behind as the STA investigation was undertaken in a stream of dry nitrogen (insufficient oxygen content).

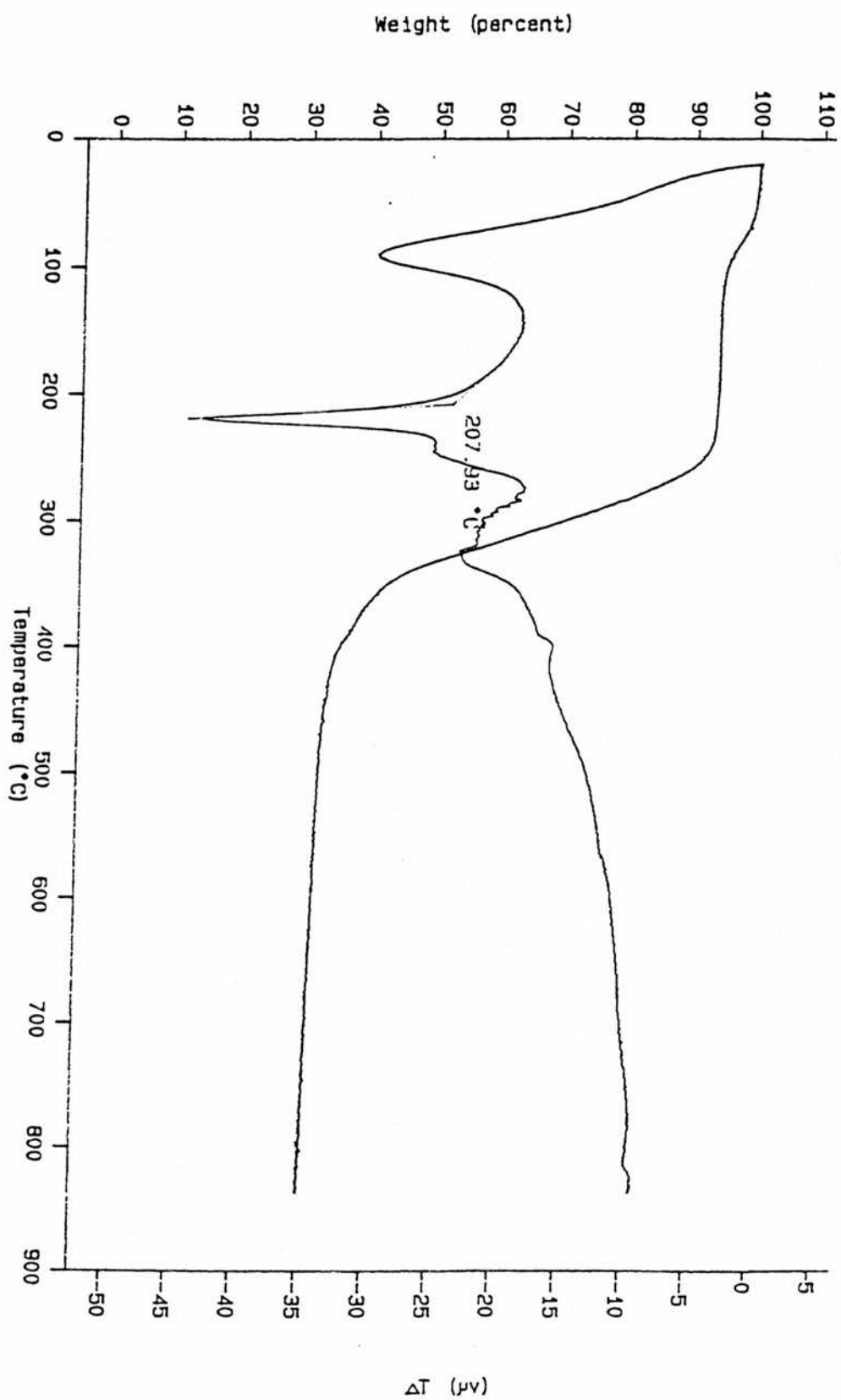


Fig 4.4.3.2.5.a. STA of [N,N'- bis (carboxymethyl) -4,13-diaza-18-crown-6]
barium (II) bromide dihydrate

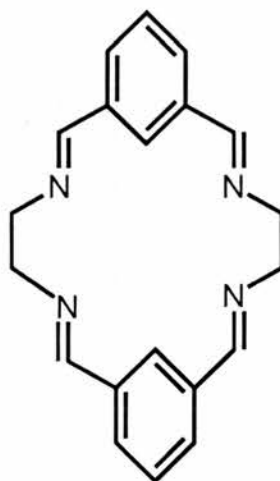
4.4.4. The Preparation and analysis of the barium schiff-base bibracchial pendant arm macrocycles (4) and (5)

4.4.4.1. The Preparation of the macrocycles (4) and (5) and their barium complexes

In order to exploit the potential advantages gained by multidentate systems around the barium centre, it was decided to produce 2 other pendant arm macrocycles based on Schiff base condensation macrocycles.

Macrocycle (4A) was produced via the nontemplate condensation reaction between 1,2-diaminoethane and benzene-1,3-dicarboxyaldehyde. An unsaturated 18-membered macrocycle was isolated.

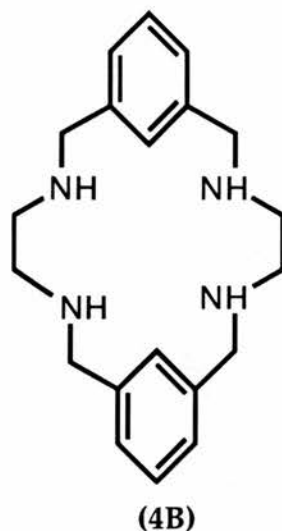
Fig.4.4.4.1.a.



(4A)

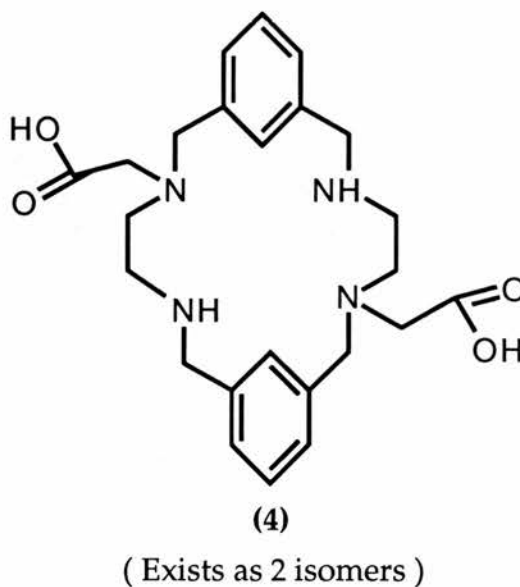
(Exists as 2 isomers)

Sodium borohydride was then added to a solution of the unsaturated macrocycle (4A) in CHCl_3 and ethanol to reduce the imine $\text{C}=\text{N}$ bonds of the macrocycle.

Fig.4.4.4.1.b.

As a consequence of the reduction of the unsaturated macrocycle, two of the bridgehead nitrogen atoms can now be deprotonated with potassium hydroxide and reacted further with bromoacetic acid and sodium carbonate in methanol to produce the pendant arm macrocycle.

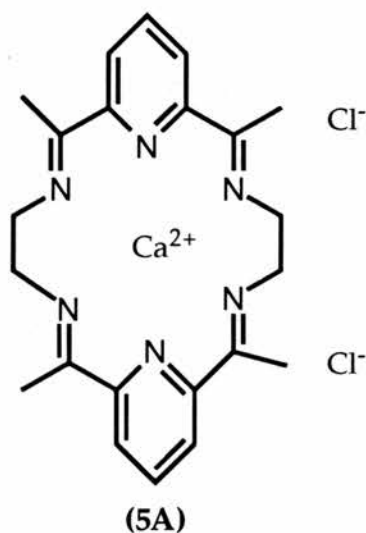
Several N-alkylations of macrocycles have been investigated. However, the incorporation of only 2 pendant arms onto a macrocycle has proven very difficult.

Fig.4.4.4.1.c.

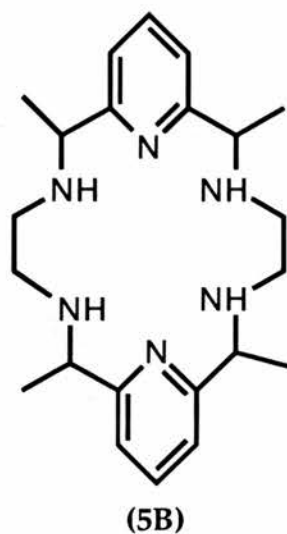
The attempted preparation of the barium complex was undertaken by reacting $\text{Ba}(\text{OH})_2 \cdot 8\text{H}_2\text{O}$ and the pendant arm macrocycle (4).

The pendant arm bibracchial macrocycle (5) was produced by a similar synthetic strategy to that employed for (4). This also involved a 4 stage reaction sequence. The first intermediate (5A) was produced and isolated by reacting 1,2-diaminoethane and 2,6-diacetylpyridine in the presence of a calcium template²².

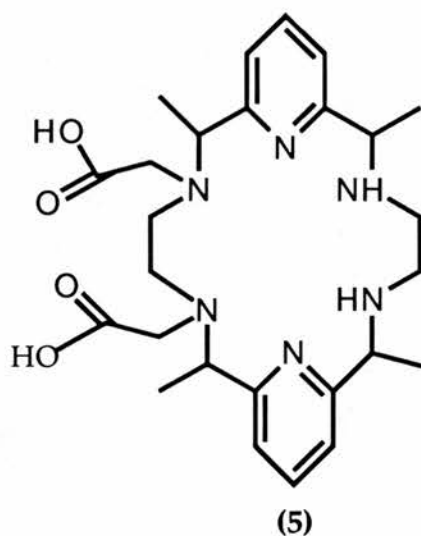
Fig.4.4.4.1.d.



Sodium borohydride was then added to the calcium macrocycle whereupon the calcium metal cation was eliminated and the corresponding imine $\text{C}=\text{N}$ bonds were reduced to the saturated uncomplexed macrocycle (5B)²².

Fig.4.4.4.1.e.

Again, as with macrocycle (4), alkylation was carried out in a suspension of bromoacetic acid, potassium hydroxide and sodium carbonate in methanol to produce the pendant arm macrocycle. The attempted preparation of the barium complex was undertaken by reaction between $\text{Ba}(\text{OH})_2 \cdot 8\text{H}_2\text{O}$ and the pendant arm macrocycle (5).

Fig.4.4.4.1.f.

4.4.4.2. The analysis of the bibracchial pendant arm schiff-base macrocycles

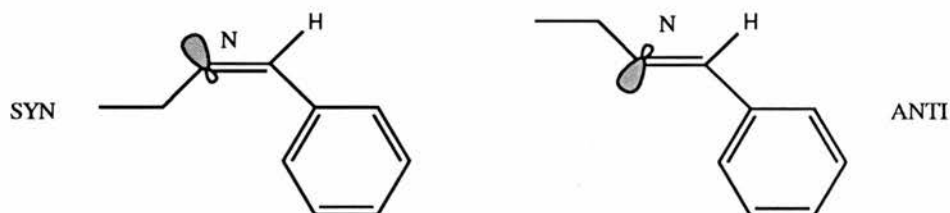
4.4.4.2.1. IR spectral analysis of macrocycle (4A)

The IR spectra of these macrocycles (**4**, **4A** and **B**) show considerable differences in absorption frequencies. However, peaks between 1641 and 1581 cm^{-1} correspond to weak aryl ν (C=C) which are characteristic of these 3 macrocycles. In the IR spectrum of (**4A**), these peaks are observed at $1641, 1595$ and 1581 cm^{-1} . These 3 bands are typical of aryl stretching modes and are probably shifted to a lower frequency as a consequence of the cyclisation of the macrocycle and the added conjugation of the sp^2 hybridised CH and N in the imine part of the macrocycle. The absorptions at $801, 724$ and 691 cm^{-1} are bands which are typical of meta-substituted aryl rings. In spite of the apparent predicted weakness of intensity of C=N band, a sharp absorption at 1732 cm^{-1} is observed for ν (C=N). The stretching frequencies at 1153 and 1073 cm^{-1} correspond to ν (C-C).

4.4.4.2.2. ^1H N.M.R. analysis

The ^1H .N.M.R. of the unsaturated macrocycle (**4A**) shows a combination of peaks which seems to suggest that the macrocycle has been isolated as a series of isomers. As seen in Fig 4.4.4.2.2.a., the rotation around the C-N bond can arise to give syn and anti isomers. A maximum of 16 stereoisomers can occur, although some of the stereoisomers will be equivalent to one another (7 inequivalent stereoisomers).

Fig 4.4.4.2.2.a.



Although, the resonance peaks in the ^1H N.M.R. spectrum indicate the presence of only two isomers. The two sets of singlets at δ 3.9-4.0 represent the ethylene protons from both of the isomers. Furthermore, the integration ratios of these singlets suggests that the relative abundance of one of these isomers is 3 times greater than the other isomer.

It can be also shown that the doublet which appears in the spectrum at δ 7.72 is represented by the protons on the aryl ring positions Hb,b' as indicated in Fig4.4.4.2.2.b. The multiplet at δ 7.37 corresponds to the protons at ring positions Ha. The two singlets at δ 7.87 and 8.07 are attributable to the protons at the ring position Hc. The singlets at δ 8.15 and 8.23 show the proton signals from the hydrogens directly bound to the imine carbons.

The singlet at δ 1.6 is due to the residual water in the compound which is as a consequence of the condensation reaction..

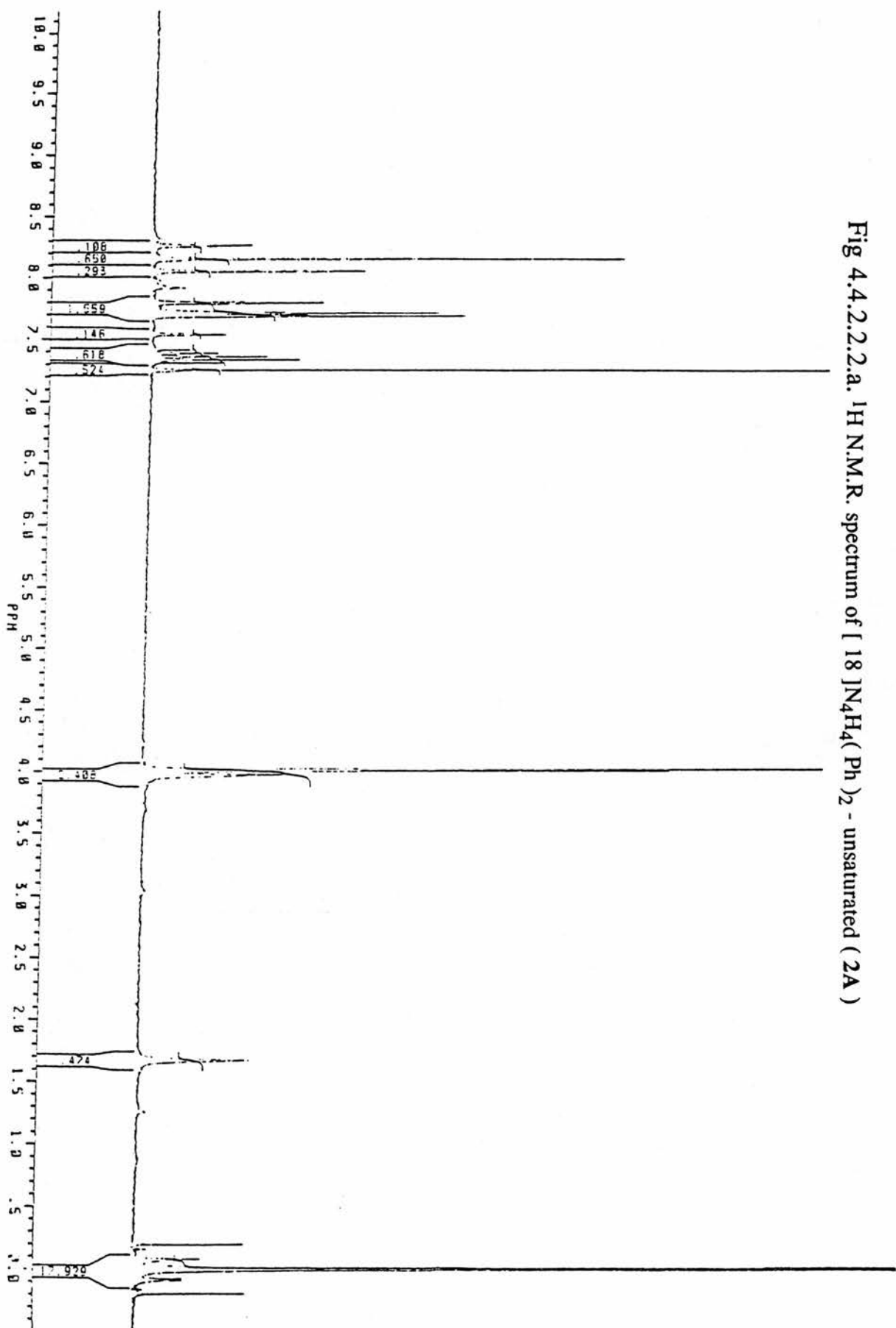
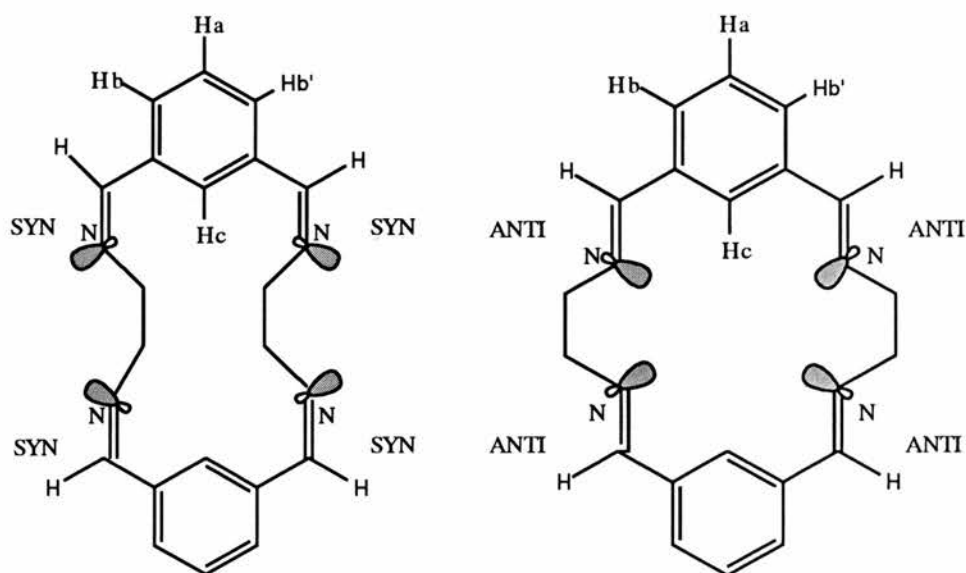
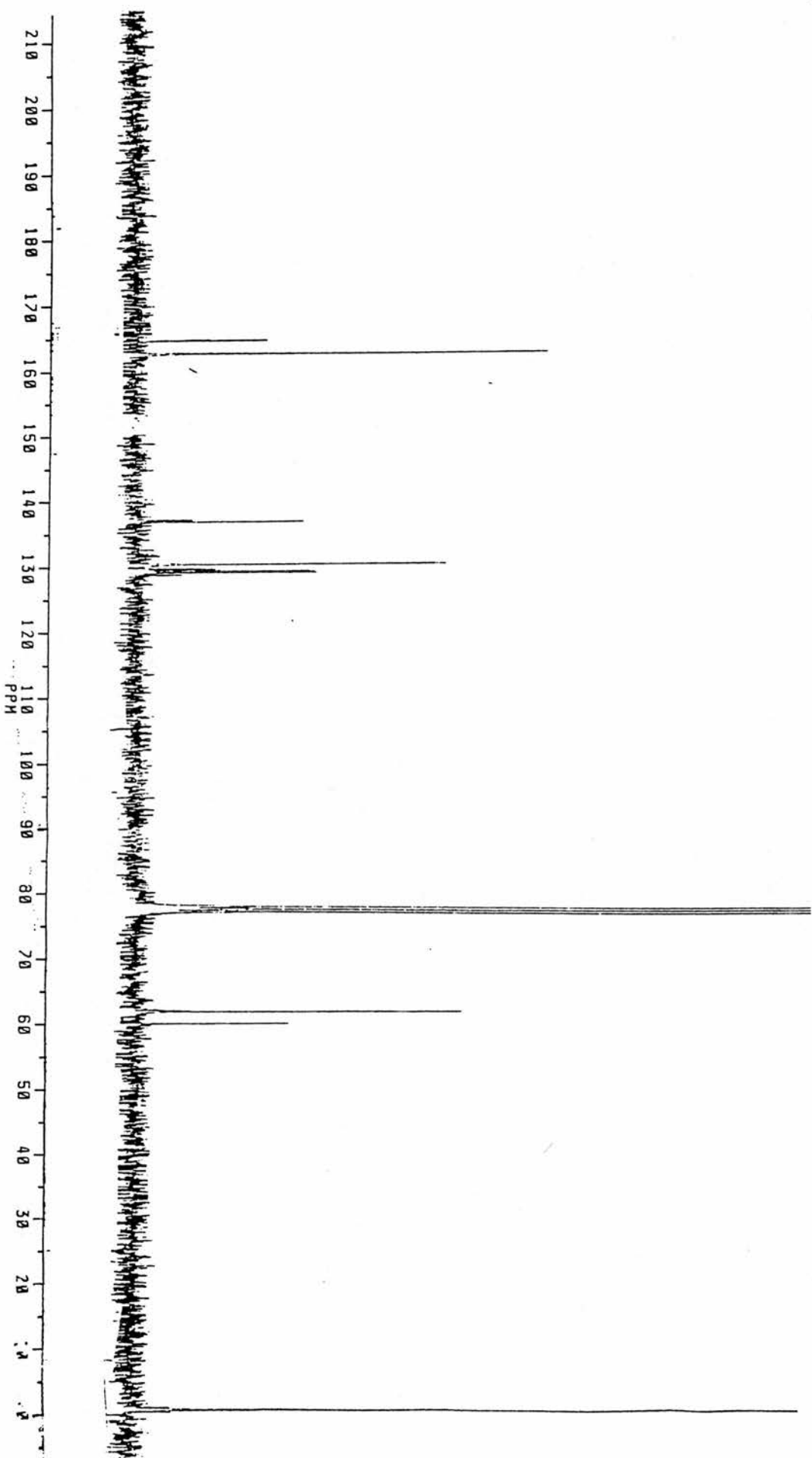
Fig 4.4.2.2.2.a. ^1H N.M.R. spectrum of $[\text{18 } ^{14}\text{N}_4\text{H}_4(\text{Ph})_2 - \text{unsaturated} (2\text{A})]$ 

Fig 4.4.4.2.2.b



4.4.4.2.3. ^{13}C N.M.R. spectrum of macrocycle (4A)

The observation of 12 separate carbon peaks seems to support the initial findings in the ^1H N.M.R. spectrum, in that the macrocycle (4A) exists in two isomeric forms. The two isomers in solution are likely to have the AAAA and the SSSS conformation (A = Anti, S = Syn). As shown in fig 4.4.4.2.2.b., the two isomers would each give rise to 6 inequivalent carbon signals. This is compared with the other possible stereoisomers which would result in giving the wrong number of peaks in the ^{13}C N.M.R. spectrum. Resonance peaks due to the two isomeric forms (AAAA) and (SSSS) are shown in the two carbon peaks resonating at δ 164.04 and 162.15. These signals are attributable to the imine carbons. 8 inequivalent phenyl carbon peaks are observed in the region of δ 136.51-128.49. The two isomeric forms of the macrocycle (4A) are also represented in the ^{13}C N.M.R. spectrum at δ 59.44 and 61.19 which is the cause of the ethylene carbons resonating. This is in comparison with the observed single resonance for 1,2-diaminoethane at δ 45.06.

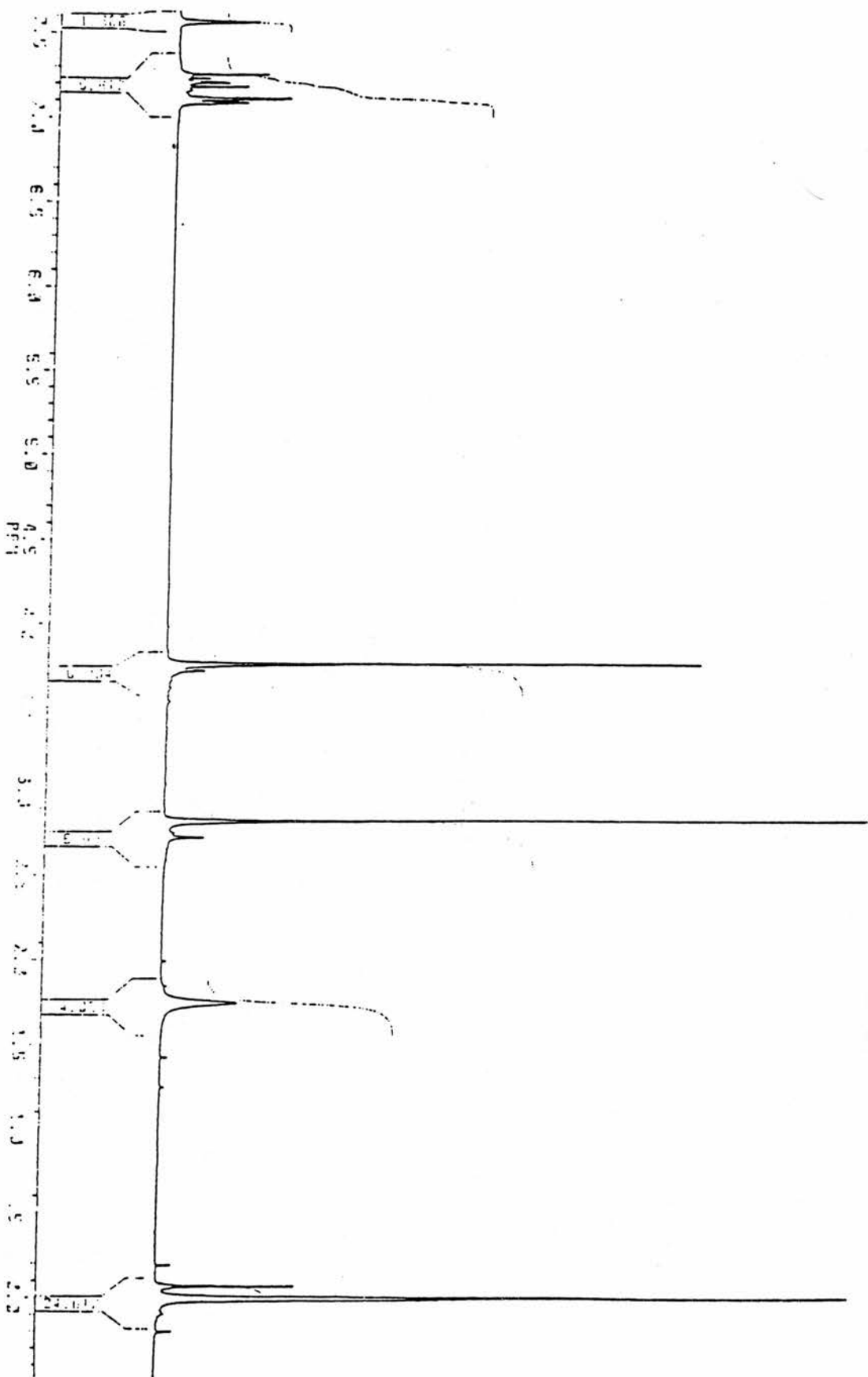
Fig 4.4.2.2.3.a. ^{13}C N.M.R. spectrum of [18] $\text{N}_4\text{H}_4(\text{Ph})_2$ - unsaturated (2A)

4.4.4.2.4. IR spectral analysis of the macrocycle (4B)

As a consequence of the reduction of the imine bonds in the unsaturated macrocycle (4A), the infrared spectrum of the saturated macrocycle (4B) shows two characteristic N-H stretching frequencies at 3295 and 3245 cm^{-1} . The IR spectrum also shows no absorption band at 1732 cm^{-1} which is observed in the unsaturated macrocycle (4A), thus, indicating that the imine bond C=N has been removed. The rest of the absorbances shown in the IR spectrum of (4B) are attributable to either the aryl stretching / bending modes or aliphatic vibrational modes, i.e., ν (C-C) and ν (C-N). These stretching and bending modes are characteristic of the macrocycles (4A, 4B and 4) and as a result, the modes of vibration have already been discussed in section 4.4.4.2.1.

4.4.4.2.5. ^1H N.M.R. analysis

As seen in Fig 4.4.4.2.5.a., the ^1H N.M.R. spectrum shows a broad singlet at δ 1.74 which corresponds to the NH protons resonating. Not surprisingly, upon saturation, the ethylene protons at δ 2.81 occur upfield to that of ethylene protons in the unsaturated macrocycle (4A) at δ 3.9-4.0. As a consequence of the saturation of the imine bond, macrocycle (4B), has 4 new CH_2 units which are adjacent to the phenyl rings. These protons are represented by a singlet which occurs at δ 3.65. The aryl protons occur between the region of δ 7.08 and 7.55.

Fig 4.4.2.2.5.a. ^1H N.M.R. spectrum of [18] $\text{N}_4\text{H}_4(\text{Ph})_2$ - saturated (2B)

4.4.4.2.6. ^{13}C N.M.R. analysis

There are half as many signals observed in this spectrum compared to the ^{13}C N.M.R. spectrum of the unsaturated macrocycle (**4A**). It appears also that imine carbons are absent from the spectrum.

The ^{13}C N.M.R. spectrum of macrocycle (**4B**) shows 6 resonating signals. Four of these signals arise between δ 141.06 and 126.44 and correspond to aryl resonances of the saturated macrocycle (**4B**).

The peak at δ 53.69 corresponds to the 4 new CH_2 carbon centres which have been produced as a result of the saturation of the imine bond. The ethylene carbons which originate from the 1,2-diaminoethane part of the macrocycle occur at δ 48.63.

The ^{13}C N.M.R. spectrum of (**4B**) is shown in Fig 4.4.4.2.6.a.

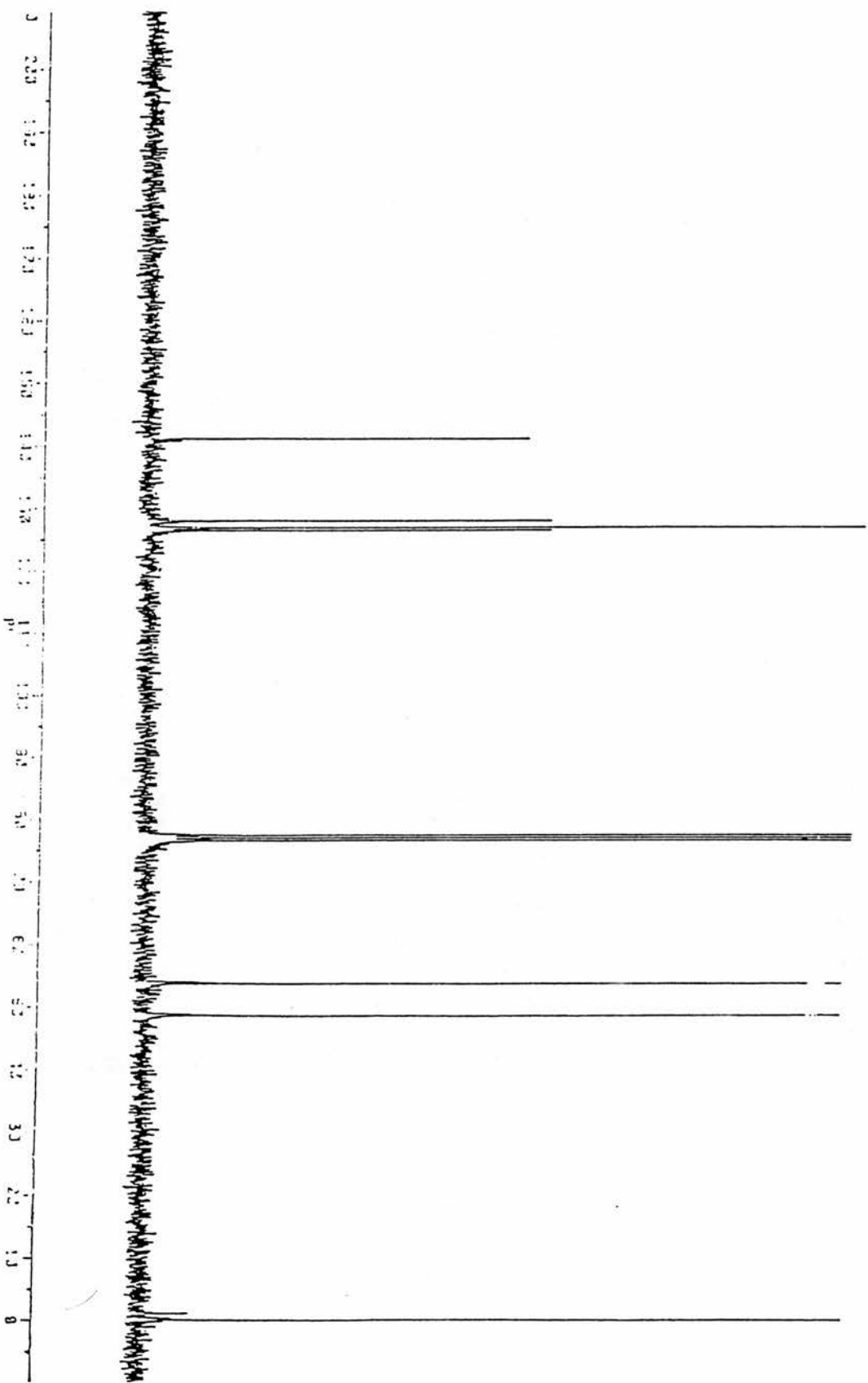
4.4.4.2.7. IR spectral analysis of the pendant arm macrocycle (**4**)

Two fundamental differences are observed in the IR spectra of (**4**) relative to that of (**4B**). The OH groups are involved in extensive hydrogen bonds.

This is shown by the strong, broad absorption at 3420 cm^{-1} which corresponds to the ν (OH). In fact, the ν (N-H) is obscured by the ν (O-H).

The absorption at 1735 cm^{-1} is attributable to ν (O-C=O) of the carboxylic acid which is absent in the corresponding parent saturated macrocycle. The absorption frequencies arising from either the stretching / bending modes of the aryl rings or the aliphatic vibrational modes are similar to the ones encountered in the other macrocycles (**4A and 4B**).

Fig 4.4.2.2.6.a. ^{13}C N.M.R. spectrum of [18] $\text{N}_4\text{H}_4(\text{Ph})_2$ - saturated (2B)



4.4.4.2.8. Mass Spectral analysis

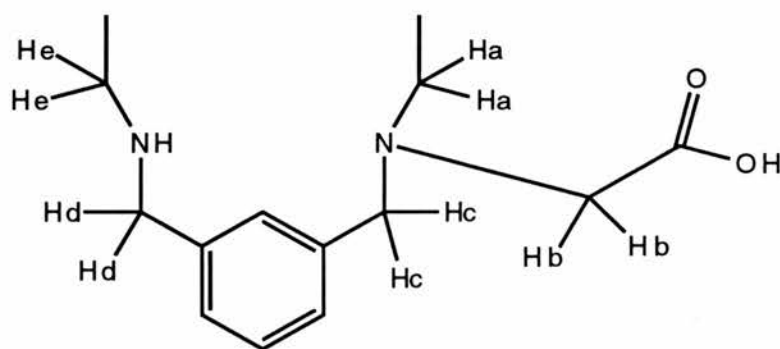
The observation of ions in the EI mass spectra of (4) at masses greater than that of the molecular ion of the pendant arm macrocycle, seems to suggest that the macrocycle is associated. Ions are observed at 579 and 552 mass units. A softer form of mass ion detection is needed to observe these ions.

4.4.4.2.9. ^1H N.M.R. analysis

A broad peak at δ 2.0 represents the remaining 2 NH protons resonating.

Fig 4.4.4.2.9.a. shows the different sets of inequivalent protons that do exist as a consequence of alkylating the macrocycle.

Fig 4.4.4.2.9.a.

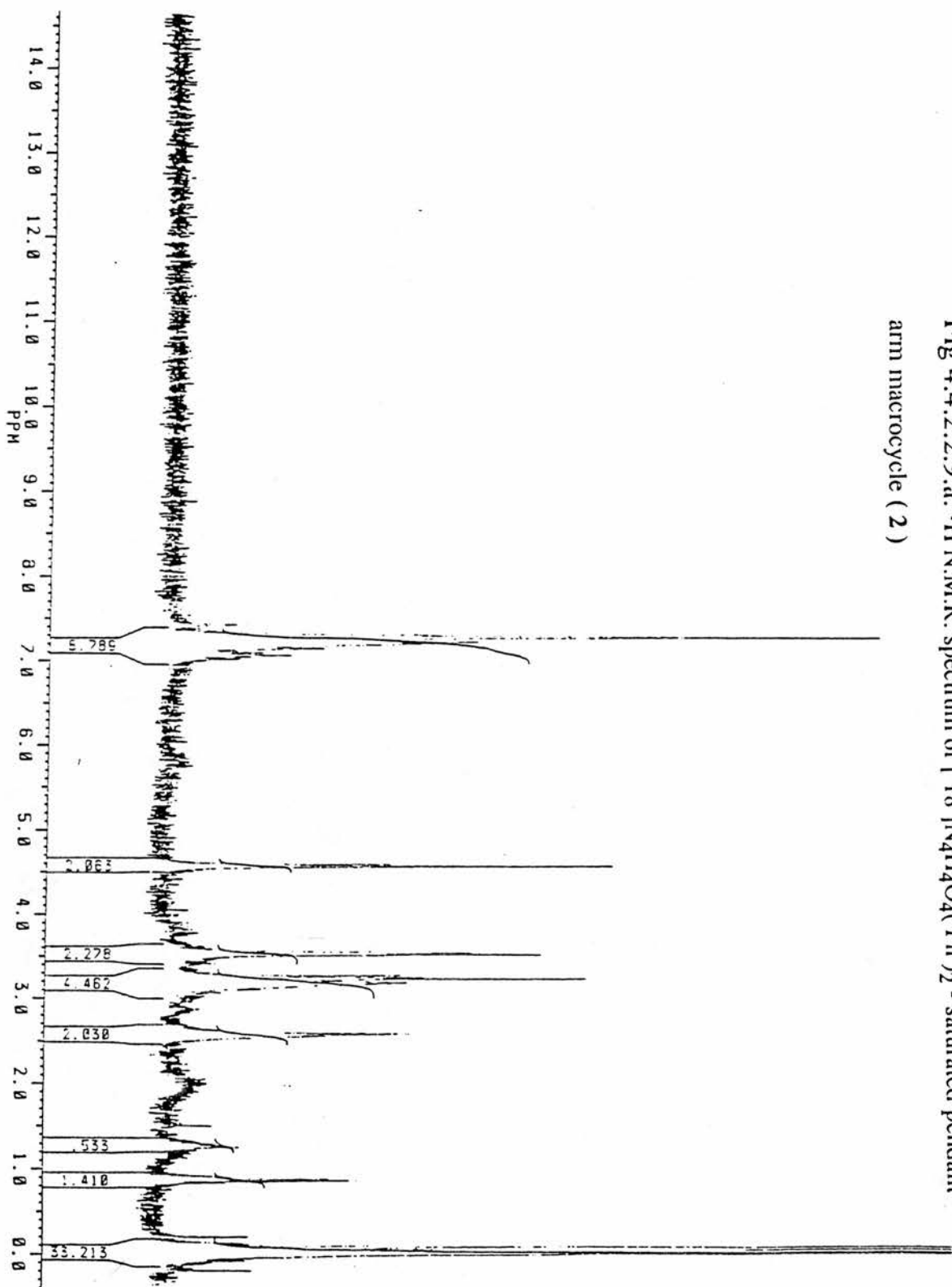


A schematic diagram of part of macrocycle (4)

It can be seen in Fig 4.4.4.2.9.b., that the triplets at δ 3.18 and δ 2.58 are attributable to the protons from the ethylene CH_2 a and e. The protons from the CH_2 a, which are adjacent to the pendant arm have moved considerably downfield from its CH_2 counterpart, CH_2 e at δ 2.58. The protons of the ethylene CH_2 c and d resonate at δ 3.54 and 4.6.

Again, the singlet at δ 4.6 arises from the protons from Hc which are adjacent to the pendant arm. Interestingly, in the saturated macrocycle (4B), the protons from the ethylene CH_2 adjacent to the phenyl rings resonate at δ 3.65. The peak at δ 3.25 is as a result of the ethylene protons on the pendant arm Hb

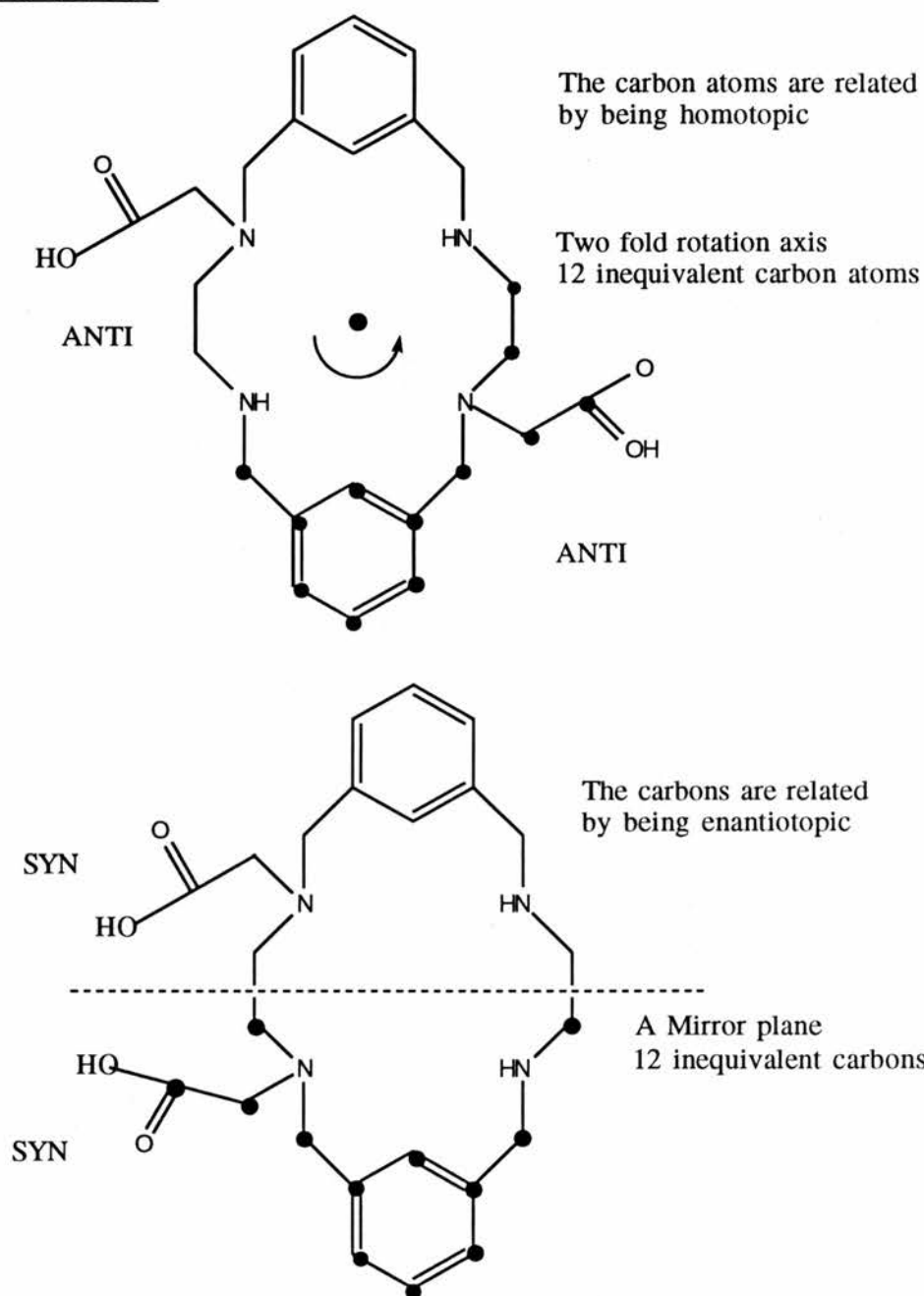
Fig 4.4.2.2.9.a. $^1\text{H N.M.R.}$ spectrum of $[18 \text{ [N}_4\text{H}_4\text{O}_4(\text{Ph})_2 - \text{saturated pendant arm macrocycle (2)}$



4.4.4.2.10. ^{13}C N.M.R. analysis

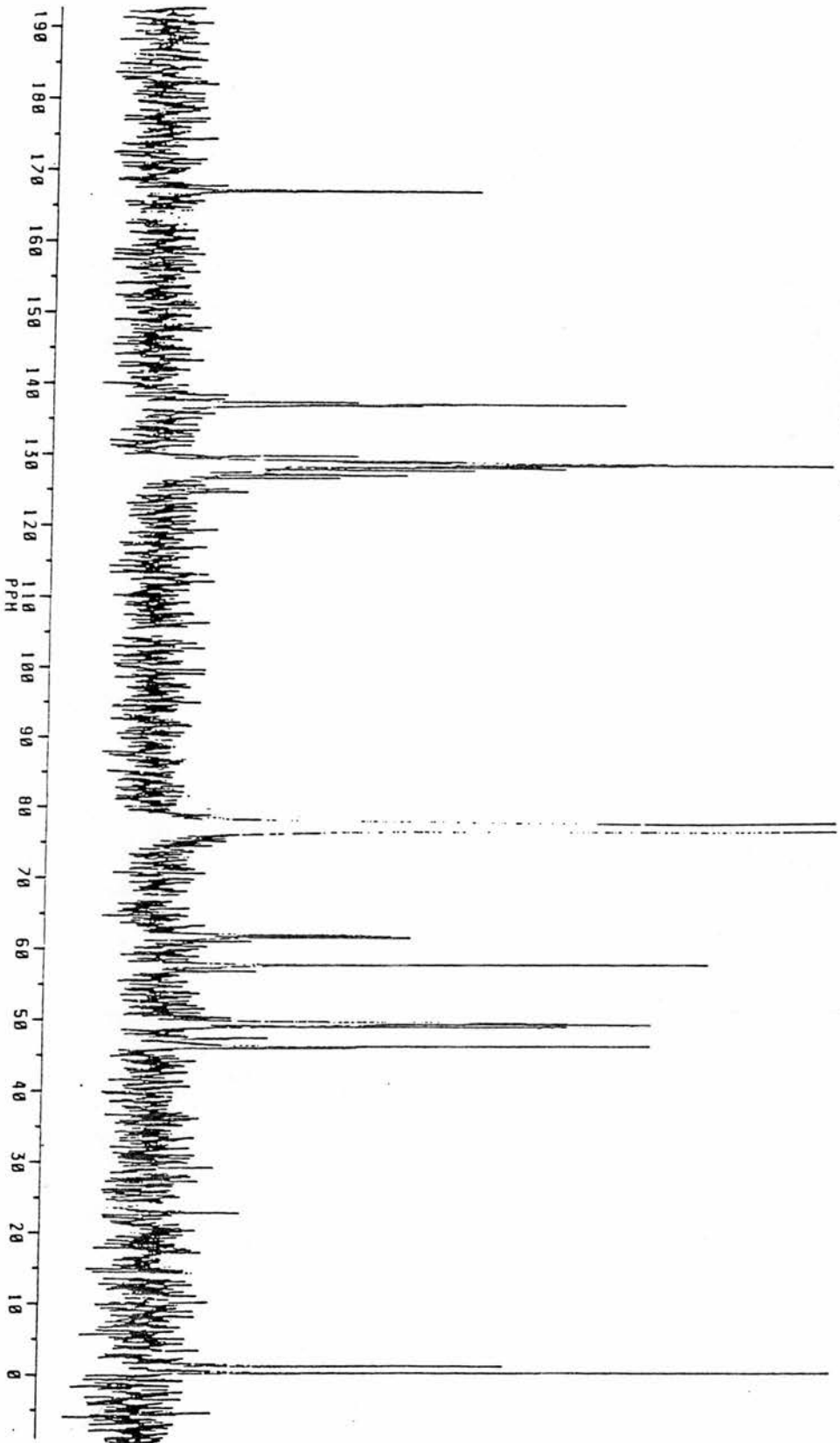
24 peaks are observed in the ^{13}C N.M.R. spectrum of macrocycle (4). The predicted number of non-equivalent carbon atoms for two stereoisomers of macrocycle (4) is 24. The number arises from the constitutional difference occurring at the apical nitrogen atoms where the pendant arm may attach. The two different pendant arm arrangements which can give rise to 24 peaks in ^{13}C N.M.R. spectrum are when the pendant arms are ANTI to one another or when they are SYN to one another as shown in Fig 4.4.4.2.10.a. In Fig 4.4.4.2.10.a., the inequivalent carbons are represented by the black dots

Fig 4.4.4.2.10.a



As predicted from the above diagram, two different carbonyl resonances are seen at δ 166.97 and 166.73. These two peaks seem to appear upfield from the single carbonyl signal which is observed for 1-bromoacetic acid at δ 173.74. 12 phenyl signals are shown in the region of δ 137.29-126.95.

Fig 4.4.2.2.10.a. ^{13}C N.M.R. spectrum of [16] $\text{N}_4\text{H}_4\text{O}_4(\text{Ph})_2$ - saturated pendant arm macrocycle (2)

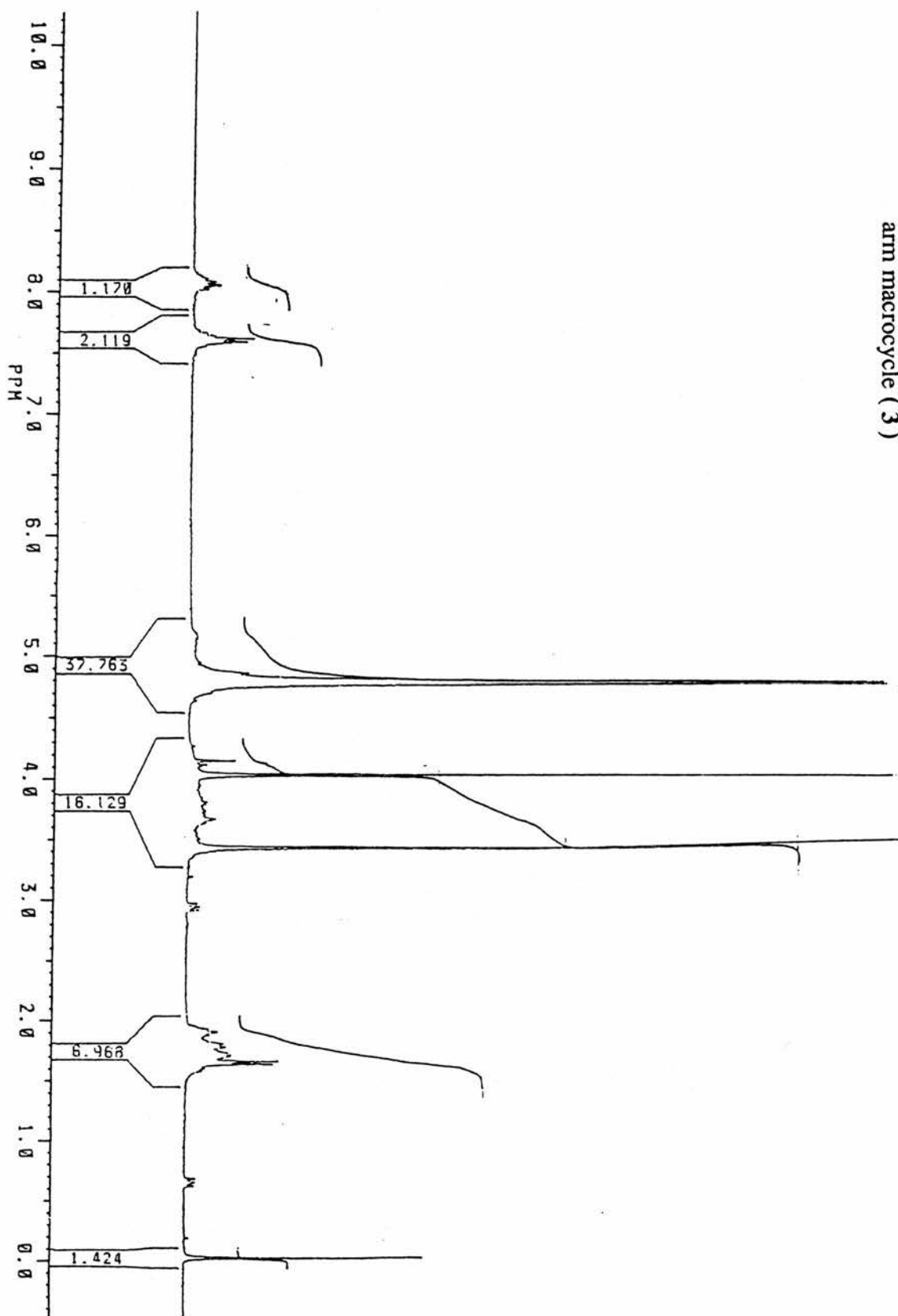


The peaks for 4 ethylene resonating carbons are seen in the region of δ 61.99 - 61.44 for the two isomers. The peaks at δ 57.70 and 57.60 are attributable to the carbon atoms adjacent to the carboxylate carbons on the pendant arms. This is in comparison with the single carbon peak observed for the resonating ethylene carbon atom in 1-bromoacetic acid at δ 25.27. Four other peaks remain between δ 49.36 and 46.17 which correspond to the ethylene carbon atoms originating from the 1,2-diaminoethane part of the macrocycle.

4.4.4.2.11. ^1H N.M.R. analysis of the macrocycle (5)

The ^1H N.M.R. spectrum of macrocycle (5) has the methyl protons resonating at δ 1.61. As seen in Fig 4.4.4.2.11.a., the singlet at δ 3.43 is attributed to the ethylene protons in the macrocyclic ring. The protons directly attached to the chiral centres occur at δ 3.70. The remaining NH signals resonate at δ 4.00 and the pyridyl signals in the region of δ 7.59 and 8.07.

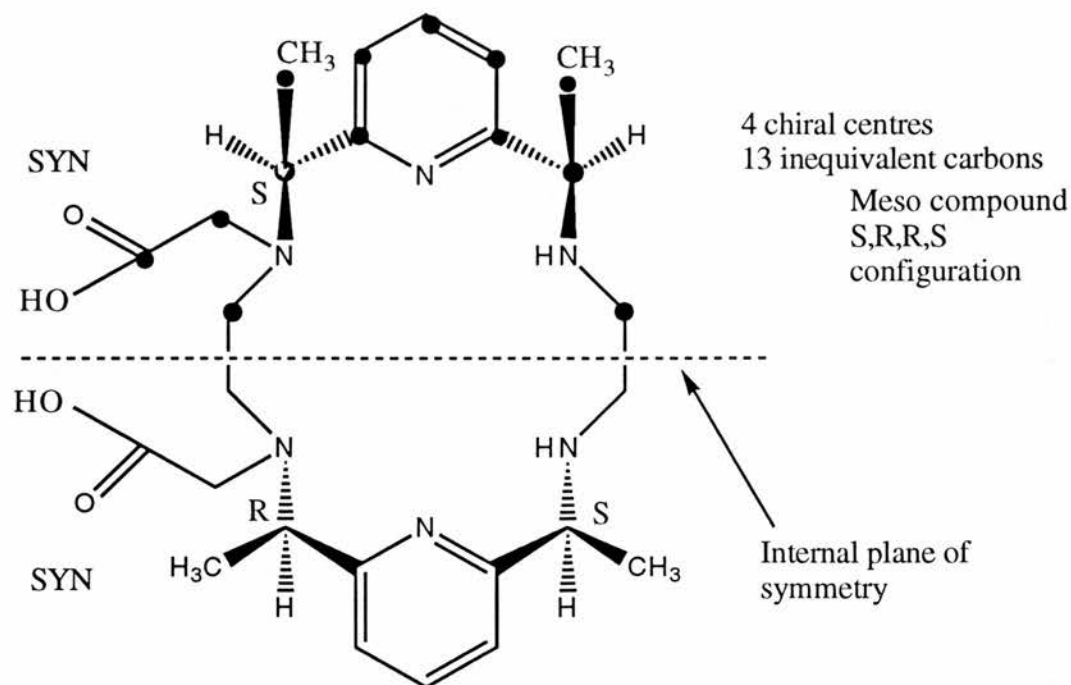
Fig 4.4.2.2.12.a. ^1H N.M.R. spectrum of [18 IN₄H₄O₄(Py)₂ - saturated pendant arm macrocycle (3)



4.4.4.2.12. ^{13}C N.M.R. analysis of the macrocycle (5)

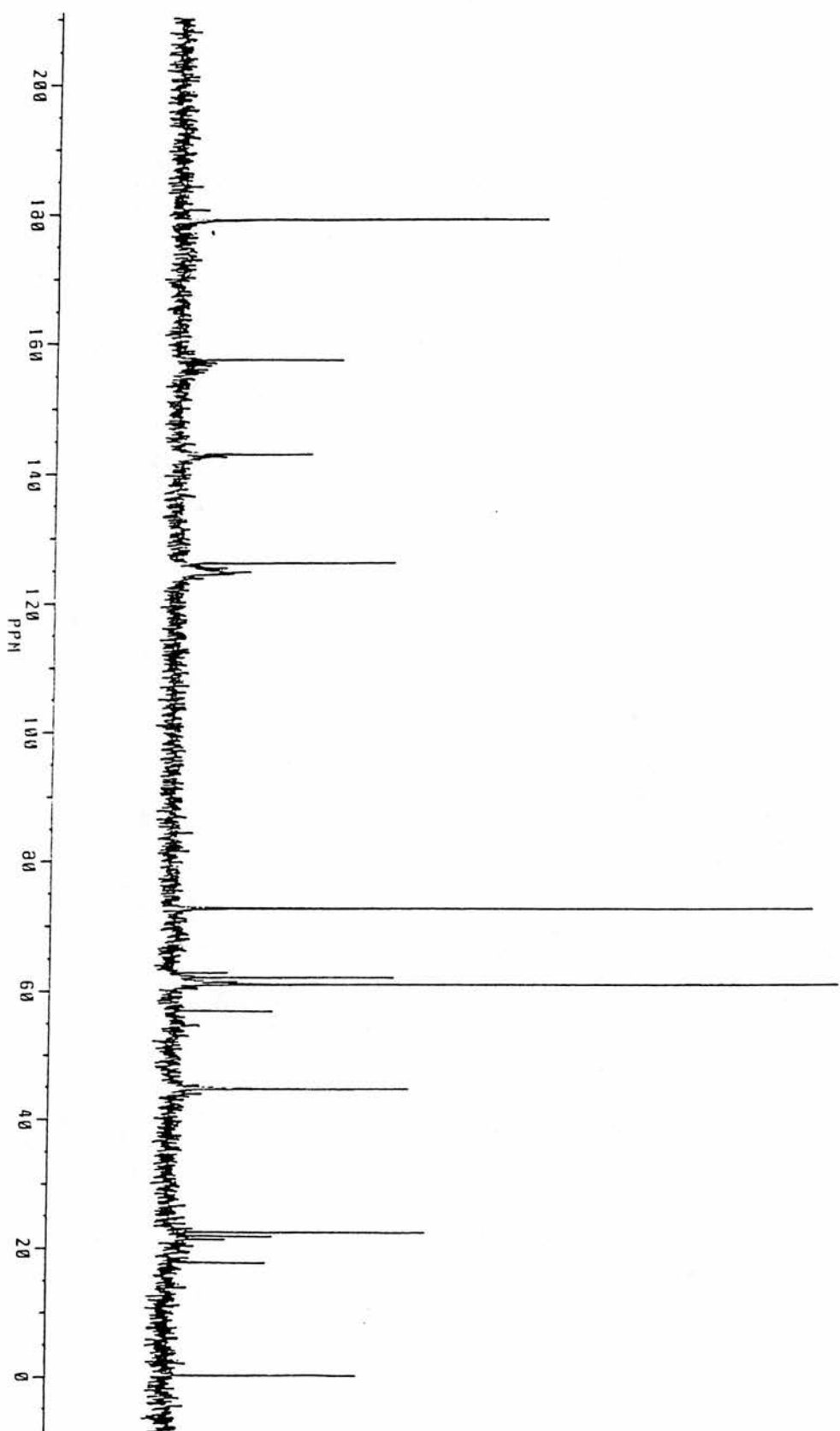
It seems from the ^{13}C N.M.R. spectrum of macrocycle (5) that one isomer exists in solution. This is quite surprising when taking into account that macrocycle (5) contains 4 chiral centres and therefore, has the possibility of forming 16 stereoisomers. In addition, another 3 geometrically different isomers can arise from the positioning of the pendant arm on the macrocycle. Although the absolute configuration about the chiral centres cannot be anticipated by means of ^{13}C N.M.R. spectra alone, a schematic diagram of one of the possible configurations is shown in Fig 4.4.4.2.12.a. In the ^{13}C N.M.R. spectrum of macrocycle (5), 13 carbon resonances are observed, which would tend to indicate the formation of the meso compound as shown in Fig 4.4.4.2.12.a. The 13 inequivalent carbons are represented by the black dots in the diagram.

Fig 4.4.4.2.12.a.



As predicted from Fig 4.4.4.2.12.a., one carbonyl resonance is observed at δ 178.96 for the macrocycle (**5**). Upon alkylation, the C=O resonance has shifted downfield compared to the C=O resonance obtained for 1-bromoacetic acid at δ 173.74 (CDCl₃). The apparent chemical shift may be due to the slight increase in the electron-withdrawing effect of the nitrogen atom compared to the bromine atom. The pendant arm CH₂ carbon occurs at δ 61.03. 5 inequivalent pyridyl carbons occur in the region δ 124.83-157.56. The peaks at δ 61.44 and 62.10 are attributable to the two inequivalent chiral carbons in the macrocycle. Interestingly, the ethylene carbons adjacent to the pendant arm also occur at a different chemical shift at δ 56.92 compared to the ethylene carbons adjacent to the N-H at δ 44.72. Finally, the two methyl peaks are observed at δ 22.27 and 21.66 for this meso compound.

Fig 4.4.2.2.13.a. ^{13}C N.M.R. spectrum of [18] $\text{N}_4\text{H}_4\text{O}_4(\text{Py})_2$ - saturated pendant arm macrocycle (3)



4.4.5. The attempted metal template assisted reaction between [Ba(TMHD)₂], 2,6-diacetylpyridine and 1,2-diaminoethane

As described by SYNTHETIC STRATEGY 4 , the synthesis of a macrocycle by a metal template assisted reaction was undertaken. It seems that a metal template macrocyclic reaction did occur. However, in the two routes adopted to produce the macrocycle, neither produced a neutral barium macrocycle. In the first route, ["Ba(TMHD)₂"] (previously produced by reacting BaBr₂.2H₂O with HTMHD in an aqueous ethanol medium) was reacted with two equivalents of 2,6-diacetylpyridine and 1,2-diaminoethane. From the recrystallisation of an oily mixture, crystals of [Ba([18](Me)₄N₄(Py₂)(Cl₂).3H₂O] were obtained from a CH₂Cl₂ and ethanol. An X-ray crystallographic structure of this macrocycle is seen in Fig 4.4.5.a-b. Interestingly in the second route that was adopted to produce a neutral barium macrocycle, [Ba₄(TMHD)₈] (previously produced by reacting barium metal with HTMHD in dry pentane) was reacted with 2,6-diacetylpyridine and 1,2-diaminoethane. The products that were obtained in second route seemed to also indicate that a metal template macrocyclic reaction had taken place, although, the barium cation had been eliminated from the macrocyclic ring. Therefore, the products that were obtained from the second route obtained - [[18](Me)₄N₄(Py₂)] and unreacted [Ba₄(TMHD)₈]. The reaction scheme of both routes are represented schematically in Fig 4.4.5.c. It is interesting to postulate that in the first route the chloride counter ion must be obtained from the recrystallisation solvent (CH₂Cl₂), as in the second route, toluene and diethyl ether were used as a recrystallisation solvent. Furthermore, it seems in the second route for producing the macrocycle, that the reaction goes catalytically and therefore may have some research or commercial value for making unsaturated macrocycles.

The barium macrocycle - [Ba([18](Me)₄N₄(Py₂)(Cl₂).3H₂O] is a nine coordinate, monomeric solid with 3 molecules of water binding to the barium cation. The other coordination arises from the nitrogen atoms of the partially folded macrocycle. The chloride counterions are not coordinated to the barium centre.

Fig 4.5.a

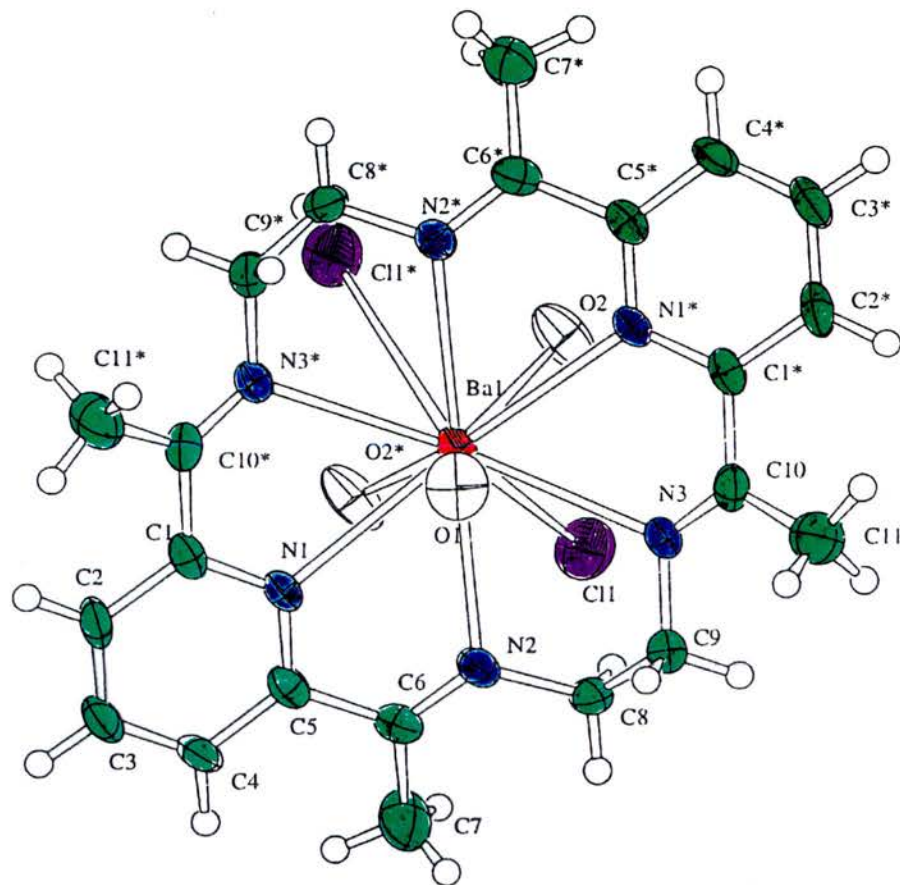


Fig 4.5.b

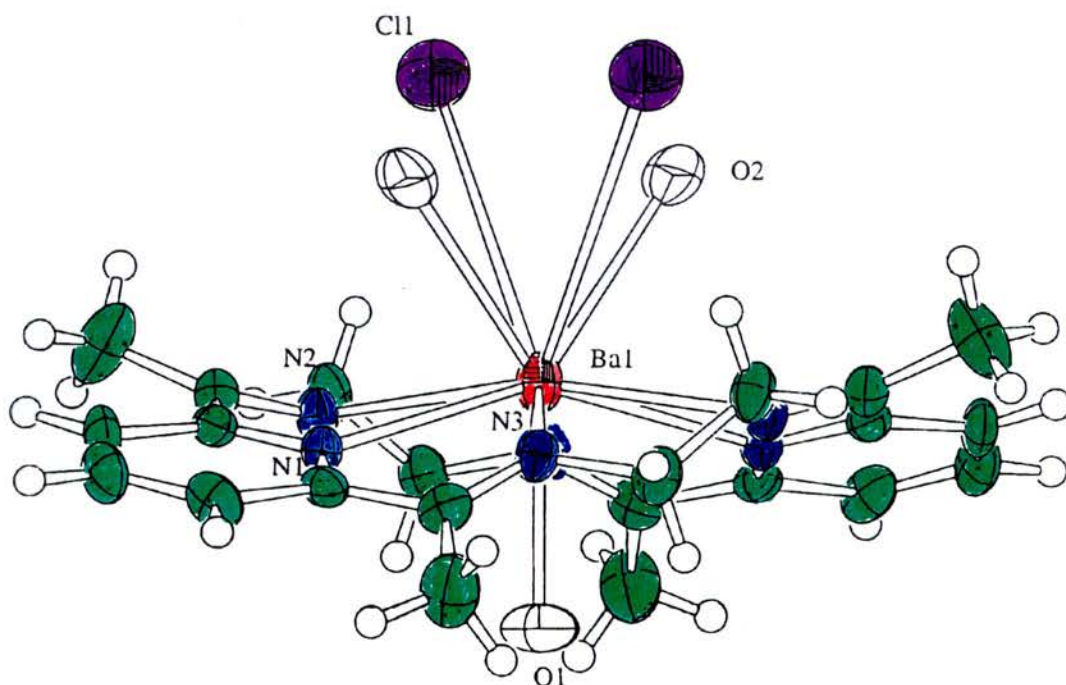
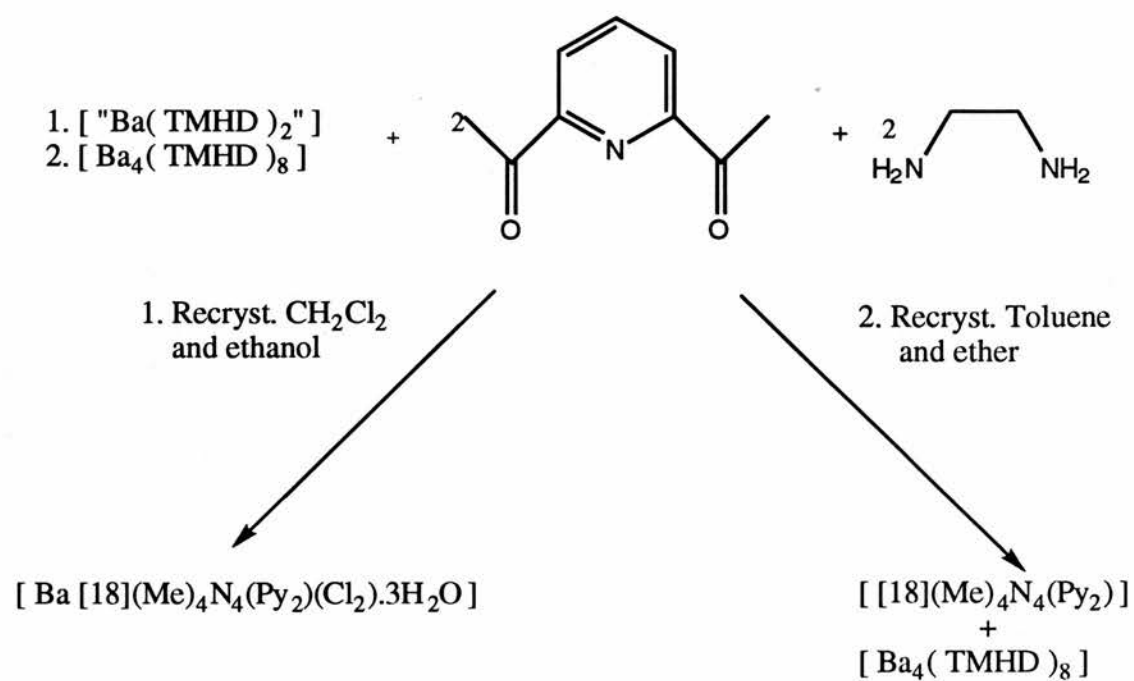


Fig 4.4.5.c.

4.5. Experimental

4.5.1. The Preparation of 1-amino-N,N-bis(2-toluene-p-sulphonylaminoethyl)ethyl ethanoate

A clear solution of recently purified and distilled ethylglycinate^{23*} (3.08 g, 2.99×10^{-2} mol) in acetonitrile (30 cm³) (previously dried over anhydrous MgSO₄ for 1 hour) was transferred to a yellow solution of N-(p-tolylsulphonyl)aziridine (11.16 g, 5.66×10^{-2} mol) in acetonitrile (150 cm³). This resulted in a yellow solution which seemed to get more viscous, whilst the addition commenced. During 12 hours of stirring at room temperature there seemed to be evidence of refluxing. The reaction system was then left at room temperature for a further 2.5 days. The flask was then cooled with a ice / water bath, which resulted in some precipitation. The solid was filtered and the yellow filtrate was condensed to leave a yellow oil. Yield = 12.67 g, 90 %. Found : C 53.38, H 6.56, N 8.12 ; C₂₂H₃₁O₆N₃S₂ requires C 53.10, H 6.28, N 8.44 %.

4.5.1.1. IR data

λ_{\max} : 3272 (s, sp), 2979 (s, sp), 1922 (s, sp), 1729 (s, sp), 1597 (s, sp), 1495 (s, sp), 1360 (s, sp), 1154 (s, br), 1096 (s, br), 909 (s, sp), 817 (s, sp), 668 (s, sp) and 549 (s, sp) cm⁻¹(neat film).

* Once ethylglycinate is produced, a reasonably rapid self condensation reaction takes place (after 12 hours at room temperature). It is therefore necessary for the ethyl glycinate to be used within 12 hours. Storage of ethylglycinate in the dark and at -30°C seems to reduce the rate of self condensation

4.5.1.2. ^1H N.M.R. data

Signals are found at δ 1.20 (3H, t), 2.41 (6H, s), 2.68 (4H, t), 2.87 (4H, t), 3.20 (2H, s), 4.08 (2H, q), 5.81 (2NH, s), 7.31 (4H, d) and 7.79 (4H, d).

4.5.1.3. ^{13}C N.M.R. data

^{13}C N.M.R. signals are observed at : δ 14.28 (CH_3), 21.64 (CH_3), 41.10 (CH_2), 53.84 (CH_2), 54.39 (CH_2), 60.93 (CH_2), 127.30, 129.86, 136.89, 143.42 (Phenyl rings) and 171.96 ($\text{C}=\text{O}$).

4.5.2. The reductive detosylation of 1-amino-N,N-bis (2-toluene-p-sulphonylaminoethyl)ethyl ethanoate by sodium dihydronaphthylide

A dark green solution was produced when a THF solution (300 cm^3) of naphthalene (34.80 g, 0.27 mol) was transferred to a 3-necked flask containing sodium metal pieces (7.23 g, 0.314 mol) in THF (50 cm^3). This green solution was stirred for 16 hours whereupon 1-amino-N,N-bis(2-toluene-p-sulphonylaminoethyl)ethyl ethanoate (13.50 g, 2.71×10^{-2} mol) in THF (50 cm^3) was added to give a deep orange solution. The solution was stirred for 2.5 hours and then added to water (75 cm^3). Upon careful addition of the deep orange solution to water, a yellow gelatinous precipitate was produced. The THF was then removed under normal distillation conditions.

The residue was then dissolved in CH_2Cl_2 (300 cm^3). The CH_2Cl_2 solution was then extracted with dilute hydrochloric acid ($3 \times 100\text{ cm}^3$, 1 mol dm^{-3}). Upon separation of the layers, the acidic layer was cooled to 0°C using ice-water bath and basified with aqueous potassium hydroxide (200 cm^3 , 7 mol dm^{-3}).

The aqueous solution was extracted with dichloromethane ($3 \times 100 \text{ cm}^3$) and the combined organic extracts were dried over anhydrous MgSO_4 , filtered and evaporated to dryness. The ^1H and ^{13}C N.M.R. spectra of the residue showed no signals attributable to the N-functionalised amine in the organic phase.

4.5.3. The reductive detosylation of 1-amino-N,N-bis (2-toluene-p-sulphonylaminoethyl)ethyl ethanoate by the action of sodium metal in liquid ammonia

1-amino-N,N-bis(2-toluene-p-sulphonylaminoethyl)ethyl ethanoate (12.08 g, 2.43×10^{-2} mol) was transferred into a 3-necked flask fitted with a dry ice condenser. Liquid ammonia (300 cm^3) was added to the ester to form a suspension . Sodium metal (8.1 g, 3.52×10^{-1} mol) was added to give an initial uniform blue solution. However, whilst stirring an orange-brown suspension was produced. After 1 hour, ammonium chloride (18.90 g, 0.35 mol) was added, whereupon the remaining ammonia was left to evaporate overnight. Distilled water (300 cm^3) was added to the brown solid that remained. The resultant solution was extracted with CH_2Cl_2 ($3 \times 100 \text{ cm}^3$).

The combined extracts were dried with anhydrous magnesium sulphate, filtered and evaporated to dryness. The organic residue did not show any signals in ^1H N.M.R. which would correspond to the detosylated product in the organic phase. However, the ^1H and ^{13}C N.M.R. spectra of the aqueous phase did show signals which corresponded to the detosylated product, but due to difficulties in purification, the detosylated product was not isolated.

4.5.3.1. ^1H N.M.R. data of the aqueous phase

Signals are observed at : δ 2.31 (impurity), 2.84 (2H,t), 2.85 (2H,t), 3.21 (2H,dt), 3.22 (2H,dt), 3.30 (2H,s) and 3.40 (2NH,t).

4.5.3.2. ^{13}C N.M.R. data of the aqueous phase

^{13}C N.M.R. peaks were seen at : δ 39.10 (impurity), 50.38 (CH_2), 55.52 (CH_2), 55.62 (CH_2), 57.81 (CH_2), 60.18 (CH_2) and 174.25 ($\text{C}=\text{O}$).

4.5.4. The preparation of the preformed barium macrocycle [Ba(24)(Me)₄N₆(py)₂(ClO₄)₂]⁹

Under refluxing methanol (150 cm³), 2,6-diacetylpyridine (2.00 g, 1.22 x 10⁻²mol) and barium perchlorate (2.10 g, 6.24 x 10⁻³ mol) were added to a 3-necked flask under N₂. To this clear colourless solution, a methanolic solution of diethylenetriamine (1.28 g, 1.24 x 10⁻² mol) was added. After 0.5 hour of reflux the solution changed to a yellow solution. After 3 hours the flask was allowed to cool to room temperature, whereupon the system was allowed to stand for two days.

Beige / colourless crystals were produced and isolated using filtration. Yield = 2.23 g, 45.87%. Found : C 39.31, H 4.59, N 13.51 ; C₂₆H₃₆N₈Cl₂O₈Ba requires C 39.18, H 4.55, N 14.06

4.5.5. The attempted reaction between the preformed barium macrocycle $[\text{Ba}[\text{24}](\text{Me})_4\text{N}_6(\text{py})_2(\text{ClO}_4)_2]$, triethylamine and 1-bromoacetic acid

In a 3-necked flask, DMF (40 cm³) was added to the preformed barium macrocycle $[\text{Ba}[\text{24}](\text{Me})_4\text{N}_6(\text{py})_2(\text{ClO}_4)_2]$ (1.13 g, 1.41 x 10⁻³ mol) to give a yellow solution. Triethylamine (80 cm³) was added to the yellow solution. A DMF solution (40 cm³) of 1-bromoacetic acid (0.46 g, 3.30 x 10⁻³ mol) was added via a catheter to the solution. The reaction was then left overnight where upon a solid precipitate had formed on the sides of the reaction flask. The reaction was left for a further 2 days. Unfortunately, the solid precipitate appeared to be a perchlorate salt. No reaction occurred.

4.5.6. The attempted reaction between the preformed barium macrocycle $[\text{Ba}[\text{24}](\text{Me})_4\text{N}_6(\text{py})_2(\text{ClO}_4)_2]$ and sodium acetate

Into a 3-necked flask, methanol (150 cm³) (previously dried with molecular sieves) was syringed and heated to refluxing temperature. The preformed macrocycle $[\text{Ba}[\text{24}](\text{Me})_4\text{N}_6(\text{py})_2(\text{ClO}_4)_2]$ (0.94 g, 1.18 x 10⁻³ mol) was then added to the refluxing solution. To the mixture, a methanolic solution (50 cm³) of sodium acetate (0.22 g, 2.68 x 10⁻³ mol) was transferred. After 5 mins the colour of the solid changed from beige to white. Finally a pale yellow solution was produced after refluxing for 4 hours. Some undissolved reactant was filtered and a light brown solution was condensed to 50 cm³ whereupon a white precipitate was produced. However, analysing the solid by IR and microanalysis showed only starting material. No reaction occurred.

4.5.7. The preparation of 7,16-bis(3-carboxypropanoyl)-1,4,10,13-tetraoxa-7,16-diazacyclooctadecane (1)¹⁷

A solution of 4,13-diaza-18-crown-6 (0.7 g, 2.67×10^{-3} mol) in THF (35 cm^3) was added dropwise to a stirred solution of succinic anhydride (0.53 g, 5.29×10^{-3} mol) in THF (10 cm^3). A cloudy solution developed after a minute. The reaction mixture was stirred for a further 2 hours at room temperature, whereupon the suspension was decanted. The main solution was stripped to dryness, leaving a clear oil. CH_2Cl_2 and diethyl ether were added to the oil. Within 12 hours at -30°C , a white crystalline solid crystallised out which was filtered and dried in vacuo at 70°C for 3 hours.

Yield = 0.70 g, 57 %. Found : C 50.77, H 7.16, N 5.81 ; $\text{C}_{20}\text{H}_{35}\text{O}_{10.5}\text{N}_2$ requires C 50.95, H 7.48, N 5.94 %.

4.5.8. The preparation of [{7,16-bis(3-carboxypropanoyl)-1,4,10,13-tetraoxa-7,16-diazacyclooctadecane} barium (II)]

A solution of barium(II) hydroxide.octahydrate (0.45 g, 1.43×10^{-3} mol) in distilled water (35 cm^3) was added dropwise to a filtered solution of 7,16-bis(carboxypropanoyl)-1,4,10,13-tetraoxa-7,16-diazacyclooctadecane (0.65 g, 1.41×10^{-3} mol) in distilled water (45 cm^3). A fine white suspension developed at room temperature within 0.5 hour. The suspension was then heated at reflux for 13 hours and then cooled to ambient temperature. The suspension was filtered and the filtrate was stripped to dryness to leave a white solid.

The white solid was then recrystallised with the minimum amount of hot water to give a white crystalline solid. The solid was filtered and then dried at 80°C for 3 hours.

M.p = 198°C (dec). Yield = 0.65 g, 77 %. Found : C 38.54, H 4.99, N 4.50 ; $\text{C}_{20}\text{H}_{34}\text{O}_{11}\text{N}_2\text{Ba}$ requires C 39.00, H 5.56, N 4.69 %.

4.5.8.1. IR data

λ_{\max} : 3397 (s, br), 1625 (s, sp), 1548 (s, sp), 1297 (s, sp), 1213 (s, sp), 1113 (m, sp), 874 (w, sp), 817 (w, sp) and 724 (w, sp) cm^{-1} .

4.5.8.2. ^1H N.M.R. data

Proton resonances are seen at : δ 2.46 (t, 4H), 2.67 (t, 4H), 3.73 (m, 24H).

4.5.8.3. ^{13}C N.M.R. data

Peaks are seen at : δ 27.45 (CH_2 pendant arm), 30.67 (CH_2 pendant arm), 45.30 (CH_2 -N diaza ring), 46.94 (CH_2 -N diaza ring), 66.59, 66.64, 67.14, 67.21, 67.95, 68.09 (CH_2 -O diaza ring), 173.70 (N-CO), 179.49 (COOH).

4.5.8.4. Sublimation Test

Under vacuum (0.01 Torr), the barium complex was heated to 240°C using a Woods metal bath. Some white crystalline solid was noticed on the sides of the schlenk at 225-230°C. However, the barium complex appeared to decompose between 230-240°C leaving a brown solid / oil.

4.5.9. The preparation of 7,16-bis(Z-3-carboxypropenoyl)-1,4,10,13-tetraoxa-7,16-diazacyclooctadecane (2)¹⁷

An immediate white precipitate developed whilst adding a THF solution (10 cm³) of 4,13-diaza-18-crown-6 to a solution of maleic anhydride (0.53 g, 5.35 x 10⁻³ mol) in THF (10 cm³). The suspension was stirred for a further two hours whereupon the suspension was filtered. The filtrate was stripped to dryness to leave a clear oil. A similar procedure was then followed as to that described in section 4.5.7.

Yield = 0.52 g, 43 %. Found : C 48.02, H 6.50, N 5.48 ; C₂₀H₃₄O₁₂N₂ requires C 48.58, H 6.93, N 5.67.

4.5.10. The preparation of [7,16-bis(Z-3-carboxypropenoyl)- 1,4,10,13-tetraoxa-7,16-diazacyclooctadecane } barium(II)]

A solution of barium(II) hydroxide.octahydrate (0.36 g, 1.13 x 10⁻³ mol) in distilled water (30 cm³) was added dropwise to a filtered solution of 7,16-bis(Z-3-carboxypropenoyl)-1,4,10,13-tetraoxa-7,16-diazacyclooctadecane (0.52 g, 1.13 x 10⁻³ mol) in distilled water (30 cm³). The work-up and crystallisation procedures were undertaken to those similarly described in section 4.5.8. Yield = 0.30 g, 44 %.

4.5.10.1. ¹H N.M.R. data

Peaks are observed at : δ 3.14 (impurity), 3.59 (m, 24H), 5.95 (d, 2H) and 6.60 (d, 2H)

4.5.10.2. ¹³C N.M.R. data

¹³C peaks are observed at : δ 173.12 (C=O), 172.64 (C=O), 139.68 (C=C), 137.66 (C=C), 72.21, 71.60, 71.08 and 70.77 (CH₂-O diaza ring), 67.98 (impurity), 50.09 and 49.91 (CH₂-N diaza ring).

**4.5.11. The preparation of N,N'-bis(carbethoxymethyl)
4,13-diaza-18-crown-6 (3A)19.20**

A solution of ethylbromoacetate (2.77 g, 1.65×10^{-2} mol) in acetonitrile (50 cm^3) was transferred to a white suspension of 4,13-diaza-18-crown-6 (1.91 g, 7.28×10^{-3} mol), and sodium carbonate (1.67 g, 1.58×10^{-2} mol) in acetonitrile (80 cm^3). The white suspension was heated at reflux for 36 hours, cooled, and filtered through Hyflosupercel to leave a white solid and pale yellow liquid. The pale yellow liquid was evaporated to dryness and the oily residue dissolved in chloroform (80 cm^3) to form a cloudy solution. Water (80 cm^3) was added to the chloroform layer whereupon 2 clear layers were formed. The layers were separated and the organic layer was dried with anhydrous magnesium sulphate.

The chloroform layer was filtered and evaporated to dryness. The orange-brown liquid was then purified by Kügelrohr distillation at $190\text{-}192^\circ\text{C} / 0.01\text{mm Hg}$.

Yield = 2.47 g, 78 %.

**4.5.12. The preparation of N,N'-bis(carboxymethyl)-4,13-
diaza-18-crown-6 (3)19.20**

N, N'-bis(carbethoxymethyl)-4,13-diaza-18-crown-6 (2.47 g, 5.68×10^{-3} mol) was transferred to a schlenk and distilled H_2O (30 cm^3) was added to form a white collidial suspension. It was then refluxed for 45 hours. The pale yellow solution which had resulted was allowed to cool to room temperature. The solution was evaporated to give an off-white solid. The residue was dissolved in ethanol (50 cm^3) and the solution was allowed to stand overnight. A white crystalline solid (1.62 g, 4.28×10^{-3} mol) was produced upon standing which was filtered and dried under vacuum for 1 hour at $100^\circ\text{C} / 0.1 \text{ mm Hg}$. Yield = 1.62 g, 75 %.

4.5.13. The preparation of [N,N'-bis(carboxymethyl)-4,13-diaza-18-crown-6 barium(II) bromide dihydrate]

Under a nitrogen atmosphere, a methanolic solution (50 cm³) of N,N-bis(carboxymethyl) 4,13-diaza-18-crown-6 (0.77 g, 2.03 x 10⁻³ mol) was added to a methanolic solution (70 cm³) of barium(II) bromide dihydrate (0.70 g, 2.10 x 10⁻³ mol). The solution was stirred overnight at room temperature and refluxed for a further 5 hours. The reaction mixture was cooled, filtered and evaporated to 15 cm³. THF (30 cm³) was added to precipitate a white solid. The white solid was filtered and dried in vacuo for 4 hours. M.p.= 210°C (dec). Yield = 0.75 g, 52 %. Found : C 26.4, H 4.07, N 3.73 ; C₁₆H₃₄BaBr₂N₂O₁₀ requires C 27.0, H 4.82, N 3.93 %.

4.5.13.1. IR data

λ_{\max} : 3377 (s, br), 1733 (m, sp), 1616 (s, br), 1295 (s, br),
1118 (s, br), 938 (w, br), 720 (w, sp) and 668 (w, br) cm^{-1} .

4.5.13.2. Mass Spectral data

M / e : The mass spectrum showed an extensive fragmentation pattern with the highest observed peak occurring at 231. Smaller fragments were observed. The molecular ion was not observed.

4.5.13.3. ^1H N.M.R. data

Peaks are observed at : δ 1.85, 2.55 (m, $8\text{H}^{3,5,12,14}$)*, 2.90 (m, $8\text{H}^{3,5,12,14}$)
3.10 (t, $8\text{H}^{2,6,11,15}$), 3.31 (t, $8\text{H}^{2,6,11,15}$)*, 3.45 (s, 4H, pendant arm)*,
3.50 (s, 4H, pendant arm), 3.73 (s, $8\text{H}^{8,9,17,18}$) and 3.75 (s, $8\text{H}^{8,9,17,18}$)*.

* Indicates the main isomer

The numbers in bold refer to the atom positions on the 4,13-diaza-18-crown-6 ether ring.

4.5.13.4. ^{13}C N.M.R. data

^{13}C N.M.R. signals are seen at : δ 56.26 ($\text{C}^{3,5,12,14}$), 57.03 ($\text{C}^{3,5,12,14}$)*, 58.38 ($\text{C}^{2,6,11,15}$), 58.66 ($\text{C}^{2,6,11,15}$)*, 69.51 (C pendant arm), 69.60 (C pendant arm)*, 70.98 ($\text{C}^{8,9,17,18}$), 71.35 ($\text{C}^{8,9,17,18}$)*, 178.66 (C=O) and 179.10 (C=O)*.

*Indicates the main isomer

The bold numbers refer to the atom positions on the 4,13-diaza-18-crown-6-ether ring.

4.5.14. The attempted reaction between

[N,N'-bis(carboxymethyl)-4,13-diaza-18-crown-6 barium(II) bromide dihydrate] and pyridine

Under N_2 atmosphere, pyridine (50 cm^3) was added to

[N,N'-bis(carboxymethyl) 4,13-diaza-18-crown-6 barium(II) bromide dihydrate] (0.53 g, 7.45×10^{-4} mol) to give a brown solution. A slight exotherm was noticed. It was then refluxed for 16 hours and the resultant solution was cooled and evaporated to dryness to leave a off white solid. The residue was dissolved in CH_2Cl_2 (80 cm^3) and a white solid was precipitated with THF (20 cm^3). The solid was filtered and dried in a vacuum overnight. The white solid was shown to be the protonated pendant arm starting material.

4.5.15. The attempted reaction between barium(II) hydride and N,N'-bis(carboxymethyl)-4,13-diaza-18-crown-6

A suspension of barium hydride (0.43 g, 3.09×10^{-3} mol) and N,N'-bis(carboxymethyl) 4,13-diaza-18-crown-6 (0.80 g, 2.11×10^{-3} mol) in dry THF (80 cm³) was heated at reflux. It was then cooled and filtered using Hyflosuper cel. The filtrate was evaporated to dryness. Unfortunately, the liquid was found to be THF. The white solid which was filtered was shown to be unreacted BaH₂ and N,N'-bis (carboxymethyl)-4,13-diaza-18-crown-6.

4.5.16. The preparation of the unsaturated macrocycle (4A)

In a 3-necked flask, a yellow solution of benzene-1,3-dicarboxyaldehyde (15.03 g, 1.12×10^{-1} mol) in acetonitrile (250 cm³) was added dropwise to a solution of 1,2-diaminoethane (7.45 g, 1.24×10^{-1} mol) in acetonitrile (200 cm³). Addition was complete after 5 hours stirring at room temperature. A white precipitate started to form after 3 hours. After the addition, the suspension was stirred at room temperature for a further 14 hours and then filtered to give a white solid and a clear solution. The white solid was dried in vacuo and CH₂Cl₂ (200 cm³) was added to form a yellow suspension. After trituration, acetonitrile (300 cm³) was added. The white precipitate so formed was collected and dried in vacuo. The solid was then recrystallised from a CH₂Cl₂ / acetonitrile mixture. The white solid was dried under vacuum at 80°C for 16 hours. Yield = 6.15 g, 35%. M.p. = 140-160°C (dec).

Found : C 75.99, H 6.28, N 17.82 ; C₂₀H₂₀N₄ requires C 75.92, H 6.37, N 17.71 %.

4.5.16.1. IR data

λ_{\max} : 3125 (w, sh), 2700 (m, sp), 2625 (m, sp), 1732 (s, sp), 1641 (m, sh),
1595 (m, sp), 1581 (m, sp), 1285 (s, br), 1153 (m, sp), 1073 (m, sp),
1017 (m, sp), 971 (m, sp), 801 (m, sp), 724 (s, sp), 691 (m, sp),
491 (w, sp) cm^{-1} .

4.5.16.2. Mass spectral data

M/e : 316, 287, 157, 130, 117, 104, 91, 77, 55, 44, 32.

The molecular ion was observed at 316.

4.5.16.3. ^1H N.M.R. data

Proton resonances are observed at : δ 1.6 (s, 2H - H_2O), 3.9 (s, 8H)*, 4.0 (s, 8H),
7.37 (td, 2H)*, 7.72 (dd, 4H)*, 7.87 (s, 2H), 8.07 (s, 2H)*, 8.15 (s, 4H)* and
8.23 (s, 4H).

* The major isomer

4.5.16.4. ^{13}C N.M.R. data

Peaks are observed at δ : 59.44 (en - CH_2), 61.19 (en - CH_2), 128.49*, 128.69,
128.78*, 128.99, 129.11, 129.76*, 136.31*, 136.51 (phenyl rings),
162.15 ($\text{C}=\text{N}$)* and 164.04 ($\text{C}=\text{N}$).

* The major isomer

4.5.17. The preparation of the saturated macrocycle (4B)

Sodium borohydride (0.65 g, 1.72×10^{-2} mol) was dissolved in ethanol (150 cm^3) and added under N_2 to a pale yellow solution of the unsaturated macrocycle (4A) (0.98 g, 3.09×10^{-3} mol) in chloroform (80 cm^3). Upon addition of 40 cm^3 of the ethanolic solution, the pale yellow solution became cloudy and some effervescence was noticed. After the addition was complete, a clear, colourless solution was apparent. After 16 hours of stirring at room temperature, the solution was evaporated to dryness to leave a white solid. This was dissolved in chloroform (300 cm^3) and water (150 cm^3). The two layer mixture was separated and the aqueous layer was extracted with chloroform ($3 \times 150 \text{ cm}^3$). The combined chloroform extracts were dried using anhydrous magnesium sulphate, filtered and evaporated to dryness to give a white, sticky solid. The sticky solid was recrystallised from a chloroform / petrol mixture.

Yield = 0.70 g, 14 %. M.p = $144 - 148^\circ\text{C}$ (dec).

Found : C 72.43, H 8.42, N 16.36 ; $\text{C}_{20}\text{H}_{28}\text{N}_4$ requires C 74.03, H 8.70, N 17.27 %.

4.5.17.1. IR Data

λ_{max} : 3295 (w, sp), 3245 (m, sp), 1604 (m, sp), 1560 (w, sp), 1280 (w, sp), 1135 (m, sp), 1080 (m, sp), 800 (m, sp), 780 (m, sp), 720 (m, sp), 698 (m, sp) cm^{-1} .

4.5.17.2. Mass spectral data

M / e : 324, 264, 254, 239, 196, 175, 163, 147, 117, 104, 91, 78, 69, 43. This spectrum shows extensive fragmentation with the molecular ion observed at 324.

4.5.17.3. ^1H N.M.R. data

Resonances are seen at δ 1.74 (s, 4NH), 2.81 (s, 8H), 3.65 (s, 8H), 7.08 (d, 4H), 7.20 (m, 2H) and 7.55 (s, 2H)

4.5.17.4. ^{13}C N.M.R. data

Carbon peaks are seen at δ 48.63 (ethylene carbons), 53.69 (CH_2), 126.44, 126.91, 127.97, and 141.06 (phenyl rings)

4.5.18. The preparation of the pendant arm bibracchial macrocycle (4)

A fine white suspension of the saturated macrocycle (**4B**) (0.65 g, 2.00×10^{-3} mol) and anhydrous sodium carbonate (0.42 g, 3.96×10^{-3} mol) in methanol (80 cm^3) was transferred through a wide bore catheter to a methanolic solution (150 cm^3) of bromoacetic acid (0.50 g, 4.03×10^{-3} mol) and potassium hydroxide (0.22 g, 3.92×10^{-3} mol). The empty flask was washed with a further ($2 \times 30 \text{ cm}^3$) of methanol and transferred to the reactant flask. The reaction mixture was then heated at 70°C for 31 hours, whereupon the white solid was filtered to leave a pale yellow solution. This solution was evaporated to dryness. Water (50 cm^3) was added to form a pale yellow solution (pH10). After trituration, the yellow solution was acidified with HCl (20 cm^3 , 1 mol dm^{-3}) to pH5.4. The acidic solution was then extracted with chloroform ($20 \times 15 \text{ cm}^3$) whereupon the collected chloroform extracts were dried with anhydrous magnesium sulphate, filtered and evaporated to 25 cm^3 . Petroleum ether (20 cm^3) was added to precipitate a white solid which was filtered and dried in vacuo. A further crop of solid was precipitated by adding successive amounts of petrol to the remaining chloroform extracts. Again, the white solid was dried in vacuo. Yield = 0.41 g, 46 %. M.p = $> 320^\circ\text{C}$ (dec).

4.5.18.1. IR data

λ_{\max} : 3420 (s, br), 1735 (w, sp), 1630 (s, br), 1268 (s, br), 1132 (s, br), 1065 (s, br), 801 (w, sp), 740 (w, sp), 720 (w, sp) and 695 (w, sp) cm^{-1} .

4.5.18.2. Mass spectrum data

M/e : 579, 552, 404, 375, 365, 274, 246, 203, 175, 133, 105, 91, 82, 72, 60. The molecular ion was not observed.

4.5.18.3. ^1H N.M.R. data

Peaks are observed at : δ 2.0 (br, NH), 2.58 (s, 4H - en), 3.18 (s, 4H - en)*, 3.25 (s, 4H - pendant arm), 3.54 (s, 4H), 4.60 (s, 4H) and 7.20 (m, 8H).

4.5.18.4. ^{13}C N.M.R. data

Peaks are observed at : δ 46.17, 48.86, 49.17, 49.36 (CH_2 en), 57.60 (CH_2 arm), 57.70 (CH_2 arm), 61.44, 61.57, 61.78, 61.99 (CH_2), 126.95, 127.73, 128.30, 128.43, 128.59, 128.85, 129.01, 129.67, 136.73, 136.87, 137.04, 137.29 (phenyl rings), 166.73 (C=O) and 166.97 (C=O).

4.5.21. The preparation of macrocycle (5)

Macrocycle (5) was prepared by a similar method to macrocycle (4). A white suspension of the saturated macrocycle (5B) (0.79 g, 2.09×10^{-3} mol) and sodium carbonate (0.44 g, 4.17×10^{-3} mol) in methanol (60 cm^3) was added to a methanolic solution of potassium hydroxide (0.23 g, 4.17×10^{-3} mol) and 1-bromoacetic acid (0.58 g, 4.17×10^{-3} mol) under a stream of N_2 . Once the addition had taken place the pH of the solution was 11.8. The reaction was refluxed for 32 hours whereupon the flask was cooled to room temperature. The suspension was stripped to dryness and distilled water (10 cm^3) was added to form a yellow suspension (pH of suspension - 11.37).

Dilute hydrochloric acid (10.80 cm^3 , 1 mol dm^{-3}) was added by a biruette to adjust the pH to 2.95, in which most of the solid had disappeared. The cloudy solution was filtered and carefully transferred to amberlite resin IRC-50 (H^+) chromatography column ($25 \times 15 \text{ cm}^3$) and eluted with ammonium hydroxide (300 cm^3 , 1 mol dm^{-3}). Several aliquots were collected and the separate fractions stripped to dryness. However, analysis of these residues still gave the incorrect microanalysis, although the compound was shown to be present in the ^1H and ^{13}C N.M.R. spectra.

4.5.21.1. ^1H N.M.R. data

Peaks are observed at : δ 1.61 (s, 12H), 3.43 (s, 8H), 3.70 (m, 4H), 4.00 (s, 4H), 7.59 (dd, 4H) and 8.07 (t, 2H) in D_2O .

Peaks observed for 1-bromoacetic acid in CDCl_3 - δ 3.9 (CH_2) and 11.78 (COOH).

4.5.21.2. ^{13}C N.M.R. data

Carbon resonances are observed at : δ 21.66 (CH_3), 22.27 (CH_3), 44.72 (CH_2 - en), 56.92 (CH_2 - N en), 61.03 (CH_2 pendant arm), 61.44 (CH), 62.10 (CH), 72.78 (impurity), 124.83, 126.24, 142.80, 143.03, 157.56 (pyridyl) and 178.96 (C=O) in D_2O .

The peaks seen in the ^{13}C N.M.R. spectrum of 1-bromoacetic acid in CDCl_3 are as follows : δ 25.27 (CH_2) and 173.74 (C=O).

4.5.23. The attempted metal template assisted reaction between [Ba(TMHD)₂], 2,6-diacetylpyridine and 1,2-diaminoethane

A methanolic suspension (350 cm³) of 2,6-diacetylpyridine (1.87 g, 1.15 x 10⁻² mol) and ["Ba[TMHD]₂"]* (2.36 g, 4.68 x 10⁻³ mol) was stirred at room temperature. To this suspension, 1,2-diaminoethane (1.11 g, 1.83 x 10⁻² mol) was added dropwise. Upon refluxing for 2 hours an orange suspension had developed. The suspension was filtered and the orange filtrate was condensed to leave a residue. CH₂Cl₂ (100 cm³) was added to the residue to form a purple solution . Ethanol (40 cm³) was then added to the solution. Upon standing for 7 days, colourless barium containing crystals were isolated from an oily residue.

X-ray crystallography showed that a 9 coordinate, monomeric, barium macrocycle had formed but the barium compound was ionic and therefore, not suitable for volatility studies. A repeated experiment using recently prepared [Ba₄(TMHD)₈]†, 2,6-diacetylpyridine and 1,2-diaminoethane gave the unsaturated macrocycle and [Ba₄(TMHD)₈] when recrystallised from toluene and diethyl ether.

In neither case was there evidence of neutral barium macrocycle had been formed.

* Made from BaBr₂.2H₂O and HTMHD in water / ethanol

† Made from Ba metal and HTMHD in pentane (anhydrous conditions).

4.6. References

1. K.B.Mertes and J.M.Lehn in "Comprehensive Coordination Chemistry", Eds. G.Wilkinson, R.D.Gilland and J.A.McCleverty, Pergamon Press, Oxford, **21.3**, 915.
2. J.A.P.Nash, S.G.Thompson, D.F.Foster, D.J.Cole-Hamilton and J.C.Barnes, *J.Chem.Soc.Dalton Trans.*, in press 1994.
3. K.Timmer and H.A.Meinama, *Inorg.Chim.Acta.*, 1991, **187** 99.
4. N.A.Bailey, D.E.Fenton, P.C.Hellier, P.D.Hempstead, U.Casellato and P.A.Vigato, *J.Chem.Soc.Dalton Trans.*, 1992, 2809.
5. H.Adams, N.A.Bailey, D.E.Fenton, R.J.Good, R.Moody and C.O.R.de Barbarin, *J.Chem.Soc.Dalton.Trans.*, 1987, 207.
6. S.M.Nelson, F.S.Esho and M.G.B.Drew, *J.Chem.Soc.Dalton Trans.*, 1982, 407.
7. D.B.Hope and K.C.Horncastle, *J.Chem.Soc.*, **C**, 1966, 1098.
8. A.E.Martin, T.M.Ford and J.E.Bulkowski, *J.Org.Chem.*, 1982, **3**,47.
9. M.G.B.Drew, J.Nelson and S.M.Nelson, *J.Chem.Soc.Dalton Trans.*, 1981, 1678.
10. T.Uechi, I.Ueda, M.Tazake, M.Takagi and K.Ueno, *Acta.Cryst.*, 1982, **B38**,433.
11. P.Gluzínski, J.W.Krajewski, R.A.Kolínski, Z.Urbánczyk, A.Mishnyov and A.Kemme, *J.Cryst and Spectro Res.*, 1989, **19**, 2, 369.
12. C.A.Chang, and V.O.Ochaya, *Inorg.Chem.*, 1986, **25**, 355.
13. V.K.Manchanda, *Radiochem.Acta.*, 1989, **48**, 213.
14. C.A.Chang, and V.C.Sekhar, *Inorg Chem.*, 1987,**26**, 1981.
15. C.A.Chang and M.E.Rowland, *Inorg Chem.*, 1983, **22** 3866.
16. V.K.Manchanda and C.A.Chang, *Anal.Chem.*, 1986, **58**, 2269.
17. F.De Jong, A.Van Zon, D.N. Reinhoudt, G.J.Torny and H.P.M.Tomassen, *Recl.Trav.Chim.Pays-Bas.*, 1983, **102**, 164.
18. R.Delgado, J.J.R.Fráustoda Silva, M.C.T.A.Vaz, P.Paoletti and M.Micheloni, *J.Chem.Soc.Dalton Trans.*, 1989, 133.
19. S. Kulstad and L.Å.Malmsten, *Acta.Chem.Scand.*, 1979, **B33**, 469.

20. V.J.Gatto and G.W.Gokel, *J.Am.Chem.Soc.*, 1984, **106** 8240.
21. R.A.Kolínski and J.Mrozínski, *Polyhedron.*, 1983, **2**, 11 1217.
22. J.F.Carvalho and S.P.Crofts, International Patent., 25/07/91 WO 91/10645.
23. M.Goodman and W.J.McGahren, *Tetrahedron.*, 1967, **23**, 2048.

CHAPTER 5

**THE BARIUM COMPLEXES OF THE TETRAGLYME
ADDUCTS OF β - DIKETONES AND THE COMPLEXES
OF THIO- β -DIKETONES**

CHAPTER 5

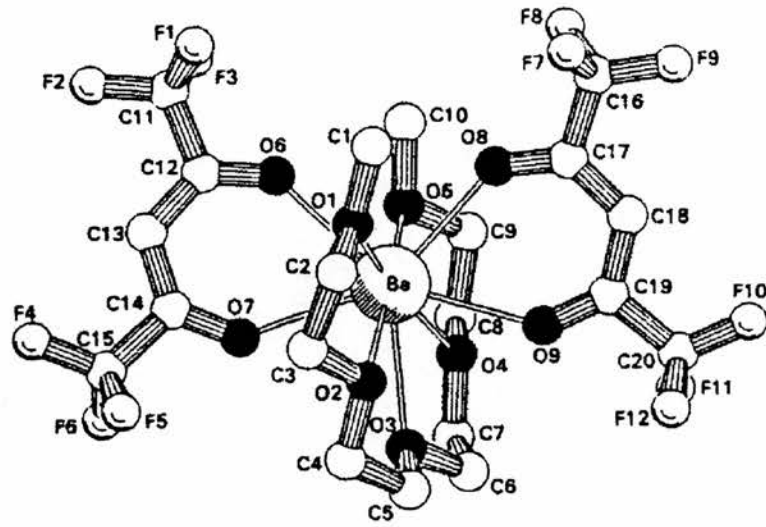
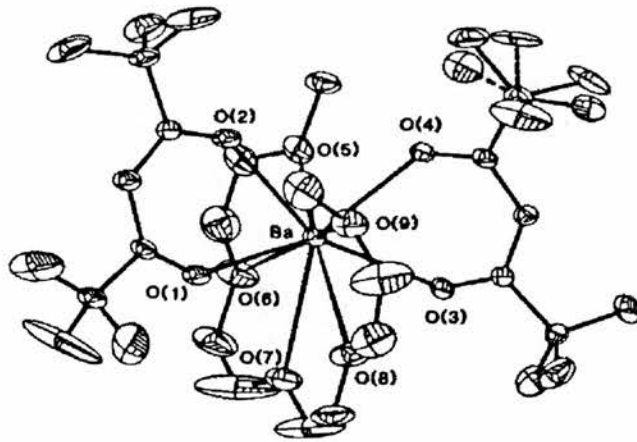
5.1. Introduction

5.1.1. Barium β -diketonate tetraglyme adducts

As discussed in the start of chapter 4, tetraglyme ligands (podands) and 18-crown-6 ether ligands (coronands) add to the stability and volatility of barium β -diketonates. However, it appears that the tetraglyme ligand, encounters a far higher stability and volatility than does the corresponding 18-crown-6 ether . This result is very surprising when taking in account that the measured stability of the complexes in solution containing 18-crown-6 ether are 3-4 magnitudes higher than those of the complexes containing tetraglyme¹.

As a consequence of the thermal advantages of the tetraglyme adducts in the solid state, the first part of this chapter details the chemistry of the tetraglyme adducts of barium β -diketonates.

Investigations into the thermal properties of various tetraglyme adducts seem to suggest that β -diketonates with stronger electron-withdrawing β -substituents, can sublime with no dissociation of the tetraglyme ligand -[Ba(HFA)₂.tetraglyme]². However, dissociation of the tetraglyme occurs with electron donating groups at the β position, such as - [Ba(TMHD)₂.tetraglyme]³. In this case there is too much electron density on the metal centre, consequently reducing the binding ability of the tetraglyme. In the case of [Ba(HFA)₂.tetraglyme], the perfluorinated groups attract electron density away from the metal centre, thus, increasing the strength of the binding of the tetraglyme ligand. The crystal structures of [Ba(HFA)₂.tetraglyme] and [Ba(TMHD)₂.tetraglyme] are shown in Figs 5.1.1 and 5.1.2.

Fig 5.1.1.[Ba(HFA)₂.tetraglyme]Fig 5.1.2.[Ba(TMHD)₂.tetraglyme]

The first half of this chapter is concerned with the synthesis and characterisation of a series of tetraglyme adducts of barium β -diketonates. By effectively changing the β -substituent from CH_3 to phenyl an increase in the electron-withdrawing power will hopefully result in a reduction in the tendency for the tetraglyme ligand to dissociate from the complex upon heating.

The reactions were undertaken in situ with barium hydride or barium metal, the β -diketone ligand and tetraglyme. The attempted synthesis of the tetraglyme adduct of $[\text{Ba}(\text{acac})_2]$ led to the formation of the tetraglyme free barium complex - $[\text{Ba}(\text{acac})_2]$. Interestingly, Norman et al⁴ tried to synthesise $[\text{Ba}(\text{acac})_2 \cdot 18\text{-crown-6-ether}]$ from BaH_2 , Hacac and the 18-crown-6 ether ligand. Similarly, no reaction was reported. However, Timmer et al succeeded in producing $[\text{Ba}(\text{acac})_2 \cdot 18\text{-crown-6} \cdot 0.5\text{H}_2\text{O}]$ from $[\text{Ba}(\text{acac})_2]$ and 18-crown-6 ether. It appears, the main function of the tetraglyme ligand is to disassemble any association in the barium β -diketonate complex by filling all available coordination sites around each Ba atom. If, however, the barium β -diketonate complex is strongly associated i.e. highly polymeric, then the tetraglyme ligand has difficulty in breaking down the polymeric structure.

$[\text{Ba}(\text{TDFND})_2 \cdot \text{tetraglyme}]$ was made by the reaction between barium hydride, HTDFND and tetraglyme in toluene. The X-ray crystal structure was deduced and is shown in section 5.2.

The synthesis of barium and copper thio β -diketonates are detailed in the second part of this chapter and the chemistry will be discussed in section 5.5.

5.2. The X-ray crystal structure of [Ba(TDFND)₂.tetraglyme]

A single crystal of [Ba(TDFND)₂.tetraglyme] was grown from a solution of hexane by slow evaporation over 8 days. The crystal was mounted in an oil drop and the data set collected at 150K. The complete data set was collected on an Enraf-Nonius FAST area detector diffractometer (SERC service, Cardiff) and the solution of the crystal structure was aided by Dr. John Barnes of the University of Dundee.

[Ba(TDFND)₂.tetraglyme] is a nine coordinate, monomeric solid with no evidence of hydrogen bonding or van der Waals bonding, which may explain why the barium complex is so volatile. As seen in fig 5.2.b., the two β-diketonate ligands are planar but deviate from being coplanar by 26°. All five oxygen atoms of the tetraglyme ligand coordinate to the barium and the oxygen atoms are essentially coplanar. Interestingly, the tetraglyme ligand does not bisect the two β-diketonate moieties unlike [Ba(HFA)₂.tetraglyme] and [Ba(TMHD)₂.tetraglyme]. The dihedral angle between the mean plane of the tetraglyme oxygen atoms and the plane of the two β-diketonate planes are at 88.8(1)° and 67.4(1)°. The nearest intermolecular contact is between F(49) of one molecule and H(70) of another at 2.606(8) Å. However, this is unlikely to be of any significance in terms of intermolecular bonding when considering the sum of the van der Waal radii of the F and H amounting to 2.55 Å. As a consequence of the lack of short or long range intermolecular interactions, [Ba(TDFND)₂.tetraglyme] sublimes.

Fig 5.2.a

The X-ray crystal structure of [Ba(TDFND)₂.tetraglyme] from the z plane. As shown below in the ball and stick diagram, the barium complex is a monomeric, nine-coordinate solid.

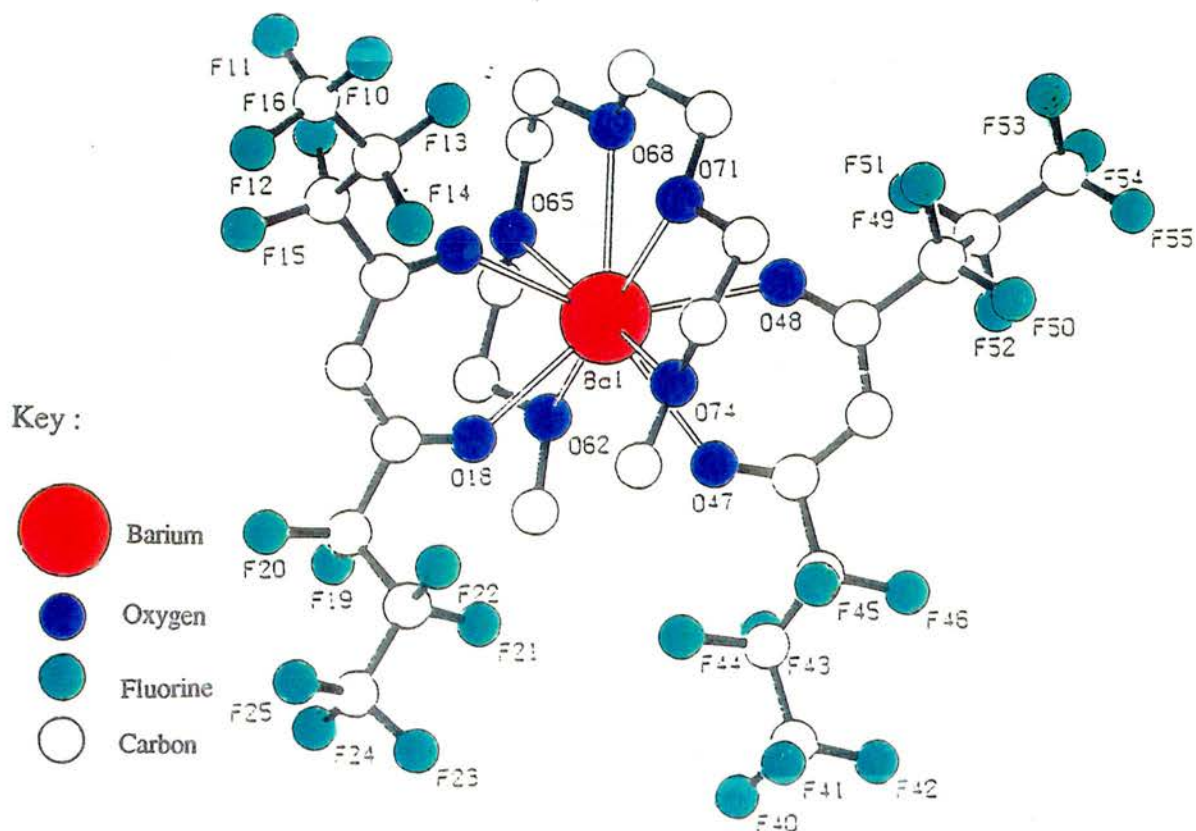


Fig 5.2.b

A view from the x-plane of the X-ray crystal structure of [Ba(TDFND)₂.tetraglyme].

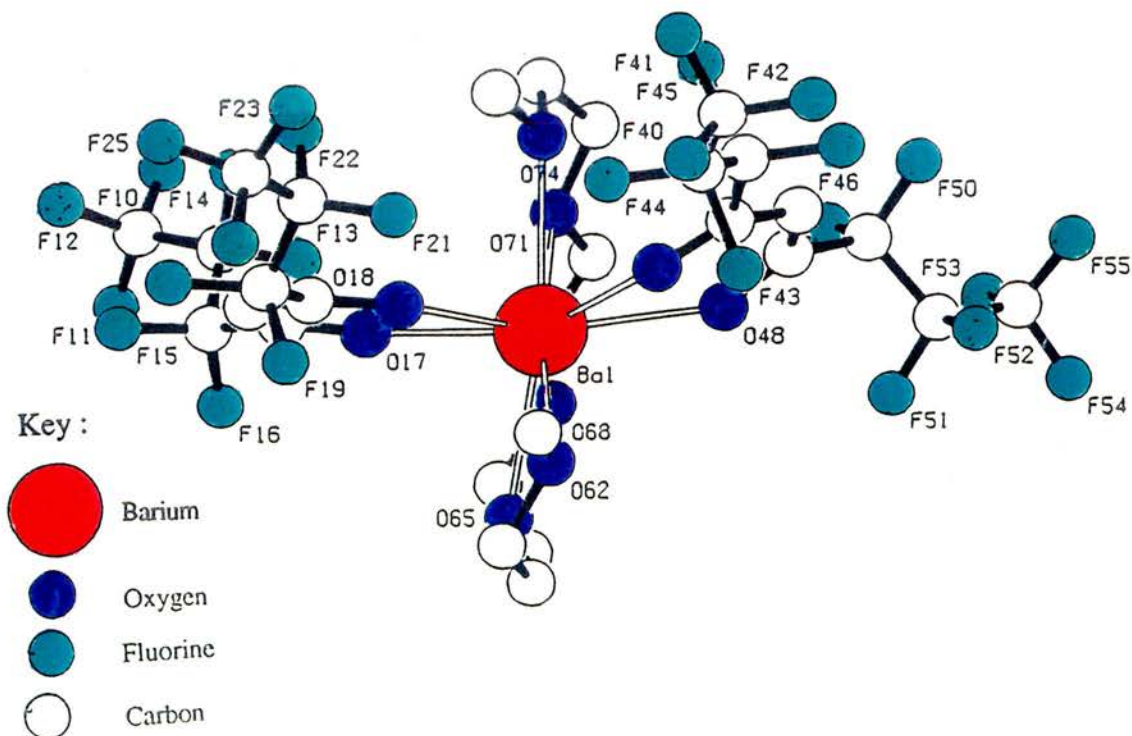
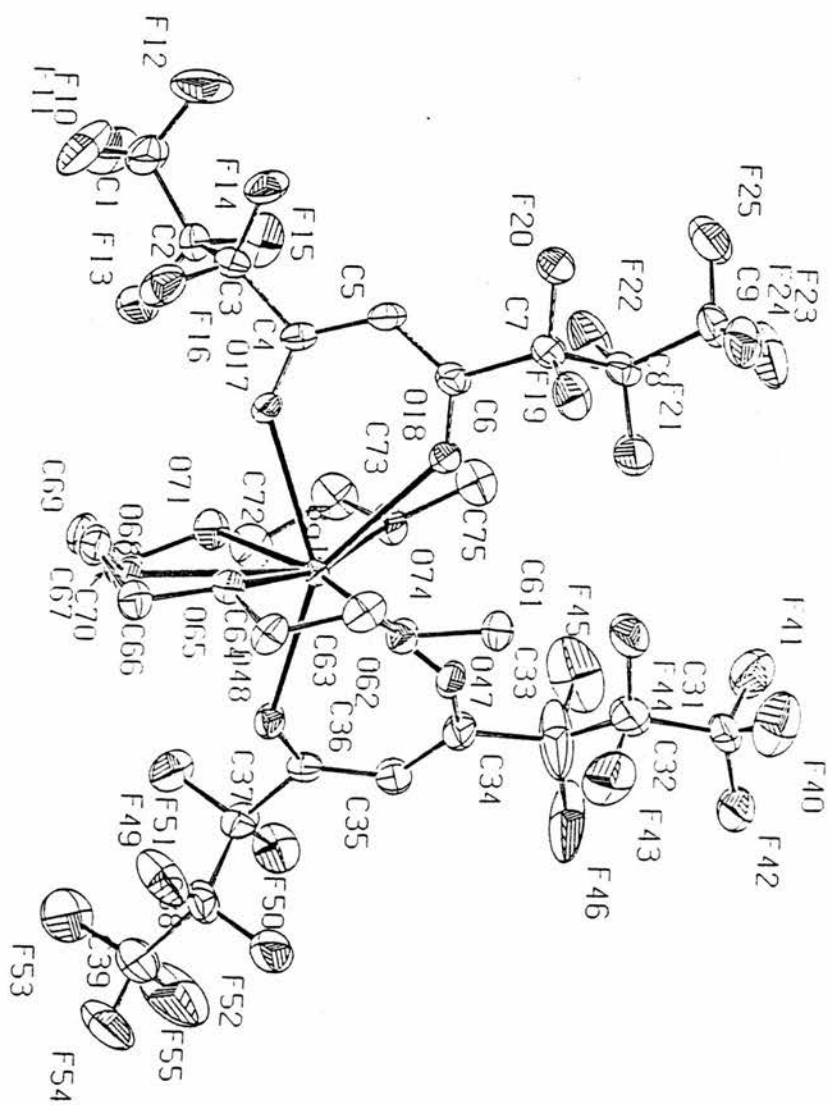


Fig. 5.2.c.

The ortep diagram below shows the crystal structure of Ba[TDFEND]₂tetraglyme. The ellipsoids at 50% and from the diagram the carbon atom C33 is rocking sideways due to some disorder.



As seen in Fig 5.2.d., the Ba-O keto distances range from 2.692(3) - 2.736(3) Å (Average 2.711 Å) for [Ba(TDFND)₂.tetraglyme]. These are similar to the Ba-O keto bond distances of [Ba(HFA)₂.tetraglyme] (Average 2.700 Å) and [Ba(TMHD)₂.tetraglyme] (Average 2.676 Å). Interestingly, comparing a series of average Ba-O β-diketonate distances for the tetraglyme adducts of [Ba(TMHD)₂], [Ba(HFA)₂] and [Ba(TDFND)₂] there seems to be a trend. It seems the greater the electron withdrawing effect of a group on the β-diketonate moiety, the greater the Ba-O β-diketonate distance. This is because the less negative O atoms experience less electrostatic attraction to the positive barium atom. To compensate, the strength of binding of the tetraglyme ligand would be expected to increase as the Ba atom becomes more δ⁺ (i.e. for the less electron donating β-diketonate ligands, thus, resulting in a decrease in Ba-O tetraglyme bond length as the series progresses from R = C₃F₇ > CF₃ > ^tBu). However, in practice, this trend is followed for R = ^tBu and CF₃ but for R = C₃F₇ there is no significant difference between the average Ba-O bond length to the tetraglyme ligand and those for R = CF₃.

Fig.5.2.d.**Bond lengths (Ba-O) of the tetraglyme adducts**

[Ba(TDFND)₂.tetraglyme] [Ba(HFA)₂.tetraglyme] [Ba(TMHD)₂.tetraglyme]

Ba-O (β -diketonate)

Ba(1)-O(17) 2.692(3)	Ba-O 2.706(2)	Ba-O 2.667(8)
Ba(1)-O(18) 2.704(3)	Ba-O 2.683(2)	Ba-O 2.656(7)
Ba(1)-O(48) 2.711(3)	Ba-O 2.713(2)	Ba-O 2.675(8)
Ba(1)-O(47) 2.736(3)	Ba-O 2.711(1)	Ba-O 2.713(7)

Ba-O (tetraglyme)

Ba(1)-O(62) 2.846(4)	Ba-O 2.809(2)	Ba-O 2.863(8)
Ba(1)-O(65) 2.848(3)	Ba-O 2.872(2)	Ba-O 2.895(9)
Ba(1)-O(68) 2.865(3)	Ba-O 2.855(2)	Ba-O 2.959(9)
Ba(1)-O(71) 2.874(4)	Ba-O 2.855(2)	Ba-O 2.918(9)
Ba(1)-O(74) 2.851(4)	Ba-O 2.893(2)	Ba-O 2.872(9)

R(1)=4.35%

R(1)=2%

R(1)=4.93%

Average Ba-O(β -diketonate) lengths

[Ba(TDFND)₂.tetraglyme] [Ba(HFA)₂.tetraglyme] [Ba(TMHD)₂.tetraglyme]

2.71075 Å

2.70325 Å

2.67775 Å

Average Ba-O(tetraglyme) lengths

2.8568 Å

2.8568 Å

2.9014 Å

5.2.1. STA studies

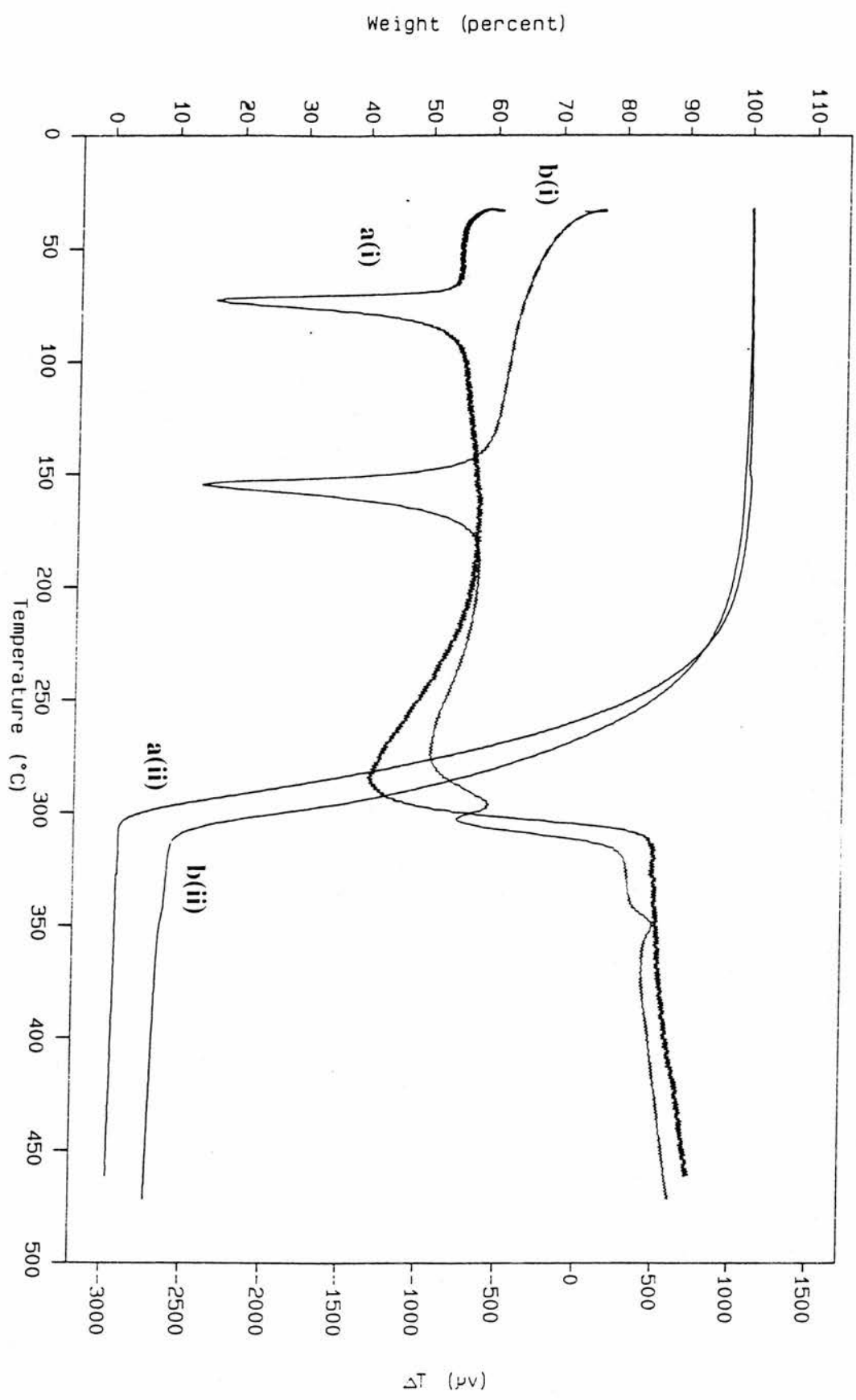
STA studies of the tetraglyme adducts indicate that [Ba(TMHD)₂.tetraglyme] loses tetraglyme prior to sublimation, [Ba(HFA)₂.tetraglyme] dissociates the polyether during sublimation and [Ba(TDFND)₂.tetraglyme] undergoes complete sublimation without decomposition.

The higher volatility and low melting point (70°C) of [Ba(TDFND)₂.tetraglyme] may be due to the lower intermolecular forces between individual molecules. This is as a result of the large amount of molecular shielding provided by the C₃F₇ groups of the β-diketonate. The fact that [Ba(HFA)₂.tetraglyme] sublimates but decomposes at 275°C seems to support the suggestion that the larger the perfluorinated group, the greater the volatility and thermal stability. As shown in Fig 5.2.1.a., [Ba(TDFND)₂.tetraglyme] sublimates without decomposition between 120-305°C. In comparison, the STA traces show that [Ba(HFA)₂.tetraglyme] starts subliming first, but [Ba(TDFND)₂.tetraglyme] has a faster evaporation rate which results in a greater volatility than [Ba(HFA)₂.tetraglyme] after 240°C. At 275°C there is sharp exotherm in the DTA trace of [Ba(HFA)₂.tetraglyme] which represents decomposition. This may be attributable to the intermolecular interactions which may exist in [Ba(HFA)₂.tetraglyme].

It can be shown from the space filling diagram of [Ba(HFA)₂.tetraglyme] in Fig 5.2.1.b. that there can be a possibility of intermolecular hydrogen bonding between the H atoms of the tetraglyme ligand, which are δ⁺ and the fluorine atoms of the CF₃ groups which are δ⁻. The space filling diagram of [Ba(TDFND)₂.tetraglyme] in Fig 5.2.1.c., illustrates that the tetraglyme ligand sits in a cleft between the C₃F₇ substituents on the β-diketonate moiety.

Fig 5.2.1.a.

Fig 5.2.2.d shows the comparison between the two STA traces of Bal TDEND]2,tetraglyme and Bal HFA]2,tetraglyme



This means that the H atoms of the tetraglyme ligand are less available than in [Ba(HFA)₂.tetraglyme] for intermolecular H-F interactions. The higher thermal stability and volatility of [Ba(TDFND)₂.tetraglyme] is attributable to the lack of these H-F interactions.

The space filling diagram of [Ba(HFA)₂.tetraglyme] is shown below

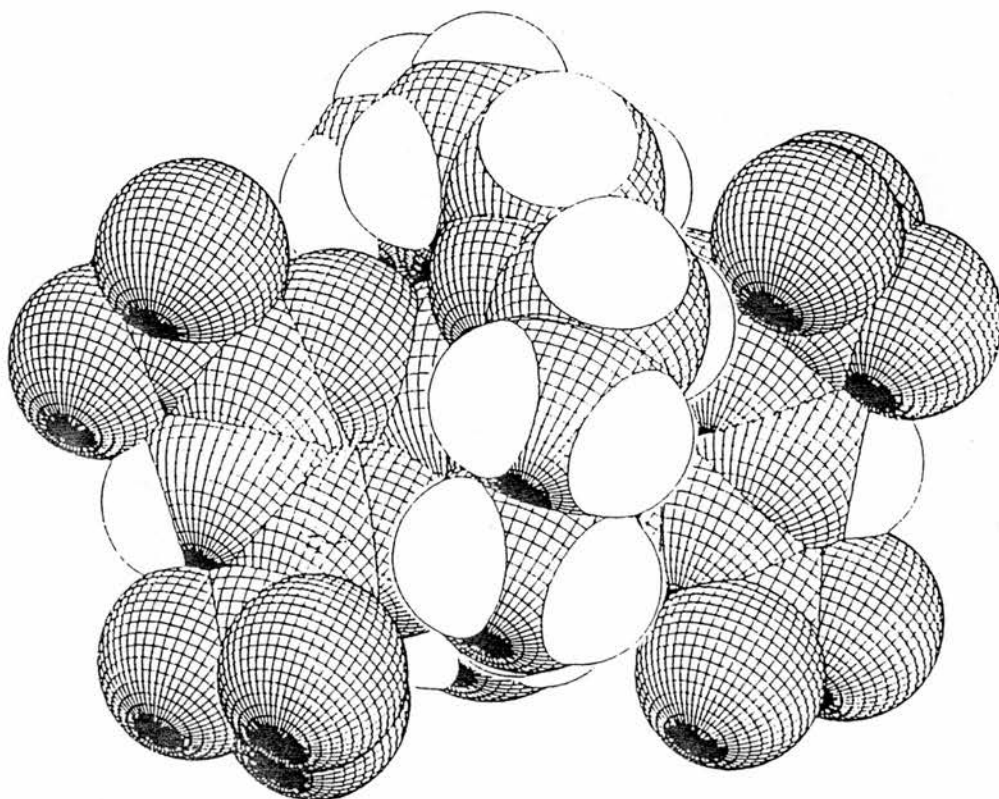
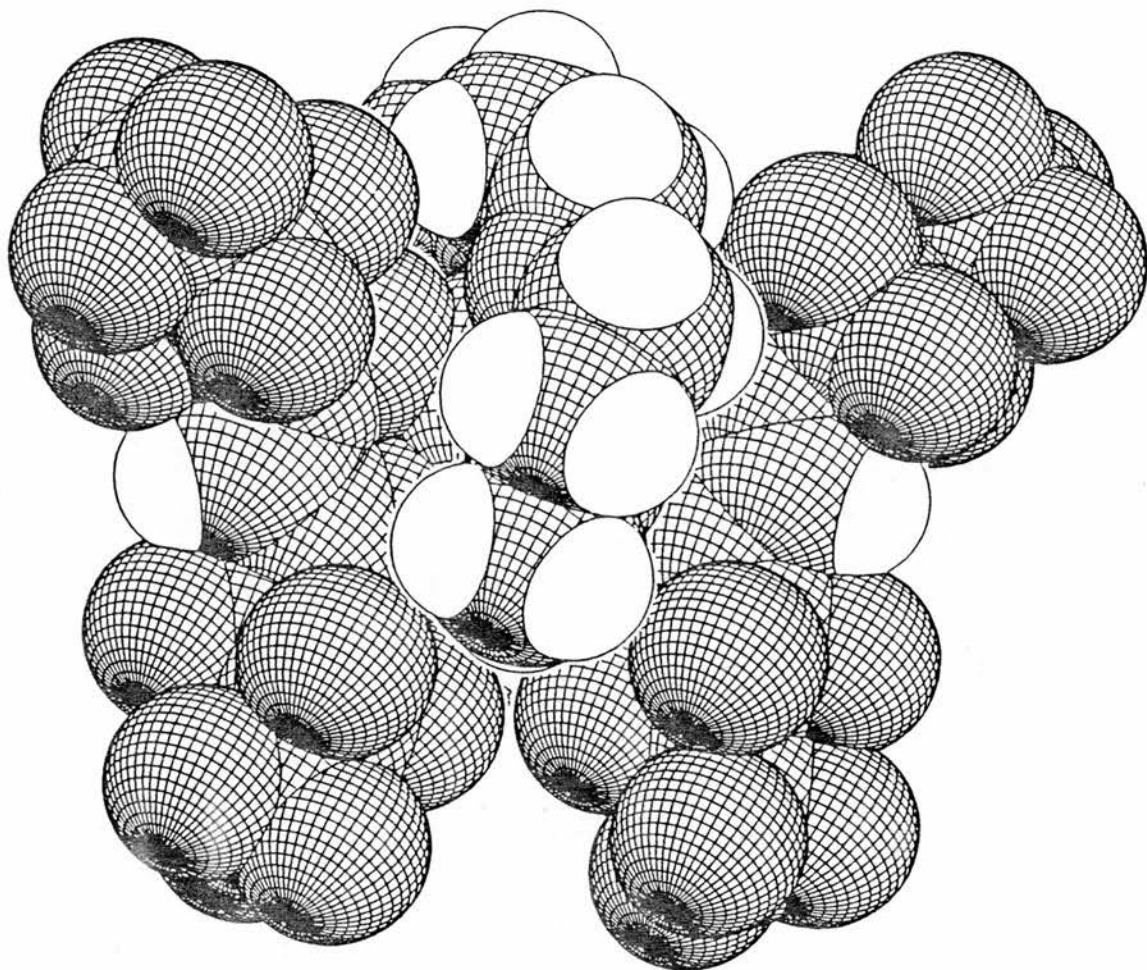


Fig 5.2.1.c.

The space filling diagram of [Ba(TDFND)₂.tetraglyme] is shown below. It can be seen from this diagram that the tetraglyme ligand has more molecular shielding from the C₃F₇ groups than [Ba(HFA)₂.tetraglyme]. From this we can deduce that there would be a reduced amount of intermolecular interactions between other [Ba(TDFND)₂.tetraglyme] molecules.



5.2.2. Experimental

8 days slow evaporation of a concentrated solution of [Ba(TDFND)₂.tetraglyme] in hexane gave colourless crystals. A crystal of [Ba(TDFND)₂.tetraglyme] was suspended in an oil drop at 150K. Using an Enraf-Nonius FAST area detector diffractometer (SERC service, Cardiff), 14529 total and 6091 independent reflections [$R(\text{int}) = 0.052$] were collected.

Data was collected in the range $1.80 < \theta < 24.98^\circ$ for the index limits $-19 < h < 16$, $11 < k < 11$, $-23 < l < 26$, and corrected for absorption using DIFABS (maximum and minimum transmission factors 1.074 and 0.956). The final refinement gave $R_1 = 0.0418$ for 4947 reflections and 0.0530 for all 6091 data, $WR = 0.1095$.

5.2.3. Crystallographic Data

Formula = [Ba(C₉H₂F₁₄O₂)₂.(C₁₀H₂₂O₅)], Mr = 1173.92, Monoclinic, P2₁/C,

a = 17.1447(1), b = 10.739(0), c = 22.8296(0), $\beta = 97.56^\circ$.

V = 4165.19 Å³, Z = 4, D_x = 1.872 Mg m⁻³

(Mo K α) = 0.71069 Å, $\mu = 1.13 \text{ mm}^{-1}$ F(000) = 2288, T = 298K, R(1) = 4.35 % for 4942 Fo > 4.sigma (Fo) and 5.48 for all 6148 data, wR2 = 0.1152.

5.2.4. Crystal data and structure refinement for
[Ba(TDFND)₂.tetraglyme]

5.2.4.1.

Identification code	jn107
Empirical formula	C ₂₈ H ₂₄ Ba F ₂₈ O ₉
Formula weight	1173.81
Temperature	150 K
Wavelength	0.71069 Å
Crystal system	monoclinic
Space group	P ₂₁ /c
Unit cell dimensions	a = 17.15(2) Å alpha = 90 deg. b = 10.735(5) Å beta = 97.56(7) deg. c = 22.830(7) Å gamma = 90 deg.
Volume	4165(5) a ³
Z	4
Density (calculated)	1.872 Mg/m ³
Absorption coefficient	1.126 mm ⁻¹ Abs ⁿ correction by DIFABS ^{1,2} corrections max. 1.074 min.
0.956	
F(000)	2288
Crystal size	0.4 x 0.4 x 0.3
Theta range for data collection	1.80 to 24.98 deg.
Index ranges	-19<=h<=16, -11<=k<=11, -23<=l<=26
Reflections collected	14529
Independent reflections	6091 [R(int) = 0.522]
Refinement method	Full-matrix least-squares on F ²
Data / restraints / parameters	6084 / 0 / 598
Goodness-of-fit on F ²	0.762
Final R indices [I>2sigma(I)]	R1 = 0.0418, wR2 = 0.1054
R indices (all data)	R1 = 0.0530, wR2 = 0.1120

Largest diff. peak and hole 1.596 [near F46 (disordered)] and -0.766 e.A⁻³

- (1) Walker and Stuart, 1983, *Acta. Cryst.* A39, 158-166.
- (2) Modified for FAST system by A. Karaulov and M. Hursthouse (personal communication).

5.2.4.2. Atomic coordinates ($\times 10^4$) and equivalent isotropic displacement parameters ($\text{\AA}^2 \times 10^3$) for 1. $U(\text{eq})$ is defined as one third of the trace of the orthogonalized U_{ij} tensor.

	x	y	z	$U(\text{eq})$
Ba(1)	2140(1)	-119(1)	523(1)	21(1)
C(1)	5255(3)	-4194(6)	1350(2)	49(2)
C(2)	4616(3)	-3266(4)	1108(2)	31(1)
C(3)	3973(3)	-3783(4)	631(2)	29(1)
C(4)	3498(2)	-2723(4)	296(2)	26(1)
C(5)	3564(2)	-2557(4)	-304(2)	29(1)
C(6)	3157(3)	-1625(4)	-640(2)	29(1)
C(7)	3231(3)	-1565(4)	-1307(2)	31(1)
C(8)	3530(3)	-285(4)	-1516(2)	29(1)
C(9)	3787(3)	-257(5)	-2134(2)	44(1)
F(10)	5715(2)	-3671(4)	1798(2)	74(1)
F(11)	4950(3)	-5201(3)	1549(2)	81(1)
F(12)	5707(2)	-4529(4)	948(2)	81(1)
F(13)	4291(2)	-2841(3)	1565(1)	49(1)
F(14)	4979(2)	-2317(3)	873(1)	52(1)
F(15)	4325(2)	-4532(3)	271(1)	45(1)
F(16)	3491(2)	-4512(3)	909(1)	46(1)
O(17)	3096(2)	-2117(3)	607(1)	30(1)
O(18)	2707(2)	-815(3)	-478(1)	33(1)
F(19)	2511(2)	-1781(3)	-1622(1)	42(1)
F(20)	3713(2)	-2456(3)	-1477(1)	46(1)
F(21)	2959(2)	557(3)	-1495(1)	53(1)
F(22)	4153(2)	29(3)	-1123(1)	55(1)
F(23)	3924(3)	900(3)	-2271(2)	78(1)
F(24)	3231(2)	-717(3)	-2529(1)	53(1)
F(25)	4435(2)	-899(4)	-2152(1)	64(1)
C(31)	1896(4)	4954(5)	-1377(3)	54(2)
C(32)	1815(5)	3953(7)	-912(4)	93(3)
C(33)	1864(9)	4151(7)	-337(4)	146(6)
C(34)	1692(3)	3160(4)	121(2)	44(1)
C(35)	1611(3)	3620(4)	684(2)	35(1)
C(36)	1551(2)	2846(4)	1155(2)	26(1)
C(37)	1458(3)	3454(4)	1754(2)	32(1)
C(38)	611(3)	3449(5)	1899(2)	39(1)
C(39)	470(4)	4071(6)	2483(3)	55(2)
F(40)	1592(2)	4516(4)	-1900(2)	79(1)
F(41)	2646(2)	5186(3)	-1422(2)	60(1)
F(42)	1549(3)	5992(4)	-1288(2)	90(1)
F(43)	915(2)	3564(3)	-976(2)	62(1)
F(44)	2189(2)	2932(3)	-1070(2)	80(1)
F(45)	2749(2)	4451(4)	-282(2)	86(1)
F(46)	1476(5)	5232(4)	-239(2)	180(4)
O(47)	1711(2)	2067(3)	-46(1)	32(1)
O(48)	1543(2)	1680(3)	1168(1)	30(1)
F(49)	1909(2)	2848(3)	2191(1)	48(1)
F(50)	1705(2)	4659(3)	1779(1)	50(1)
F(51)	346(2)	2285(3)	1905(2)	65(1)
F(52)	168(2)	4062(4)	1462(1)	67(1)
F(53)	877(3)	3492(5)	2931(2)	102(2)
F(54)	-276(2)	3950(4)	2563(2)	84(1)
F(55)	621(3)	5230(4)	2492(2)	111(2)
C(61)	920(3)	-84(4)	-958(2)	35(1)
O(62)	865(2)	-567(3)	-384(1)	28(1)
C(63)	560(3)	-1807(4)	-420(2)	36(1)

C(64)	370(3)	-2185(5)	167(2)	36(1)
O(65)	1078(2)	-2141(3)	586(1)	29(1)
C(66)	946(3)	-2593(5)	1153(2)	35(1)
C(67)	1717(3)	-2594(4)	1552(2)	34(1)
O(68)	1987(2)	-1344(3)	1616(1)	29(1)
C(69)	2654(3)	-1251(4)	2067(2)	37(1)
C(70)	2929(3)	63(4)	2097(2)	39(1)
O(71)	3234(2)	363(3)	1563(1)	34(1)
C(72)	3598(3)	1558(5)	1578(2)	40(1)
C(73)	3997(3)	1677(5)	1044(2)	46(1)
O(74)	3433(2)	1552(3)	533(1)	35(1)
C(75)	3778(3)	1754(5)	4(2)	44(1)

Ba(1)-O(17)	2.690(3)
Ba(1)-O(18)	2.702(3)
Ba(1)-O(48)	2.710(3)
Ba(1)-O(47)	2.736(3)
Ba(1)-O(62)	2.847(4)
Ba(1)-O(65)	2.849(3)
Ba(1)-O(74)	2.850(4)
Ba(1)-O(68)	2.863(3)
Ba(1)-O(71)	2.873(4)
C(1)-F(11)	1.308(7)
C(1)-F(12)	1.326(6)
C(1)-F(10)	1.331(6)
C(1)-C(2)	1.530(7)
C(2)-F(13)	1.328(5)
C(2)-F(14)	1.342(5)
C(2)-C(3)	1.546(6)
C(3)-F(15)	1.348(5)
C(3)-F(16)	1.356(5)
C(3)-C(4)	1.543(6)
C(4)-O(17)	1.237(5)
C(4)-C(5)	1.402(6)
C(5)-C(6)	1.390(6)
C(6)-O(18)	1.251(5)
C(6)-C(7)	1.545(6)
C(7)-F(20)	1.354(5)
C(7)-F(19)	1.366(5)
C(7)-C(8)	1.564(7)
C(8)-F(21)	1.338(5)
C(8)-F(22)	1.345(6)
C(8)-C(9)	1.532(7)
C(9)-F(23)	1.309(6)
C(9)-F(25)	1.313(6)
C(9)-F(24)	1.319(6)
C(31)-F(42)	1.291(6)
C(31)-F(40)	1.325(8)
C(31)-F(41)	1.327(7)
C(31)-C(32)	1.530(8)
C(32)-C(33)	1.320(11)
C(32)-F(44)	1.343(7)
C(32)-F(43)	1.587(9)
C(33)-F(46)	1.371(9)
C(33)-F(45)	1.540(14)
C(33)-C(34)	1.548(9)
C(34)-O(47)	1.235(6)
C(34)-C(35)	1.402(7)
C(35)-C(36)	1.373(6)
C(36)-O(48)	1.252(5)
C(36)-C(37)	1.543(6)
C(37)-F(49)	1.347(5)
C(37)-F(50)	1.360(5)
C(37)-C(38)	1.530(7)
C(38)-F(51)	1.331(6)
C(38)-F(52)	1.345(6)
C(38)-C(39)	1.537(7)
C(39)-F(55)	1.271(7)
C(39)-F(53)	1.317(7)
C(39)-F(54)	1.322(7)
C(61)-O(62)	1.423(6)
O(62)-C(63)	1.428(5)
C(63)-C(64)	1.477(7)

C(64)-O(65)	1.443(6)
O(65)-C(66)	1.429(6)
C(66)-C(67)	1.505(7)
C(67)-O(68)	1.421(5)
O(68)-C(69)	1.439(6)
C(69)-C(70)	1.486(7)
C(70)-O(71)	1.425(6)
O(71)-C(72)	1.425(6)
C(72)-C(73)	1.480(7)
C(73)-O(74)	1.421(6)
O(74)-C(75)	1.430(6)
O(17)-Ba(1)-O(18)	63.68(9)
O(17)-Ba(1)-O(48)	143.07(9)
O(18)-Ba(1)-O(48)	149.30(9)
O(17)-Ba(1)-O(47)	147.25(9)
O(18)-Ba(1)-O(47)	86.58(9)
O(48)-Ba(1)-O(47)	63.20(9)
O(17)-Ba(1)-O(62)	108.63(10)
O(18)-Ba(1)-O(62)	70.48(10)
O(48)-Ba(1)-O(62)	101.93(10)
O(47)-Ba(1)-O(62)	70.55(10)
O(17)-Ba(1)-O(65)	77.06(11)
O(18)-Ba(1)-O(65)	97.78(10)
O(48)-Ba(1)-O(65)	103.06(10)
O(47)-Ba(1)-O(65)	122.96(10)
O(62)-Ba(1)-O(65)	58.23(9)
O(17)-Ba(1)-O(74)	92.02(11)
O(18)-Ba(1)-O(74)	79.33(11)
O(48)-Ba(1)-O(74)	84.04(11)
O(47)-Ba(1)-O(74)	67.92(11)
O(62)-Ba(1)-O(74)	129.37(10)
O(65)-Ba(1)-O(74)	168.78(9)
O(17)-Ba(1)-O(68)	72.34(10)
O(18)-Ba(1)-O(68)	133.96(9)
O(48)-Ba(1)-O(68)	76.65(9)
O(47)-Ba(1)-O(68)	139.26(9)
O(62)-Ba(1)-O(68)	113.99(10)
O(65)-Ba(1)-O(68)	58.24(9)
O(74)-Ba(1)-O(68)	116.26(10)
O(17)-Ba(1)-O(71)	76.06(10)
O(18)-Ba(1)-O(71)	118.69(10)
O(48)-Ba(1)-O(71)	71.02(10)
O(47)-Ba(1)-O(71)	110.09(10)
O(62)-Ba(1)-O(71)	170.71(9)
O(65)-Ba(1)-O(71)	116.57(9)
O(74)-Ba(1)-O(71)	57.14(10)
O(68)-Ba(1)-O(71)	59.13(9)
F(11)-C(1)-F(12)	108.2(5)
F(11)-C(1)-F(10)	107.8(5)
F(12)-C(1)-F(10)	107.8(5)
F(11)-C(1)-C(2)	111.3(5)
F(12)-C(1)-C(2)	112.5(4)
F(10)-C(1)-C(2)	109.1(5)
F(13)-C(2)-F(14)	108.6(4)
F(13)-C(2)-C(1)	107.1(4)
F(14)-C(2)-C(1)	106.9(4)
F(13)-C(2)-C(3)	110.0(4)
F(14)-C(2)-C(3)	108.4(4)
C(1)-C(2)-C(3)	115.5(4)
F(15)-C(3)-F(16)	106.9(4)
F(15)-C(3)-C(4)	112.8(4)
F(16)-C(3)-C(4)	110.1(3)
F(15)-C(3)-C(2)	108.0(4)

F(16)-C(3)-C(2)	107.4(4)
C(4)-C(3)-C(2)	111.4(4)
O(17)-C(4)-C(5)	128.1(4)
O(17)-C(4)-C(3)	113.7(4)
C(5)-C(4)-C(3)	118.2(4)
C(6)-C(5)-C(4)	122.1(4)
O(18)-C(6)-C(5)	128.4(4)
O(18)-C(6)-C(7)	113.4(4)
C(5)-C(6)-C(7)	118.2(4)
F(20)-C(7)-F(19)	105.9(4)
F(20)-C(7)-C(6)	112.6(4)
F(19)-C(7)-C(6)	109.1(4)
F(20)-C(7)-C(8)	107.2(4)
F(19)-C(7)-C(8)	107.3(4)
C(6)-C(7)-C(8)	114.3(4)
F(21)-C(8)-F(22)	109.2(4)
F(21)-C(8)-C(9)	108.7(4)
F(22)-C(8)-C(9)	108.1(4)
F(21)-C(8)-C(7)	108.1(4)
F(22)-C(8)-C(7)	106.2(4)
C(9)-C(8)-C(7)	116.4(4)
F(23)-C(9)-F(25)	108.1(5)
F(23)-C(9)-F(24)	109.2(5)
F(25)-C(9)-F(24)	108.7(5)
F(23)-C(9)-C(8)	108.7(4)
F(25)-C(9)-C(8)	111.5(4)
F(24)-C(9)-C(8)	110.7(4)
C(4)-O(17)-Ba(1)	139.3(3)
C(6)-O(18)-Ba(1)	138.3(3)
F(42)-C(31)-F(40)	108.2(6)
F(42)-C(31)-F(41)	108.8(5)
F(40)-C(31)-F(41)	105.5(5)
F(42)-C(31)-C(32)	114.3(5)
F(40)-C(31)-C(32)	108.3(6)
F(41)-C(31)-C(32)	111.3(6)
C(33)-C(32)-F(44)	115.3(6)
C(33)-C(32)-C(31)	125.2(8)
F(44)-C(32)-C(31)	107.3(5)
C(33)-C(32)-F(43)	93.9(8)
F(44)-C(32)-F(43)	104.7(6)
C(31)-C(32)-F(43)	107.3(6)
C(32)-C(33)-F(46)	109.3(7)
C(32)-C(33)-F(45)	92.8(8)
F(46)-C(33)-F(45)	107.7(8)
C(32)-C(33)-C(34)	124.6(8)
F(46)-C(33)-C(34)	109.3(7)
F(45)-C(33)-C(34)	111.2(8)
O(47)-C(34)-C(35)	128.9(5)
O(47)-C(34)-C(33)	115.4(5)
C(35)-C(34)-C(33)	115.4(5)
C(36)-C(35)-C(34)	122.1(4)
O(48)-C(36)-C(35)	128.7(4)
O(48)-C(36)-C(37)	113.5(4)
C(35)-C(36)-C(37)	117.7(4)
F(49)-C(37)-F(50)	106.4(4)
F(49)-C(37)-C(38)	107.9(4)
F(50)-C(37)-C(38)	107.1(4)
F(49)-C(37)-C(36)	109.6(4)
F(50)-C(37)-C(36)	111.8(4)
C(38)-C(37)-C(36)	113.7(4)
F(51)-C(38)-F(52)	107.8(4)
F(51)-C(38)-C(37)	109.9(4)
F(52)-C(38)-C(37)	107.3(4)
F(51)-C(38)-C(39)	107.8(4)

F(52)-C(38)-C(39)	107.0(4)
C(37)-C(38)-C(39)	116.6(4)
F(55)-C(39)-F(53)	111.3(6)
F(55)-C(39)-F(54)	107.0(5)
F(53)-C(39)-F(54)	105.7(5)
F(55)-C(39)-C(38)	112.6(5)
F(53)-C(39)-C(38)	109.9(5)
F(54)-C(39)-C(38)	110.0(5)
C(34)-O(47)-Ba(1)	133.2(3)
C(36)-O(48)-Ba(1)	133.9(3)
C(61)-O(62)-C(63)	110.9(3)
C(61)-O(62)-Ba(1)	118.0(3)
C(63)-O(62)-Ba(1)	116.0(2)
O(62)-C(63)-C(64)	109.1(4)
O(65)-C(64)-C(63)	108.9(4)
C(66)-O(65)-C(64)	111.6(3)
C(66)-O(65)-Ba(1)	118.9(3)
C(64)-O(65)-Ba(1)	118.6(2)
O(65)-C(66)-C(67)	108.5(4)
O(68)-C(67)-C(66)	108.0(4)
C(67)-O(68)-C(69)	110.9(3)
C(67)-O(68)-Ba(1)	114.3(2)
C(69)-O(68)-Ba(1)	115.8(3)
O(68)-C(69)-C(70)	108.5(4)
O(71)-C(70)-C(69)	108.9(4)
C(70)-O(71)-C(72)	113.0(4)
C(70)-O(71)-Ba(1)	113.2(3)
C(72)-O(71)-Ba(1)	114.7(3)
O(71)-C(72)-C(73)	107.8(4)
O(74)-C(73)-C(72)	109.3(4)
C(73)-O(74)-C(75)	111.6(4)
C(73)-O(74)-Ba(1)	120.7(3)
C(75)-O(74)-Ba(1)	119.8(3)

Symmetry transformations used to generate equivalent atoms:

5.2.4.4. Anisotropic displacement parameters ($\text{Å}^2 \times 10^{-3}$) for 1.

The anisotropic displacement factor exponent takes the form:

$$-2 \pi^2 [h^2 a^{*2} U_{11} + \dots + 2 h k a^* b^* U_{12}]$$

	U11	U22	U33	U23	U13	U12
Ba(1)	26(1)	20(1)	15(1)	-1(1)	3(1)	4(1)
C(1)	51(4)	64(4)	27(3)	-2(3)	-8(3)	23(3)
C(2)	36(3)	35(3)	22(3)	3(2)	6(2)	4(2)
C(3)	33(3)	28(3)	29(3)	-4(2)	9(2)	7(2)
C(4)	24(2)	23(2)	30(3)	-5(2)	1(2)	5(2)
C(5)	28(2)	34(3)	24(3)	-6(2)	-1(2)	13(2)
C(6)	30(3)	33(3)	24(3)	-5(2)	5(2)	4(2)
C(7)	40(3)	33(3)	23(3)	-5(2)	8(2)	7(2)
C(8)	29(3)	41(3)	18(2)	-11(2)	1(2)	3(2)
C(9)	59(4)	47(4)	28(3)	0(2)	17(3)	5(3)
F(10)	61(2)	103(3)	47(2)	-15(2)	-27(2)	32(2)
F(11)	95(3)	59(2)	83(3)	27(2)	-16(2)	30(2)
F(12)	46(2)	138(4)	57(2)	-19(2)	-4(2)	52(2)
F(13)	55(2)	65(2)	26(2)	-7(1)	3(1)	24(2)
F(14)	43(2)	57(2)	53(2)	11(2)	-5(2)	-16(1)
F(15)	55(2)	43(2)	34(2)	-11(1)	-3(1)	26(1)
F(16)	40(2)	32(2)	65(2)	14(2)	6(2)	1(1)
O(17)	33(2)	35(2)	20(2)	4(1)	1(1)	15(1)
O(18)	42(2)	36(2)	21(2)	1(1)	7(2)	14(1)
F(19)	44(2)	57(2)	23(2)	-7(1)	0(1)	-10(1)
F(20)	66(2)	47(2)	28(2)	-2(1)	17(1)	24(1)
F(21)	83(2)	37(2)	46(2)	7(2)	30(2)	18(2)
F(22)	53(2)	80(3)	32(2)	-13(2)	9(2)	-27(2)
F(23)	136(3)	55(2)	54(2)	2(2)	51(2)	-18(2)
F(24)	62(2)	72(2)	25(2)	0(2)	2(2)	2(2)
F(25)	54(2)	101(3)	40(2)	2(2)	21(2)	12(2)
C(31)	70(4)	48(4)	52(4)	21(3)	41(4)	19(3)
C(32)	141(7)	65(5)	91(6)	48(4)	84(5)	66(5)
C(33)	362(17)	35(4)	64(5)	21(4)	114(8)	60(7)
C(34)	73(4)	25(3)	37(3)	8(2)	21(3)	17(2)
C(35)	53(3)	21(3)	33(3)	-1(2)	16(2)	7(2)
C(36)	24(2)	22(3)	32(3)	-3(2)	6(2)	1(2)
C(37)	43(3)	19(2)	31(3)	-6(2)	1(2)	2(2)
C(38)	57(3)	39(3)	23(3)	-2(2)	14(2)	2(2)
C(39)	71(4)	66(4)	32(3)	-8(3)	16(3)	17(3)
F(40)	82(3)	75(3)	77(3)	28(2)	-1(2)	-13(2)
F(41)	47(2)	71(2)	62(2)	20(2)	3(2)	6(2)
F(42)	136(4)	65(3)	84(3)	47(2)	70(3)	55(2)
F(43)	34(2)	78(2)	69(2)	11(2)	-13(2)	-10(2)
F(44)	130(3)	55(2)	68(3)	28(2)	65(2)	47(2)
F(45)	55(2)	133(4)	67(3)	-6(3)	5(2)	-63(2)
F(46)	452(12)	48(3)	64(3)	33(2)	124(5)	116(5)
O(47)	48(2)	28(2)	21(2)	5(1)	5(2)	9(1)
O(48)	43(2)	22(2)	24(2)	0(1)	6(1)	4(1)
F(49)	64(2)	50(2)	27(2)	-10(1)	-9(1)	19(2)
F(50)	70(2)	32(2)	49(2)	-15(1)	13(2)	-11(1)
F(51)	80(2)	59(2)	65(2)	-18(2)	44(2)	-25(2)
F(52)	55(2)	111(3)	37(2)	10(2)	10(2)	32(2)
F(53)	129(4)	152(4)	24(2)	-9(2)	5(2)	68(3)
F(54)	79(3)	127(4)	54(2)	-7(2)	39(2)	23(2)
F(55)	174(5)	64(3)	114(4)	-44(3)	87(4)	-7(3)
C(61)	40(3)	45(3)	20(3)	3(2)	1(2)	6(2)
O(62)	37(2)	27(2)	20(2)	-2(1)	1(1)	2(1)
C(63)	38(3)	30(3)	36(3)	-7(2)	-8(2)	-2(2)

o(64)	35(3)	33(3)	37(3)	5(2)	-3(2)	-1(2)
o(65)	30(2)	31(2)	26(2)	2(1)	4(1)	4(1)
c(66)	38(3)	36(3)	34(3)	7(2)	10(2)	-2(2)
c(67)	46(3)	29(3)	29(3)	7(2)	7(2)	1(2)
o(68)	41(2)	24(2)	21(2)	3(1)	3(2)	6(1)
c(69)	49(3)	40(3)	22(3)	4(2)	-1(2)	9(2)
c(70)	52(3)	43(3)	18(3)	-6(2)	-6(2)	1(2)
o(71)	38(2)	40(2)	21(2)	-5(2)	-1(2)	-1(2)
c(72)	32(3)	52(3)	34(3)	-9(2)	-3(2)	-8(2)
c(73)	32(3)	63(4)	42(3)	-9(3)	-3(3)	-10(2)
o(74)	33(2)	45(2)	26(2)	0(2)	4(2)	-5(1)
c(75)	49(3)	47(3)	39(3)	-1(3)	11(3)	-7(2)

5.2.4.5. Hydrogen coordinates ($\times 10^4$) and isotropic displacement parameters ($\text{\AA}^2 \times 10^3$) for 1.

	x	y	z	U(eq)
H(5)	3890(2)	-3087(4)	-484(2)	28(8)
H(35)	1598(3)	4478(4)	741(2)	28(8)
H(61A)	1126(3)	748(4)	-924(2)	59(7)
H(61B)	407(3)	-73(4)	-1185(2)	59(7)
H(61C)	1264(3)	-601(4)	-1152(2)	59(7)
H(63A)	947(3)	-2372(4)	-546(2)	42(4)
H(63B)	90(3)	-1842(4)	-707(2)	42(4)
H(64A)	-22(3)	-1626(5)	292(2)	42(4)
H(64B)	156(3)	-3022(5)	148(2)	42(4)
H(66A)	732(3)	-3431(5)	1117(2)	42(4)
H(66B)	571(3)	-2062(5)	1316(2)	42(4)
H(67A)	1648(3)	-2937(4)	1935(2)	42(4)
H(67B)	2099(3)	-3101(4)	1383(2)	42(4)
H(69A)	3073(3)	-1794(4)	1973(2)	42(4)
H(69B)	2507(3)	-1504(4)	2445(2)	42(4)
H(70A)	2495(3)	614(4)	2149(2)	42(4)
H(70B)	3335(3)	171(4)	2432(2)	42(4)
H(72A)	3977(3)	1639(5)	1931(2)	42(4)
H(72B)	3205(3)	2206(5)	1583(2)	42(4)
H(73A)	4252(3)	2483(5)	1042(2)	42(4)
H(73B)	4396(3)	1036(5)	1046(2)	42(4)
H(75A)	3383(3)	1663(5)	-333(2)	59(7)
H(75B)	4189(3)	1156(5)	-20(2)	59(7)
H(75C)	3994(3)	2580(5)	8(2)	59(7)

5.3. The preparation and analysis of [Ba(DBM)₂.tetraglyme.0.25C₇H₈]

5.3.1. The preparation of [Ba(DBM)₂.tetraglyme.0.25C₇H₈]

In a toluene suspension, barium hydride was refluxed in the proper stoichiometric ratios with 1,3-diphenylpropane-1,3-dione and tetraglyme to produce [Ba(DBM)₂.tetraglyme.0.25C₇H₈]. [Ba(DBM)₂.tetraglyme.0.25C₇H₈] was recrystallised by the addition of methylene chloride to the mother liquors. The filtered solid was found to be air, moisture and light sensitive. Exposure to the air or moisture will probably result in some oxo barium containing species similar to [Ba₅(TMHD)₉(OH)(H₂O)₃]⁵. In addition, Thompson, also noticed that the [Ba(DBM)₂] complex (tetraglyme free) was light sensitive as shown by the low values obtained for %C and %H in the microanalysis and the complex turning to a yellow solid upon exposure to the light⁶. To our surprise, though, the tetraglyme ligand does not add to the stability of the barium complex - [Ba(DBM)₂]. The air, moisture and light sensitivity properties of [Ba(DBM)₂.tetraglyme.0.25C₇H₈] seem also to be in direct contrast with the air and moisture stable [Ba(TMHD)₂.tetraglyme].

As with other non-fluorinated barium β-diketonates, the tetraglyme ligand dissociates quite readily under STA conditions. [Ba(DBM)₂.tetraglyme.0.25C₇H₈] is involatile and the dissociation of the toluene and the tetraglyme finally leads to the decomposition of the "[Ba(DBM)₂]" complex at 300°C. These above properties would suggest that [Ba(DBM)₂.tetraglyme.0.25C₇H₈] is polymeric, although, the strontium analog which was produced by Drake⁷ was found to be monomeric, but involatile. [Sr(DBM)₂.tetraglyme.0.5C₇H₈] was produced by reacting [Sr(OEt)₂(EtOH)₄], HDBM and tetraglyme at room temperature.

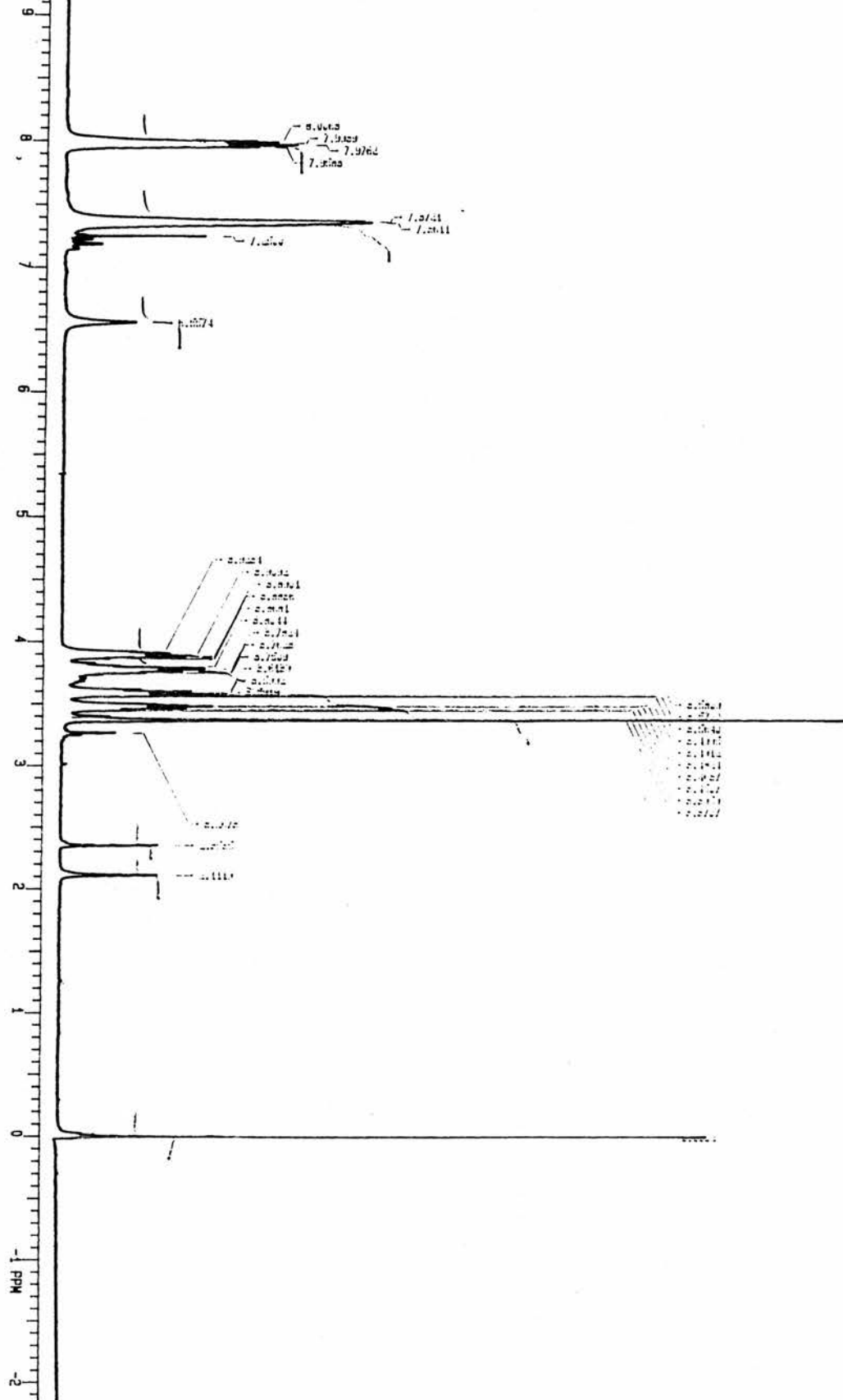
[Sr(DBM)₂.tetraglyme.0.5C₇H₈] is a air, moisture stable, monomeric, 9 coordinate solid. It, however, does not possess sufficient volatility for a mass spectrum to be obtained. The strontium analog has a rather low melting point at 96-98°C and the complex decomposes at 100°C / 10⁻³ Torr to produce the tetraglyme free strontium complex - " [Sr(DBM)₂]". It is interesting to note that the observed sublimation studies on [Ba(DBM)₂.tetraglyme.0.25C₇H₈] seem to show dissociation of the tetraglyme between 95-104°C. The synthesis and characterisation of Mg²⁺,⁸, Sr²⁺,⁹, Ca²⁺,¹⁰, Ho³⁺,¹¹ and rare earths complexes of 1,3-diphenyl-1,3-propanedione have also been undertaken by several workers. The adducts of ethanol, acetone and water of the Sr²⁺ and Ca²⁺ complexes have been isolated and characterised by means of X-ray crystallography. The latter adduct seems very surprising in light of the barium complex being so moisture sensitive. This sensitivity, however, must be as a result of the affinity for barium to maximise its coordination sphere (10-12 coordination number) and its affinity to bond to oxygen.

5.3.2. Analysis of [Ba(DBM)₂.tetraglyme.0.25C₇H₈]

5.3.2.1. ¹H N.M.R

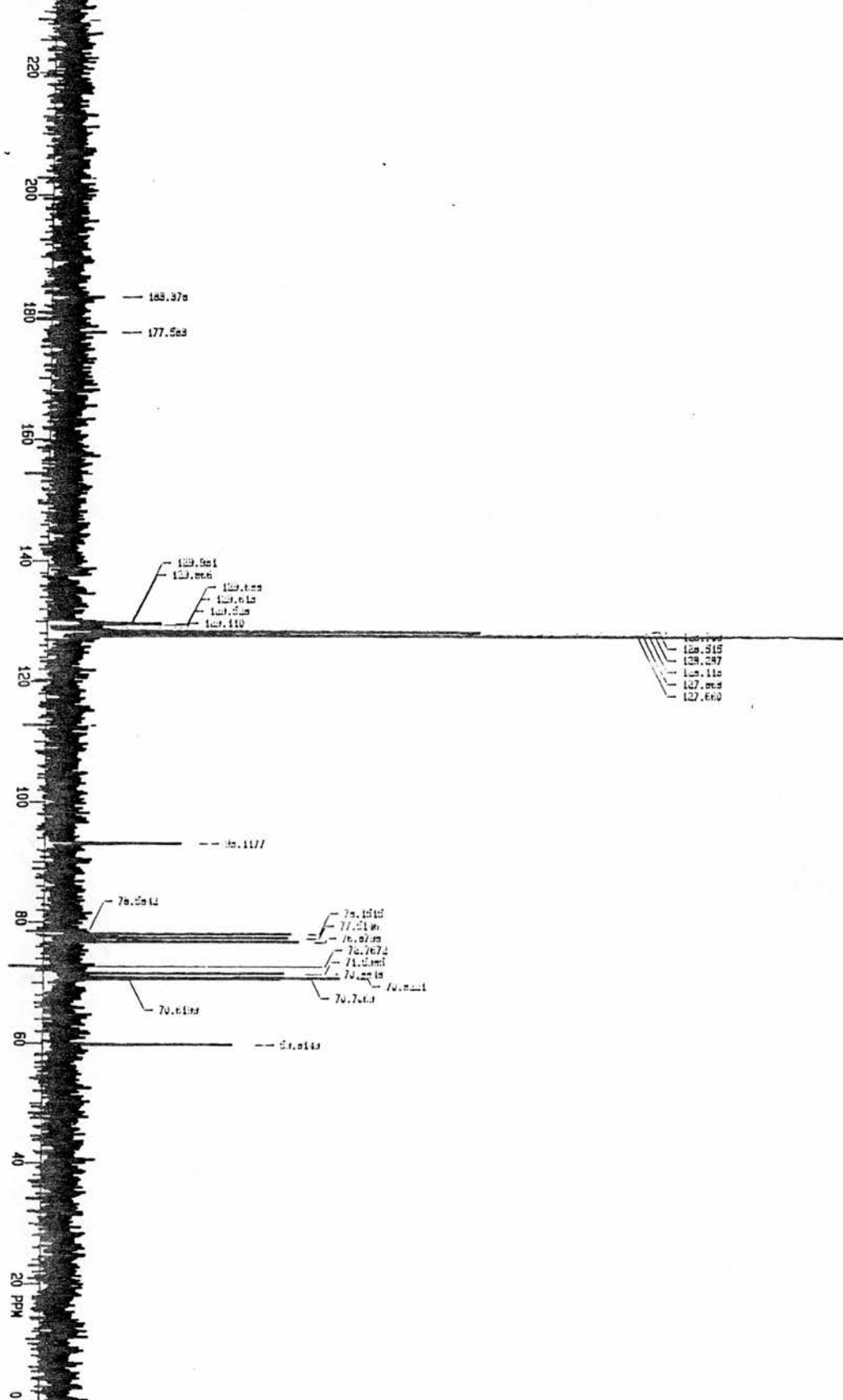
The ¹H N.M.R. spectrum in d⁸ toluene shows that the integration ratios of the C₇H₈ : tetraglyme : β-diketone to be in the appropriate ratio for the proposed empirical formula - [Ba(DBM)₂.tetraglyme.0.25C₇H₈]. As shown in Fig 5.3.2.1.a., the peak at δ 2.12 corresponds to the methyl protons of the residual toluene. Upon complexation to the barium metal, the methylene protons of the tetraglyme ligand seem possess different magnetic environments, as 4 separate sets of methylene (OCH₂) protons occur at different chemical shifts.

This is in direct contrast to what is observed in the ¹H N.M.R. spectra of tetraglyme or the [Ba(TMHD)₂.tetraglyme] complex . It seems that in these 2 spectra, the OCH₂ protons of the tetraglyme overlap one another at a similar chemical shift (tetraglyme - δ 3.42-3.70). The methylene signals of the tetraglyme ligand also occur downfield to that of the tetraglyme ligand when complexed to the barium centre in [Ba(DBM)₂.tetraglyme.0.25C₇H₈] at δ 3.37-3.93. The methylene proton from the β-diketonate moieties is observed at δ 6.56 which occurs upfield from that in the corresponding ligand. The 2 peaks at δ 7.37 and 7.99 correspond to protons of the phenyl rings of the β-diketonate.



5.3.2.2. ^{13}C N.M.R.

In the ^{13}C N.M.R. spectrum of the barium complex the peaks between δ 59.81-71.59 corresponds to the methyl and methylene carbon atoms of the tetraglyme ligand. The methylene carbon of the β -diketonate moieties occurs slightly upfield at δ 93.11 compared to that of the parent β -diketone ligand at δ 93.66. As shown in Fig 5.3.2.1.b., the phenyl carbons occur between δ 127.66 and 129.53. It appears upon complexation to the barium metal that the phenyl signals move upfield from their portion of the parent β -diketone at δ 121.53-136.04 and all 4 phenyl signals in the barium complex occur at a similar chemical shift. Due to the fact that 1,3-diphenylpropane-1,3-dione exists totally in the enol form (100% enol), one signal arises in the carbonyl region of the ^{13}C spectrum at δ 186.27. The barium complex exhibits 2 signals in the carbonyl region at δ 177.58 and 183.38 which strongly suggests that the β -diketonates are in a non-symmetrical environment. This is expected since the two carbonyl groups will be close to the open end of the β -diketone whilst the other two will be close to the centre of its backbone.

Fig. 5.3.2.2.a ^{13}C N.M.R. spectrum of BaI DBM [2-tetralyl]me.0.25C₇H₈

5.3.2.3. Mass spectral analysis

The mass spectrum of this barium complex shows extensive fragmentation. Peaks are observed up to 900 amu suggesting that the barium complex may be slightly volatile. The molecular ion is seen at 829 amu. Unfortunately, the solid did not sublime up to 225°C in vacuo.

5.3.2.4. STA studies

The DTA trace shows 5 major endotherms at 120, 190, 300, 485 and 875°C and one major exotherm at 420°C. As seen in fig.5.3.2.4.a, the first endotherm which is seen at 120°C is accompanied by a weight loss of 2% in the TGA. This seems to fit quite closely to the loss of 0.25 C₇H₈ in the proposed empirical formula -

[Ba(DBM)₂.tetraglyme.0.25C₇H₈] (2.77%). Between the temperatures of 120°C and 420°C there are 2 other endotherms. The DTA trace shows the first endotherm at 190°C which is accompanied by a gradual weight loss of 24%, ending at 420°C.

{ The calculated loss of the tetraglyme ligand in the barium complex

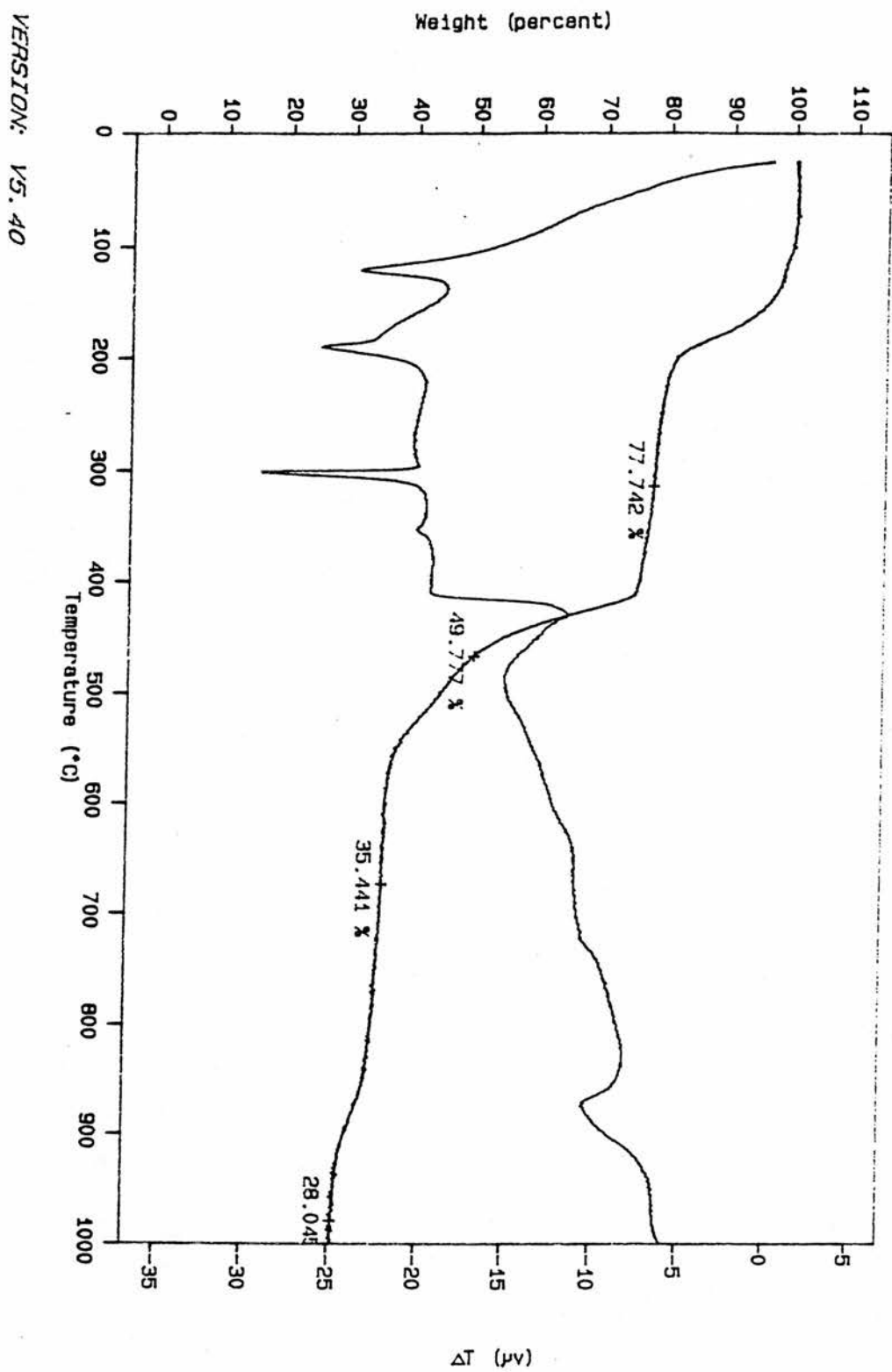
[Ba(DBM)₂.tetraglyme.0.25 C₇H₈] is 26.8% }. The STA also includes a very sharp melt at 300°C which is indicated by the third endotherm. The sharp melt can be tentatively assigned to the melting point of "[Ba(DBM)₂]".

After 420°C, the barium complex slowly decomposes. This is represented by an abrupt exotherm at 420°C. At first the "[Ba(DBM)₂]" complex loses one of its DBM ligands. The loss of a DBM ligand corresponds to a broad endotherm at 485°C.

The calculated loss of one of the DBM ligands from the barium complex -

[Ba(DBM)₂.tetraglyme.0.25 C₇H₈] corresponds to 27.05% weight loss.

Interestingly, the observed % weight loss from the exotherm at 420°C to the endotherm at 485°C corresponds to 27.28% weight loss. From 485°C to 875°C, the TGA trace shows only slight weight loss. The endotherm at 875°C is accompanied by a 6% weight loss which then finally decomposes to leave a % weight residue of 28%. The residue does not correspond to the formation of the expected barium oxide (18.50%). This discrepancy of 9.50% is probably due to residual decomposed carbon fragments. As a consequence of running the STA in a N₂ gas stream, decomposition to the oxide will not occur readily.

Fig 5.3.2.4.a. The STA of Bal DBM 1,2 tetraglyme, 0.25C₇H₈ in N₂

5.4. Experimental

5.4.1. The preparation of [bis(1,3-diphenylpropane-1,3-dionato) barium(II).tetraglyme.0.25C₇H₈]

In a 3-necked flask, a white suspension of barium hydride (0.95 g, 6.82×10^{-3} mol), 1,3-diphenylpropane-1,3-dione (3.38 g, 1.51×10^{-2} mol) and tetraglyme (1.67 g, 7.5×10^{-3} mol) in dry toluene (200 cm³) was initially stirred at room temperature under dry N₂. Some effervescence was noticed during the addition of the reactants. The suspension was stirred at room temperature for 1 hour and then refluxed for a further 16 hours whereupon a yellow suspension had resulted. Following the return to ambient temperature the suspension was filtered. The yellow solid (0.65 g) which had been filtered proved to insoluble in most organic solvents. The yellow filtered solution was then condensed to 80 cm³ whereupon a creamy, off-white solid was precipitated from solution. The solid was filtered and then recrystallised from methylene chloride. The recrystallised compound was found to be [bis(1,3-diphenylpropane-1,3-dionato) barium(II).tetraglyme.0.25 C₇H₈]. Yield = 2.05 g, 74%. Found % : C 60.93, H 5.21; C₄₀H₄₄O₉Ba.0.25C₇H₈ requires C 60.48, H 5.59.

It appears the compound is slightly light sensitive, moisture and air sensitive.

5.4.1.1. ¹H N.M.R.data

¹H N.M.R signals are observed at : δ 2.12 (CH₃ -0.25 C₇H₈), 3.37 (3H, s), 3.48 (2H,t), 3.57 (2H,t), 3.76 (2H,t), 3.89 (2H,t), 6.56 (2H,s), 7.37 (12H,m) and 7.99 (8H,m).

5.4.1.2. ^{13}C N.M.R. data

δ : 59.81, 70.62, 70.71, 70.82, 71.60, 93.11, 127.66, 127.87, 128.11, 128.29, 128.52, 128.71, 129.11, 129.53, 129.69 and 129.87.

5.4.1.3. Mass spectral data

Peaks were observed at 847, 829, 787, 720, 669, 581, 500, 452, 420, 279, 205, 164, 110, 72 and 42 mass units. The molecular ion is observed at 829 along with extensive fragmentation to give low intensity peaks. The largest peak is at 42.

5.4.1.4. Sublimation studies

The off-white solid was heated to 225°C at 40 Torr (dry stream of N_2 causing a dynamic vacuum). A small amount of liquid was condensed on the sides of the schlenk at temperatures between 95-104°C. ^1H N.M.R analysis of the liquid showed that it was tetraglyme. A colour of the solid changed to give a highly intense yellow once the solid was heated.

5.4.2. The attempted preparation of [bis(pentane-2,4-dionato) barium(II).tetraglyme] via Ba metal or BaH₂ routes

Pentane-2,4-dione (4.94 g, 4.93×10^{-2} mol) (previously washed with NaOH (2 Mol dm⁻³) and H₂O, dried and distilled at 45°C / 30 mmHg) was added to a white toluene suspension (250 cm³) of barium hydride (3.44 g, 2.47×10^{-2} mol) and tetraglyme (5.49 g, 2.47×10^{-2} mol.) at room temperature under N₂.

The suspension was stirred for 1 hour and then refluxed for a further 10 hours.

The white suspension was filtered at ambient temperature and the filtered solution was evaporated to a small volume. The clear solution which resulted was shown by ¹H and ¹³C N.M.R. analysis to be tetraglyme and the white solid to be the tetraglyme free complex. A similar result was obtained from refluxing barium granules, the β-diketone and tetraglyme.

5.5. Introduction

5.5.1. Metal thio- β -diketonates

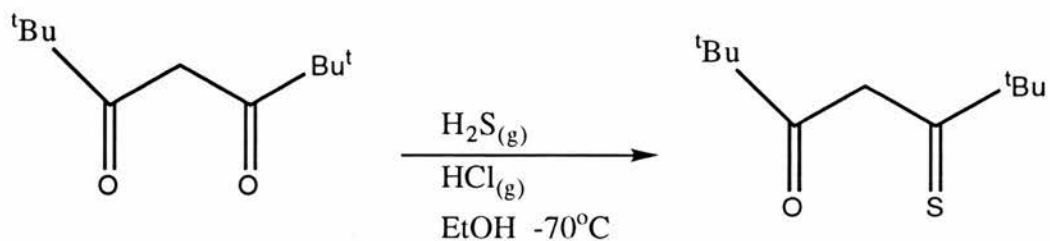
Several divalent metal β -diketonates of pentane-2,4-dione and other 1,3-diketones have been produced and isolated. X-ray analysis of most of these metal β -diketonates have shown them to be polymeric in nature. In particular, $[\text{Ni}(\text{acac})_2]^{12}$ and $[\text{Co}(\text{acac})_2]^{13}$ possess trimeric and tetrameric structures respectively.

On the other hand, the sulphur analogues $[\text{Ni}(\text{Sacac})_2]^{14}$ and $[\text{Co}(\text{Sacac})_2]^{14}$ are simple monomeric square planar complexes. By the simple replacement of an oxygen atom by a sulphur atom, depolymerisation can be achieved, as well as probably some extra stabilisation. Most of the thio- β -diketones that have been synthesised have been complexed to metal cations in the first and second row transition series ($\text{Fe}^{2+,15}$, $\text{Co}^{2+,15}$, $\text{Ni}^{2+,16}$, $\text{Ag}^{+,17}$, $\text{Cd}^{2+,17}$, $\text{Cu}^{2+,17}$ and $\text{Hg}^{2+,17}$).

In addition, Sugawara¹⁸ produced several monothio-perfluorinated β -diketonate barium complexes and observed that the sulphur analogues possessed a better or equivalent volatility to that of the sulphur free barium β -diketonate complexes. He found that $[\text{Ba}(\text{SHFA})_2]$ sublimed at $178^\circ\text{C} / 20\text{-}30$ Torr. This is in comparison to the sulphur free barium β -diketonate complex - $[\text{Ba}(\text{HFA})_2]$ which sublimes at a higher temperature - $220^\circ\text{C} / 20\text{-}30$ Torr¹⁹. In order to capitalise on the properties of depolymerisation, extra stabilisation and extra volatility demonstrated by the monothio and dithio- β -diketonate complexes, a series of barium and copper metal chelates of 2,2,6,6-tetramethyl-5-mercaptohept-4-en-3-one were produced, isolated and characterised. It was hoped that the copper and barium complexes would be monomeric and volatile.

The ligand 2,2,6,6-tetramethyl-5-mercaptohept-4-en-3-one was produced in a similar manner to that described by Chaston et al²⁰ as is illustrated in fig 5.5.1.a.

Fig 5.5.1.a



2,2,6,6-tetramethylheptane-3,5-dione was dissolved in ethanol and cooled down to -70°C using a cardice / ethanol bath. Dry gaseous hydrogen sulphide was passed through the solution, followed by dry gaseous hydrogen chloride gas. The flask was then left to stand at room temperature for 24 hours whereupon the thio- β -diketone was extracted using petroleum ether. It was purified and characterised by GC-MS. The preparation and analysis of the barium and copper compounds now follows.

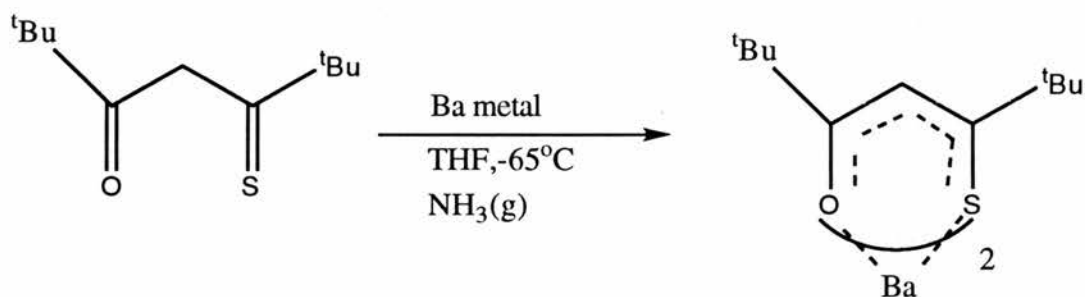
5.5.2. The preparation and analysis of the barium and copper complexes of 2,2,6,6-tetramethyl-5-mercaptohept-4-en-3-one

5.5.2.1. The preparation of [Ba(TMMHD)₂]

Attempts to produce [bis(2,2,6,6-tetramethyl-5-mercaptohept-4-en-3-oate) barium(II)] by aqueous methods using BaCl₂·2H₂O and sodium hydroxide and barium acetate proved to be unsuccessful. However, using anhydrous conditions, activated barium metal was reacted with 2,2,6,6-tetramethyl-5-mercaptohept-4-en-3-one to produce the barium complex. The activated barium metal was produced by a similar method to that described by Drake²¹.

Dry gaseous ammonia was bubbled through a mixture containing the ligand (in this case 2,2,6,6-tetramethyl-5-mercaptohept-4-en-3-one) and barium metal granules in THF solvent at -65°C. The equation is shown below.

Fig 5.5.2.1a

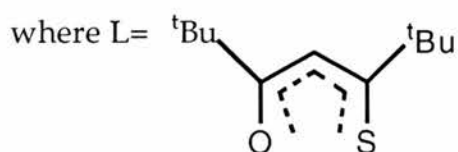


Upon the flask returning to ambient temperature a yellow, oily mixture was produced. The mixture was purified by adding methanol and diethyl ether. [Bis(2,2,6,6-tetramethyl-5-mercaptohept-4-en-3-oate)barium(II)] crystallised out from this solvent system.

5.5.2.3. The Preparation of [Cu(TMMHD)₂]

The preparation of [Cu(TMMHD)₂] has been described before by Dietrich and co-workers^{15,16}. However, in their first publication no experimental or analytical data was given on the copper complex. After a period of 13 years, a second publication in 1988 described the preparation of the copper complex. Although, no thermal or X-ray crystallographic data was reported. For this reason, the copper complex was also synthesised to observe its volatility and its structural characteristics. STA, volatility and X-ray crystallographic studies have been undertaken for the copper complex. Following a similar procedure to Dietrich, copper (II) acetate monohydrate was refluxed in methanolic solution of the thio-β-diketone.

Fig 5.5.2.3.



Upon addition of the thio-β-diketone to the copper (II) acetate an immediate red-brown precipitate was formed. The precipitate was filtered and the complex was purified by sublimation using a paraffin oil bath (120-140°C / 0.01 mm Hg). Upon sublimation of [Cu(TMMHD)₂], crystals fit for X-ray diffraction were obtained.

5.5.2.4. The analysis of [Cu(TMMHD)₂]

5.5.2.4.1. Sublimation studies

The red solid was sublimed at 120-140°C / 0.01mm Hg without decomposition (the heating rate was at 2° / minute using a paraffin oil bath). It would appear from this observation that [Cu(TMMHD)₂] has a lower sublimation temperature than its dioxygen analog [Cu(TMHD)₂]. Nakamori et al reported that [Cu(TMHD)₂] sublimed at 140-155°C under vacuum conditions. In conclusion it seems [Cu(TMMHD)₂] has a greater volatility than [Cu(TMHD)₂]. [Cu(TMMHD)₂] decomposes above 235°C but information on the decomposition temperature of [Cu(TMHD)₂] is not available.

5.5.2.4.2. The crystal structure of [Cu(TMMHD)₂]

A single crystal of [bis(2,2,6,6-tetramethyl-5-mercaptohept-4-en-3-olate) copper(II)] was obtained by sublimation, and the crystal structure was determined by the use of a Rigaku AFC7S diffractometer with graphite monochromated Cu-K α radiation under the guidance of Dr. Phil Lightfoot of the University of St. Andrews. As shown in Fig 5.5.2.4.2.a., the copper complex is a four coordinate, monomeric solid with the sulphur atoms existing in a cis configuration.

[Cu(TMMHD)₂] was found to be almost planar, however the calculated torsion angles shown in table 5 (Appendix 5.5.3) show that the molecule is slightly distorted towards to a tetrahedral structure. Although, the intraligand S(1)-Cu-S(2) and the O(1)-Cu-O(2) bond angles are < 90° [89.28(7) and 83.9° (2)] which suggest that the copper complex favours a square planar more than a tetrahedral geometry.

[Cu(TMMHD)₂] exists as a series of molecules oriented in two well defined planes within the unit cell. There are 4 molecules of [Cu(TMMHD)₂] per unit cell in which each molecule possesses a pseudo mm symmetry.

Fig 5.5.2.4.2.a

The copper complex $\text{Cu}[\text{TMMHD}]_2$ is viewed on the z plane. The ortep diagram shows ellipsoids at 25% probability.

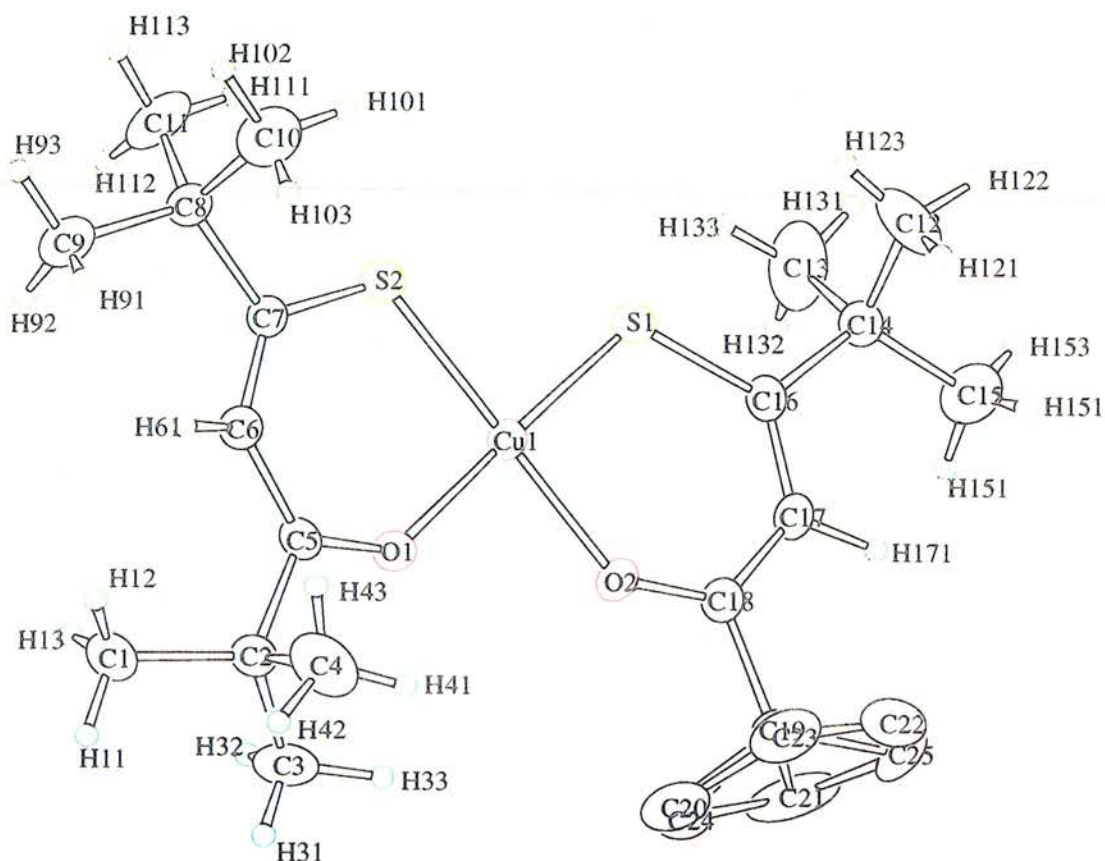


Fig 5.5.2.4.2.b

The figure below shows a ball and stick diagram from the x-plane. The diagram also shows that the copper atom does not achieve a totally square planar environment. The black hexagon of dots in all of the diagrams represents disorder in 'butyl groups.

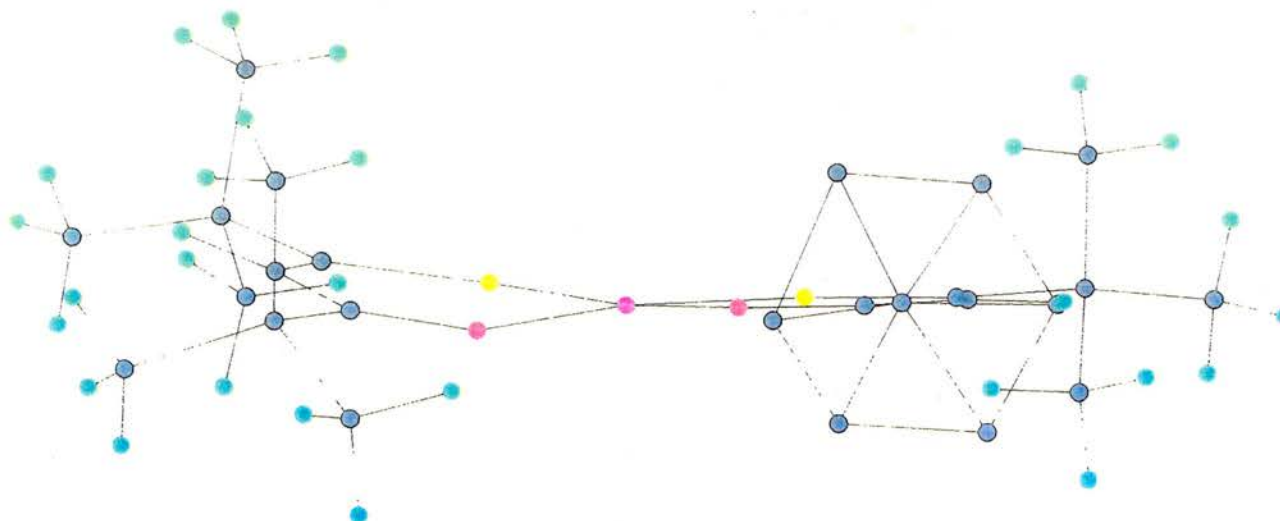
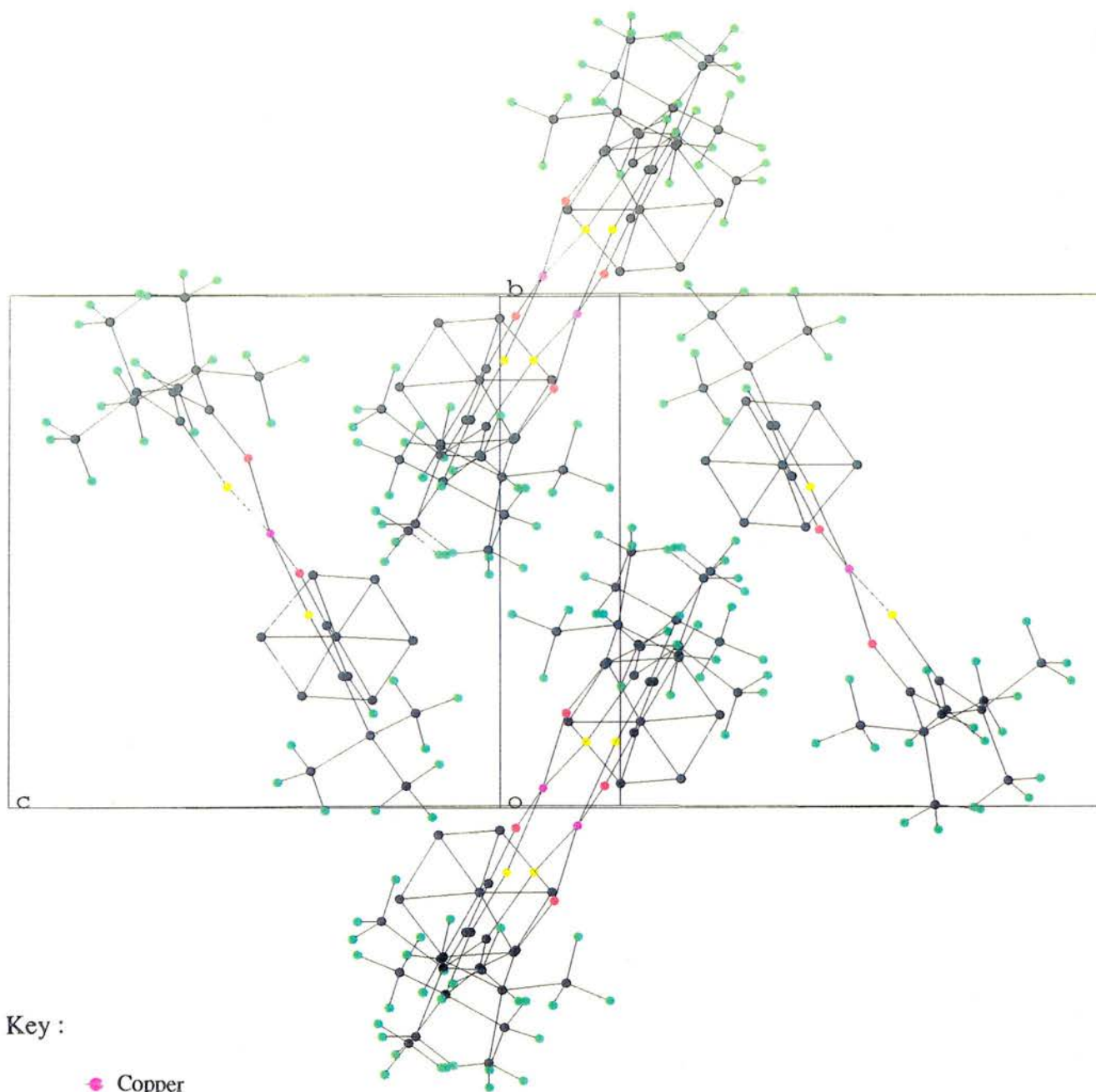


Fig.5.5.2.4.2.c.

Fig 5.5.2.4.2.c. illustrates the $\text{Cu}[\text{TMMHD}]_2$ molecules in the unit cell viewed from the x-plane. The diagram shows that $\text{Cu}[\text{TMMHD}]_2$ is essentially monomeric.

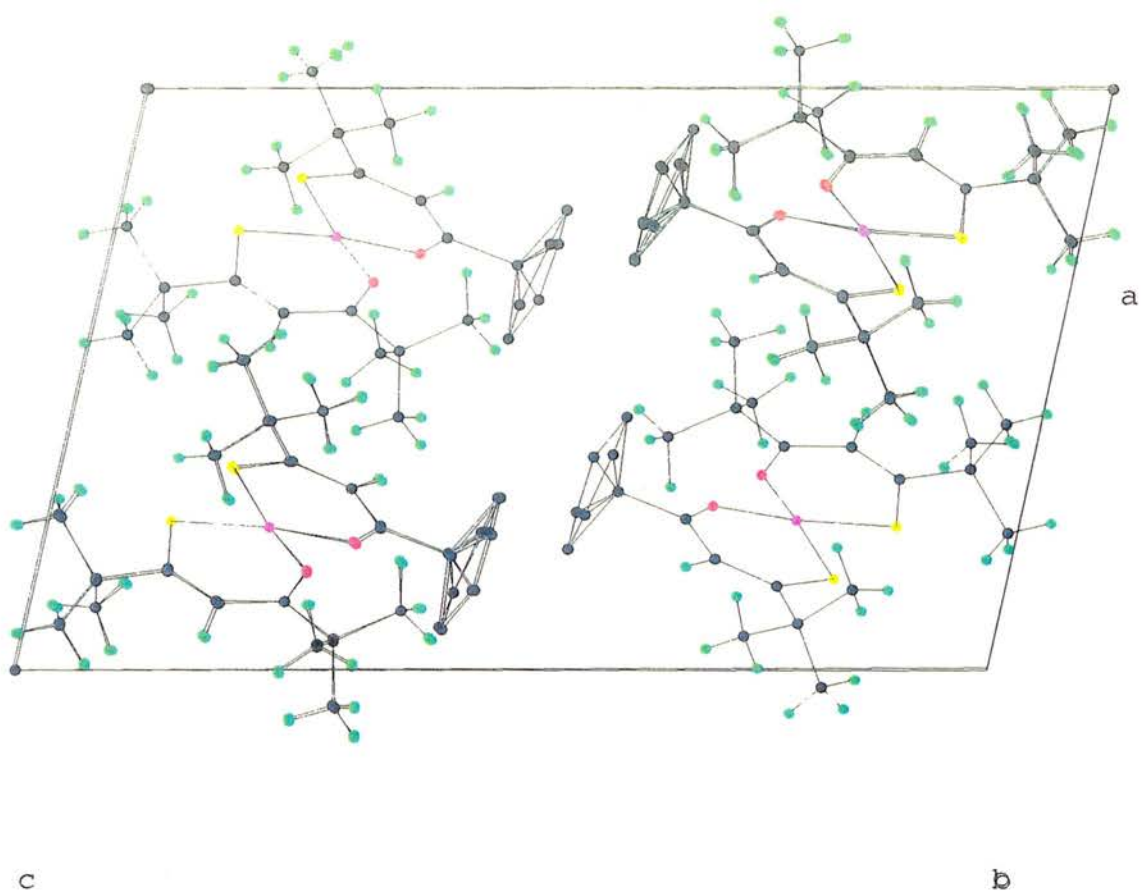


Key :

- Copper
- Sulphur
- Oxygen
- Hydrogen
- Carbon

Fig 5.5.2.4.2.d

$\text{Cu}[\text{TMMHD}]_2$ is viewed from the z plane where there are 4 individual molecules of $\text{Cu}[\text{TMMHD}]_2$ per unit cell. A birds eye view shows that the 4 molecules are eclipsed by adjacent molecules in another unit cell.



Key :

- Copper
- Sulphur
- Oxygen
- Hydrogen
- Carbon

Fig 5.5.2.4.2.e

A ball and stick diagram is shown of 2 individual molecules of $\text{Cu}[\text{TMMHD}]_2$ in the unit cell. Some of the closest interactions from other molecules are labelled. The figures for the closest intermolecular interactions are given in table 6 (Appendix 5). The diagram and table 6 show no short intermolecular interactions between adjacent $\text{Cu}[\text{TMMHD}]_2$ molecules.

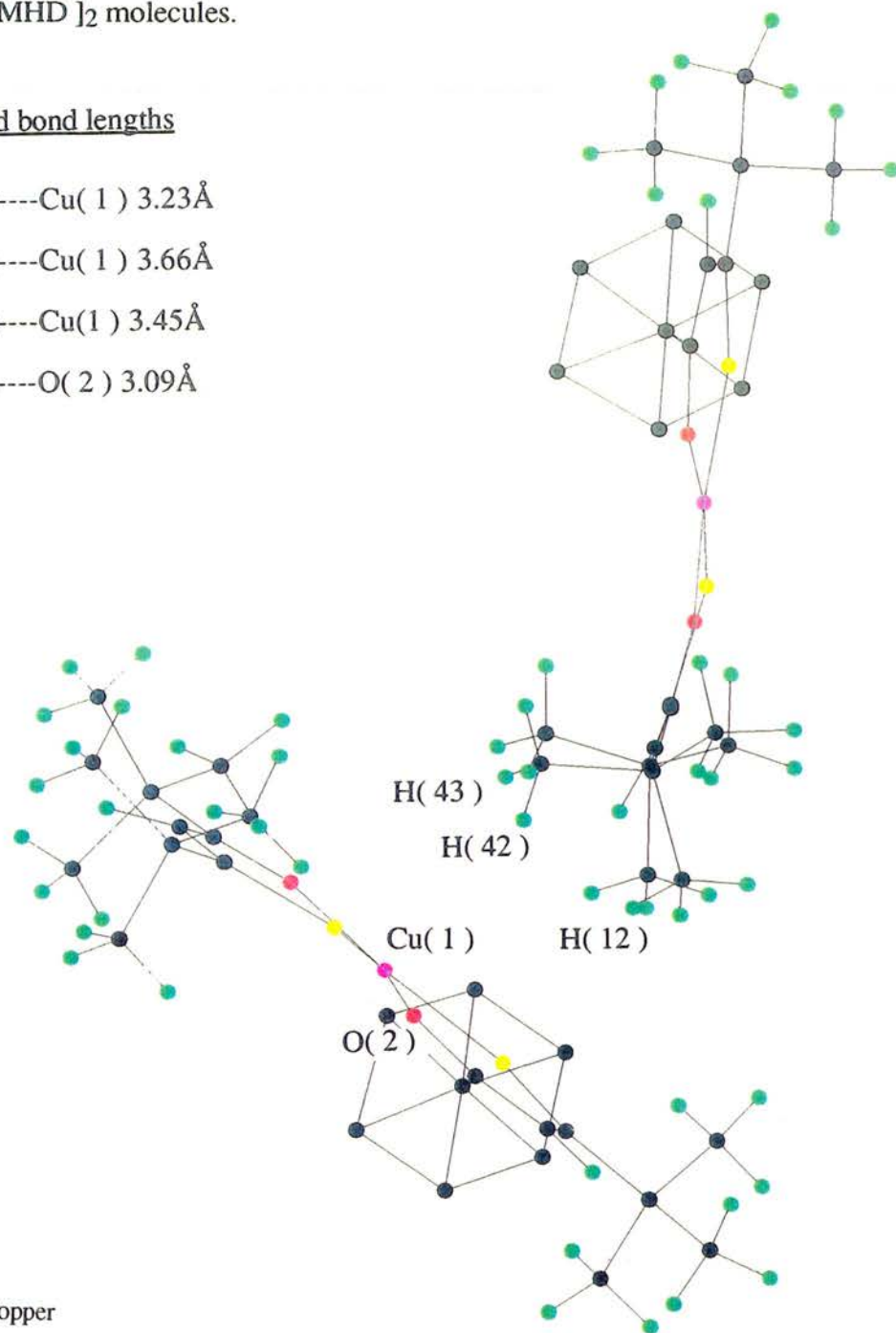
Selected bond lengths

$\text{H}(43) \cdots \text{Cu}(1)$ 3.23Å

$\text{H}(42) \cdots \text{Cu}(1)$ 3.66Å

$\text{H}(12) \cdots \text{Cu}(1)$ 3.45Å

$\text{H}(42) \cdots \text{O}(2)$ 3.09Å



Key:

- Copper
- Oxygen
- Sulphur
- Hydrogen
- Carbon

The copper complex has no short range intermolecular interactions occurring between individual $[\text{Cu}(\text{TMMHD})_2]$ molecules. The nearest copper interaction between one molecule and another is at 3.03\AA , which is a copper to hydrogen interaction $[\text{Cu}(1) \cdots \text{H}(153)]$. This interaction is unlikely to occur because there seems to be no other crystallographic evidence to support the occurrence of $\text{Cu} \cdots \text{H}$ interactions. As a consequence of the lack of short intermolecular interactions, $[\text{Cu}(\text{TMMHD})_2]$ sublimes. In $[\text{Ni}(\text{TMHD})_2]$ the nearest neighbour to the Ni atom is at 3.78\AA whilst the closest ring atom is a carbon atom at 4.46\AA . The $[\text{Ni}(\text{TMHD})_2]$ crystal structure was deduced by Cotton and coworkers in which the Nickel derivative was found to be isomorphous to the copper analog²². However, no structural data was individually published on the crystal structure of $[\text{Cu}(\text{TMHD})_2]$.

The Cu-O bond lengths in $[\text{Cu}(\text{TMMHD})_2]$ at $1.928(4)\text{\AA}$ $[\text{Cu}(1)-\text{O}(1)]$ and $1.947(4)\text{\AA}$ $[\text{Cu}(1)-\text{O}(2)]$ are slightly longer than the short Cu-O bond lengths that occur in $[\text{Cu}(\text{acac})_2]$ (Cu-O - $1.912(4)$ and $1.914(4)\text{\AA}$)²³ but are still in the range for a typical Cu(II) slightly distorted square planar complex.

Ligand atoms involving larger donor atom radii such as sulphur provide intermediate bond lengths for the Cu (II) distorted square planar complexes. These Cu-S bond lengths occur at $2.219(2)$ and $2.220(2)\text{\AA}$ in $[\text{Cu}(\text{TMMHD})_2]$. This is in close agreement with the Cu-S bond lengths in CuS at 2.19 and 2.32\AA . As a result of the larger size of the sulphur, weaker binding may be experienced in the copper complex. This may explain the observed thermal properties of the copper complex $[\text{Cu}(\text{TMMHD})_2]$ in the STA as shown in Fig 5.5.2.4.4.a. At temperatures greater than 235°C , decomposition may occur as a consequence of the cleavage of the Cu-S bond. The oxygen derivative - $[\text{Cu}(\text{TMHD})_2]$, which has 4 shorter and stronger Cu-O bonds is thermally stable at this temperature.

The bond lengths and bond orders of $\text{C}=\text{O}$, $\text{C}=\text{C}$ are consistent with those of other β -diketonates with similar π delocalisation occurring within the chelate ring.

It is interesting to note that the C=C bond adjacent to C=S is slightly shorter at [C(7) - C(6) - 1.357(8) Å] than C=C next to C=O at [C(6) - C(5) - 1.412(8) Å]. It follows that C=O has more double bond character than C=S, which is to be expected. The cis arrangement of the sulphur atoms, rather than trans arrangement is preferred in [Cu(TMMHD)₂]. The fact that favourable nonbonded π interactions can occur between adjacent cis sulphurs may suggest a reason why the sulphur atoms adopt a cis configuration, as opposed to trans. In addition, another reason for the sulphur atoms to occur cis and not trans to one another may be due to the fact that ligands of high trans effect tend not to favour being mutually trans²⁴.

In this particular crystal structure as well as many other metal β -diketonates which have bulky β -substituents, disorder is observed.

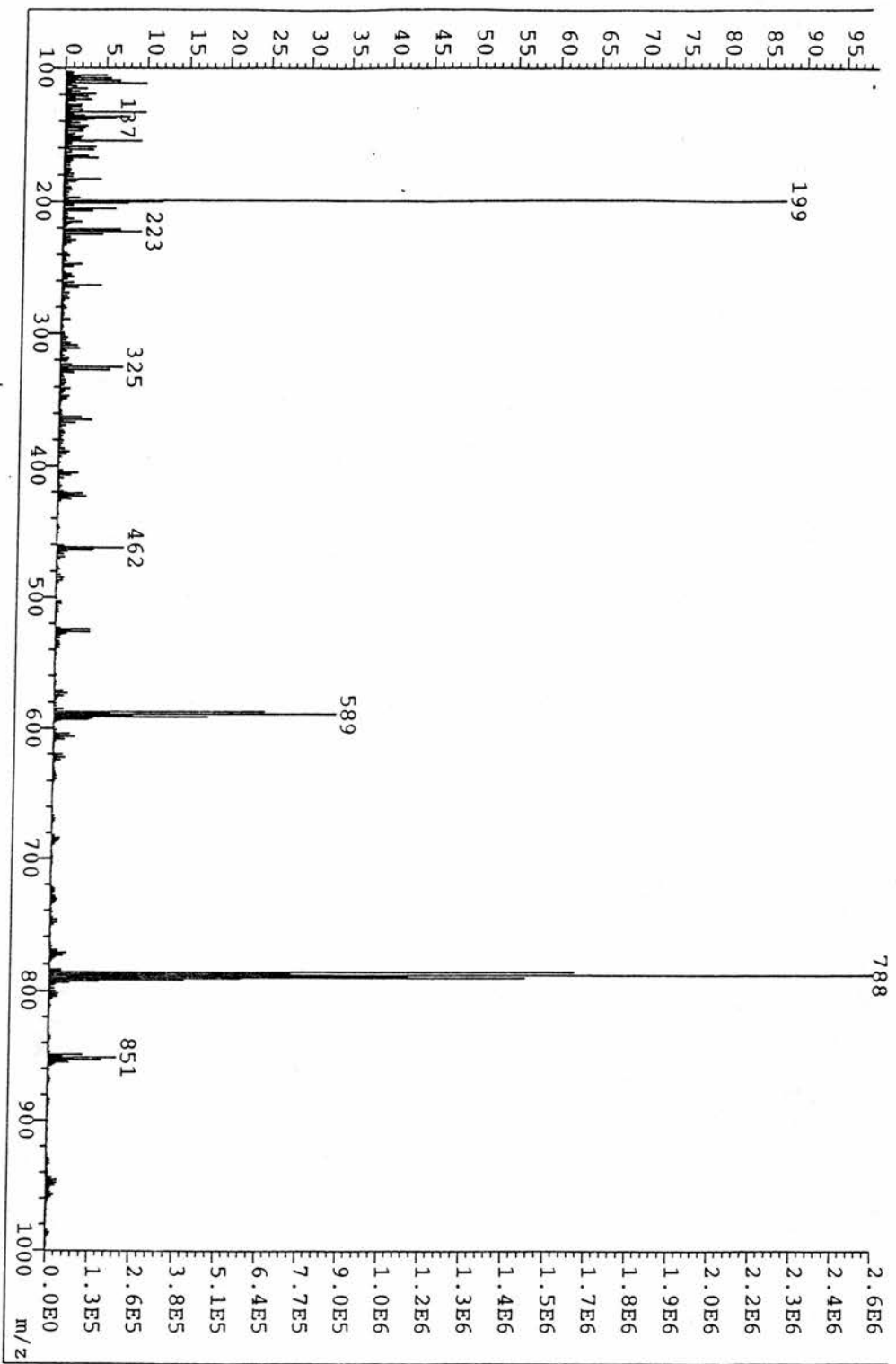
Disorder occurs around the ^tbutyl groups of the thio- β -diketonate moiety and hence in Fig 5.5.2.4.2.a., some disorder is represented by amalgamation of carbon atoms on the ^tbutyl groups. The distinction between one individual ^tbutyl group and another ^tbutyl cannot be resolved due to the large amount of electron density observed for the butyl groups. Similar disorder was noticed in the crystal structure of [Ni(TMMHD)₂] obtained by Coetzer²⁵ with which the copper derivative is isostructural.

5.5.2.4.3. Mass spectral analysis of [Cu(TMMHD)₂]

The FAB mass spectrum of the copper complex shows 5 major peaks at 199, 462, 589, 788 and 851 mass units. A significant feature of a mass spectrum of most metal β -diketonates is a peak corresponding to a small molecular ion, and the FAB mass spectrum of [Cu(TMMHD)₂] is no exception, showing a small peak at 462. Larger intensity peaks due to oligomeric species are seen at 589- Cu₃L₂, 788- Cu₃L₃, 851- Cu₄L₃ and 924- Cu₂L₄ where L = 2,2,6,6-tetramethyl-5-mercaptohept-4-en-3-one. The peak at 199 corresponds to L-H.

At first, the results showing oligomeric species in the vapour phase of the FAB mass spectrum for $[\text{Cu}(\text{TMMHD})_2]$, seem to be somewhat puzzling, since $[\text{Cu}(\text{TMMHD})_2]$ is essentially monomeric in the solid state.

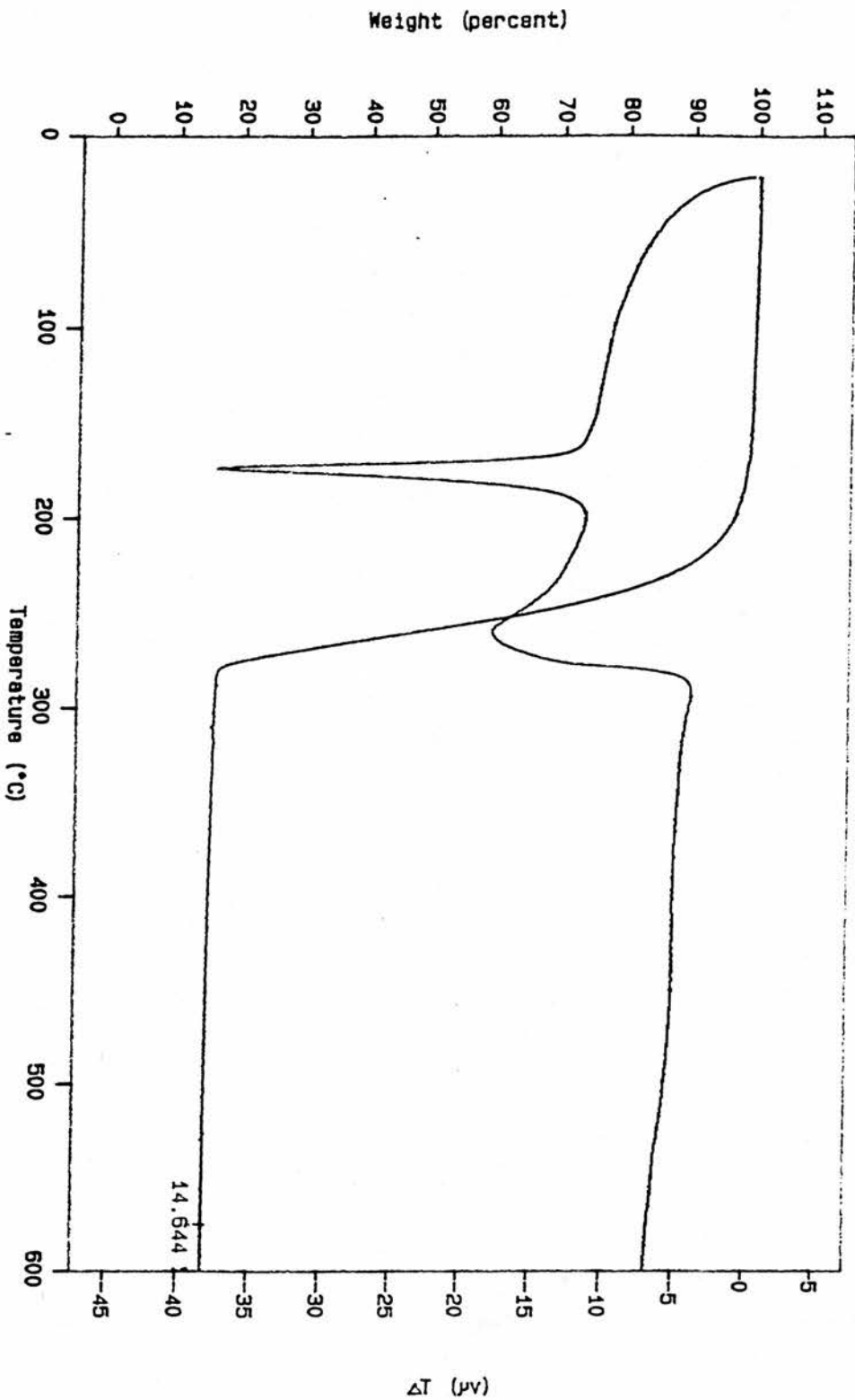
However, McDonald and Shannon²⁶ showed with simple metal acetylacetonates, valency changes in the metal could account for polymeric species in the vapour phase of the mass spectrum. Unfortunately, most of the complexes that were studied were not characterised by X-ray diffraction techniques. As a consequence, some of the simple acetylacetonates did possess polymeric structures, and therefore, some of the oligomeric species observed in the vapour phase of the mass spectrum were indeed, attributable to 'true' polymeric species and not due to any valency changes caused by monomeric ion- monomeric molecule interactions. However, some of metal β -diketonates that were studied did have monomeric structures and in the mass spectrum, polymeric species were observed.



5.5.2.4.4. STA studies

The STA of this copper complex shows two endotherms. The first endotherm corresponds to the melting point of [Cu(TMMHD)₂] at 175°C. The observed melting point is slightly lower than that determined experimentally and that quoted in the literature (186-187°C). Although, the first endotherm occurs at 175°C, weight loss seems to occur before melting, at 140°C. This may be attributable to partial sublimation taking place. The second endotherm at 275°C is shown to occur in two stages . From the DTA trace, an inflexion in the curve suggests that sublimation takes place, but at higher temperatures > 235°C sublimation is accompanied by decomposition. The sublimation of [Cu(TMMHD)₂] under vacuum using an oil bath or a heat gun seems to support the observed sublimation and decomposition in the STA. Using controlled temperature conditions (a heating rate of 2° / min in an oil bath), the copper complex [Cu(TMMHD)₂] can be sublimed intact. However, using a heat gun to sublime the complex the temperature rises too high (> 300°C) too quickly and thus, some decomposition occurs during the sublimation. This decomposition is also noticed in the STA where a % weight residue of 14.64% was obtained at 600°C (heating rate 10° / minute). This residue seems to suggest that sublimation has taken place, but at higher temperatures decomposition sets in . The calculated values for copper oxide (17.19 %) or copper sulphide (20.67 %) formation are higher than the experimentally observed % weight residue.

Fig. 5.5.2.4.4. The STA of CuI TMMHD₂ in N₂



VERSION: V5.40

5.5.3. APPENDIX

a) X-ray crystal structure of [Cu(TMMHD)₂]

5.5.3.1. Crystal data and structural refinement of [Cu(TMMHD)₂]Data Collection

A brown plate crystal of C₂₂H₃₈CuO₂S₂ having approximate dimensions of 0.40 x 0.40 x 0.10 mm was mounted on a glass fiber. All measurements were made on a Rigaku AFC7S diffractometer with graphite monochromated Cu-K α radiation.

Cell constants and an orientation matrix for data collection, obtained from a least-squares refinement using the setting angles of 25 carefully centered reflections in the range 51.15 < 2 θ < 54.92° corresponded to a primitive monoclinic cell with dimensions:

$$\begin{aligned} a &= 12.510(4) \text{ \AA} \\ b &= 10.333(3) \text{ \AA} \quad \beta = 102.34(1)^\circ \\ c &= 19.895(2) \text{ \AA} \\ V &= 2512.4(10) \text{ \AA}^3 \end{aligned}$$

For Z = 1 and F.W. = 462.21, the calculated density is 1.22 g cm⁻³. The systematic absences of:

$$\begin{aligned} h0l: h \neq 2n \\ 0k0: k \neq 2n \end{aligned}$$

uniquely determine the space group to be:

$$P2_1/a \text{ (#14)}$$

The data were collected at a temperature of 20 ± 1°C using the ω -2 θ scan technique to a maximum 2 θ value of 120.1°. Omega scans of several intense reflections, made prior to data collection, had an average width at half-height of 0.35° with a take-off angle of 6.0°. Scans of (1.57 + 0.35 tan θ)° were made at a speed of 16.0°/min (in omega). The weak reflections (I < 15.0 σ (I)) were rescanned (maximum of 4 scans) and the counts were accumulated to ensure good counting statistics. Stationary background counts were recorded on each side of the reflection. The ratio of peak counting time to background counting time was 2:1. The diameter of the incident beam collimator was 1.0 mm and the crystal to detector distance was 235 mm. The computer-controlled slits were set to 9.0 mm (horizontal) and 13.0 mm (vertical).

Data Reduction

Of the 4185 reflections which were collected, 3982 were unique (R_{int} = 0.091). The intensities of three representative reflection were measured after every 150 reflections. No decay correction was applied.

The linear absorption coefficient, μ , for Cu-K α radiation is 28.3 cm⁻¹. An empirical absorption correction based on azimuthal scans of several reflections was applied which resulted in transmission factors ranging from 0.56 to 1.00. The data were corrected for Lorentz and polarization effects.

Structure Solution and Refinement

The structure was solved by direct methods¹ and expanded using Fourier techniques². The non-hydrogen atoms were refined anisotropically. Hydrogen atoms were included but not refined. The final cycle of full-matrix least-squares refinement³ was based on 3168 observed reflections ($I > 3.00\sigma(I)$) and 263 variable parameters and converged (largest parameter shift was 4.47 times its esd) with unweighted and weighted agreement factors of:

$$R = \Sigma||Fo| - |Fc||/\Sigma|Fo| = 0.073$$

$$R_w = \sqrt{(\Sigma w(|Fo| - |Fc|)^2/\Sigma wFo^2)} = 0.081$$

The standard deviation of an observation of unit weight⁴ was 6.92. The weighting scheme was based on counting statistics and included a factor ($p = 0.004$) to downweight the intense reflections. Plots of $\Sigma w(|Fo| - |Fc|)^2$ versus $|Fo|$, reflection order in data collection, $\sin \theta/\lambda$ and various classes of indices showed no unusual trends. The maximum and minimum peaks on the final difference Fourier map corresponded to 0.83 and -0.91 $e^-/\text{\AA}^3$, respectively.

Neutral atom scattering factors were taken from Cromer and Waber⁵. Anomalous dispersion effects were included in F_{calc} ⁶; the values for $\Delta f'$ and $\Delta f''$ were those of Creagh and McAuley⁷. The values for the mass attenuation coefficients are those of Creagh and Hubbel⁸. All calculations were performed using the teXsan⁹ crystallographic software package of Molecular Structure Corporation.

References

- (1) SIR92: Altomare, A., Burla, M.C., Camalli, M., Cascarano, M., Giacovazzo, C., Guagliardi, A., Polidori, G. (1994). *J. Appl. Cryst.*, in preparation.
- (2) DIRDIF92: Beurskens, P.T., Admiraal, G., Beurskens, G., Bosman, W.P., Garcia-Granda, S., Gould, R.O., Smits, J.M.M. and Smykalla, C. (1992). The DIRDIF program system, Technical Report of the Crystallography Laboratory, University of Nijmegen, The Netherlands.

(3) Least-Squares:

Function minimized: $\Sigma w(|Fo| - |Fc|)^2$

$$\text{where } w = \frac{1}{\sigma^2(F_o)} = \frac{4Fo^2}{\sigma^2(F_o^2)}$$

$$\sigma^2(F_o^2) = \frac{S^2(C+R^2B)+(pFo^2)^2}{Lp^2}$$

S = Scan rate

C = Total integrated peak count

R = Ratio of scan time to background counting time

B = Total background count

Lp = Lorentz-polarization factor

p = p-factor

(4) Standard deviation of an observation of unit weight:

$$\sqrt{\sum w(|F_o| - |F_c|)^2 / (N_o - N_v)}$$

where: N_o = number of observations

N_v = number of variables

(5) Cromer, D. T. & Waber, J. T.: "International Tables for X-ray Crystallography". Vol. IV. The Kynoch Press, Birmingham, England. Table 2.2 A (1974).

(6) Ibers, J. A. & Hamilton, W. C.: Acta Crystallogr., 17, 781 (1964).

(7) Creagh, D. C. & McAuley, W.J.: "International Tables for Crystallography", Vol C, (A.J.C. Wilson, ed.), Kluwer Academic Publishers, Boston. Table 4.2.6.8, pages 219-222 (1992).

(8) Creagh, D. C. & Hubbell, J.H.: "International Tables for Crystallography", Vol C, (A.J.C. Wilson, ed.), Kluwer Academic Publishers, Boston. Table 4.2.4.3, pages 200-206 (1992).

(9) teXsan: Crystal Structure Analysis Package. Molecular Structure Corporation (1985 & 1992).

EXPERIMENTAL DETAILS

A. Crystal Data

Empirical Formula	$C_{22}H_{38}CuO_2S_2$
Formula Weight	462.21
Crystal Color, Habit	brown, plate
Crystal Dimensions	0.40 X 0.40 X 0.10 mm
Crystal System	monoclinic
Lattice Type	Primitive
No. of Reflections Used for Unit	
Cell Determination (2θ range)	25 ($51.2 - 54.9^\circ$)
Omega Scan Peak Width at Half-height	0.35°
Lattice Parameters	$a = 12.510(4) \text{ \AA}$ $b = 10.333(3) \text{ \AA}$ $c = 19.895(2) \text{ \AA}$ $\beta = 102.34(1)^\circ$ $V = 2512.4(10) \text{ \AA}^3$
Space Group	$P2_1/a$ (#14)
Z value	4
D_{calc}	1.222 g/cm^3
F_{000}	988.00
$\mu(\text{CuK}\alpha)$	28.26 cm^{-1}

B. Intensity Measurements

Diffractometer	Rigaku AFC7S
Radiation	CuK α ($\lambda = 1.54178 \text{ \AA}$) graphite monochromated
Attenuator	Ni foil (factors = 1.00, 9.06, 9.06, 9.06)
Take-off Angle	6.0°
Detector Aperture	9.0 mm horizontal 13.0 mm vertical
Crystal to Detector Distance	235 mm
Temperature	20.0°C
Scan Type	ω -2 θ
Scan Rate	16.0°/min (in ω) (up to 4 scans)
Scan Width	(1.57 + 0.35 tan θ)°
$2\theta_{max}$	120.1°
No. of Reflections Measured	Total: 4185 Unique: 3982 ($R_{int} = 0.091$)
Corrections	Lorentz-polarization Absorption (trans. factors: 0.5578 - 1.0000)

C. Structure Solution and Refinement

Structure Solution	Direct Methods (SIR92)
Refinement	Full-matrix least-squares
Function Minimized	$\Sigma w(F_o - F_c)^2$
Least Squares Weights	$\frac{1}{\sigma^2(F_o)} = \frac{4F_o^2}{\sigma^2(F_o^2)}$
p-factor	0.004
Anomalous Dispersion	All non-hydrogen atoms
No. Observations ($I > 3.00\sigma(I)$)	3168
No. Variables	263
Reflection/Parameter Ratio	12.05

Residuals: R: Rw	0.073 ; 0.081
Goodness of Fit Indicator	6.92
Max Shift/Error in Final Cycle	4.47
Maximum peak in Final Diff. Map	$0.83 \text{ e}^-/\text{\AA}^3$
Minimum peak in Final Diff. Map	$-0.91 \text{ e}^-/\text{\AA}^3$

5.5.3.2. Atomic coordinates

atom	x	y	z	B _{eq}
Cu(1)	0.25538(7)	0.03792(7)	0.22873(4)	3.76(2)
S(1)	0.1535(1)	-0.1253(1)	0.17847(7)	4.56(4)
S(2)	0.2440(1)	0.1281(2)	0.12623(8)	5.26(4)
O(1)	0.3323(3)	0.1832(3)	0.2772(2)	4.40(9)
O(2)	0.2821(3)	-0.0413(4)	0.3196(2)	5.0(1)
C(1)	0.4581(6)	0.4994(6)	0.3029(3)	6.6(2)
C(2)	0.4499(5)	0.3557(5)	0.3199(3)	4.3(1)
C(3)	0.3989(6)	0.3444(7)	0.3826(3)	7.4(2)
C(4)	0.5635(6)	0.2960(8)	0.3355(4)	8.7(2)
C(5)	0.3819(4)	0.2782(5)	0.2601(3)	3.8(1)
C(6)	0.3845(5)	0.3131(5)	0.1919(3)	4.2(1)
C(7)	0.3284(4)	0.2581(5)	0.1330(3)	3.6(1)
C(8)	0.3433(5)	0.3128(5)	0.0624(3)	4.2(1)
C(9)	0.3909(6)	0.4491(7)	0.0683(3)	7.1(2)
C(10)	0.4220(7)	0.2233(8)	0.0366(4)	8.6(2)
C(11)	0.2352(6)	0.3182(7)	0.0104(3)	7.3(2)
C(12)	0.1330(8)	-0.4287(7)	0.1561(5)	9.8(3)
C(13)	-0.0323(7)	-0.3181(8)	0.1639(5)	10.5(3)
C(14)	0.0747(5)	-0.3609(5)	0.2051(3)	4.3(1)
C(15)	0.0566(7)	-0.4597(7)	0.2566(4)	9.5(3)
C(16)	0.1421(4)	-0.2436(5)	0.2358(3)	3.8(1)
C(17)	0.1895(5)	-0.2416(5)	0.3049(3)	4.2(1)
C(18)	0.2557(5)	-0.1459(5)	0.3432(3)	4.1(1)
C(19)	0.3044(5)	-0.1651(6)	0.4214(3)	4.9(2)

atom	x	y	z	B_{eq}
C(20)	0.364(2)	-0.044(2)	0.4527(9)	10.9(6)
C(21)	0.206(1)	-0.176(3)	0.4589(8)	9.2(6)
C(22)	0.369(2)	-0.283(2)	0.4332(9)	11.4(6)
C(23)	0.430(1)	-0.167(2)	0.4285(7)	7.0(4)
C(24)	0.269(1)	-0.055(1)	0.4583(7)	7.5(4)
C(25)	0.266(1)	-0.292(1)	0.4496(7)	8.1(5)
H(11)	0.4907	0.5454	0.3435	7.6105
H(12)	0.5037	0.5070	0.2702	7.6105
H(13)	0.3882	0.5325	0.2842	7.6105
H(31)	0.4480	0.3866	0.4191	6.5386
H(32)	0.3157	0.3758	0.3706	6.5386
H(33)	0.3944	0.2510	0.4010	6.5386
H(41)	0.5653	0.2190	0.3570	10.2524
H(42)	0.6134	0.3579	0.3621	10.2524
H(43)	0.5857	0.2877	0.2916	10.2524
H(61)	0.4430	0.3731	0.1850	3.0000
H(91)	0.4643	0.4460	0.0924	8.1110
H(92)	0.3491	0.5024	0.0918	8.1110
H(93)	0.3869	0.4827	0.0232	8.1110
H(101)	0.3923	0.1395	0.0302	10.0991
H(102)	0.4356	0.2560	-0.0053	10.0991
H(103)	0.4895	0.2211	0.0702	10.0991
H(111)	0.2039	0.2344	0.0055	8.3995
H(112)	0.1883	0.3773	0.0254	8.3995

atom	x	y	z	$B_{\varepsilon q}$
H(113)	0.2493	0.3456	-0.0328	8.3995
H(121)	0.2067	-0.4486	0.1801	11.6401
H(122)	0.0971	-0.5090	0.1416	11.6401
H(123)	0.1351	-0.3768	0.1180	11.6401
H(131)	-0.0691	-0.3886	0.1377	12.1760
H(132)	-0.0769	-0.2855	0.1931	12.1760
H(133)	-0.0215	-0.2512	0.1327	12.1760
H(151)	0.1211	-0.5071	0.2728	11.4605
H(151)	0.0342	-0.4176	0.2938	11.4605
H(153)	-0.0007	-0.5180	0.2352	11.4605
H(171)	0.1735	-0.3176	0.3326	3.0000

$$B_{\varepsilon q} = \frac{8}{3} \pi^2 (U_{11}(aa^*)^2 + U_{22}(bb^*)^2 + U_{33}(cc^*)^2 + 2U_{12}aa^*bb^* \cos \gamma + 2U_{13}aa^*cc^* \cos \beta + 2U_{23}bb^*cc^* \cos \alpha)$$

5.5.3.3. Anisotropic displacement parameters

atom	U_{11}	U_{22}	U_{33}	U_{12}	U_{13}	U_{23}
Cu(1)	0.0665(5)	0.0372(4)	0.0419(4)	-0.0094(4)	0.0176(4)	0.0027(4)
S(1)	0.082(1)	0.0481(9)	0.0437(8)	0.0214(8)	0.0136(8)	-0.0047(7)
S(2)	0.082(1)	0.0481(9)	0.0437(8)	0.0214(9)	0.0136(8)	-0.0047(7)
O(1)	0.086(3)	0.044(2)	0.041(2)	-0.021(2)	0.021(2)	-0.001(2)
O(2)	0.105(3)	0.043(2)	0.042(2)	-0.021(2)	0.015(2)	0.008(2)
C(1)	0.132(6)	0.052(4)	0.066(4)	-0.028(4)	0.023(4)	-0.014(4)
C(2)	0.076(4)	0.045(3)	0.046(3)	-0.011(3)	0.017(3)	-0.005(3)
C(3)	0.145(7)	0.088(5)	0.051(4)	-0.047(5)	0.032(4)	-0.020(4)
C(4)	0.107(6)	0.089(6)	0.113(7)	0.002(5)	-0.023(5)	-0.035(5)
C(5)	0.062(4)	0.037(3)	0.048(3)	-0.005(3)	0.022(3)	-0.006(3)
C(6)	0.073(4)	0.042(3)	0.047(3)	-0.019(3)	0.022(3)	0.001(3)
C(7)	0.058(3)	0.038(3)	0.043(3)	-0.002(3)	0.020(3)	0.003(3)
C(8)	0.072(4)	0.048(3)	0.044(3)	-0.012(3)	0.020(3)	0.004(3)
C(9)	0.140(6)	0.078(5)	0.056(4)	-0.040(5)	0.029(4)	0.015(4)
C(10)	0.160(7)	0.104(6)	0.085(5)	0.021(6)	0.079(5)	0.015(5)
C(11)	0.099(5)	0.112(6)	0.060(4)	-0.033(5)	0.002(4)	0.038(4)
C(12)	0.173(8)	0.075(5)	0.137(7)	-0.032(6)	0.061(6)	-0.053(5)
C(13)	0.104(6)	0.082(6)	0.186(10)	-0.046(5)	-0.032(6)	0.026(6)
C(14)	0.068(4)	0.044(3)	0.051(3)	-0.015(3)	0.011(3)	0.001(3)
C(15)	0.181(8)	0.089(5)	0.082(5)	-0.081(5)	0.007(6)	0.013(5)
C(16)	0.057(3)	0.037(3)	0.053(3)	-0.004(3)	0.022(3)	0.001(3)
C(17)	0.073(4)	0.038(3)	0.050(3)	-0.010(3)	0.018(3)	0.009(3)
C(18)	0.070(4)	0.042(3)	0.048(3)	-0.001(3)	0.022(3)	0.005(3)
C(19)	0.094(5)	0.053(4)	0.037(3)	-0.005(3)	0.007(3)	0.007(3)

atom	U_{11}	U_{22}	U_{33}	U_{12}	U_{13}	U_{23}
C(20)	0.23(2)	0.11(1)	0.049(10)	-0.11(2)	-0.03(1)	0.00(1)
C(21)	0.09(1)	0.22(3)	0.044(8)	0.01(1)	0.037(8)	0.02(1)
C(22)	0.22(2)	0.11(1)	0.06(1)	0.12(1)	-0.06(1)	-0.02(1)
C(23)	0.068(9)	0.13(1)	0.060(8)	0.004(9)	-0.013(7)	0.014(9)
C(24)	0.16(2)	0.08(1)	0.044(7)	0.03(1)	0.028(9)	-0.004(8)
C(25)	0.17(2)	0.074(10)	0.054(8)	-0.04(1)	-0.003(10)	0.034(8)

The general temperature factor expression:

$$\exp(-2\pi^2(a^2U_{11}h^2 + b^2U_{22}k^2 + c^2U_{33}l^2 + 2a^*b^*U_{12}hk + 2a^*c^*U_{13}hl + 2b^*c^*U_{23}kl))$$

5.5.3.4. Bond lengths

atom	atom	distance	atom	atom	distance
Cu(1)	S(1)	2.220(2)	Cu(1)	S(2)	2.219(2)
Cu(1)	O(1)	1.928(4)	Cu(1)	O(2)	1.947(4)
S(1)	C(16)	1.701(6)	S(2)	C(7)	1.698(6)
O(1)	C(5)	1.248(7)	O(2)	C(18)	1.256(7)
C(1)	C(2)	1.534(9)	C(1)	H(11)	0.95
C(1)	H(12)	0.95	C(1)	H(13)	0.94
C(2)	C(3)	1.533(9)	C(2)	C(4)	1.514(10)
C(2)	C(5)	1.535(8)	C(3)	H(31)	0.95
C(3)	H(32)	1.06	C(3)	H(33)	1.03
C(4)	H(41)	0.89	C(4)	H(42)	0.96
C(4)	H(43)	0.99	C(5)	C(6)	1.412(8)
C(6)	C(7)	1.357(8)	C(6)	H(61)	0.99
C(7)	C(8)	1.555(8)	C(8)	C(9)	1.519(9)
C(8)	C(10)	1.526(10)	C(8)	C(11)	1.516(9)
C(9)	H(91)	0.95	C(9)	H(92)	0.95
C(9)	H(93)	0.95	C(10)	H(101)	0.95
C(10)	H(102)	0.94	C(10)	H(103)	0.96
C(11)	H(111)	0.95	C(11)	H(112)	0.94
C(11)	H(113)	0.96	C(12)	C(14)	1.51(1)
C(12)	H(121)	0.96	C(12)	H(122)	0.95
C(12)	H(123)	0.94	C(13)	C(14)	1.50(1)
C(13)	H(131)	0.96	C(13)	H(132)	0.92
C(13)	H(133)	0.96	C(14)	C(15)	1.501(9)
C(14)	C(16)	1.526(8)	C(15)	H(151)	0.96

atom	atom	distance	atom	atom	distance
C(15)	H(151)	0.93	C(15)	H(153)	0.96
C(16)	C(17)	1.378(8)	C(17)	C(18)	1.402(8)
C(17)	H(171)	1.00	C(18)	C(19)	1.537(8)
C(19)	C(20)	1.54(2)	C(19)	C(21)	1.55(2)
C(19)	C(22)	1.37(2)	C(19)	C(23)	1.494(8)
C(19)	C(24)	1.28(1)	C(20)	C(22)	1.49(3)
C(20)	C(23)	0.08(2)	C(21)	C(22)	1.48(3)
C(21)	C(25)	1.64	C(22)	C(23)	1.41(3)

5.5.3.5. Bond angles

atom	atom	atom	angle	atom	atom	atom	angle
S(1)	Cu(1)	S(2)	89.28(7)	S(1)	Cu(1)	O(1)	174.2(1)
S(1)	Cu(1)	O(2)	93.9(1)	S(2)	Cu(1)	O(1)	93.4(1)
S(2)	Cu(1)	O(2)	173.9(2)	O(1)	Cu(1)	O(2)	83.9(2)
Cu(1)	S(1)	C(16)	111.5(2)	Cu(1)	S(2)	C(7)	110.2(2)
Cu(1)	O(1)	C(5)	134.4(4)	Cu(1)	O(2)	C(18)	134.6(4)
C(2)	C(1)	H(11)	109.4	C(2)	C(1)	H(12)	108.1
C(2)	C(1)	H(13)	109.8	H(11)	C(1)	H(12)	109.6
H(11)	C(1)	H(13)	110.1	H(12)	C(1)	H(13)	109.9
C(1)	C(2)	C(3)	108.5(6)	C(1)	C(2)	C(4)	109.8(6)
C(1)	C(2)	C(5)	112.6(5)	C(3)	C(2)	C(4)	109.6(6)
C(3)	C(2)	C(5)	109.4(5)	C(4)	C(2)	C(5)	106.9(5)
C(2)	C(3)	H(31)	105.0	C(2)	C(3)	H(32)	110.5
C(2)	C(3)	H(33)	114.7	H(31)	C(3)	H(32)	118.4
H(31)	C(3)	H(33)	103.9	H(32)	C(3)	H(33)	104.6
C(2)	C(4)	H(41)	113.0	C(2)	C(4)	H(42)	108.0
C(2)	C(4)	H(43)	105.7	H(41)	C(4)	H(42)	113.4
H(41)	C(4)	H(43)	111.0	H(42)	C(4)	H(43)	105.1
O(1)	C(5)	C(2)	115.0(5)	O(1)	C(5)	C(6)	125.4(5)
C(2)	C(5)	C(6)	119.5(5)	C(5)	C(6)	C(7)	127.7(5)
C(5)	C(6)	H(61)	117.5	C(7)	C(6)	H(61)	113.8
S(2)	C(7)	C(6)	126.6(5)	S(2)	C(7)	C(8)	114.1(4)
C(6)	C(7)	C(8)	119.3(5)	C(7)	C(8)	C(9)	112.8(5)
C(7)	C(8)	C(10)	107.1(5)	C(7)	C(8)	C(11)	111.9(5)
C(9)	C(8)	C(10)	108.2(6)	C(9)	C(8)	C(11)	107.0(6)

atom	atom	atom	angle	atom	atom	atom	angle
C(10)	C(8)	C(11)	109.9(6)	C(8)	C(9)	H(91)	109.4
C(8)	C(9)	H(92)	109.3	C(8)	C(9)	H(93)	109.3
H(91)	C(9)	H(92)	110.0	H(91)	C(9)	H(93)	109.5
H(92)	C(9)	H(93)	109.3	C(8)	C(10)	H(101)	109.1
C(8)	C(10)	H(102)	109.6	C(8)	C(10)	H(103)	108.4
H(101)	C(10)	H(102)	110.6	H(101)	C(10)	H(103)	109.3
H(102)	C(10)	H(103)	109.8	C(8)	C(11)	H(111)	108.9
C(8)	C(11)	H(112)	109.5	C(8)	C(11)	H(113)	108.6
H(111)	C(11)	H(112)	110.7	H(111)	C(11)	H(113)	109.1
H(112)	C(11)	H(113)	110.1	C(14)	C(12)	H(121)	108.7
C(14)	C(12)	H(122)	109.6	C(14)	C(12)	H(123)	110.0
H(121)	C(12)	H(122)	108.7	H(121)	C(12)	H(123)	109.7
H(122)	C(12)	H(123)	110.0	C(14)	C(13)	H(131)	108.6
C(14)	C(13)	H(132)	111.1	C(14)	C(13)	H(133)	108.2
H(131)	C(13)	H(132)	110.9	H(131)	C(13)	H(133)	107.1
H(132)	C(13)	H(133)	110.9	C(12)	C(14)	C(13)	107.9(7)
C(12)	C(14)	C(15)	107.4(7)	C(12)	C(14)	C(16)	109.0(6)
C(13)	C(14)	C(15)	108.3(7)	C(13)	C(14)	C(16)	109.7(6)
C(15)	C(14)	C(16)	114.4(5)	C(14)	C(15)	H(151)	108.9
C(14)	C(15)	H(151)	110.6	C(14)	C(15)	H(153)	109.1
H(151)	C(15)	H(151)	110.5	H(151)	C(15)	H(153)	107.8
H(151)	C(15)	H(153)	109.9	S(1)	C(16)	C(14)	114.8(4)
S(1)	C(16)	C(17)	125.5(5)	C(14)	C(16)	C(17)	119.6(5)
C(16)	C(17)	C(18)	128.9(5)	C(16)	C(17)	H(171)	116.3

atom	atom	atom	angle	atom	atom	atom	angle
C(18)	C(17)	H(171)	114.8	O(2)	C(18)	C(17)	125.5(6)
O(2)	C(18)	C(19)	114.4(5)	C(17)	C(18)	C(19)	120.0(5)
C(18)	C(19)	C(20)	108.6(8)	C(18)	C(19)	C(21)	113.3(7)
C(18)	C(19)	C(22)	116.4(9)	C(18)	C(19)	C(23)	109.2(5)
C(18)	C(19)	C(24)	110.0(7)	C(20)	C(19)	C(21)	118(1)
C(20)	C(19)	C(22)	61(1)	C(20)	C(19)	C(23)	2.4(8)
C(20)	C(19)	C(24)	108(1)	C(21)	C(19)	C(22)	60(1)
C(21)	C(19)	C(23)	116.6(9)	C(21)	C(19)	C(24)	97(1)
C(22)	C(19)	C(23)	59(1)	C(22)	C(19)	C(24)	133.4(10)
C(23)	C(19)	C(24)	109.9(9)	C(19)	C(20)	C(22)	53.7(9)
C(19)	C(20)	C(23)	55(12)	C(22)	C(20)	C(23)	5(13)
C(19)	C(21)	C(22)	53.5(9)	C(19)	C(21)	C(25)	104.2
C(22)	C(21)	C(25)	136.9	C(19)	C(22)	C(20)	64(1)
C(19)	C(22)	C(21)	65(1)	C(19)	C(22)	C(23)	65.0(10)
C(20)	C(22)	C(21)	126(1)	C(20)	C(22)	C(23)	0.3(7)
C(21)	C(22)	C(23)	126(1)	C(19)	C(23)	C(20)	122(13)
C(19)	C(23)	C(22)	56.0(8)	C(20)	C(23)	C(22)	174(13)

5.5.3.6. Torsion angles

atom	atom	atom	atom	angle	atom	atom	atom	atom	angle
Cu(1)	S(1)	C(16)	C(14)	-179.2(4)	Cu(1)	S(1)	C(16)	C(17)	-0.4(6)
Cu(1)	S(2)	C(7)	C(6)	-8.6(6)	Cu(1)	S(2)	C(7)	C(8)	169.4(4)
Cu(1)	O(1)	C(5)	C(2)	-168.3(4)	Cu(1)	O(1)	C(5)	C(6)	8.3(10)
Cu(1)	O(2)	C(18)	C(17)	-2(1)	Cu(1)	O(2)	C(18)	C(19)	173.8(5)
S(1)	Cu(1)	S(2)	C(7)	-171.8(2)	S(1)	Cu(1)	O(1)	C(5)	-133(1)
S(1)	Cu(1)	O(2)	C(18)	1.8(6)	S(1)	C(16)	C(14)	C(12)	66.1(7)
S(1)	C(16)	C(14)	C(13)	-51.9(8)	S(1)	C(16)	C(14)	C(15)	-173.8(6)
S(1)	C(16)	C(17)	C(18)	0(1)	S(2)	Cu(1)	S(1)	C(16)	174.3(2)
S(2)	Cu(1)	O(1)	C(5)	-16.1(6)	S(2)	Cu(1)	O(2)	C(18)	-118(1)
S(2)	C(7)	C(6)	C(5)	-2(1)	S(2)	C(7)	C(8)	C(9)	163.2(5)
S(2)	C(7)	C(8)	C(10)	-77.9(6)	S(2)	C(7)	C(8)	C(11)	42.6(7)
O(1)	Cu(1)	S(1)	C(16)	-67(1)	O(1)	Cu(1)	S(2)	C(7)	13.3(3)
O(1)	Cu(1)	O(2)	C(18)	176.4(6)	O(1)	C(5)	C(2)	C(1)	-149.3(6)
O(1)	C(5)	C(2)	C(3)	-28.5(8)	O(1)	C(5)	C(2)	C(4)	90.0(7)
O(1)	C(5)	C(6)	C(7)	5(1)	O(2)	Cu(1)	S(1)	C(16)	-0.4(3)
O(2)	Cu(1)	S(2)	C(7)	-50(1)	O(2)	Cu(1)	O(1)	C(5)	158.4(6)
O(2)	C(18)	C(17)	C(16)	0(1)	O(2)	C(18)	C(19)	C(20)	-55(1)
O(2)	C(18)	C(19)	C(21)	169(1)	O(2)	C(18)	C(19)	C(22)	-122(1)
O(2)	C(18)	C(19)	C(23)	-58.3(7)	O(2)	C(18)	C(19)	C(24)	62(1)
C(1)	C(2)	C(5)	C(6)	33.9(8)	C(2)	C(5)	C(6)	C(7)	-178.4(6)
C(3)	C(2)	C(5)	C(6)	154.6(6)	C(4)	C(2)	C(5)	C(6)	-86.8(7)
C(5)	C(6)	C(7)	C(8)	179.5(6)	C(6)	C(7)	C(8)	C(9)	-18.7(8)
C(6)	C(7)	C(8)	C(10)	100.2(7)	C(6)	C(7)	C(8)	C(11)	-139.3(6)
C(12)	C(14)	C(16)	C(17)	-112.8(7)	C(13)	C(14)	C(16)	C(17)	129.2(7)

atom	atom	atom	atom	angle	atom	atom	atom	atom	angle
C(14)	C(16)	C(17)	C(18)	179.2(6)	C(15)	C(14)	C(16)	C(17)	7.4(9)
C(16)	C(17)	C(18)	C(19)	-175.0(7)	C(17)	C(18)	C(19)	C(20)	120(1)
C(17)	C(18)	C(19)	C(21)	-13(1)	C(17)	C(18)	C(19)	C(22)	53(1)
C(17)	C(18)	C(19)	C(23)	118.0(6)	C(17)	C(18)	C(19)	C(24)	-121(1)
C(18)	C(19)	C(20)	C(22)	-110(1)	C(18)	C(19)	C(20)	C(23)	-104(14)
C(18)	C(19)	C(21)	C(22)	108(1)	C(18)	C(19)	C(21)	C(25)	-113.2
C(18)	C(19)	C(22)	C(20)	97(1)	C(18)	C(19)	C(22)	C(21)	-103(1)
C(18)	C(19)	C(22)	C(23)	97.4(9)	C(18)	C(19)	C(23)	C(20)	76(14)
C(18)	C(19)	C(23)	C(22)	-109.9(10)	C(19)	C(20)	C(22)	C(21)	-23(1)
C(19)	C(20)	C(22)	C(23)	108.4	C(19)	C(20)	C(23)	C(22)	-68.2
C(19)	C(21)	C(22)	C(20)	23(1)	C(19)	C(21)	C(22)	C(23)	23(1)
C(19)	C(22)	C(20)	C(23)	-108.4	C(19)	C(22)	C(21)	C(25)	-70.0
C(19)	C(22)	C(23)	C(20)	71.5	C(19)	C(23)	C(20)	C(22)	68.2
C(19)	C(23)	C(22)	C(20)	-71.5	C(19)	C(23)	C(22)	C(21)	-23(1)
C(20)	C(19)	C(21)	C(22)	-20(1)	C(20)	C(19)	C(21)	C(25)	117.6
C(20)	C(19)	C(22)	C(21)	159(1)	C(20)	C(19)	C(22)	C(23)	-0.3(7)
C(20)	C(19)	C(23)	C(22)	173(14)	C(20)	C(22)	C(19)	C(21)	-159(1)
C(20)	C(22)	C(19)	C(23)	0.3(7)	C(20)	C(22)	C(19)	C(24)	-88(2)
C(20)	C(22)	C(21)	C(25)	-46.2	C(20)	C(23)	C(19)	C(21)	-153(14)
C(20)	C(23)	C(19)	C(22)	-173(14)	C(20)	C(23)	C(19)	C(24)	-44(14)
C(20)	C(23)	C(22)	C(21)	47.8	C(21)	C(19)	C(20)	C(22)	20(1)
C(21)	C(19)	C(20)	C(23)	26(14)	C(21)	C(19)	C(22)	C(23)	-159(1)
C(21)	C(19)	C(23)	C(22)	20(1)	C(21)	C(22)	C(19)	C(23)	159(1)
C(21)	C(22)	C(19)	C(24)	70(1)	C(21)	C(22)	C(20)	C(23)	-132.3

atom	atom	atom	atom	angle	atom	atom	atom	atom	angle
C(22)	C(19)	C(20)	C(23)	5(14)	C(22)	C(19)	C(21)	C(25)	138.5
C(22)	C(20)	C(19)	C(23)	-5(14)	C(22)	C(20)	C(19)	C(24)	130(1)
C(22)	C(21)	C(19)	C(23)	-19(1)	C(22)	C(21)	C(19)	C(24)	-136(1)
C(22)	C(23)	C(19)	C(24)	129(1)	C(23)	C(19)	C(21)	C(25)	118.8
C(23)	C(20)	C(19)	C(24)	135(14)	C(23)	C(22)	C(19)	C(24)	-88(1)
C(23)	C(22)	C(21)	C(25)	-46.5	C(24)	C(19)	C(21)	C(25)	2.2

5.5.3.7. Non-bonded contacts

atom	atom	distance	ADC	atom	atom	distance	ADC
C(18)	H(11)	3.48	45504	C(18)	H(12)	3.49	45504
C(18)	H(42)	3.54	45504	C(20)	H(151)	3.30	54504
C(20)	C(25)	3.54	54504	C(22)	H(11)	3.15	54501
C(22)	H(31)	3.48	65603	C(22)	H(13)	3.60	54501
C(23)	H(151)	3.34	54504	C(23)	C(25)	3.56	54504
C(23)	H(11)	3.58	54501	C(24)	H(42)	3.39	45504
C(25)	H(33)	2.37	54602	C(25)	H(32)	2.68	54602
C(25)	H(31)	2.82	54602	C(25)	H(42)	3.41	65603
C(25)	H(41)	3.57	65603	H(12)	H(132)	3.32	4
H(13)	H(121)	2.73	56501	H(13)	H(132)	3.26	4
H(13)	H(151)	3.32	56501	H(13)	H(171)	3.41	56501
H(32)	H(151)	3.02	56501	H(32)	H(41)	3.24	45504
H(32)	H(43)	3.42	45504	H(32)	H(42)	3.48	45504
H(41)	H(151)	2.93	54504	H(41)	H(153)	3.16	54504
H(41)	H(151)	3.35	54504	H(43)	H(151)	2.97	54504
H(43)	H(153)	3.11	54504	H(61)	H(121)	3.47	56501
H(91)	H(133)	3.25	4	H(91)	H(93)	3.33	66503
H(92)	H(121)	2.80	56501	H(92)	H(133)	3.05	4
H(92)	H(111)	3.06	2	H(92)	H(123)	3.10	56501
H(92)	H(122)	3.50	56501	H(92)	H(132)	3.56	4
H(93)	H(111)	2.85	2	H(93)	H(93)	3.18	66503
H(93)	H(102)	3.56	66503	H(93)	H(133)	3.56	4
H(101)	H(123)	2.90	2	H(101)	H(112)	3.02	54502
H(101)	H(122)	3.30	54504	H(101)	H(131)	3.33	54504

atom	atom	distance	ADC	atom	atom	distance	ADC
Cu(1)	H(153)	3.03	54504	Cu(1)	H(43)	3.23	45504
Cu(1)	H(12)	3.45	45504	Cu(1)	H(131)	3.49	54504
Cu(1)	H(132)	3.51	54504	S(1)	H(12)	3.13	45504
S(1)	H(91)	3.20	45504	S(1)	H(113)	3.39	54502
S(1)	H(132)	3.45	54504	S(2)	H(131)	3.38	54504
S(2)	H(93)	3.42	54502	S(2)	H(113)	3.47	54502
S(2)	H(91)	3.51	45504	S(2)	H(103)	3.51	45504
O(1)	H(153)	2.96	54504	O(1)	H(43)	3.17	45504
O(1)	H(42)	3.54	45504	O(2)	H(42)	3.09	45504
O(2)	H(151)	3.33	54504	O(2)	H(12)	3.43	45504
O(2)	H(153)	3.54	54504	O(2)	H(43)	3.55	45504
C(1)	H(121)	3.59	56501	C(3)	C(25)	2.80	55602
C(4)	H(151)	3.38	54504	C(4)	H(153)	3.50	54504
C(4)	H(32)	3.55	4	C(5)	H(153)	3.15	54504
C(6)	H(121)	3.30	56501	C(6)	H(153)	3.40	54504
C(9)	H(111)	3.39	2	C(9)	H(133)	3.47	4
C(10)	H(123)	3.18	2	C(10)	H(122)	3.48	54504
C(10)	H(112)	3.54	4	C(11)	H(131)	3.30	3
C(11)	H(133)	3.53	3	C(11)	H(103)	3.55	45504
C(12)	H(92)	3.30	54501	C(12)	H(112)	3.46	54501
C(12)	H(102)	3.51	54502	C(13)	H(113)	3.35	3
C(15)	H(41)	3.33	44504	C(15)	H(43)	3.47	44504
C(16)	H(12)	3.16	45504	C(17)	H(12)	3.34	45504
C(17)	H(11)	3.43	45504	C(17)	H(13)	3.49	54501

atom	atom	distance	ADC	atom	atom	distance	ADC
H(101)	H(113)	3.52	54502	H(102)	H(123)	2.62	2
H(102)	H(133)	2.96	2	H(102)	H(111)	3.32	4
H(102)	H(112)	3.38	4	H(103)	H(122)	2.80	54504
H(103)	H(112)	2.99	4	H(103)	H(111)	3.25	4
H(111)	H(133)	3.18	3	H(111)	H(131)	3.38	3
H(112)	H(122)	3.03	56501	H(112)	H(131)	3.27	3
H(112)	H(123)	3.29	56501	H(112)	H(121)	3.53	56501
H(113)	H(131)	2.76	3	H(113)	H(133)	3.26	3
H(113)	H(123)	3.36	2	H(113)	H(132)	3.50	3
H(121)	H(132)	3.60	54504				

The ADC (atom designator code) specifies the position of an atom in a crystal. The 5-digit number shown in the table is a composite of three one-digit numbers and one two-digit number: TA (first digit) + TB (second digit) + TC (third digit) + SN (last two digits). TA, TB and TC are the crystal lattice translation digits along cell edges a, b and c. A translation digit of 5 indicates the origin unit cell. If TA = 4, this indicates a translation of one unit cell length along the a-axis in the negative direction. Each translation digit can range in value from 1 to 9 and thus ± 4 lattice translations from the origin (TA=5, TB=5, TC=5) can be represented.

The SN, or symmetry operator number, refers to the number of the symmetry operator used to generate the coordinates of the target atom. A list of symmetry operators relevant to this structure are given below.

For a given intermolecular contact, the first atom (origin atom) is located in the origin unit cell and its position can be generated using the identity operator (SN=1). Thus, the ADC for an origin atom is always 55501. The position of the second atom (target atom) can be generated using the ADC and the coordinates of the atom in the parameter table. For example, an ADC of 47502 refers to the target atom moved through symmetry operator two, then translated -1 cell translations along the a axis, +2 cell translations along the b axis, and 0 cell translations along the c axis.

An ADC of 1 indicates an intermolecular contact between two fragments (eg. cation and anion) that reside in the same asymmetric unit.

Symmetry Operators:

(1)	X.	Y.	Z	(2)	1/2-X.	1/2+Y.	-Z
(3)	-X.	-Y.	-Z	(4)	1/2+X.	1/2-Y.	Z

5.5.3.8. Least square planes

Summary

plane mean deviation λ^2

Dihedral angles between planes ($^\circ$)

plane

Table of Least-Squares Planes

----- Plane number 1 -----

Atoms Defining Plane	Distance	esd
S(2)	-0.0010	0.0019
O(1)	0.0112	0.0039
C(11)	0.0157	0.0058
C(16)	0.0049	0.0052
C(17)	-0.0288	0.0053

Additional Atoms	Distance
Cu(1)	0.3205

Mean deviation from plane is 0.0123 angstroms
Chi-squared: 42.8

Table of Least-Squares Planes

----- Plane number 1 -----

Atoms Defining Plane	Distance	esd
S(1)	0.0005	0.0017
O(2)	-0.0047	0.0042
C(15)	-0.0004	0.0058
C(20)	0.0091	0.0056
C(21)	-0.0055	0.0052

Additional Atoms	Distance
Cu(1)	0.0057

Mean deviation from plane is 0.0040 angstroms
Chi-squared: 4.7

Table of Least-Squares Planes

----- Plane number 1 -----

Atoms Defining Plane	Distance	esd
S(1)	-0.0220	0.0017
S(2)	0.0271	0.0019
O(1)	-0.1423	0.0039
O(2)	0.1643	0.0042

Additional Atoms	Distance
Cu(1)	0.0052

Mean deviation from plane is 0.0889 angstroms
Chi-squared: 3234.3

5.5.4. Experimental

5.5.4.1. The Preparation of [bis(2,2,6,6-tetramethyl-5-mercaptohept-4-en-3-olate)barium(II)]using Ba granules and gaseous ammonia

2,2,6,6-tetramethyl-5-mercaptohept-4-en-3-one (1.30 g, 6.49×10^{-3} mol) in dry tetrahydrofuran (250 cm^3) was transferred into a 3-necked flask containing barium metal granules (0.60 g, 4.36×10^{-3} mol). No apparent reaction seemed to take place upon addition. The flask was then cooled to -65°C using a cardice / acetone bath. Dry gaseous ammonia was bubbled through the reaction mixture for 40 minutes. After 10 minutes of bubbling ammonia through the reaction mixture, one or two bubbles appeared, closely followed by a cloudy suspension. Several colour changes were observed during the 40 minutes of the addition of the ammonia gas which resulted in the production of a cherry red suspension. A further 25 minute addition of dry gaseous ammonia was undertaken after stirring the reaction mixture at -65°C for 2 hours. The flask was then left for 10 hours at room temperature whereupon all the gaseous ammonia had evaporated. An oily, off-white mixture remained.

Methanol (30 cm^3) was added to produce a yellow suspension. The suspension was filtered to leave a yellow solution . Ether (30 cm^3) was then added to this yellow solution to precipitate a white solid. The white solid was filtered and washed with ether ($3 \times 10 \text{ cm}^3$). The white solid was dried in vacuum.

5.5.4.2. The attempted preparation of [bis(2,2,6,6-tetramethyl-5-mercaptohept-4-en-3-one)barium(II)] using BaCl₂.2H₂O

2,2,6,6-tetramethyl-5-mercaptohept-4-en-3-one (1.00 g, 4.99×10^{-3} mol) in methanol (40 cm³) was transferred to a stirred solution of barium (II) chloride dihydrate (0.68 g, 2.78×10^{-3} mol) in distilled water (30 cm³) and 3 drops of concentrated hydrochloric acid. Upon addition a cloudy, oily suspension was produced. A homogenous solution was produced when methanol (35 cm³) was added. The solution was stirred for 24 hours and refluxed for a further 2 hours. The solution was then cooled to room temperature and stripped to dryness whereupon toluene (200 cm³) was added to give a yellow suspension. The suspension was filtered to give a yellow solution and a white solid. After evaporation of the yellow solution ¹H N.M.R. analysis showed it to contain the starting thio-β-diketone . The white filtered solid was found to be soluble in water and thus was assumed to be unreacted barium (II) chloride.

5.5.4.3. The attempted preparation of [bis(2,2,6,6-tetramethyl-5-mercaptohept-4-en-3-one)barium(II)] using barium (II) acetate

Into a 50% v/v methanol / water solution (100 cm³) of barium acetate (0.68 g, 2.66×10^{-3} mol), 2,2,6,6-tetramethyl-5-mercaptohept-4-en-3-one (1.10 g, 5.49×10^{-3} mol) was added dropwise to form a cloudy oily suspension. The suspension was then refluxed for 10 hours and cooled to ambient temperature, whereupon the suspension was filtered and the filtrate was evaporated almost to dryness.

Toluene (200 cm³) was added to the remaining residue, in which a white solid and yellow solution was produced. The white solid was filtered and was found to be soluble in water.

It was assumed that this was unreacted barium acetate. The yellow solution was then condensed to give the starting thio- β -diketone.

5.5.4.4. The preparation of [bis(2,2,6,6-tetramethyl-5-mercaptohept-4-en-3-one)copper(II)]

The copper complex was produced by similar methods to Dietrich, but the reaction time and conditions and the purification procedures are different from the ones described by Dietrich.

A methanolic solution (35 cm³) of 2,2,6,6-tetramethyl-5-mercaptohept-4-en-3-one (1.50 g, 7.49 x 10⁻³ mol) was added dropwise to a light green solution of copper(II) acetate. monohydrate (0.75 g, 3.75 x 10⁻³ mol) in methanol (25 cm³). Immediately, an instant red-brown precipitate developed. Once the addition was complete, the suspension was then refluxed for 15 hours and cooled to ambient temperature. The red-brown precipitate was filtered and washed with distilled water (3 x 15 cm³). The solid was then sucked dry in vacuo. The red-brown solid was then dissolved in ether (300 cm³) whereupon two layers were formed. The ethereal layer was separated and filtered. The homogenous solution was then evaporated to dryness to form a red brown solid. The complex was purified by sublimation 120-140°C / 0.01 mmHg, heating rate 2° / minute. M.P.=186-187°C, STA M.P. = 175°C, Lit M.P.= 187-188°C. Yield = 58% . Found % : C = 56.73, H = 8.66 ; C₂₂H₃₈O₂S₂Cu requires:C = 57.04, H = 8.27.

5.5.4.4.1. Mass spectral data

M / e : 996, 948, 945, 851, 788, 589, 524, 462, 420, 364, 325, 223, 199 and 137.

The FAB mass spectrum of the copper complex [Cu(TMMHD)₂] showed the molecular ion was present at 462 (monomer formation.).

5.6. References

1. K.B.Mertes and J.M.Lehn in "Comprehensive Coordination Chemistry", Eds. G.Wilkinson, R.D.Gillard and J.A.Mc.Cleverty, Pergamon press, Oxford, **21.3**, 915.
2. K.Timmer, C.I.M.A.Spee, A.Mackor and H.A.Meinema, Eur.Pat.Appl., 1991, 405 634, **A2**.
3. J.A.P.Nash, S.C.Thompson, D.F.Foster, D.J.Cole-Hamilton and J.C.Barnes, *J.Chem.Soc.Dalton.Trans.*, in press, 1994.
4. J.AT.Norman and G.P.Pez, *J.Chem.Soc.Chem.Commun.*, 1991, 971.
5. L.Huang, S.B.Turnipseed, C.Haltiwanger, R.M.Barkley and R.E.Sievers, *Inorg.Chem.*, 1994, **33**, 798, 803.
6. S.C.Thompson, Ph.D.Thesis, University of St.Andrews, 1991.
7. S.R.Drake, S.A.S.Miller, M.B.Hursthouse and K.B.Abdul-Malik, *Polyhedron*, 1993, **12**, 13, 1621.
8. F.J.Hollander, D.H.Templeton and A.Zalkin, *Acta.Cryst.*, 1973, **B29**, 1289.
9. F.J.Hollander, D.H.Templeton and A.Zalkin, *Acta.Cryst.*, 1973, **B29**, 1303.
10. F.J.Hollander, D.H.Templeton and A.Zalkin, *Acta.Cryst.*, 1973, **B29**, 1295.
11. A.Zalkin, D.H.Templeton and D.G.Karraker, *Inorg.Chem.*, 1969, **8**, 12, 2680.
12. G.J.Bullen, *Nature.*, 1956, **177**, 537.
13. F.A.Cotton and R.C.Elder, *J.Am.Chem.Soc.*, 1964, **86**, 2294.
14. R.Beckett and B.F.Hoskins, *J.Chem.Soc.Dalton.Trans.*, 1974, 622.
15. K.Dietrich, K.Konig, G.Mattern and H.Musso, *Chem Ber.*, 1988, **121**, 1277.
16. K.Dietrich, H.Musso and R.Allman, *J.Organomet.Chem.*, 1975, **93**, 15.
17. D.H.Gerlach and R.H.Holm, *Inorg.Chem.*, 1969, **8**, 11, 2292.
18. S.Sugawara and S.Koji, *Jpn.Kokai.Tikkyo.Kohlo.*, J.P. 05 65647 19/03/93.
19. S.Sugawara and S.Koji, *Jpn.Kokai.Tikkyo.Kohlo.*, J.P. 04 260640 16/09/92.
20. S.H.Chaston, S.E.Livingstone, T.N.Lockyer, V.A.Pickles and J.S.Shannon, *Aust.J.Chem.*, 1965, **18**, 673.

21. S.R.Drake and D.J.Otway, *J.Chem.Soc.Chem.Commun.*, 1991, 517.
22. F.A.Cotton and J.J.Wise, *Inorg.Chem.*, 1966, **5**, 7, 1200.
23. P.C.Le Brun, W.D.Lyon and H.A.Kuska, *J.Crystallogr. and Spectr.Res.*, 1986, **16**, 889.
24. T.G.Appleton, H.C.Clark and L.E.Manzer, *Coord.Chem.Rev.*, 1973, **10**, 355.
25. J.Coetzer and J.C.A.Boeyens, *J.Cryst.Mol.Struct.*, 1971, **1**, 277.
26. C.G.Macdonald and J.S.Shannon, *Aust.J.Chem.*, 1966, **19**, 1545.

APPENDICES

CONCLUSIONS

Several barium "scorpion-tail" and pendant arm bibracchial macrocyclic complexes have been produced and analysed for their volatility. It appears that the barium complexes with the "scorpion tail" appendages attached were found to be involatile and decompose upon heating.

The reason for this lack of volatility is probably due to the formation of a polymeric network within the complex which severely hinders the solid to vapourise into the gaseous state. The formation of a polymeric network is further supported by the X-ray crystallographic evidence of $[\text{Cu} (\text{POUD})_2]$ which shows a (4+2) Jahn-Teller distorted system. In this case, the polyether "scorpion tail" appendage would rather be binding to another metal centre than chelating to the same metal centre to that of the β -diketonate function.

The barium pendant arm bibracchial macrocyclic complexes (**1,2,3**) produced, were also found to decompose when heated and do not sublime.

Barium macrocyclic complexes (**1, and 2**) were produced using the ligands (**1 and 2**) and $\text{Ba} (\text{OH})_2 \cdot 8\text{H}_2\text{O}$ in water. In all three barium macrocyclic complexes, cis and trans isomers are isolated in solution in which the pendant carboxylate arms are chelating to a single barium centre.

Complexes **2** and **3** were isolated as dihydrate or monohydrate barium complexes. Thus, the possibility of inter/intra moleccular hydrogen bonding may cause the barium complexes to become involatile.

The barium macrocyclic complexes affinity for protic solvents such as water and methanol indicates that inter/intramolecular hydrogen bonding takes place within the barium macrocyclic complexes. This is supported by the observation that the barium macrocyclic complexes (**1,2,3**) do not sublime.

The tetraglyme adduct of [Ba (DBM)₂] was shown to decompose on heating. It was found that in this particular case increase in electron negativity on the β-substituents did not increase the stability of the barium complex as observed in the perfluorinated β-diketonate tetraglyme complexes. In contrast, [Cu (TMMHD)₂] is very volatile and even has a higher volatilisation temperature than [Cu (TMHD)₂].

ANALYTICAL EQUIPMENT

The analysis of the compounds was undertaken using a series of instruments. IR spectra were obtained on a Perkin Elmer FTIR 1710 spectrometer and ^1H , ^{13}C and ^{135}Ba N.M.R. spectra were obtained on the Bruker 300 MHz spectrometer (^1H , ^{13}C and ^{135}Ba N.M.R.) or on a Varian Associates 200 MHz spectrometer (^1H and ^{13}C N.M.R.). The UV / visible spectra were obtained on a Phillips UV / Visible spectrometer. Mass spectra data was collected on a AEI MS50 electron impact mass spectrometer and FAB mass spectrometer. Simultaneous Thermal Analysis was undertaken at Associated Octel Ltd using a Stanton Redcroft STA 1000 analyser.

Typical peaks in the IR spectra are defined as follows: s = strong, m = medium and w = weak absorption. The characteristic shapes of the absorbance in the IR spectra are defined as: b = broad, sp = sharp and sh = shoulder. The UV/Visible data is represented by absorbance and wavelength in nm (λ_{max}). In the ^1H and ^{13}C N.M.R., the peaks are defined as s = singlet, d = doublet, t = triplet, tt = triplet of triplets and m = multipet. The symbols k and e represent the keto and enol forms in the ^1H and ^{13}C N.M.R. spectra. The figures in the brackets for the ^1H N.M.R. assignments correspond to the number of protons giving rise to that peak. The figures in the brackets for the ^{13}C N.M.R. assignments correspond to the position in the carbon chain. However, the numbers do not correspond to the systematic IUPAC nomenclature.